DESIGN AND IMPLEMENTATION OF A CONTROL SYSTEM FOR

A

POWERED RECIPROCATING GAIT ORTHOSIS

A thesis submitted to

THE UNIVERSITY OF SALFORD

for the degree of

DOCTOR OF PHILOSOPHY

BY

ARAFAT ABDUL-RAHMAN ZAIDAN

SCHOOL OF ACOUSTICS AND ELECTRONIC ENGINEERING

UNIVERSITY OF SALFORD

ENGLAND

NOVEMBER 2000

ABSTRACT

The University of Salford has developed a program in order to improve the control of lower limb orthotics thus improving the ability of paraplegics to walk. Although the system is greatly needed for rehabilitation it is hoped that the final system would enable paraplegics to walk in the community. The present project, which is based on previous designs such as the R.G.O (Reciprocating Gait Orthosis), strives to add external power at the hips of the R.G.O. The constructed prototype is made of a mechanical skeleton with each leg driven by a brushless motor and a lead screw.

The main purpose of this project is to design a control system to control the motion of the legs. The first step in achieving this task was to model the various components of the system separately and then derive a model using system identification that will describe the behaviour of the whole system.

The starting point was a mechanical device with two motors mounted one at either hip. A full mathematical analysis of the system is carried out. Once a mathematical model is derived for the R.G.O with the two motors it can be used to carry out real time simulations using MATLAB.

Once the model is derived it must be validated to make sure it is actually a mathematical representation of the system. The identified model is usually very accurate as it is based on the actual system performance. Then real time simulations of the theoretical and the

identified model are compared. If the theoretical model behaves in the same way as the identified model then it is validated and may be used for further work.

The models derived using system identification were validated and gave a good comparison when compared to real data. A pole placement controller was designed and tested based on these models. The controller performance was tested with the orthosis unloaded, loaded with artificial loads (a plaster leg weighing 10 Kg). The controller managed to follow the pre-set trajectory reasonably well. The orthosis was then tested with a volunteer in it. Again the performance was very encouraging.

The final Project will be P.C driven System with the possibility of using NiCAD Batteries as the power source. The main tools, which will be used in order to carry out simulations and comparisons of theoretical and practical results, are MATLAB. The software used was C

Acknowledgements

I would like to express my deepest gratitude and thanks to Dr Medrano-Cedra for his help and guidance and supervision throughout the course of this project. Also many thanks go to Professor John Grey for his over all supervision.

I would also like to thank Mr. Ken Taylor for his continuing advice and support when it was most needed during the duration of the project. Finally I would like to thank Dr Hill for his help.

Special thanks go to my friends whose patients with me for coming late to work during the whole period of this project was an essential part in completing this project

To the most important people in my life. Thank you for your

Patient Support

My Mother

Ibrahim, Mouin, Jamal. Salam, Mazin, Mohammed, My Sisters

My Wife and My friend.

Contents

CHAPTER 4

CHAPTER 5

CHAPTER 6

CHAPTER 7

CHAPTER 1

INTRODUCTION

Human gait has been investigated for several decades. It is one of the most sophisticated forms of locomotion existing in the animal kingdom. It consists of two main functions.

1. Propulsion: A sequence of movements permitting displacement in several directions.
2. Dynamic Stabilization: This permits balance of an upright structure moving over rugged terrain or an incline. These functions are acquired at a young age, and that it would take approximately 18 months for a baby to walk using all his feedback sensors such as sight, hearing, feelings and finally pressure [Rabischong P., 1975].

In recent years there were many attempts to develop an exoskeleton for paraplegics with paralysis of lower extremities in order to give paraplegics at least a minimum ability to walk [Vukobratovich M., 1976; Grundman J. and Seireg A., 1976]. All efforts so far did not result in an efficient suitable device. The principal disadvantages of the developed devices were a low degree of anthropomorphism and a high technical complexity.

An anthropomorphic active exoskeleton is usually defined as a portable mechanism whose configuration and degrees of mobility corresponds to those of patients body and which can be made to produce walking motions that closely resemble those of a healthy human being by means of a continuous execution of special control programs with the help of slave drives.

For many disabled people, particularly paraplegics, polio patients or those with deformities of the lower limbs with a loss of the gait function, some compensation is required, if the upper limbs are functional then for some patients crutches may help others are confined to a wheel chair. Therefore there is a tremendous need for a device which would counter the flaccidity of the muscles in paraplegics and assist in the propelling forward of the subject. The device also needs to counter the hip extensor weakness in paraplegics thus helping the subject to adopt the upright posture.

Hip extensor weakness in myelomeningocele causes problems in ambulating thus creating difficult challenges for effective Orthotic design, hip extension by the gluteus maximus (muscles in the buttocks) is innervated by signals from the sacrum (bone between the two hips). Hip flexion is innervated by upper lumbar levels (upper part of body, on both sides of the spine between the floating ribs and hip bone)

For many disabled people, particularly paraplegics, Polio victims and patients with myelomeningocele who have paralytic levels in the lumbar region (lower back) have paralysed hip extensor. This means that these patients may assume a posture of hip flexion while attempting to stand or walk figure (1). This depends on the level of paralysis in the lower back. One solution has been the addition of a reciprocating mechanism to the hip joints of a lightweight Orthosis that controls the hips knees, ankles and feet (KAFO).

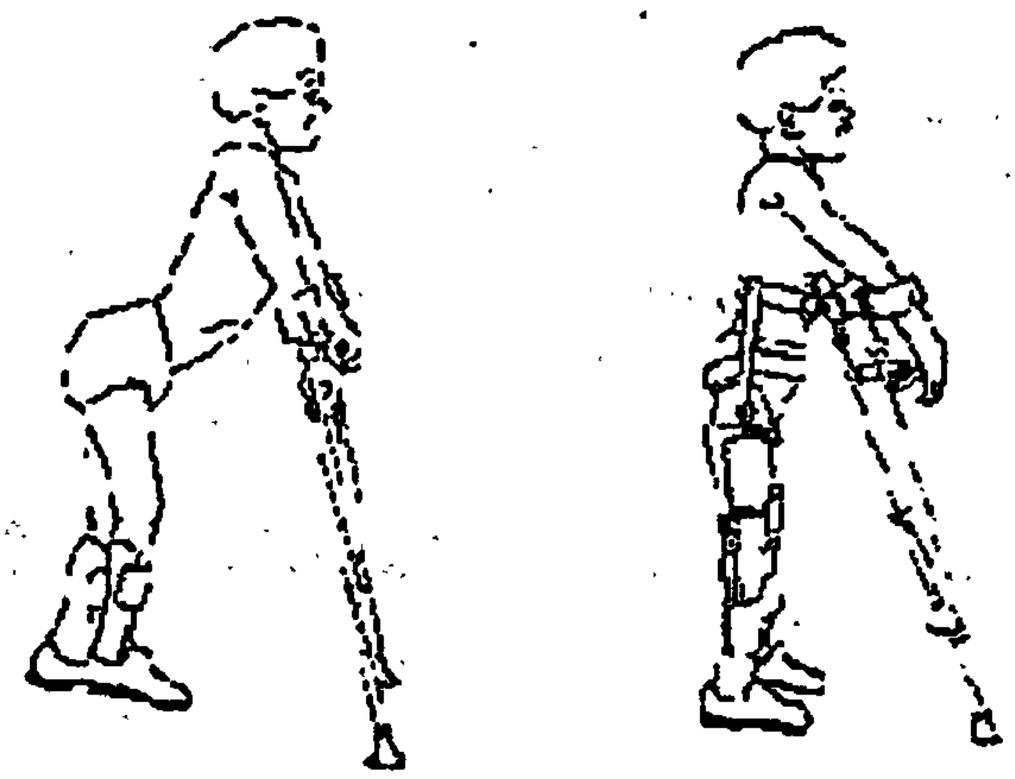

Figure 1 Standing Postures with and without Orthosis for paraplegics

The basic principle of these devices is that they provide a rigid support structure upon which the patient's weight may be borne during the stance phase of a gait cycle, therefore facilitating either functional ambulation or exercise. Hence these devices are prescribed so that the patient may be rehabilitated as far as possible, through the restoration of some degree of mobility to an otherwise wheelchair bound subject.

The Amol project [Rabischong P., 1975] considers the three problems faced by any person working on this complex problem.

1. The concept of an Orthosis and its adaptation to the patient.
2. . The problems of a portable energy source and the choice of actuators.
3. The control problem.

The classical Orthotic approach relies on the application of an external skeleton supporting the impaired limb, such an arrangement involves force transfer over the man-machine interface as well as external control adapted to the patients need and body attitude.

In the late 1960s, a number of reciprocating Orthoses were devised for children, quite independently of one another. David Scrutton of Guy's Hospital, London, designed a polyplanar hip hinged brace [Scrutton D., 1971] used for children with cerebral palsy and spinal bifida. To find out the outcome of this type of bracing [Stauffer E.S., 1972] followed up 100 adults and 91 children five years after discharge. On the basis of this group of patients it was concluded that functional ambulation was realistic only for children and adults who are not completely paralyzed. This effectively means that these systems are limited and only a few people will benefit from them. They also found that children generally tended to ambulate for longer periods than adults after being braced. However, of the children studied, those with complete lesions stopped walking when they reached adolescence.

[Hoffer M.M, 1973] reported similar findings, namely that 56 children with myelomeningocele, non with thoracic lesions walked at all.

[Guttman L., 1976] reported paraplegics with mid thoracic or lower lesions walking with non-weight-bearing callipers (using Duralumin for younger adults and children) and in some cases, with pelvic bands or leather corsets for additional support.

All these bracing programmes came up against a variety of problems and were eventually discontinued. These problems include the failure in designing appropriate control systems and lack of funding.

Other ideas and developments followed some years later, for example the swivel walker [Stallard J. & Rose G.K., 1981]. The swivel walker is a standing frame, which will move forward when the patient leans his trunk from side to side. Progress is very slow and it only works on flat surfaces. It is mainly used by small children. The study of [Hyde S.A., 1982] showed that, of 30 boys with Duchenne muscular dystrophy braced with a lightweight Orthosis (by John Florence), 24 managed to walk and delay deterioration of the muscles.

Until recently, the only form of walking available to paraplegics was with swing through gait using a hip-knee-ankle-foot Orthosis. This brace effectively makes the patient into a rigid structure from the waist downwards and enables walking to be achieved using a pair of crutches. Both legs move forward while the body weight is taken through the crutches. The legs then take the weight while the crutches are moved forwards. The gait is ungainly and tiring, but nonetheless can be fast and effective.

There have been a number of attempts over the years to permit the paralysed to walk using reciprocal gait. Prominent among recent work are two designs, which have emerged as practical systems. One is the reciprocating gait Orthosis or RGO developed by Roy Douglas and his colleagues [David A.Y., Roy D., & John M.R., 1984]. The

R.G.O itself is a development from earlier device such as the KAFO (Knee-Ankle-Foot-Orthosis) used to lock the knee and ankle joints within a rigid framework supporting the subject's stance. This device was initially tested at the Ontario Crippled Children's centre (1969) and later at the Louisiana State University [David A.Y., Roy D., & John M.R., 1984]. The second device is the hip guidance Orthosis HGO also called the 'Para Walker' developed by Gordon Rose and his colleagues at the Orthotic research and Locomotion Assessment Unit (ORLAU) at Oswestry. England. [Rose G.K., 1981 & 1983].

For patients with a greater degree of weakness at the hips it was necessary to also incorporate an additional hip braced component as described by [Lehman J.F, Redford J.B., 1986] in both the RGO and HGO. Both devices have enabled work to proceed with the restoration of the gait in those having complete flaccidity of the lower extremities, using the subject's own upper body musculature to provide the motive effort.

Regular use of these devices proved to be a very fatiguing experience for the user. This is principally due to the transfer of the physical effort to the upper body and the efficiency with which this can be done. Various attempts have been made to apply an external power source under active control to an Orthosis. Much of this work can be put into two main categories, either that using Functional Electrical Stimulation (F.E.S) of the subjects own leg and lower trunk muscles, or that utilizing external actuators,

Functional Electrical Stimulation F.E.S in conjunction with the mechanical Orthosis was jointly developed by Louisiana State University Medical center and Durr-Fillaver

Medical, Inc to overcome four problems encountered with the existing model [Solomonow M., 1989].

1. The high energy cost of locomotion
2. The great arm strength required for patients to stand up from the seated position without assistance.
3. Difficulty in remaining standing owing to failure of the knee latch to lock except in full extension.
4. Problems in balancing when ambulating on an incline.

FES can produce sequences of controlled muscle contractions leading to functional motions such as standing, ambulation, and hand actions. However FES rehabilitation technology is not effective in all cases of paralysis. In order to extend the scope of FES, methods combining FES and active exoskeletons, the so-called Hybrid-Assistive-Systems (HAS) have been proposed. Gait stability and posture control are maintained without machine assistance by involving the patient's upper extremities (bars, crutches, canes etc) [Handicapped, Robots For].

FES has a great advantage over exoskeletons in that it attempts to regenerate functional motions by evoking external biological reflex mechanisms and internal synergies over which voluntary control has been lost due to damages to the neural networks [Handicapped, Robots For]. The application of FES enables the patients to produce the motor function using their own energy muscles as actuators and their metabolic energy.

The idea that FES should be supported by externally controlled Orthosis in order to improve and extend the application field of FES was presented quite early. It took some time before hardware and software tools for HAS had been developed so that the clinical feasibility studies of this rehabilitation method could be started. However it must be kept in mind that FES by itself cannot restore in a satisfactory way functional motions in all instances of paralysis. With total lesion (total break of the spine, severing the neural cords) or denervated muscles, application of FES is not yet possible. Therefore in cases of severe lesions, HAS may be the only solution.

The safe transition from various static postures as described by [Mulder A.J., 1992], have in the main considered FES as the principle motive power source. FES has one major advantage over the alternative method using motor driven actuators. The latter requires bulky power packs, which burdens the subject with both additional complexity and a greater physical load. However there are also penalties that may be associated with the use of FES. These include both problems concerning the degree of actual control available and the long term fatiguing of the subject's own muscles.

Such limitations of the controllability of the FES led to the investigation of the externally powered and actuated Orthosis. The most notable amongst the earlier attempts was the AMOL project of [Rabischong P., 1975]. Developed in the mid 1970s and aimed at producing an active modular Orthosis having separate strap-on Orthotic and powered components. Since then work has progressed with certain features of the original work now being embodied within the EUREKA/CALIES project described by [Micallef J.P. &

Rabischong E., 1991]. However this application of a controlled electrically driven Orthosis is limited to the training in the clinic rather than truly free ambulation. In other words the use of these Orthoses would be limited for rehabilitation and training in hospitals or clinics.

[Hill J.W., 1981] Stanford research institute, California considers using hydraulic power on the Amol project; he quotes several advantages in the use of hydraulic systems over actuators. Great torques are required at the joints when sitting down or standing up (about 117.7 Nm), also available very light and small hydraulic actuators (1kg in weight and 25mm thickness). Hydraulic cylinders are smaller and less noisy than pneumatic cylinders. However there are disadvantages of hydraulic systems such as leaks, and even the power capability of the system may pose a danger to the patient. Powering up these mechanical systems produces new challenges for engineers, namely the issue of control.

The control problem has been approached in two different ways. One is to consider the Orthosis as an independent autonomous machine, which solves the problems of stability and propulsion. The second assumes that stability is controlled by the patient. That is the patient must shift his body weight with his canes or walker to continue the walking process, In effect the patient becomes part of the control loop [Rabischong P., 1975].

Work reported in this field has been few and no clear evidence of working control systems has been presented. [Miyamoto H, 1985], [Rabischong P., 1975] and [Hill J.W.,

1981] reported that working control systems had been developed, but no evidence of such systems were presented in their respective papers.

The device that was selected for this project is based upon a conventional Reciprocating Gait Orthosis (R.G.O) [Edwards J. & Gray J.O, 1993], being subsequently modified as to incorporate one or two electrical drive units. Such aids have been developed to counteract flaccidity of the lower limbs of paraplegics. The lineage of this form of aid extends at least to the 1960s, with earlier designs in turn being the product of an evolution development originating from the earliest caliper designs [Grundman J., 1976, Guttmann L., 1976].

Such a device could be powered in many ways as various direct power schemes have been considered for use in the work of others. These include hydraulic power [Miyamoto H., Israel I., Mori S., Sono A. & Sakurai Y., 1985], direct electrical drives as discussed earlier and Hybrid schemes [Tomovic R. & Popovic D., 1990]. A decision was taken to adopt the directly electrically driven design as presented. The alternatives were rejected in favor of the current design in order not to compromise the improvements in mobility or the anticipated degree of control possible. However a combined FES and directly driven power schemes similar to that of [Tomovic R. & Popovic D., 1990] does have certain attractions, in that a given power output could be sustained for a greater period with more flexibility. This however would form the basis for future work to be addressed after the basic issues of control have been addressed within the current project.

Within the scope of this project as presented here the objectives are as follows: to extend the ambulatory capability beyond that provided by an unmodified RGO and to design a computer control systems to improve the performance of the RGO.

It is worth stressing at this point that it is not our intention or aim to provide all the power required for human mobility, but rather to assist the efforts of the upper body musculature still being used to maintain balance and contribute some motive effort. Adopting this approach has enabled us to minimise the size and weight of the components in the external drive. However, even without any subject motive effort, the estimated performance derived from the 26.3Nm at the hip limit indicates that 70Kg subject having a 1m leg and 0.75m stride can attain 22m per minute. This is about one third of the expected 75m per minute for an able-bodied subject [Downes C.G, Hill S.L. & Gray J.O, 1994].

The main tools used were Matlab, programming in C. The techniques were solving polynomial equations for the pole placement equation and assessing the relative stability of the closed loop systems using frequency domain techniques based on the Nyquist and Bode plots

The layout of this thesis is as follows: The first chapter is the introduction the second chapter is the background which gives the preliminaries on previous work done interms of different Orthotic devices, Energy requirement for these devices and the control systems considered for these devices by other researchers. Chapter 3 compares the

different types of Orthotic devices and the mechanical calculations for the powered Orthosis are presented. Chapter 4 shows the testing of the different components i.e. the motor torque-speed and current characteristics. Chapter 5 explains how the mathematical model for the RGO was derived using System Identification in Matlab. Chapter 6 gives detailed work of the design and background for Pole-Placement controller and chapter 7 shows the results when implementing the pole placement controller. And finally the conclusions and future work are presented in the final chapter.

CHAPTER 2

BACKGROUND

Clinicians and engineers have been involved in the walking rehabilitation of paraplegics since the early 1960s. During the early period there was no attempt at developing a full Orthosis which would enable children and adults to ambulate. The early work concentrated on bracing joints particularly for children. The idea was to help stiffen up the limbs by mechanical means compensating for the paraplegics' own flaccid muscles. This would enable the patient to stand upright and then use his upper body's strength to propel himself forward.

Work on full Orthosis and the idea of reciprocal walking for adults and children really began in the early 1970s. The concept was first introduced by Roy Douglas at the Ontario crippled center. At about the same time the North Western Orthotic unit in Salford which had an established Orthotic clinic specializing in the rehabilitation of paralyzed people was using the Salford University designed Swivel Walker [Henshaw J.T & Griffiths J.C., 1981].

The 1970s and 1980s saw rapid development of reciprocal gait Orthosis. However in the last decade there seems to be very little literature on this subject. This could be due to the lack of funding and the difficulty in producing a control system for these devices. All previous publications such as [Miyamoto H., 1983, Hill J.W., 1981, Rabischong P., Bel J.P., Hill J., 1975] talk about the high level control requirements, but non talk about the

details of the control requirements such as bandwidth or noise rejection properties. A summary of the most successful Orthotic devices developed since 1970 is given in this chapter.

2.1 Orthotic devices

The Swivel Walker was one of the first devices available for paraplegics [Butler P.B et al., 1982]. Due to the widespread success of the swivel walker among children paralyzed below the waist as a result of spina bifida and various neuro-muscular diseases, over 1000 swivel walkers were prescribed to children over a ten year period. All the children were five years and over. Most were taken from wheel chairs but some had tried unsuccessfully to use more conventional equipment first. The appliance is intended for use indoors but some patients do use it outdoors where a firm level surface is available. Measurement of distance travelled in thirteen children using a specially designed counter shows considerable variations, one child travelling as much as 1000m in one day (6 hours). However adults paraplegics found this device difficult to use with the result that only 21 swivel walkers were prescribed to adults, and just 5 patients continued to use them in the long term [Henshaw J.T & Griffiths J.C., 1981].

Whilst swivel walkers enable walking early in life to be achieved their speed, surface limitations and their somewhat penguin-like pattern of locomotion made the development of Reciprocal Orthosis with better characteristics eminently desirable. The Hip Guidance Orthosis (HGO) was therefore produced. The Orthosis enables paraplegics to walk

reciprocally with crutches over a variety of surfaces and inclines. The principle of the hip guidance articulation used in the Para Walker has been extensively described by [Rose G.K., 1979, 1980], [Butler P.B. et al., 1984], [Stallard J. et al, 1986]. It makes use of components of locomotion and components of gait [Rose G.K., 1986]. The HGO was also supposed to improve or reduce the energy requirement needed for walking. The Para Walker (name given to the Hip Guidance Orthosis) has been in use since the early 80's. A survey [Summers B.N. et al, 1986] showed that 85% of the patients were still regularly using their Para Walker at follow-up on average 20 months from the date of supply of their Orthosis.

Further developments from the swivel walker and the H.G.O brought about the Reciprocating Gait Orthosis (R.G.O) by [David A.Y. & Roy D., 1984]. The Louisiana State University Reciprocating Gait Orthosis is a prime example of the R.G.O. The L.S.U R.G.O comprises molded polypropylene Ankle-Foot Orthosis with carbon fibre inserts for added strength and stability. The side straight is made of titanium and aluminum alloys. On each side, the hip joints lock in the upright position and unlock by means of small button, enabling the patient to sit or bend forward. Two bowden cables are connected to the hip joints. The cables assist in the reciprocating gait. The L.S.U Orthosis is designed to support the patient in the upright position and assist the walking action purely by mechanical principles which are actuated by the patients upper body and arms. [Beckmann J., 1984].

The British Government's Department of Health and Social Security commissioned a trial at the Nuffield Orthopedic Centre, Oxford, running from September 1986 to April 1988. The trial was a crossover study in which 22 patients were grouped into pairs, matched as closely as possible. Each patient first underwent four weeks of exercise, followed by fitting, at least one week of training in the first brace and then four months of wearing it at home. The pattern was then repeated for the other brace. At the end of the second four months wearing period, the patient chose whichever brace he preferred. One member of each pair used the H.G.O first, followed by the R.G.O, and the other member was given the R.G.O first, followed by the H.G.O. The fact that a trial was needed at all suggests that neither brace is clearly much better than the other. The aim of the trial was not to find a "winner'' but rather to give guidance to fitters as to which patients are likely to be unsuitable for either brace, which can be expected to do best in one and which in the other [Michael W. W., 1988].

Long term compliance with the reciprocating gait Orthosis (RGO) has been found to be poor [Sykes et al., 1995]. One contributory factor for this may be the energy requirements associated with its use. It has been suggested that reducing the energy cost of walking will allow the patient to use the device "over longer distances and periods of time, and thereby incorporate it in his daily living" [Hirokawa et al., 1990]. To achieve this the mechanical Orthosis has been combined with electrical stimulation of the thigh muscles to produce a "hybrid" system [Solomonow et al, 1989]. Stimulation is used to assist the propulsion of the patient. This system has been reported to improve ambulatory efficiency [Hirokawa et al., 1990], [Petrofsky and Smith, 19991], [Phillips and

Hendershot, 1991], [Isakov et al, 1992]. However the evaluation of the RGO has been carried out largely in the laboratory environment.

The R.G.O was taken further by different researchers, the issue of comfort and adding external power to the R.G.O was addressed by [Miyamoto H., 1983, Hill J.W., 1981, Rabischong P., Bel J.P, Hill J., 1975].

The AMOL project discusses the issues of comfort of the Orthosis and applying external power. The device consists of a set of soft but firm clothing segments. One fitting around the hips and the other fitting around the thighs and lower legs. The segments are fabricated from cloth and pressurized pneumatic tubes to stiffen the structure. The built in tubes provide firm contact with the patient and support for a metal skeleton of pins pinched between the inflated tubes.

A prototype of a powered Orthosis for paralyzed lower limbs was designed by [Miyamoto H., 1983]. The powered Orthosis consists of the exoskeletal frame, four electrohydraulic servo actuators, sensory system, and a microprocessor with specially designed hardware. The electrohydraulic linear servo actuators were supplied with oil pressure of 686.7 N/cm^2 by a power unit. Hip and knee joints were motorized by these actuators while ankle joints had no driven torque. The servo amplifiers and servo valves were installed in a wagon separate from the exoskeltal frame. The powered Orthosis was controlled via a prescribed reference gait pattern that was originally taken from a normal

subject's walk. The method was effective for a stationary level walk [Miyamoto H., 1983].

A similar prototype Orthosis but with two fixation mechanisms for ankle joints added was later developed by [Miyamoto H., 1985]. Again the gait patterns were based on a normal subject. Various sensors were included such as potentiometers, foot switch sensors and posture sensors. The weight of the Orthosis was 19.5 Kg compared to 15Kg in the 1983 experience [Miyamoto H., 1983].

[Hill J.W, 1981] considers some of the problems encountered using hydraulic actuators. He considers the conventional approach and a new approach. The conventional approach has constant speed motor drives, a pump with pressure regulator. The maximum necessary pressure and maximum necessary flow must be continuously available at the output of the pump. The power derived with that system is worked out by multiplying the maximum torque with the max speed. In his case 120 Nm × 2.2 rad/s = 264 watts

The second system uses an accumulator to store the hydraulic energy for peak demand time. The pump generates only the mean flow required not the peak flow. Therefore the maximum power is again the maximum torque multiplied by the mean speed. Considering the same case as above yields $120\,\text{Nm} \times 0.45\,\text{rad/s} = 54$ watts. Now considering that the mean power actually required to drive the hip is approximately 8

watts [Vukobratovic M. et al, 1973]. It can be seen how wasteful these two approaches are. This is important when the battery drain is considered [Hill J.W., 1981].

Adding external power to the mechanical Orthosis helps in reducing the energy expenditure by the patient. This is an essential requirement for the Orthosis to be successful or to be used in long distance walking.

2.2 Energy Expenditure

A disadvantage of unpowered Orthotic devices is the high-energy requirement from the user. Reduction of the energy cost of paraplegic walking is therefore an important goal. Estimating the energy expenditure of ambulation is essential for assessing the gait efficiency and the differences in orthotic systems in the spinal cord injured individual. Previous studies have demonstrated that the energy expenditure of walking with knee ankle-foot Orthoses (KAFO) is above normal after a spinal cord injury [Huang et al., 1979; Chantraine et al., 1984; Miller et al., 1984; Waters et al., (1985, 1989), Cerney et al, 1980, Merkel et al., 1984,1985] and R.G.O. [Hirokawa et al., 1990].

In order to evaluate what would be regarded as needing high-energy consumption the normal energy consumption of normal walking has to be evaluated. [Blessey R, 1978] studied energy requirement of normal walking and found energy consumption to be $4.355\,JKg^{-1}s^{-1}$ energy cost $3.25\,JKg^{-1}m^{-1}$ and speed $1.37m/s$

[Nene A.V., Patrick J.H, 1989] studied the energy cost of paraplegics locomotion with the ORLAU Para Walker (H.G.O). Ten subjects with neurological lesion levels were evaluated in the laboratory at ORLAU using their Orthosis in the mechanical form only. The results were that Para Walker subjects consumed $3.1\,JKg^{-1}s^{-1}$, at a speed of $0.213\,m/s$ at the cost of $16.0\,JKg^{-1}m^{-1}$. The energy cost was 4.9 times the normal cost at only 15.5% of normal speed. The method used was to measure the amount of Oxygen intake at rest and the same again after the walk. The oxygen consumption per minute was used to calculate energy consumption.

The assessment of functional performance by measuring oxygen uptake and other physical parameters to produce energy cost index, was found by experience not to be suitable for young children or severely handicapped patients [Nakagiri K.I, 1976, Dounis E. et al, 1980]. Face masks and cumbersome equipment either completely prevent such patients walking, or distort performance so much that assessment of function is impractical. Physiologists have shown that oxygen uptake and heart rate are linearly related and dependent on speed [Astrand P.O. and Rodhal K., 1970]. The use of small radio transmitters makes it possible to monitor ambulatory heart rate in addition to speed without causing undue stress to handicapped patients [Davies J.B, 1977], [Stallard J. et al, 1978].

While it had been shown that it is possible to measure walking performance of patients by monitoring speed and heart rate [Stallard J. and Rose G.K., 1980], the two parameters had not been combined by ORLAU to produce a single physical cost index. The problem

of comparison was further exacerbated because there were no standards by which to judge individual performances through various age groups. In addition it was often difficult to know whether to ascribe improvement in performance to increase in age or the effect of treatment.

[MacGregor, 1981] introduced the physiological cost index (PCI) which is the ratio of the heart rate increase above resting heart rate to the velocity of ambulation. He found that for normal subjects the PCI range was from 0.51-0.11 beats/meter. The minimum values found were associated with those walking speeds selected by the patients as being "Preferred". He also uses PCI as an indicator of the level of handicap.

PCI is not the only indicator of the level of handicap. In attempting to define the severity of physical impairment in a patient with a fault in the locomotor system, it was found from extensive experience with amputees [Dyson, 1977] and a wide variety of youngsters with conditions such as Polio, Spina bifida and Spasticity [Levy, 1980] that perhaps the simplest and yet one of the most repeatable and reliable indices available is a simple determination of the preferred speed of walking. Not only do attempts to vary walking speed by instruction or inducement produce additional information regarding the physical biomechanics of their locomotor system, but the preferred gait is a concept readily demonstrated by the patient and yields very reproducible performance from day-to-day [MacGregor, 1979a].

PCI has been used to demonstrate the difference in energy costs between normal and disabled children by [Butler P., Engelbrecht M. 1984] who took on the task of using the heart rate and speed to find a physical cost index (PCI) for normal children. Their method shows that the mean PCI while wearing shoes is 0.4 and while barefoot to be 0.38. The PCI for children with pathological gait is appreciatively greater than that of normal children. The PCI is an important quantitative indicator because it enables fitters to test different Orthoses and the patient's energy consumption and also it can be used as an indicator of the level of physical handicap.

A Comparison of energy costs of spastic diplegic children with and without ankle-foot Orthoses Was done by [Mossberg et al., 1990]. PCI was also used to assess the gait efficiency of a single spinal cord injured subject ambulating with the R.G.O and F.E.S [Isakov et al., 1992]. The mean PCI found with this study was 2.55 beats/metre.

In order to improve the energy cost of ambulation, a modification of the original R.G.O has become available [Motloch, 1992]. In this system (Known as the Isocentric R.G.O). the Bowden cables used to couple hip extension to contralateral hip flexion are replaced by a centrally pivoting bar and tie rod arrangement. It is claimed that this system is more efficient. To see if this claim is justified a study which examined the energy cost of ambulation using the reciprocating gait Orthosis and the modified Isocentric R.G.O. in paraplegic spinal cord injured subjects was carried out by [Winchester P.K. et al., 1993].

The mean PCI for ambulation with the RGO was 3.61 ± 0.66 beats/metre compared to 2.56 ± 0.47 beats/metre with the Isocentric R.G.O.

Comparing the studies of [Isakov et al., 1992] and [Winchester P.K., 993] clearly shows that the mean PCI for the first was much better than that of the second. This improvement could be due to the length of training. While Isakov's subjects had been ambulating with the R.G.O for two years, Winchester reported an average training time of approximately 35 ± 7.5 hours.

Another approach to the energy expenditure problem was the use of what is known as Functional Electrical Stimulation (F.E.S). That is electrically stimulating the patients own muscles to carry some of the burden carried by the Orthosis or in some cases to completely do all the work while the Orthosis is a secondary safety system to be used if necessary.

If all the muscles in the legs of a paraplegic were to be of normal strength they would be able to walk. This is the basis for functional electrical stimulation (F.E.S). The main physiological problems are muscle atrophy and muscle fatigue. The main technical problems are providing adequate electrical stimulation, developing sensitive control systems and protecting the patient in the event of system or power failure [Michael W. W., 1988].

The combination of F.E.S and the Orthosis is known as a Hybrid system. The R.G.O generation II system [Solomon M. et al, 1989] considers the advantages of such systems. It is claimed that the R.G.O generation II came about to overcome four main problems encountered with the existing model as discussed in the introduction. Testing on six Patients demonstrated an average of 30% reduction in energy expenditure at a walking speed of 0.05 m/s and a 15% reduction at 0.37 m/s. Improved mobility and better balance on inclines and unassisted rising in all patients. Walking range was increased from an average of 100m to an average of 800m [Solomonow M. et al, 1989].

Unfortunately, the higher the speed the less is the benefit gained from using F.E.S. [Hirokawa et al, 1990] showed that at speeds over 0.37 m/s walking with the R.G.O. on its own consumes less energy than when F.E.S is used with R.G.O.

[Sykes et al., 1996] carried out an evaluation of the RGO and hybrid system while being used in the home environment. Five adult subjects participated in the study. Three methods were tried for the measurement of steps taken in the RGO and hybrid system. Firstly a commercial digital Pedometer was used. This Pedometer records the acceleration and deceleration movements in one direction. This approach was first adopted by [Bessey et al, 1988] who successfully used a Pedometer to measure the step score of elderly Patients over the course of a week thus measuring their level of walking activity. However this approach was rejected by this study because it required operation by the patient.

The second method was to use a magnetic switch counter. The main problem with this method was the bulk required at the hip joint in order to get a sufficient lever arm and range of movement. The device tended to catch clothes and was frequently pulled off. It also obstructed the hip joint release mechanism on the RGO and was abandoned.

Finally, a contact switch was used which was combined with an electronic counter. This was the most reliable system. The results were not encouraging. This was because of the problems encountered. Firstly it proved difficult to find a reliable measurement tool. Compliance with the RGO and hybrid system was poor and there was no apparent increase in RGO use following the supply of electrical stimulation. No improvement in efficiency of ambulation was found when subjects used the hybrid system [Sykes et al., 1996].

Other published reports on the use of RGO have relied on subjective information recalled by the patient. [Guidars et al, 1993] assessed RGO use in children with myelodysplasia by interviewing the patient and family. Mean daily usage of the RGO was 6.9 hours. Adult patients were not included in the study. [Sykes et al, 1995] used a questionnaire format. Median RGO use by patients aged under eighteen was 3 hours/day compared with 2 hours/day by adult patients. Median weekly usage was 5 days by patients aged under 18 and 3.5 days by adult patient. Self-reporting behaviour has been used successfully in other studies [Stephens et al. 1983].

In 1984 at Wright State University, Dayton Ohio, U.S.A, Roy Douglas and Jerrold Petrofsky combined the L.S.U Reciprocating Gait Orthosis with functional electrical stimulation in a hybrid system [Petrofsky J.S., 1985]. The R.G.O provides the patient with support should the F.E.S system fail. With F.E.S many paralyzed muscles had to be stimulated and, as [Patrick J.H., 1986] points out, the fatigue caused by continuous stimulation to keep the patient upright and the possibility of this causing damage as well were also limiting factors to walking with F.E.S only. In Oswestry, [Watkin E.M. et al, 1987] reported on four adults using the Para Walker combined with F.E.S. At the Walk Fund Spinal Unit, as part of a research project, four paraplegics were fitted with the L.S.U Reciprocating Gait Orthosis and F.E.S walking. Testing of patients using a hybrid system showed a considerably lower use of oxygen and energy for walking. This has been proved by testing the speeds and heart rates of children using their Para Walker combined with F.E.S. and comparing it with the speeds and heart rates of the same children using their previous Orthoses. For the patients tested there was a mean increase in speed of 87.3% and a mean decrease in heart of 10 beats per minute.

The energy consumption is also effected by the status of the knee. The effect of bending or not bending the knee while walking is very significant. Biomechanical studies have shown that having to walk with fixed extended knees is a major consumer of energy in R.G.O. walking. [Ralston H.J., 1965] investigated the effect of restricting knee movement in normal subjects during walking. He observed an increase of 18% in energy consumption when they walked with one knee held straight. When both knees were fixed, he found that the energy consumption of walking was increased by an average of 45%.

2.3 Orthotic Control Systems

Power assisted walking can reduce the patient's energy expenditure however this introduces the problem of control.

The rules in applying a control system to what is called a Hybrid Assistive Systems (HAS) are discussed by [Tomovic R., Popovic D., 1990]. The term HAS relates to numerous different combination of bracing techniques. Common to all HAS designs is the man machine interaction in order to improve the gait performance. Three rules were discussed. Rule 1, the pressure difference between the two feet must change the sign within walking cycle, Rule 2, the prospective leg in the "swing" phase must not be completely off the ground. It can be dragged maintaining the contact to the ground, or touch the ground intermittently. Rule 3 states that the hip flexion terminal angle must cross the vertical line (through the hip joint) if the forward body displacement has to take place [Tomovic R., Popovic D., 1990]. Rule 2 seems to contradict itself. Not lifting the leg off the ground introduces great difficulty in walking special over a carpet or on an incline. Also the energy required to drag the leg will be much more than that required to lift the leg. However rule 2 gives the patient more confidence in walking if his legs does not clear the ground. This is because the patient would feel he is less likely to fall if the swing leg is dragged rather than lifted. Further training could eliminate this problem.

The AMOL project describes the use of 60W DC motors for external power. It has four actuators, two at the hips and two at the knees with one degree of freedom. It also

considers two ways of controlling the powered Orthosis. The first is entirely automatic and includes propulsion and stabilization. In this case the patient may feel foreign to the device and ill at ease with it. The second case is for the patient to take care of the stability factor by himself while propulsion and regulation of gait are provided by the artificial system. The control system used has automatic feedback to limit the torque. It also allows the patient to intervene in the control program using simple switches. The patient can control, Start, Standing up, Sitting down, Speed, Stop both normal and emergency. However the paper does not give any details of the type of controller used or show any results of the control system performance. [Rabischong P., Bel J.P., Hill J., 1975].

A method for improving the response of the powered Orthosis during a stationary level walk was described by H. Miyamoto. A corresponding signal based on the error of the output from the reference gait pattern was calculated, The input signal was adjusted to reduce the error. It has been verified that this method is effective for a stationary level walk [Miyamoto H., 1983].

All the movements of the Orthosis are controlled by microcomputers. Again two control systems are considered. Autonomous control uses the measurement system of the centre of gravity displacement where the gait is entirely controlled by the microcomputer. The second method is an interactive control using the crutch floor contact plate. With the latter method the patient can transmit some commands to the powered Orthosis and it is not put entirely under the control of the computer. The controller used was described only as a following controller but no further details were given. However typical controllers

that can be used as following controllers are PID and Pole Placement controllers. [Miyamoto H., 1985].

[Hill J.W., 1981] considers a prototype control system which has appropriate sensors for measuring the electrical power input, the intermediate hydraulic power, and the power supplied to each of the four leg joints. An efficient solution to the hydraulic power source can be obtained by letting the pressure at the output of the pump fluctuate according to the demand, Thus, if the pump is driven at a constant speed corresponding to the joint velocity we desire at a particular instant, only the pressure required to move the joint will be seen at the pump.

It is important to highlight that there was no detailed information for the low level controllers used in previous Orthotic devices. Furthermore control system specifications and evaluations are also very poor. This has also been the motivation for this dissertation.

In addition, non-of the papers reviewed, which consider the control problem, discuss the issue of Modelling. There are no details on how they derived the model for the control systems. In this thesis the Modelling of an RGO is considered and the use of least squares identification method is investigated.

2.4 Pole Placement Controller Background

Introducing the concept of power walking introduces the concept of control. Many control systems are based on deriving models for the system to be controlled. A basic issue in the control of linear time-invariant systems is the investigation of the effect of modelling errors on the performance of the control system. Typical modelling errors resulting from neglecting fast parasitic modes are considered by [Hassan K.K., 1981]. A suitable approach suggested by the author is to employ singular perturbation analysis. Fast parastic modes arise from small inductance, capacitance and inertia etc. In practice the parastic elements may be neglected. This is equivalent to having a reduced order model. If the neglected components are sufficiently small then the actual performance is arbitrarily close to the one predicted by the design model. Then it is reasonable to say that the control strategy is robust with respect to these kinds of modelling errors. [Hassan K.K., 1981].

A high order model will give a high order regulator. To obtain a simple regulator it is therefore important to base the design on a simplified model. It is then of interest to investigate the sensitivity of the closed loop system to variations in the model used for the design. Astrom considers a linear time invariant single output and gives inequality for condition of stability. [Astrom K.J., 1980].

Nowadays due to the availability of powerful and cheap computers, virtually any conceivable control algorithm can be implemented. In theory we could sprinkle poles and zeros like salt and pepper over the complex plane if this should turn out to be desirable [Garcia C.E., 1982]. The difficulty in tuning these more complex controllers does not present any practical difficulties because of the widespread availability of powerful CAD packages and commercial tuning aids which can perform the tuning in a semi-automatic or fully automatic mode.

In many control applications, it is not unusual that several specifications such as stability margins, servo response, noise rejection are needed. These are not fully compatible with each other. When such situations occur the designer has to perform the delicate task of balancing depending on what is considered to be a priority. Because there is no general relationship between these specifications, there is no easy way of designing the controller, which can give some kind of trade-off between these contradicting requirements. The usual approach is to resort to 'trial and error' methods.

The pole assignment controller has a strong appeal to control practitioners because of its close relationship to the classical design approach [Mustafa M.M., 1989]. Another advantage with pole assignment controllers is that they can easily cope with unknown or variable time delay and non-minimum phase systems, which occur quite commonly in sampled data systems. They also have the advantage that for any given set of closed loop poles the computation is a straightforward task of solving a set of linear equations. The

stability margin is also dependent on the chosen closed loop poles location. It is not true to think that locating the poles at the origin will always result in the greatest stability margin. For an open loop stable system, infinite stability margin is obtained when the closed loop poles are at the open loop location, which effectively causes the loop to be opened. [Mustafa M.M., 1989].

The difficulty in choosing suitable closed loop poles location is a trade-off between stability robustness and input output behaviour and can be overcome using the fact that two different ways of implementing the same closed loop system can have different Nyquist curves (i.e. different robustness properties). Therefore this problem can be partly solved by obtaining a parameterization of the class of all controllers which can give the same closed loop input and output behaviour. In normal practice the controller with minimal order is chosen. In this thesis it is shown in theory and practice that the freedom available in using high order pole assignment controllers allows the designer to meet the specified closed loop behaviour such as tracking and noise rejection.

The use of high order controllers to improve the robustness and performance of digital pole-assignment controllers for a single input and single output systems is explored as the control system to be used in controlling the powered Orthosis. This approach enjoys a fundamental feature, which is the simplicity of the algorithm. Simplicity means the design can be carried out using basic numerical routines such as matrix inversion with a

priori known computational time, and the whole design can be fully automated, thus avoiding out any procedure involving man-machine iterative solutions.

The pole assignment method can be summarized as follows. First design a minimal order controller to assign the closed loop poles at certain location depending on the desired transient response. The order of the controller is then increased and the extra freedom available is used to obtain a more robust controller i.e. one that preserves closed loop stability for larger modelling errors. Furthermore the sensitivity of the closed loop system to model mismatch is also reduced.

There are two design methods or philosophies for adaptive pole placement controller or any control design. The explicit pole assignment self-tuner and the implicit one. For the implicit algorithm, the controller parameters are estimated directly with the help of the input output data of the system. [Bayoumi M.M., 1989]. The explicit scheme has been extensively studied and fruitful results are available. In the explicit scheme the actual system parameters or a related set of parameters are estimated. These estimates are passed on to a controller design phase where a set of linear simultaneous algebraic equation is solved to obtain the controller parameters [Allidin A.Y., 1985]. Although in this dissertation the off-line approach is used but it may useful to highlight the online methods (implicit and explicit) because it may be of some use in future work.

In any control system usually more than one requirement is needed whether it is reduction in output variance or reduction in noise. The relative merits and disadvantages of pole assignment strategy are important. The standard pole assignment strategy may give rise to an output variance that is considerably greater than the minimum achievable. The solution of increasing the order of the controller gives extra degrees of freedom that can be used for optimization purposes. [Zarrop M.B. Fischer M., 1985].

CHAPTER 3

Reciprocal walking Devices and

Mechanical calculation of powered Orthosis

Definition: DHSS definition

An Orthosis is a device applied direct and externally to the patient's body with the object of supporting, correcting or compensating for an anatomical deformity or weakness, however caused. It may be applied with the additional object of assisting, allowing or restricting movement of the body.

(Orthotics principles G.K Rose 1986)

3.0 Introduction

This chapter discusses the ideal characteristics of a powered Orthosis and compares different Orthotic designs for reciprocal walking. As well as carrying out the task it was designed for, it is imperative that the device is acceptable to potential users. Acceptability is a wide concept, which depends on many factors, these include cosmetics and cost. The powered Reciprocating Gait Orthosis is a development from the conventional R.G.O.

The powered Orthosis as shown in figure (3.1) is the principal subject of this project. Within the scope of this project the objectives are as follows: to extend the ambulatory

capability beyond that provided by an unmodified RGO, implement a natural gait cycle and improve upon the dynamical control as found with other powered approaches. To this end the powered Orthosis has been constructed from the joint experience of the Orthopaedic Mechanics Research Institute (based in the school of prosthetics & Orthotics at Salford) and the Department of Electronic & Electrical Engineering. In this chapter the mechanical assembly and calculations are also discussed. The calculations indicate that the mechanical assembly with the selected motors and gears can supply the required torques.

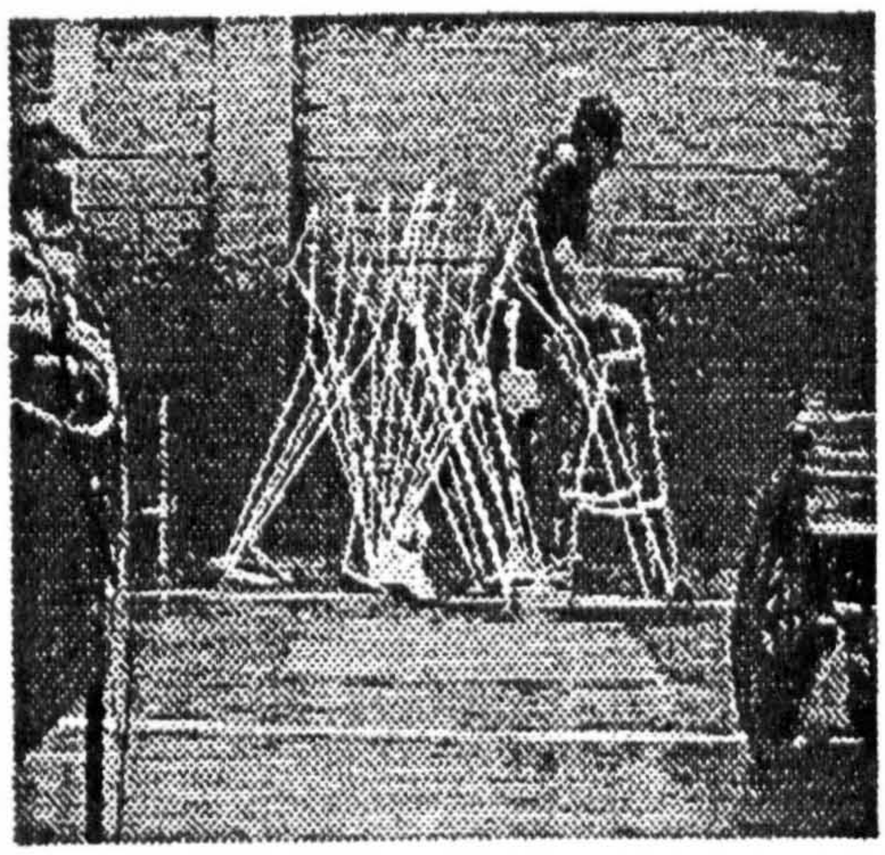

Figure 3.1 Digitally captured motion analysis of the Powered Orthosis

[Downes C.G, Hill S.L., 1994]

3.1 Ideal Characteristics of an Orthosis

Although walking is the prime function required there are factors involved which will effect the suitability of the solution for any particular patient, by considering these parameters, clinicians will better be able to select a device to match patient needs.

The way the device looks when mounted on the patient is very important for patient acceptability. Ultimately the decision whether the Orthosis is to be used or not is with the patient. If the patient rejects the device because of the way it makes him/her look then the device no matter how efficient it may be will be a non starter. Secondly it is important for the device to be socially acceptable, that is not too bulky so as to get in the way of others and more importantly not so big so it does not get through doors, lifts etc. There are additional factors these include:

3.1.1 Independence

To be of real value, walking for a paraplegic patient should be achieved completely independently. This means the patient must be able to put on and take off the complete system, transfer from sitting to standing and vice-versa, without any assistance from a helper. Other aspects of independence include problems of toiletting.

3.1.2 Energy cost

One of the main benefits expected of a reciprocal walking system is a reduction in patient energy expenditure. The degree to which this energy saving occurs will depend on the effectiveness of the system used in permitting the swing leg to be cleared from the ground.

3.1.2 Cosmesis-

Because Cosmesis is such an emotive subject it is often not considered in a suitably objective manner. It will be a compromise of a number of different factors, all of which are important. Those, which are most important, will depend on the individual patient's own attitudes. The main factors concerned in Cosmesis are:

a) The style of walking, the aim being that it should resemble normal walking as closely as possible.
b) The ability to disguise the wearing of the Orthosis, the ease with which clothes can cover the device being the important factor.
c) The clumsiness of the walking aid used in conjunction with the Orthosis.

Cosmesis must be both static and dynamic, including the elimination of noise on usage. The creaking of a long leg brace or the puff of a pneumatic valve can be

equally disturbing. At the same time it is essential to realise that desirable as Cosmesis may be it is not this that determines the acceptability of an Orthosis.

3.1.4 System Reliability

For a system to be truly practical it must have a high level of reliability so that the user is not frequently deprived of the walking function. It should also be designed so that any failure, which may occur, does not put the patient at risk of physical injury.

3.1.5 System Cost

There are no cheap options for systems, which enable the paraplegic to walk. However it is important to keep the cost as low as possible.

3.1.6 Patients acceptability

Patient acceptability includes a wide variety of factors: -

a) Comfort on sitting as well as walking.

b) Ease of toilet function.

c) Reasonable wear on clothes. Touch and close fastening.

d) Low energy usage.

e) Cosmesis.

3.2 Currently available systems

There are four fundamental approaches to the provision of reciprocal walking for high level paraplegic patients.

1) Purely Mechanical System (Unpowered Orthosis).
2) Hybrid devices comprising mechanical Orthosis with supplementary FES.
3) Purely FES system with no mechanical system.
4) Powered Orthosis.

At the present time the most widely available and the most widely used is the first system. However this system suffers from a major draw back, that is the patient's high-energy expenditure when using these devices. These devices are discussed further along in this chapter.

The hybrid system and pure FES approaches to paraplegic walking are being extensively researched. It has already been established that the hybrid approach can further improve the efficiency of walking [Watkins E.M. et al, 1987].

The fourth and final system is the same as the first system with the addition of external power. This is the subject of this thesis.

3.3 Reciprocal Walking

Because of the high-energy cost of swing through gait and the restrictions inherent in swivel walking, devices have been developed which permit patients with no control of the lower limbs to ambulate reciprocally. This is a form of walking in which one leg is placed sequentially in front of the other (i.e. normal walking). Such a method enables patients to take body weight through the stance leg, therefore providing a potential for reducing energy cost. Swing through gait effectively means that both legs are propelled forward at the same time. The hands take all the body weight. Downward force is applied to both the crutches enabling the body to be lifted. This effectively means that every step forward is similar to doing a sit up. This is a very high-energy cost and tiring process.

It is inevitable that such a system would need additional aids e.g. (crutches or walking frames) for stability and to input propulsion forces. However when mastered, the design should enable the patient to walk over a variety of surfaces including slopes and may eventually lead to the use of steps.

3.4 Clinical Considerations

Reciprocal walking systems demand the input of quite large forces from the upper limbs, which must be carefully controlled in both direction and relative timing. Therefore good upper bodies strength and co-ordination is essential. Also a reasonable degree of cardiovascular fitness and a level of intelligence which allows them to understand detailed physiotherapy instructions is needed. A good range of hip movement on both sides is an essential requirement.

3.5 Mechanics of Reciprocal Walking

Reciprocal walking includes three essential features: -

1) The 'swing leg' must be cleared from the ground.

Clearing the swing leg is achieved by tilting the body sideways or lifting on the relevant side or a combination of both of these. Downward and lateral forces are applied to one or both crutches (or other walking aid) for this purpose.

2) The 'swing leg' must pivot forwards from relative hip extension to hip flexion.

Pivoting the swing leg from relative extension to flexion. This requires a forward turning moment to be generated about the swing leg hip. This can be achieved as a result of gravitational, inertial or orthotically generated mechanism forces or a combination of these.

3) The trunk must be progressed forwards over the stance leg from hip flexion to extension.

Trunk translation (hip flexion to extension) over the stance leg occurs as a reaction to rearward forces generated in the crutches or walking aid. These may be applied unilaterally or bilaterally and require that the arm be drawn to the trunk. Usually through the action of latissimus dorsi [Rose G.K., 1986].

3.6 Existing Designs of Reciprocating Orthosis

There are two systems, which are widely used for the provisions of reciprocal walking for paraplegics, the Orlau Para Walker (H.G.O) and the Reciprocating gait Orthosis (R.G.O). Both recognise that there are a number of factors, which must be considered, and that the final design requires a compromise of these [Stallard J. et al., 1979].

Figure 3.2 the Orlau Para walker

The (H.G.O) aims for maximum efficiency of ambulating with crutches, ease of doffing and donning and transferring, and a free flowing gait style [Rose G. K., 1979, Butler and Major, 1987].

In order to achieve this the (H.G.O) consists of the following: -

1) A structure, which rigidly resists adduction abduction but which conforms for cosmetic, reasons as closely as possible to the patient.

2) Limited range of low friction flexion-extension at the hips, which can be overridden by an easily operated lock to permit a full range of flexion for sitting.

3) Easily operated fastening mechanisms for the support points, which provide limb stabilisation for the patient.

4) A high degree of mechanical safety and reliability to minimize the danger of patient injury and reduce the cost of maintenance.

5) An initial cost, which does not exceed that of conventional devices, supplied to patients for standing and limited mobility.

A particular advantage of the Para Walker is the ease with which crutches may be used- elbow crutches being the most popular and efficient. The structural basis of the design

ensures easy modification for growth or anatomical changes in the patient, a high degree of reliability, and a capacity for accommodating very large patients.

The R.G.O (Reciprocating Gait Orthosis) is a bracing system, which can give paraplegics a limited ability to walk independently. The original design in the early seventies was to help children with spina bifida and other forms of muscular dystrophy walk. The system has since been developed to also help adults with lower back spinal injuries.

The system consists of two-moulded plastic knee-ankle-foot Orthosis attached to a metal pelvic control band and upright thoracic supports, while two cables connect the reciprocating hip joints. These cables prevent both hips from flexing simultaneously, and thus support the upper body. The R.G.O consists of the following.

1) A closely conforming polypropylene Orthotic patient support structure.

2) Freely hinged metal hip joints attached to the polypropylene body brace and lower limb segments of the Orthosis.

3) Twin cables linking the two hip joints to enforce relative reciprocal flexion and extension for reciprocation during walking whilst providing stable support with the hips fully extended and both feet grounded.

4) Releasable fastenings on knee joints and the interlinking cable mechanisms at the hip to permit sitting.

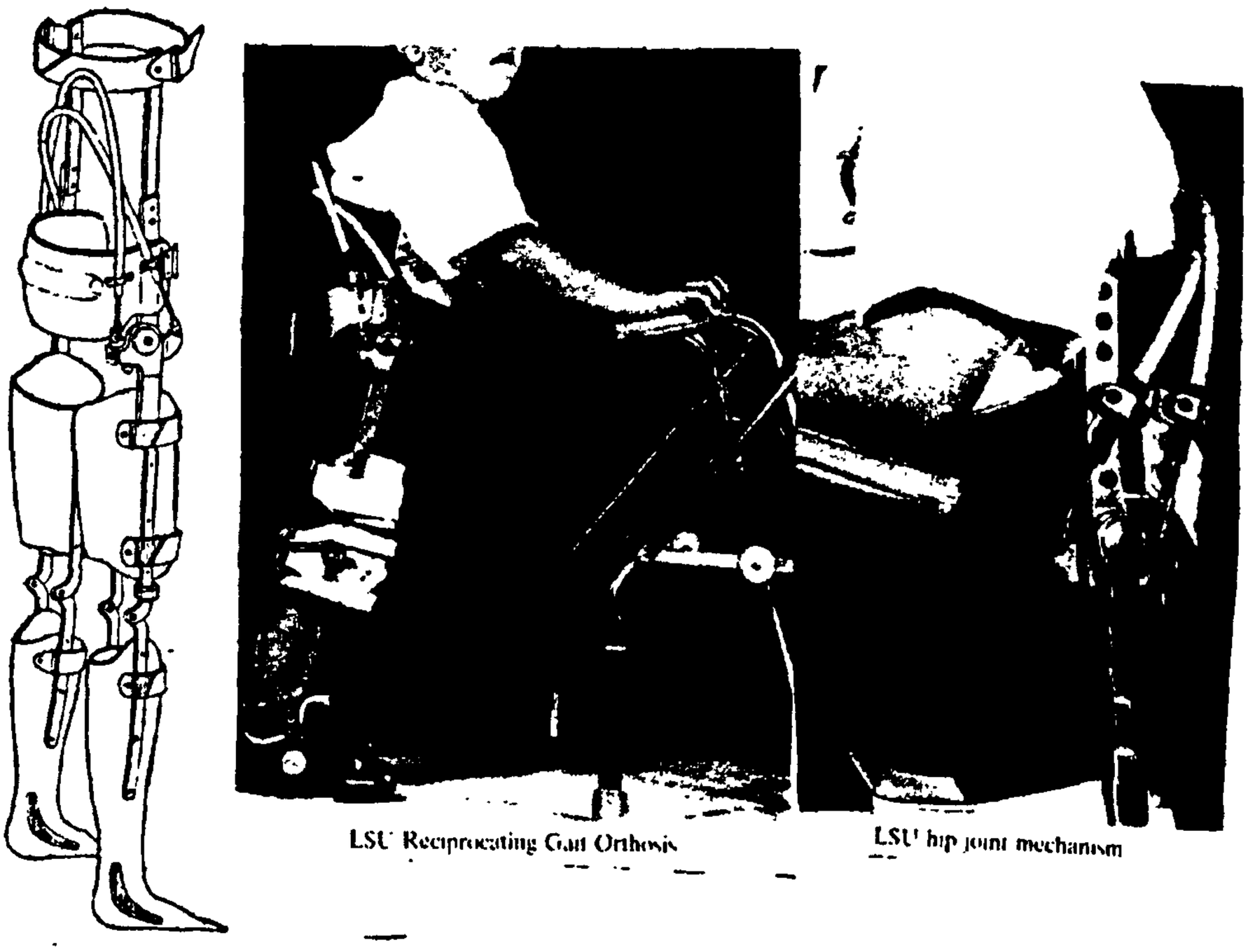

LSU Reciprocating Gait Orthosis

LSU hip joint mechanism

Figure 3.3 LSU R.G.O and Hip Joint Mechanism

3.7 Advantages [Rose G.K, 1986].

1) Low energy requirements.

2) Speed over 50% normal rate of walking.

3) Can surmount a single step of 15cm.

4) Can be used on all surfaces, for example roads and fields.

5) Very acceptable dynamic cosmetic walking pattern.

6) Independent doffs and don and transfer from sitting to walking.

7) Available for children from 4 years onwards and adults.

3.8 Disadvantages [Rose G.K., 1986].

1) Crutches or some other form of walking aid are needed.

2) Requires a fair amount of upper body strength.

3) Requires good co-ordination from the patients.

3.9 Powered Orthosis

So far two designs have been discussed which are capable of producing reciprocal walking. However a more advanced design is now being developed at the University of Salford.

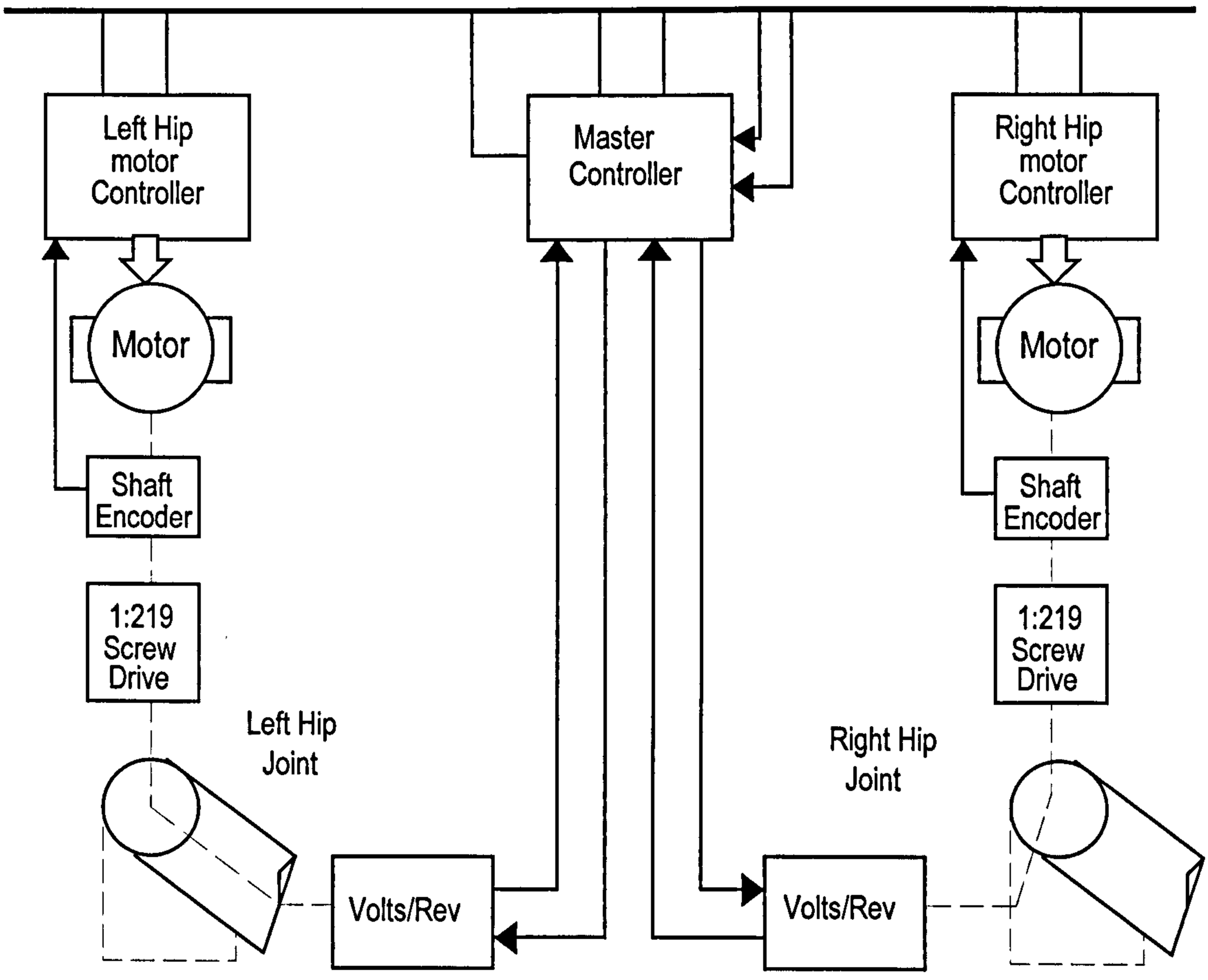

Figure 3.4 Powered Orthosis System Architecture [Downes C.G. Hill S.L., 1994]

3.10 The Powered Hip Walking Orthosis

The purpose of this design was to extend the walking capability of paraplegics beyond that presently provided through the use of reciprocating Orthosis discussed earlier, (LSU R.G.O., ORLAU Para Walker).

The devices discussed earlier do enable people who are paralysed below the waist to walk upright in a reciprocating fashion over a variety of surfaces including soft grass. Tests show that even on hard level ground the walking speeds provided by these devices was 1/8 to 1/4 of normal walking speed [Yngve D.A., 1984]. Furthermore many adult patients become excessively fatigued after walking only 100 yards.

By using functional electrical stimulation (F.E.S) of the quadriceps and hamstring muscles in conjunction with R. G. O., a few paraplegics can achieve a continuous walking speed of 1/3 to 1/2 of normal cadence over a distance of up to one mile. However paraplegics with higher spinal lesions or weak upper body strength find it extremely difficult to use the R.G.O effectively [Yngve D.A, 1984]).

Another disadvantage of using F.E.S is that it does not work on muscles with damaged secondary motorneurones. Therefore the answer for all these problems is to add an external power to the hip joints of the R.G .O to help in the forward propelling of the Orthosis. Adding external power to hip joints of the R.G.O allows a larger number of

paraplegics to achieve reciprocating gait at near normal speeds, with significantly less fatigue.

The present design allows future work to make use of the lockable/unlockable knee joint recently designed at Salford. This should allow paraplegics to achieve a more normal gait pattern by knee bending during the swing phase. As a result the height by which the hip will have to be raised to avoid stubbing the toe on the ground during swing through will be reduced therefore achieving a further reduction in energy expenditure.

3.11 General Design Specification

Previous publications reporting attempts to power lower limb Orthoses have been few in number [Miyamoto H., 1983, 1985, Rabischong P. et al, 1975]. All proved to be impractical as they were attempting to provide all the power needed for human mobility. However the projects aim is not to provide all the power required for human mobility, but rather to assist the efforts of existing upper body musculature. This made it possible to minimise the size and weight of components in the external drive unit.

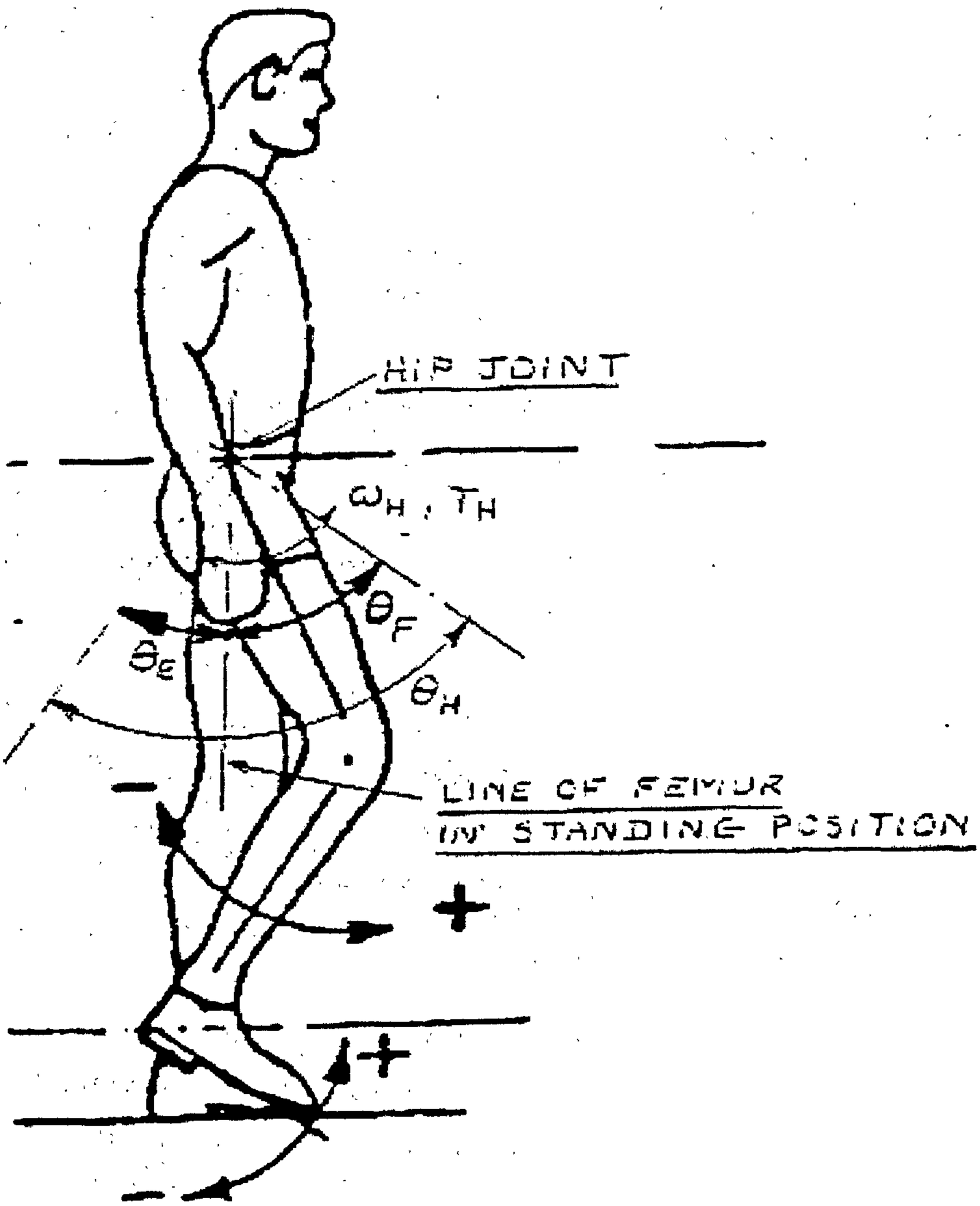

Figure 3.5 angles of the hip

To achieve anything like a normal pattern of gait, the powered Orthosis should satisfy the following requirements table (3.1) (with reference to fig 3.5).

Requirement	Variable	Value
1) Maximum angular movement of hip joint In extension, measured from neutral	θ_E	−15°
2) Maximum angular movement of hip joint In flexion, measured from neutral position	θ_F	+20°
3) Overall maximum angular movement of hip Joint.	θ_H	35°
4) Maximum angular velocity of hip (Representing range of approx. ¾ to normal walking speed where the peak occurs at mid stance and mid swing).	ω_H	+1.3 to 1.8 rad/sec (11-16 rpm)
5) Maximum hip torque in either direction (In normal walking this occurs at heel strike with another lower peak at toe	T_H	40-85 Nm

Table 3.1 Parameters for Normal Walking

[Paul J., 1975]

In addition the angular acceleration of the hip joint during the early part of the swing phase must be sufficient to create an inertia moment which flexes the knee so that the toe just clears the ground at the mid point of swing. This is normally about 25 rad/sec^2. During the latter part of the swing phase, the rate of hip flexion should decelerate sufficiently to bring the knee into near full extension by the time the heel strike (about 15 rad/sec^2).

3.12 General Description of Motor Drive Assembly

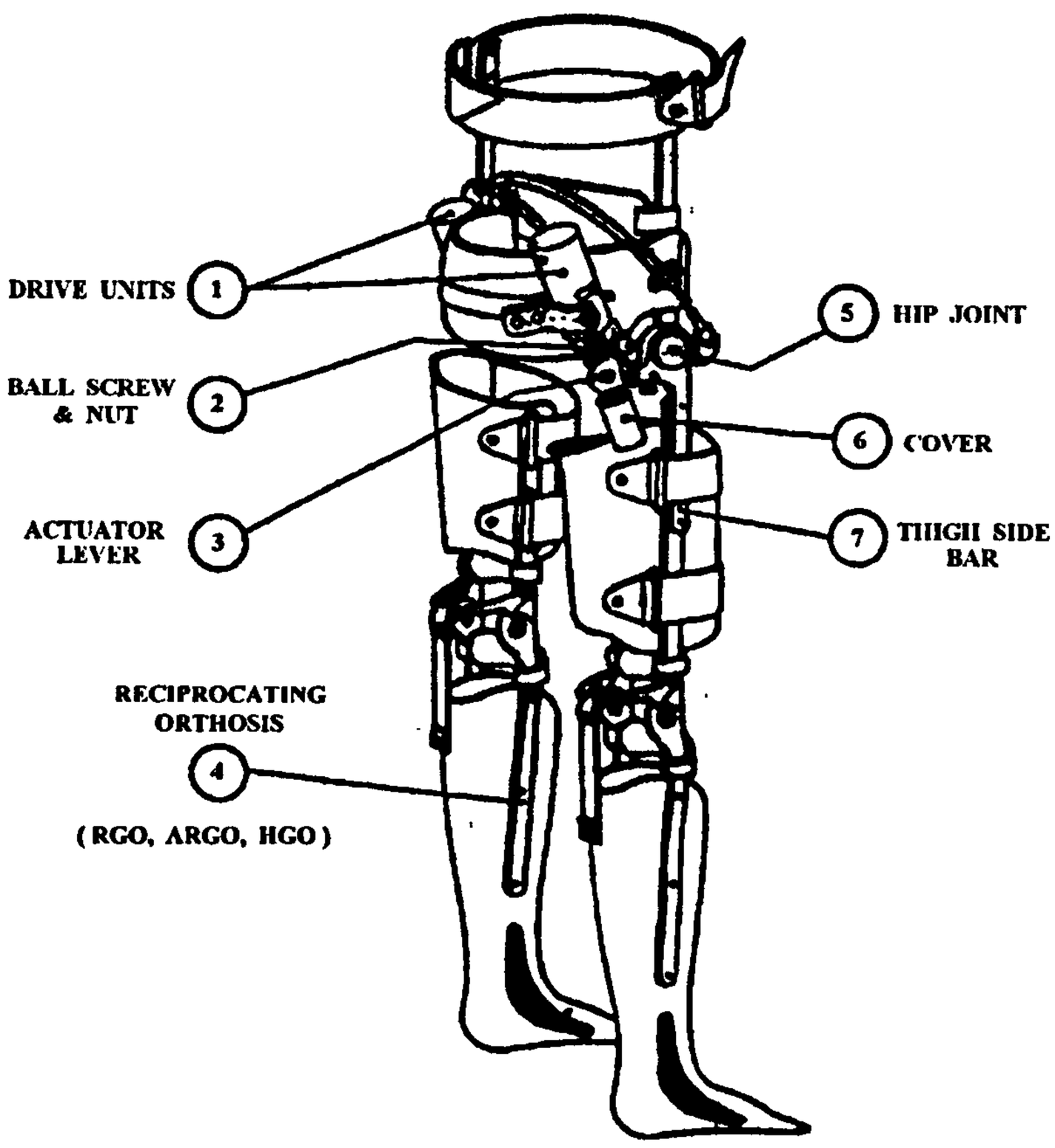

Figure 3.6 Diagram of the Powered Orthosis

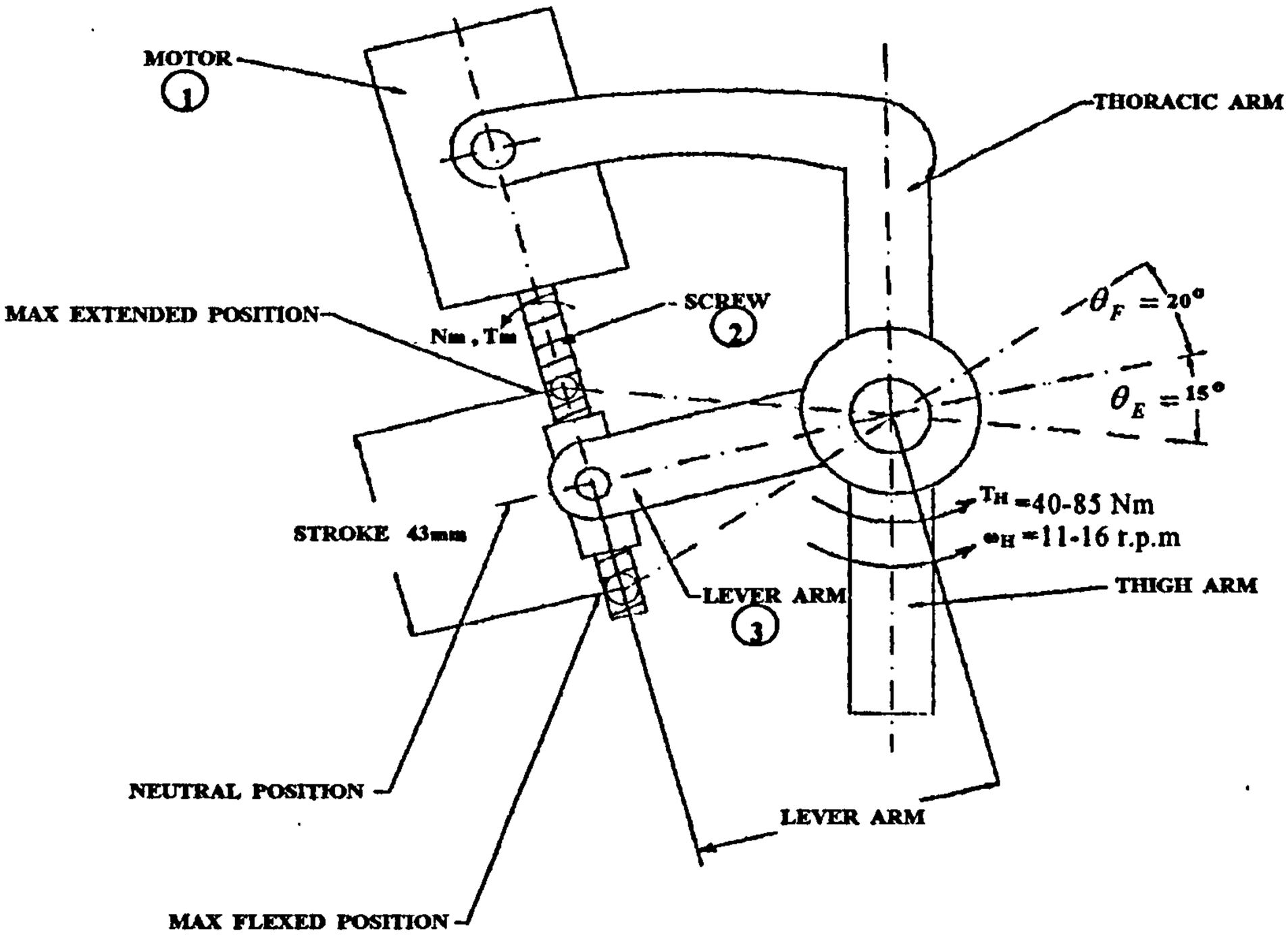

Figure 3.7 Mechanics of drive actuator system

Reference will be made to figures (3.6) and (3.7) in order to fully describe the powered Orthosis. Currently power is supplied by a power supply through a Maxon controller [Chapter 4.2], which in turn sends a P.W.M signal to the motor. However in the final design it is envisaged that NiCad batteries will be used to supply the power needed. The motor is contained within the cover of a drive unit (1), which is mounted on the sacral band of a reciprocating gate Orthosis (R.G.O). The motor actuates a lever (3) attached to the coupling at the hip joint (5) by means of a ball screw and nut arrangements (2). When the hip joint latch plunger is set in its locked position, the motor will also cause the high sidebars of the Orthosis (7) to flex or extend the hip joint, thereby assisting walking. However, disengagement of this

plunger allows the hip to rotate freely so that the user can sit down whilst still wearing the Orthosis. During walking, rotation of the motor and screw are stopped and reversed at each end of the actuator stroke by electronic control.

The motor produces a rotational torque, which is converted to a translation force by the ball screw mechanism and that is converted to a rotational motion via a lever attached directly to the hip (fig 3.7)

3.13 Coupling between the Orthosis and the Motor

The motor (EC/040/70/38) has a maximum no load speed of 4450 rpm. Therefore, the MECHANICAL RATIO (MR) required between the motor and the hip joint. Knowing that the operating speed is 4450 r.p.m. and the required speed at the hip is 16 r.p.m (table 3.1) then the following is true.

$$MR = 4450/16 = 278$$

Therefore a reduction of 278 will be required if the desired speed is to be achieved. By appropriate choice of the lead of the ball screw and the length of the actuator lever arm, it was considered feasible to achieve this mechanical ratio without using a gearbox. This was desirable since a gearbox would add considerable bulk, weight and complexity to the Orthosis. However, it was necessary to check whether existing commercial ball screws were capable of withstanding the resulting torque. Axial loads and high rotational speeds.

a) Speed Limit of Ball Screw Mechanism

Several ball screw mechanisms were investigated and it was decided to use an SKFSH ball screw of 10mm nominal diameter with 2mm thread. The speed capability for this screw is defined by the number of revolutions per minute (N) multiplied by the nominal diameter of the screw (Dn) such that:

$$N \times Dn = 60000 \quad \text{[J. Edwards, 1993]}$$

Therefore, the maximum allowable screw speed is:

$$N. = 60000/10 = 6000 \text{ r.p.m.}$$

Hence, the SKFSH screw is easily capable of handling the 4450 r.p.m. input speed of the motor. However considering the motor will be running at speeds up to 4450 r.p.m. This seems to be to close to the speed capability of the screw. In other words the safety factor allowed is too low.

b) Axial Force Delivered by Ball Screw (F) to Lever Arm

The maximum continuous dynamic torque developed by the motor is:

$$Tm = 0.23\ Nm$$

For an SKFSH Ball Screw, the relationship between input torque and axial force at the nut is given by:

$$Tm = F.S/2000\pi\rho P \qquad \text{equation 3.1}$$

Where Tm = Torque on screw

F = axial force on nut

S = thread of screw

ρP = Practical(direct efficiency =Eρ100)

E = % of theoretical direct efficiency

$$\rho = \frac{1}{1 + \frac{K.Dn}{s}}$$

Assuming S = 2mm Dn = 10 K(for SKFSH Screws) = 0.02 & E = 0.875 for a new screw

$$\rho = \frac{1}{1 + \frac{0.02 * 10}{2}} = 0.91$$

$$\rho = \frac{0.875}{100} * 0.91 = 0.975\%$$

From equation 3.1

$$F = \frac{Tm * 2000 * \pi * 0.795}{S}$$

$$= \frac{0.23 * 2000 * \pi * 0.795}{2}$$

Therefore Axial Force F = 574.5N

c) Buckling Strength of Ball Screw

Given the actual maximum axial load on the screw, we need to determine whether a screw of only 10mm diameter can withstand this load without buckling.

The maximum compression load (F) on the screw with a safety factor of 3 is given by:

$$F = \frac{34000 * b * do^4}{L^2} \qquad \text{equation 3.2}$$

Where

do = root dia of Screw shaft (mm) 8.3mm.

L = distance between the nut and the more distance bearing (mm) 150mm.

b = Screw support factor . Because the screw is supported at both ends b=1, This effectively means that regardless of the ball screw position, the screw remains evenly

supported. That is, the likely hood of the screw buckling is the same wherever the ball screw arrangement is.

Calculating equation 3.2 yields the maximum allowable value of F.

$$F = 7171N$$

Therefore the buckling strength of the screw is well within the loading with an effective safety factor of

$$7171/574.5 = 41$$

d) Maximum Torque delivered to hip by drive unit (TH)

Given an axial force of 574.5N on the end of the lever, the torque delivered at the hip joint varies with the radius of the lever arm according to the following table.

Lever Radius –R(mm)	Hip Torque – T_H (Nm)
50	31.2
60	37.4
70	43.7
80	49.9
100	62.4

Table 3.2 Summary of Torques corresponding to lever radius

To satisfy the design requirements whilst keeping the length of the lever arm as short as possible, it was decided to use a lever radius of 70mm, which delivers a maximum torque at the hip of 43.7 Nm. This torque is adequate (table 3.1).

e) Maximum Angular Velocity of hip joint

For a lever radius of 70mm,the stroke of the nut required to move the hip through an angle of 35 is 43mm (determined by geometry). At a maximum motor speed of 4450 rpm the time required to travel this stroke is:

Time=70*60/2*4450 =0.47

Max velocity at hip = 35*2pi/0.47*360 = 1.3 rad/sec

This satisfies the minimum speed requirement of the design specification table (3.1)

CHAPTER 4

Evaluation and Modelling of the Motor Driver Unit

And Legs

4.0 INTRODUCTION

In this chapter the selection of the motor and drive unit are discussed. Evaluation of these components is carried out and a conclusion of their suitability in this project was reached. Also simple mathematical models for the motor and driver and the leg of the Orthosis are derived. The motor selected was from a range of electronically commutated brushless (EC) motors based on the size and power capability of the motor.

As the motor is electronically commutated, a suitable motor driver is needed to provide control of speed. A 4-quadrant driver was chosen. It was important to select a 4-quadrant driver as it would be required not only to control speed in both directions but also to be capable of providing a holding torque at zero speed.

The driver unit, which was selected, worked as a PI speed controller. However the values of the integral and proportional gains were unknown since the manufacturers would not disclose this information. Deriving a theoretical model meant that these values must be estimated. A model for the motor and driver unit with unknown integral and proportional gains was worked out. Different values for these gains were tried to match Matlab

simulations to experimental data. That is for the same input the practical behaviour and the simulated behaviour were compared for different values of the integral and proportional gains. Then the same model was extended to include a load in the form of a gearbox.

Another unknown parameter was the amount of friction in one leg. This was also estimated using Matlab simulations. One leg was pulled to one side and released to freely swing till it came to a stop (i.e. like a pendulum). There was no external power applied. The behaviour was captured using Matlab and again parameters were varied till the Matlab simulation matched the practical data.

The motor speed torque characteristics were investigated and corresponding graphs plotted. As the motor can only be run with the motor driver unit the results shown are for both the motor and driver unit. One end of the motor shaft was connected to a 50:1 gearbox and the output shaft of the gearbox was connected to a dynamometer, where an electrical resistance was applied. The other end of the motor had a tachometer mounted so the speed can be monitored and graphs of the torque, speed and current are drawn. This experiment was carried out for three separate reference voltages and all results analysed. The Maxon controller proved to be a very good speed controller and capable of holding torque at zero speed.

4.1 Selecting the Maxon Motor

The motor chosen was selected from a new range of electronically commutated motors that use rare earth permanent magnets. These produce higher magnetic flux densities than conventional permanent magnet DC motors and therefore provide a higher power output in a more compact device.

The size of the motor is important because of the weight factor. It is desirable to have the Orthosis as light as possible for practical purposes and to save power. According to the Maxon catalogue the EC motor used (EC04007038EAA200A) has similar characteristics as a permanent magnet DC motor and according to the manufacturers recommendations the mathematical equations which describe the permanent magnet DC motor can be used to describe the Maxon motor.

The use of electronic commutation requires additional electronics to be incorporated into the motor driver, however the absence of brushes in the motor will lead to an extended motor life which is more desirable in this particular application. The present motor can produce up to 100watts peak power output into the load with 80 percent efficiency, whilst producing in excess of 0.305 Nm of peak stall torque at the peak continuous current (±10 amps). However the maximum continuous power dissipation within the motor is limited to 20 watts at room temperature, hence limiting the maximum current gives a maximum continuous torque of 0.230 Nm at the motor or 40.3 Nm at the hip. This value is consistent with the values calculated in chapter 3. They indicate that in order to achieve normal walking, the system must be capable of delivering torques at the hip between 40-

85 Nm. The calculations show that the system torque capability is close to the minimum requirement as indicated in table (3.1) in chapter 3.

In brushless motors it is usually most practical to provide a stator structure as shown in figure (4.1b) where the windings are placed in an external, slotted stator. The rotor consists of the shaft and a hub assembly with a magnet structure. The brushless motor has the active conductors in slots in the outside stator. The removal of heat produced in the active windings is easier in the brushless motor since the thermal path to the environment is shorter and the permanent magnet rotor does not contribute any heating. The result is that the brushless motor is a more stable mechanical device from a thermal point of view

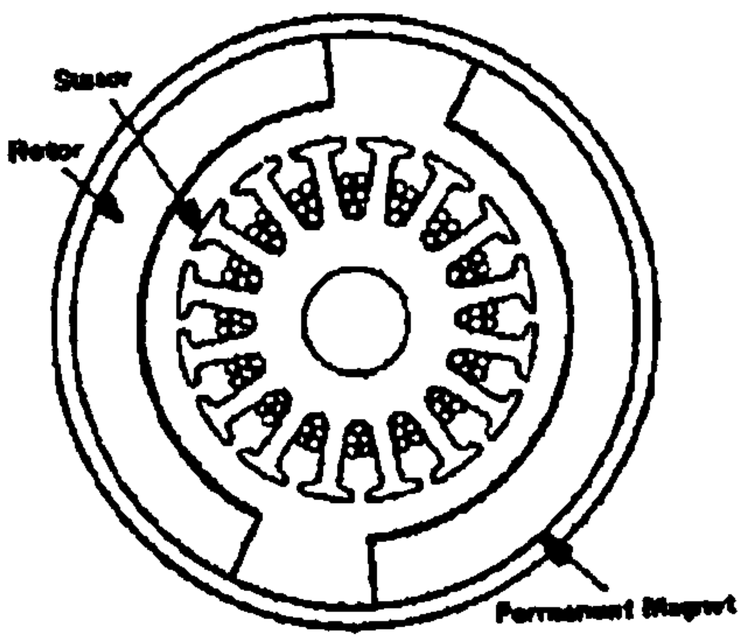

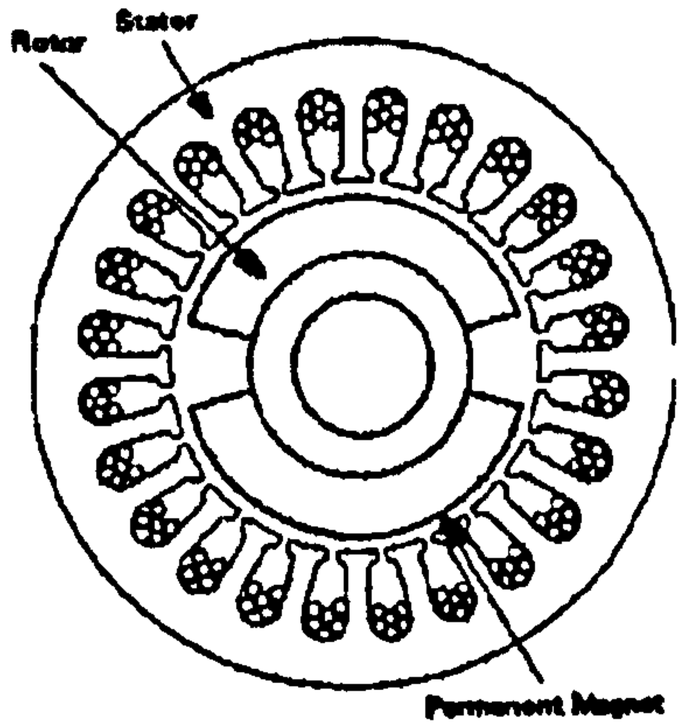

Figure 4.1a cut-away view of DC motor **Figure 4.1b A cut-away view of brushless motor**

[Dc Motors, Speed Controls, Servo Systems, 1980]

The brushless motor system is shown in figure (4.2). There are 4 transistors, and a shaft position encoder. The latter generates logic signals, which control the commutation of the windings. There are many different commutation configurations. One of the simplest practical brushless motor circuits is shown in figure (4.3)

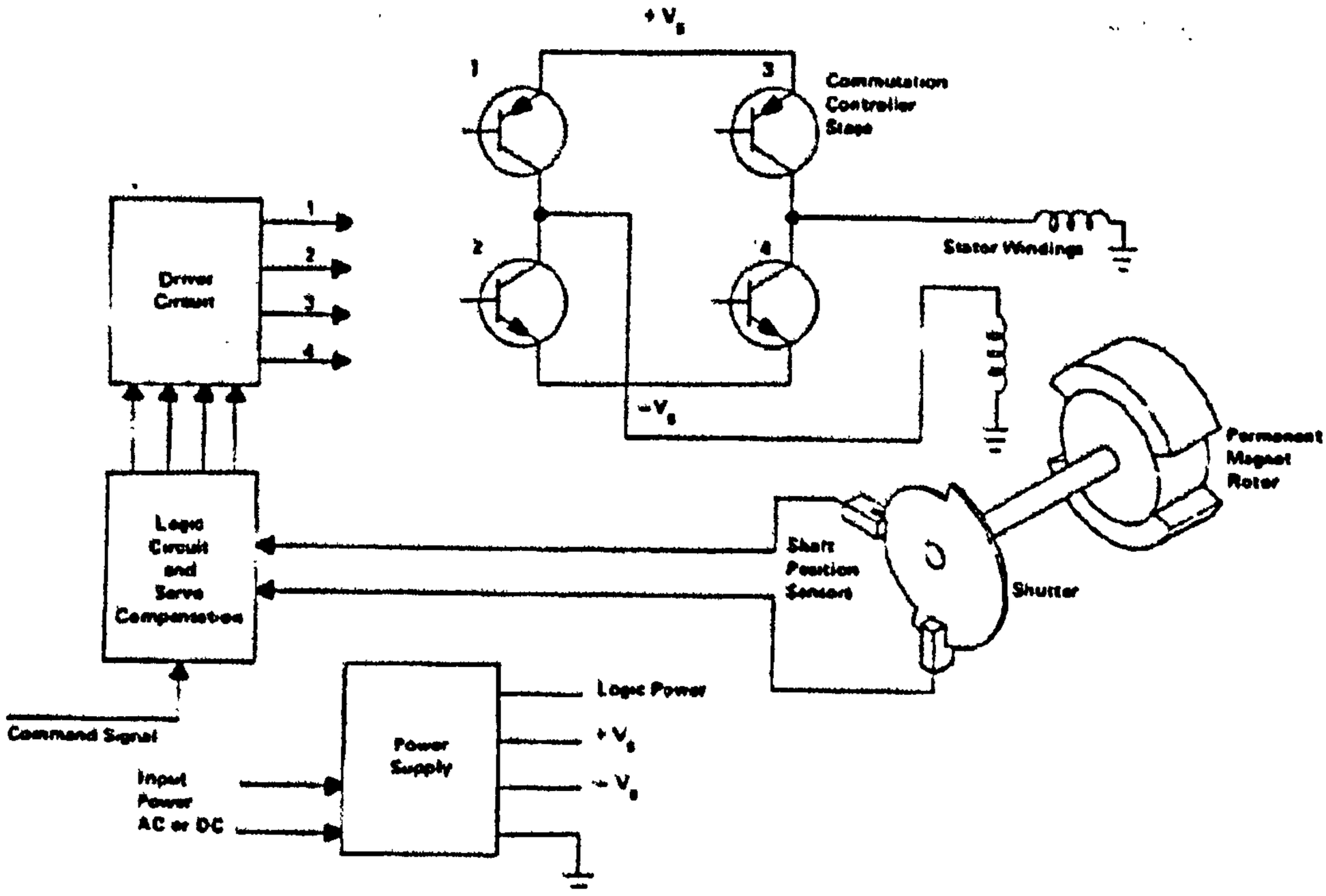

Figure 4.2 Essential parts of a brushless motor

[Dc Motors, Speed Controls, Servo Systems, 1980]

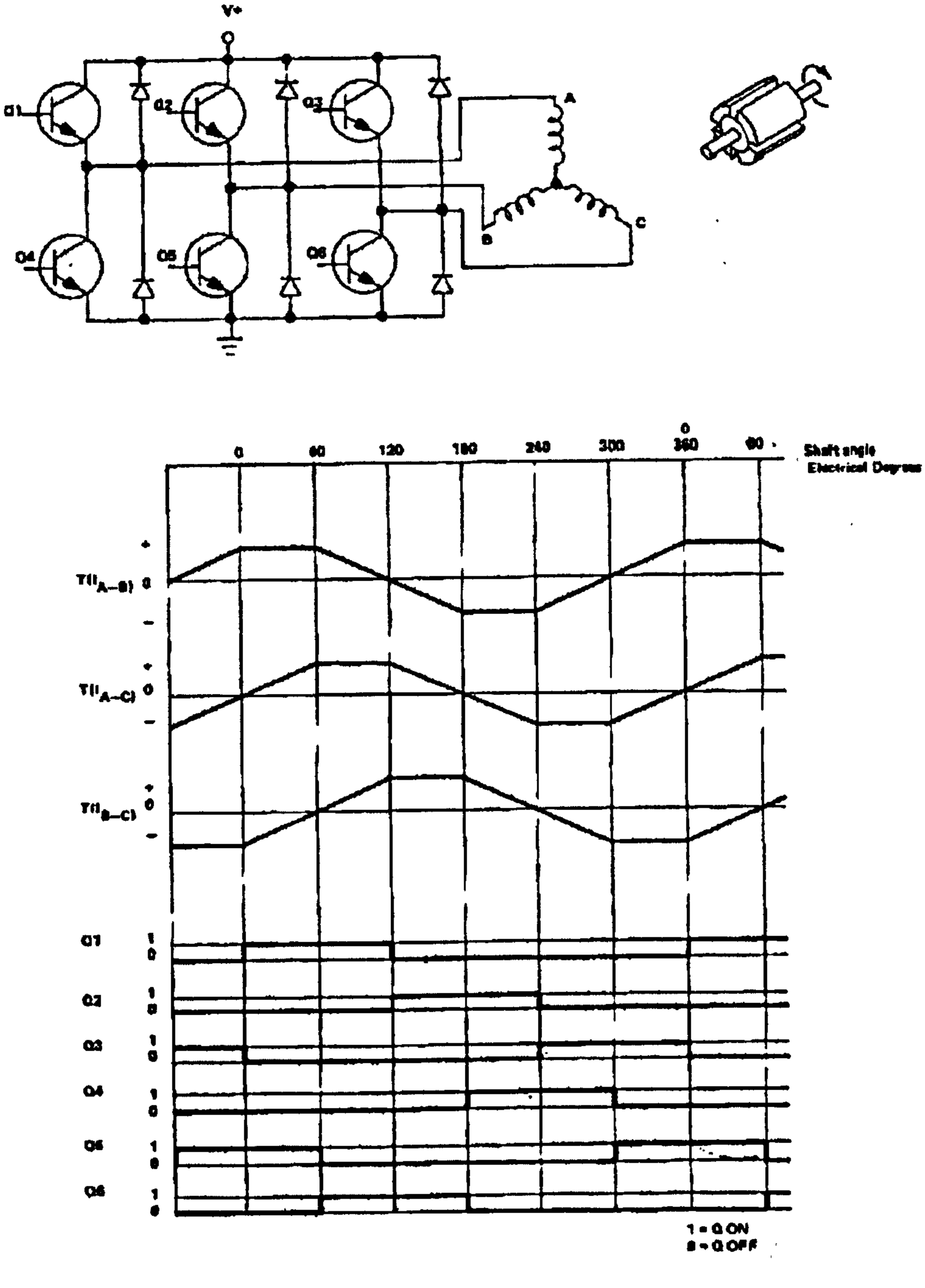

Figure 4.3 Full wave brushless motor controller

[Dc Motors, Speed Controls, Servo Systems, 1980]

Figure (4.3) shows full-wave brushless motor system. The winding configuration is based on a "star" connection stator arrangement where each winding is oriented 120° from the other. The six transistors are connected to the end points of each stator leg, and thus form a three-phase full-wave motor control. The conduction is always continuous in one leg when the other is being commutated. We can see that when Q1 is energized between 0 and 60°, Q5 is also conducting, and current is thus flowing from point A to point B. In the next sequence $(60-120^{\circ})$ Q6 is energized and the current will then flow from point A to point C. In the meantime the current through leg B declines to zero by conduction through D2. The conduction angle per phase is 120°.

4.1.1 Speed Control Using P.W.M

Pulse-width or pulse-frequency control scheme is well suited for control of voltage and current to a brushless motor. A circuit diagram of an "H" type PWM amplifier is shown in figure (4.4). The transistors of the circuit in figure (4.4) can be switched in various sequences to provide the desired voltage polarity. There are two common modes the bipolar and unipolar methods. The bipolar drive is characterized by the fact that the transistors are turned on in pairs. When we want a positive current we turn on both Q_1 and Q_4. Whereas, for negative current, we turn on Q_2 and Q_3. By alternatively switching between the two pairs we can control the current. The combination of switching on one pair of transistors at a time provides a motor voltage that varies between the $+V_s$ and $-V_s$, with an average value, which is dependent on the duty cycle.

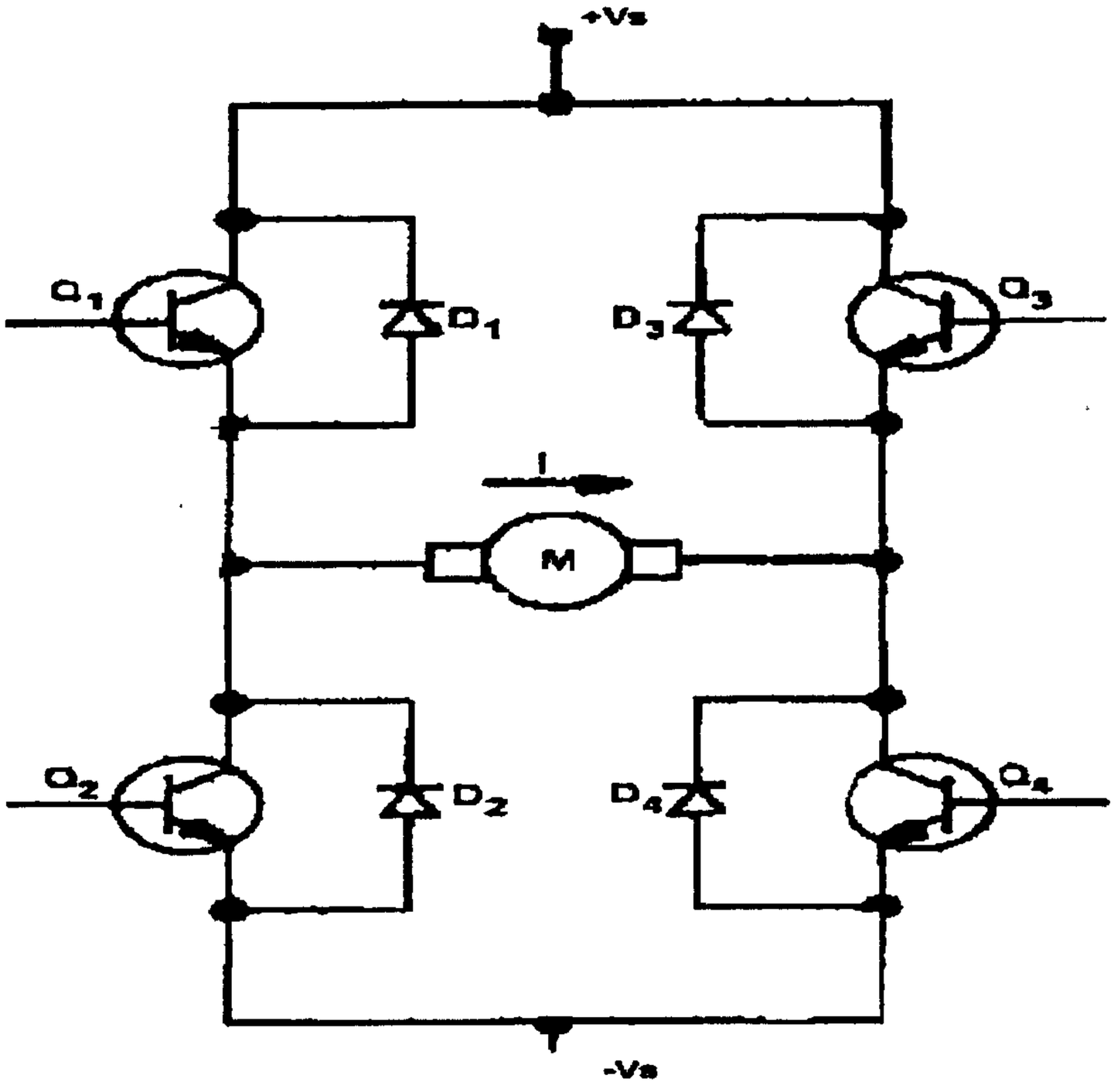

Figure 4.4 "H" type PWM amplifier

[Dc Motors, Speed Controls, Servo Systems, 1980]

The bipolar drive method has a limitation, however. When a pair of transistors is turned off, it takes a finite time for the transistors to get to the off state. Therefore, we must allow for some time delay between the turning off of one pair and the turning on of the second pair. This time delay, which is approximately $5\mu s$, limits the switching frequency to approximately 20kHz.

In bipolar drive, the switching period T is divided into three phases: phase a, phase b and the delay phase as shown in figure (4.5)

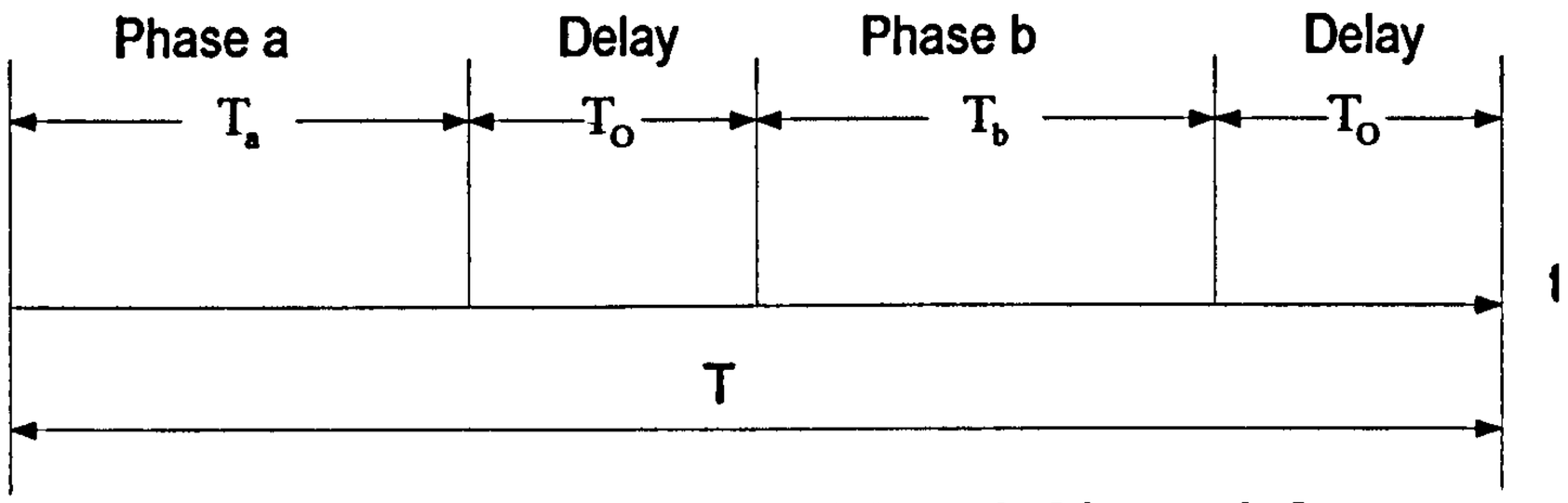

Figure 4.5 The phases of the switching period

The phases are defined as follows:

Phase a:	Q_1, Q_4	On	The motor voltage = Vs
	Q_2, Q_3	Off	
Phase b:	Q_2, Q_3	On	The motor voltage = - Vs
	Q_1, Q_4	Off	
Delay Phase:	Q_1, Q_2, Q_3, Q_4,	Off	

4.1.2 Commutation Sensor Systems

In order to know which coil to energize for effective commutation the rotor angular position must be known. There are several methods available today for the angular position sensing system. The most commonly used method is the Hall effect sensors. This system utilizes a sensor, which detects the magnitude and polarity of the magnetic field. The signals are amplified and processed to form logic compatible signal levels. The

sensors are usually mounted in the stator structure, where they sense the polarity and magnitude of the permanent magnet field in the air gap. The outputs of these sensors control the logic functions of the controller configuration to provide current to the proper coil in the stator figure (4.6).

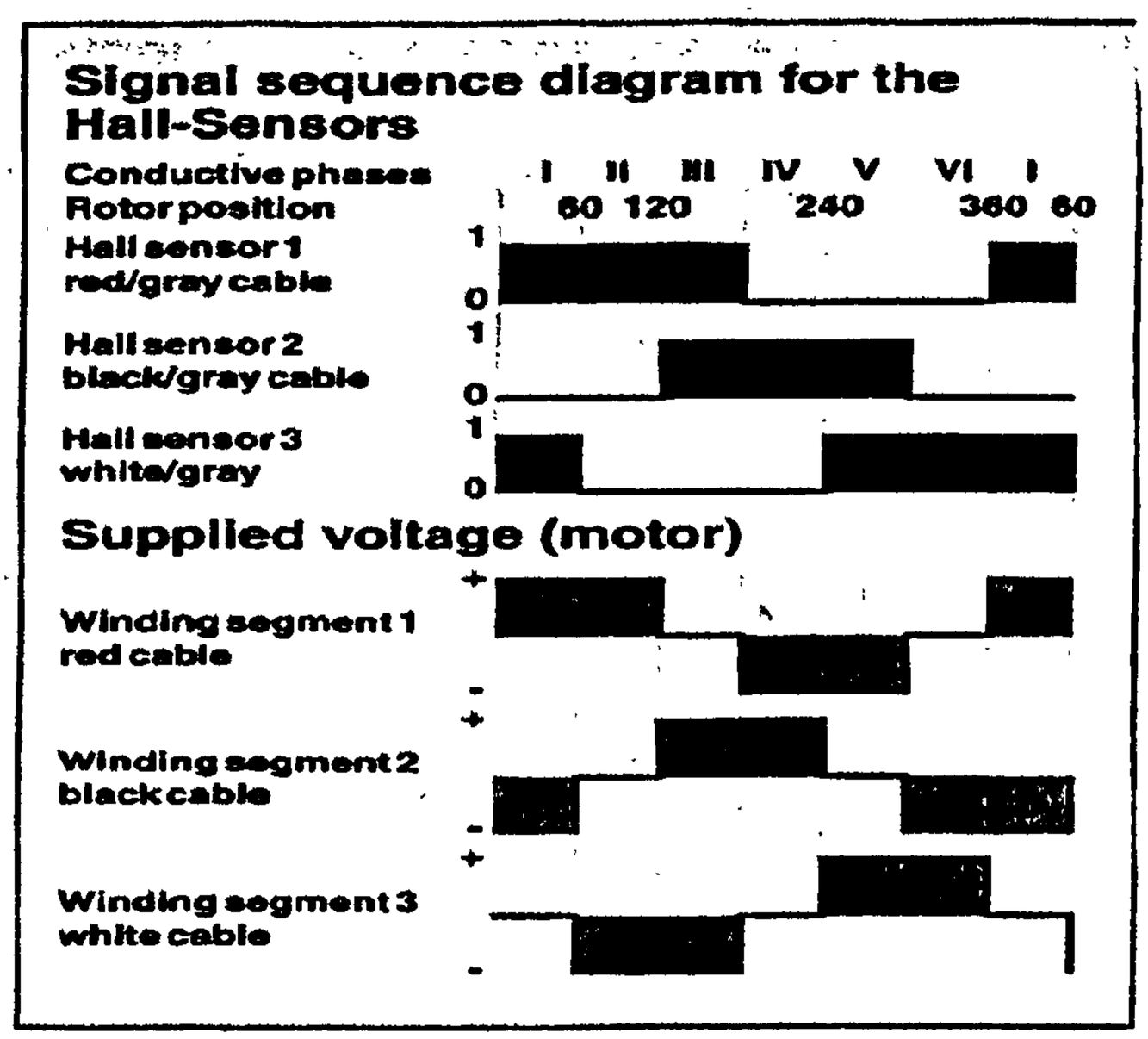

Figure 4.6 Signal sequence diagram for the Hall-Sensors

One drawback with such a location of the angular position sensor is that it is subject to stator temperature conditions, which may at times be rather severe (160-180 degrees Celsius) in high performance applications. Such temperature may adversely affect the Hall effect sensor and can therefore impair performance. This is because the Hall effect sensor is a semiconductor device. Therefore more carriers will be produced as the temperature increases thus producing a larger signal for the same field. Also the circuitry behind the Hall effect sensor will produce signals which are more noise at high temperatures. The Hall effect device can, of course be located away from the immediate stator structure and may use a separate magnet for angular sensing.

4.2 The Motor Driver Unit (132368)

The motor driver unit is an advanced 4-quadrant servoamplifier that is suitable for the chosen motor. A 4-quadrant controller means that it is capable of controlling speed in both directions and braking in both directions figure (4.7). The unit operates from a single DC supply in the range of 12-50 volts. The driver also requires a minimum inductance of 0.5mH. for each motor winding. This means that for the chosen motor an additional 0.2mH was required in each winding. The supply voltage used is calculated as a function of operating speed, torque and nominal voltage (see supply voltage section).

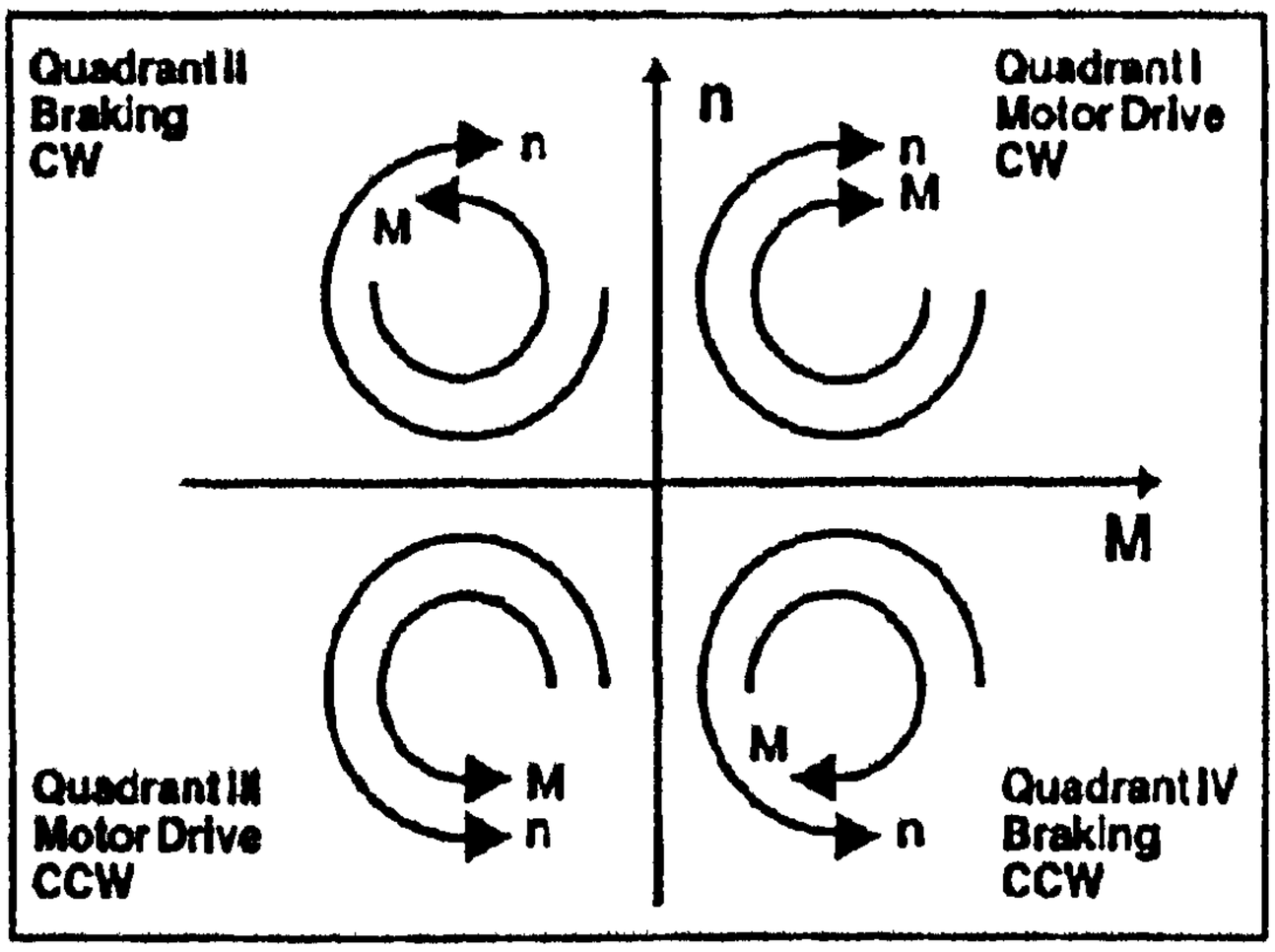

Figure 4.7 4-Quadrant operation

This motor driver unit is a PI speed controller, which uses PWM for speed regulation. It also incorporates other useful features such as a speed monitoring facility, current limiting for the protection of the components, a power (MOSFET) final stage and 5 trim potentiometers at the edge of the driver for optimal setting.

4.2.1 Speed Control section

The Maxon motor drivers include servo amplifiers for controlling the EC motors. The primary function of these servo amplifiers is to maintain a predetermined shaft speed as stable as possible, independent of load fluctuations at the motor output. To this end electronic circuitry constantly compares a preset (desired) speed according to the set value V_{ref} with the actual speed as measured by V (figure 4.8). The information thus collected provides an error-input signal for the control system. The values of the

proportional K_P and integral K_I and sensor gain H_3 are not known, as the manufacturers did not disclose this information.

The intensity of the field can be varied through a pulse-width modulator. The pulse-width modulator operates at a frequency of approximately 20kHz and receives its set value from a PI controller (PI = Proportional & integration). In order for the driver to work properly as described in the data sheet and to be able to use attractive features such as speed monitoring (see section 4.2.3) the optical encoder must have 500 pulses per revolution (PPR).

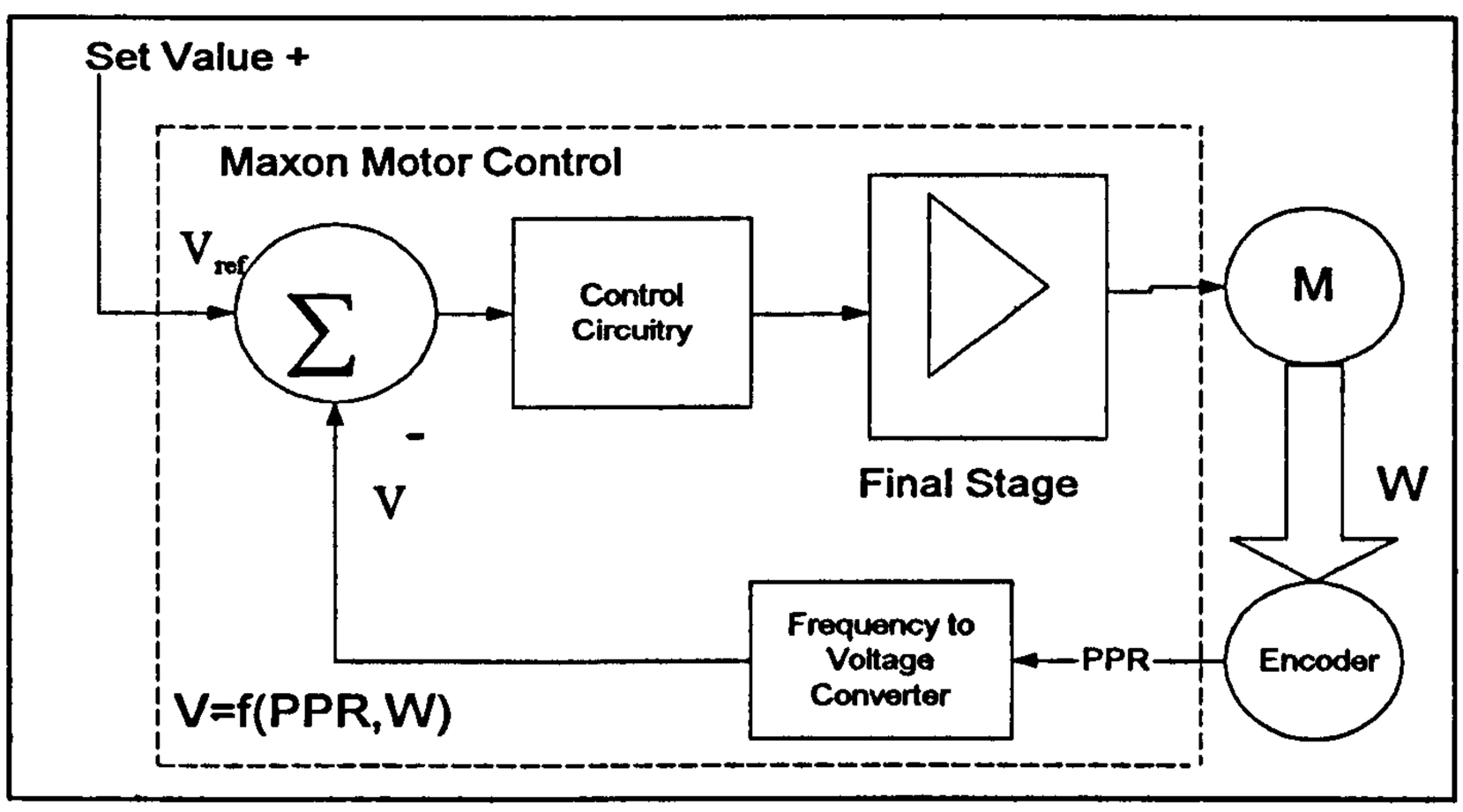

Figure 4.8 Digital encoder speed control

4.2.2 Speed Monitoring.

The monitor output signal ±5 volts corresponds to the adjusted max speed at ±10 volts set value input. This feature is particularly useful because there is a direct linear relation between the input set value and the speed monitor signal, hence the speed of the motor can be calculated using this monitor signal.

The monitor signal on the driver will swing between 5 volts and –5 volts only if the encoder produces 500 pulses per revolution. This feature would be useful if it is decided that rate feed back is required or just as a monitor for the speed.

4.2.3 Current Limiting.

A ±10 amps absolute current limiter protects the electronic components. Maximum continuous as well as maximum intermittent current can be adjusted within the range of 0.1 to 6 amps with the respective trimmers found at the card edge. The adjustment made to Imax represents the maximum continuous peak current that can be reached during normal operation 0-±6 amps. However the system may withdraw current of up to ±10 amps for a time constant of approximately 1-second. After that time constant the current is reduced to the value of the continuous current as set by the trimmers. In other words a window is opened for a defined period of time during which the motor may draw more current. If the effective motor current remains outside the continuous permissible current of ± 6 amps for more than 1-second then motor current limiting is initiated.

4.2.4 Drivers /Final stage:

The final stage is equipped with N-channel MOSFET transistors exclusively, assuring the

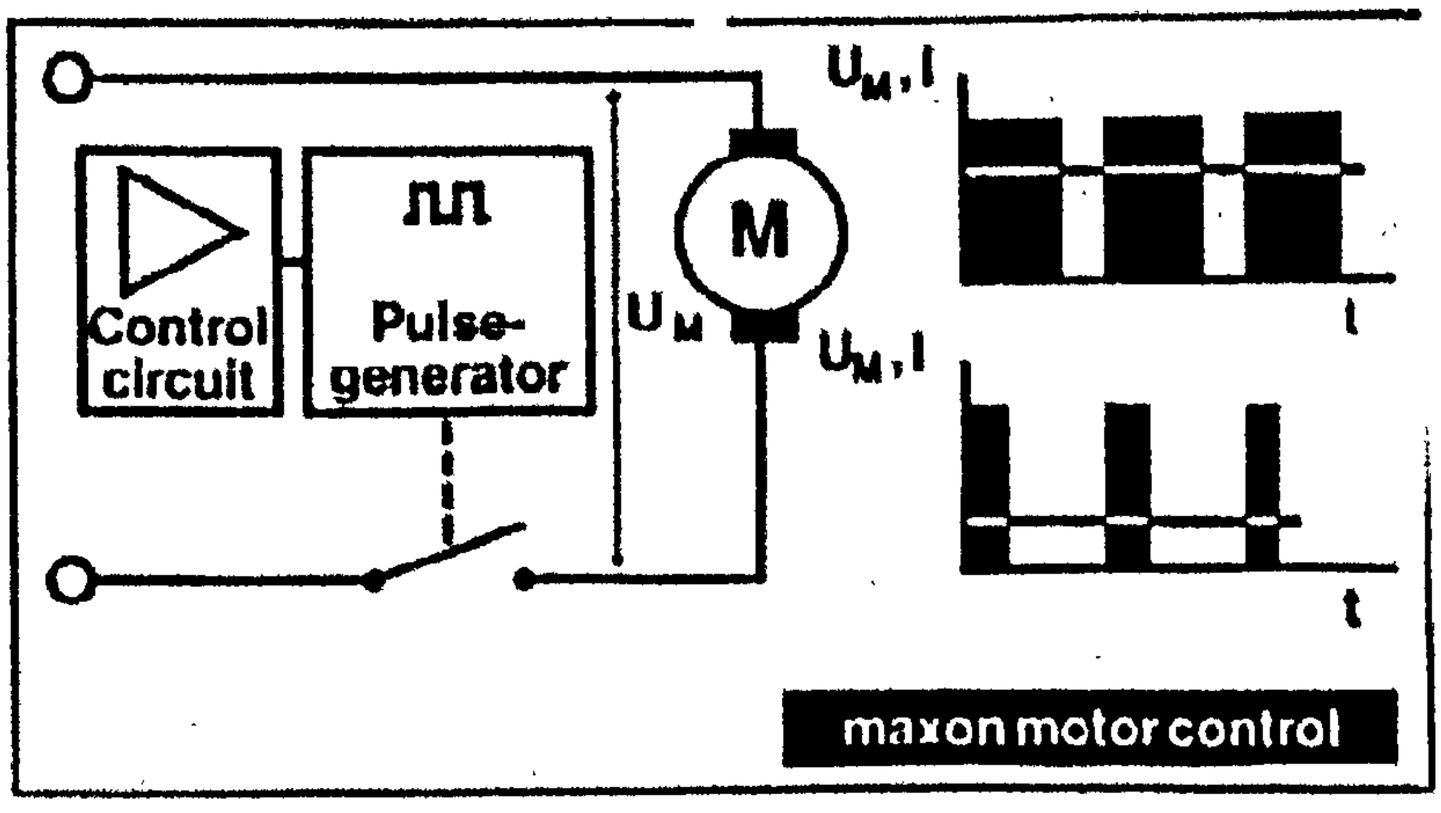

Figure 4.9 The Maxon final stage for PWM generation

excellent efficiency of up to 95%. The voltage drop across each conducting transistor (ON State) is 4V maximum.

4.2.5 Trim Potentiometer at the Edge of the Card

The 4-Q driver has 5 potentiometers at the edge allowing for adjustments.

a) Gain Speed controller potentiometer (P_1): The amplification of the speed control signal can be adjusted with the potentiometer P_1. If the system has small amplification then the controller has slow response. The proportional and integral gains are not changed separately but rather the overall gain of the system is changed.

b) Offset potentiometer (P_2): Set reference speed value to zero volts then adjust potentiometer (P_2) until the motor shaft is stationary. This is a useful feature because due to offsets and problems with electronics, when applying zero volts as a reference signal this does not mean that the voltage across the motor terminals is zero. That is to say even for zero input voltage the motor shaft might still oscillate. This feature allows us to make sure that zero input means a stationary shaft.

c) Current Limit Potentiometer (P_3): The current limit can be adjusted by the potentiometer P_3 (Imax). The maximum value it can be set to is ± 6 amps and the lowest value is 0.

d) Set Value Adjustment Speed Potentiometer (P_4): The maximum possible speed is adjusted with the potentiometer P_4. Give the maximum set value speed (e.g. 10 volts)

and turn P_4 so far that the required speed is achieved. The speed is monitored by a tachometer.

4.2.6 Supply Voltage.

The selection of the supply voltage was chosen according to the recommendation of the manufactures data sheet for optimal performance. There is an overall voltage drop across the driver of 4 volts [Appendix D, Data sheet for the driver].

$$Vs = \frac{U_n}{no} \times \left(nB + \frac{\Delta n}{\Delta M} \times M_B \right) + 4 \quad \text{[Appendix D]} \qquad \text{equation 4.1}$$

Operating speed $nB\,[rpm] = 4500$

Nominal motor voltage $U_n[volts] = 18.00$

Motor no load speed at $U_n, no[rpm] = 4500$

Speed/ torque gradient of the motor $\frac{\Delta n}{\Delta M}[rpm / mNm] = 8.2$

As stated earlier (page 46)

Operating Torque $M_B[mNm] = 230$

$\therefore$

$$Vs = \frac{18.00}{4500}(4500 + 8.2 \times 230) + 4$$

$Vs = 29.5 volts$

Vs was chosen to be 30 volts

4.3 Calibration of the Motor Driver Unit

As the supply voltage for the driver was worked out to be 30 volts. The corresponding no load motor speed at that value was worked out as follows

From motor data sheet:

$$18 \text{ volts} \rightarrow 4500 \text{ r.p.m} \rightarrow 471 \text{ rads/sec}$$

Therefore

$$30 \text{ volts} \rightarrow 7500 \text{ r.p.m} \rightarrow 785 \text{ rads/sec}$$

The 7500 r.p.m is well within the maximum speed limit of 15000 r.p.m for this motor. However we know that there is a voltage drop in the controller circuitry, therefore the 30 volts are not necessarily what the motor would see. This can be confirmed with the experimental data.

An experiment was set up to determine the relationship between the input voltage and the output speeds as measured by a tachometer. That is if the driver has been calibrated to give a linear increase in speed over the 10 volts input. A tachometer was mounted at one end of the motor shaft and the tachometer readings were taken for different input voltages. The results are recorded in tables (4.1 & 4.2). The supply voltage to the Maxon driver was 30 volts. This will always be the case for all the work to be carried out. The tachometer gives a voltage which is proportional to speed. The tachometer constant is $K_t = 41.1 * 10^{-3} V / rad / sec$ [Appendix E].

Direction = C.C.W

Input voltage (pot voltage)	Tacho voltage V_{tacho}	$W = V_{tacho}/K_t$ rad/sec
10 volts	29.5	718.0
9 volts	26.7	650.0
8 volts	23.7	577.0
7 volts	21.0	511.0
6 volts	17.9	436.0
5 volts	14.9	363.0
4 volts	11.9	290.0
3 volts	8.9	217.0
2 volts	5.9	144.0
1 volts	2.9	71.0

Table 4.1 Corresponding speeds at various voltages

Direction = C.W

Input voltage (pot voltage)	Tacho voltage V_{tacho}	$W = V_{tacho}/K_t$ rad/sec
-10 volts	29.5	-718.0
-9 volts	26.7	-650.0
-8 volts	23.7	-577.0
-7 volts	21.0	-511.0
-6 volts	17.9	-436.0
-5 volts	14.9	-363.0
-4 volts	11.9	-290.0
-3 volts	8.9	-217.0
-2 volts	5.9	-144.0
-1 volts	2.9	-71.0

Table 4.2 Corresponding speeds at various voltages

The data points in tables (4.1) and (4.2) were plotted as a graph figure (4.10) to confirm the linear relationship input voltage and speed.

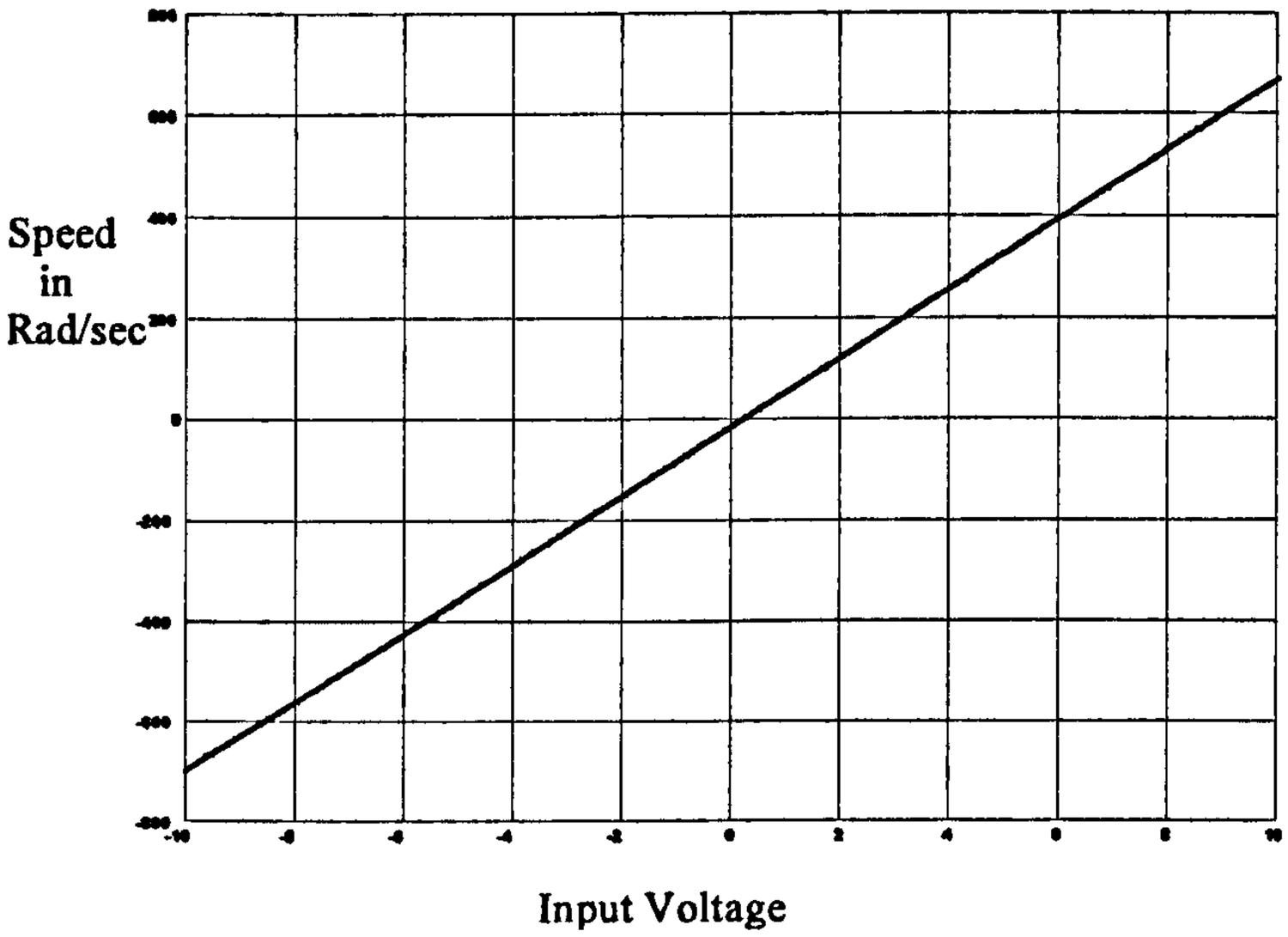

Figure 4.10 Relationship between input voltage and corresponding speed

Figure (4.10) clearly shows a linear relation between the input reference voltage and the corresponding output speed of the motor in both clockwise and anti clockwise directions. The speed control and the linear relationship is maintained even at low speeds

4.4 Mathematical Model of the Motor and Driver Unit

A DC motor can be described by a second order model with one integrator and one time constant by neglecting the armature inductance [Astrom K.J., 1990, pp511]. As the EC motor used in this case is described by the manufacturers to behave just like a DC motor then it can be taken that all the mathematical equations used for a DC motor are

applicable in this case. The input is the voltage applied to the motor driving unit and the output is the shaft position and speed.

In order to evaluate the unknown parameters K_P, K_I and the sensor gain H_3 a model must be derived. The model of interest at this point is one, which describes the motor driver unit and the motor only. Later in this chapter the effect of attaching a gearbox will be taken into account. It is also worth mentioning that the approximations in the model derivation include the use of a DC input to the motor rather than a PWM.

NO.	Characteristics	Symbols	Units
1	Nominal voltage	Vin(max)	18.00 V
2	No load speed	no	4500 r.p.m
3	Speed constant	K_b	250 r.p.m/V
4	Terminal resistance	R	1.26Ω
5	Terminal inductance (phase to phase)	L_m	0.3 mH
6	Torque constant	K	38.2 mNm/A
7	Mechanical time constant	τ_m	7 ms
8	Rotor moment of inertia	J	85e-7 Kgm^2
9	Back emf Constant	E_a	38.2 e-3 V/rad/sec

Table 4.3 Typical motor characteristics

From first principles the following equations are derived

$$\frac{dI}{dt} = -\frac{R}{L}I - \frac{E_a}{L}W + \frac{1}{L}V_t \qquad \text{equation 4.2}$$

I = current amps $\quad L_c$ = Choke inductance $\quad W$ = Velocity rad/secl $\quad L = L_m + L_c$

T = Torque Nm $\quad B_f$ = motor friction $\quad V_t$ = DC input volt s

also we know that :

$$T = KI = J\dot{W} + B_f W$$

$\therefore$

$$\dot{W} = \frac{KI}{J} - \frac{B_f W}{J} \qquad \text{equation 4.3}$$

Rearranging equation (4.2) and (4.3) in the state space representation yields:

All the parameters except the viscous friction coefficient B_f are known. This however

$$\begin{bmatrix} \dot{I} \\ \dot{W} \end{bmatrix} = \begin{bmatrix} \frac{-R}{L} & \frac{-E_a}{L} \\ \frac{K}{J} & \frac{B_f}{J} \end{bmatrix} \begin{bmatrix} I \\ W \end{bmatrix} + \begin{bmatrix} \frac{1}{L} \\ 0 \end{bmatrix} Vt \qquad \text{equation 4.4}$$

where

L_c = This is the extra choke required for the driver. Minimum choke for the maxon driver was 0.5mH. As the motor had already 0.3mH per phase an additional 0.2mH is needed

$$L = L_m + L_c$$

can be estimated using least squares. Table (4.4) gives the steady state currents and speeds for various set point input voltages.

Input Voltage	Motor Current Unloaded	Speed in rad/sec Unloaded
1	0.14	70.60
2	0.16	143.6
3	0.19	216.55
4	0.20	289.54
5	0.21	362.5
6	0.24	435.52
7	0.27	510.95
8	0.30	576.64
9	0.32	649.64
10	0.34	717.76

Table 4.4 Summary of Results for Unloaded Motor

Using the data in table (4.3) a value for friction B_f was estimated. From equation (4.3)

$$T = B_f W + T_L \qquad \text{equation 4.5}$$

Since T=KI and $T_L = 0$ (motor unloaded) in steady state the following formulae is true: -

$$KI = B_f W \qquad \text{equation 4.6}$$

From equation (4.6) and table (4.4) the least squares estimate of B_f was calculated using Matlab. $B_f = 2.045*10^{-5}$ Nms/rad for the unloaded motor. Inserting the friction value of the unloaded motor value in the state space model yields:

$$\begin{bmatrix} \dot{I} \\ \dot{W} \end{bmatrix} = \begin{bmatrix} -2520 & -76.4 \\ 4494.118 & 2.41 \end{bmatrix} \begin{bmatrix} I \\ W \end{bmatrix} + \begin{bmatrix} 2000 \\ 0 \end{bmatrix} Vt \qquad \text{equation 4.7}$$

The above model is an open loop model, which does not take into consideration the motor driver unit. Now taking the unit into consideration the model will change considerably.

4.5 Evaluation of the proportional and integral gains

Knowing that a PI controller is used a closed loop model for the motor and the driver unit can be estimated as follows:

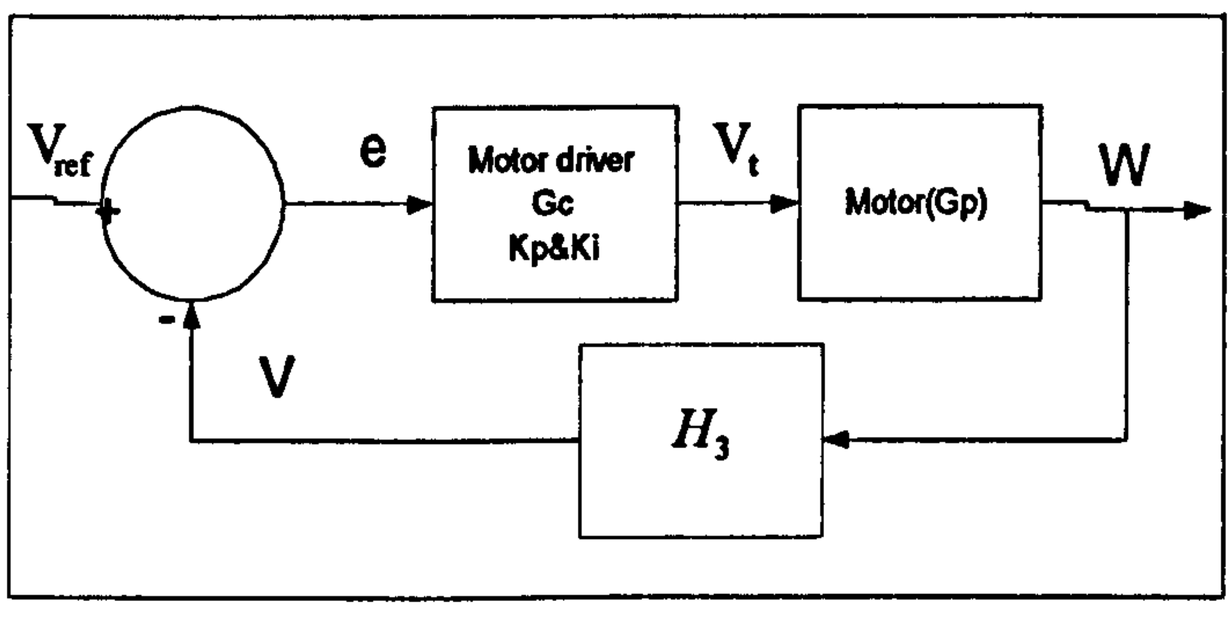

Figure 4.11 System Block Diagram

$$e = (V_{ref} - V) \qquad \text{equation 4.8}$$

$$\text{let } V_t = K_p e + K_I \int_0^t e \qquad \text{equation 4.9}$$

$$\text{and let } \quad Z = \int e \;\therefore \dot{Z} = e \qquad \text{equation 4.10}$$

$$\text{but } \; V = \begin{bmatrix} 0 & H_3 \end{bmatrix} \begin{bmatrix} I \\ W \end{bmatrix} \qquad \text{equation 4.11}$$

Where

K_P = Proportion al gain

K_I = Integral gain

H_3 = frequency to voltage converter + Encoder gain

$$\begin{bmatrix} \dot{X} \\ \dot{Z} \end{bmatrix} = \begin{bmatrix} A & 0 \\ -\begin{bmatrix} 0 & H_3 \end{bmatrix} & 0 \end{bmatrix} \begin{bmatrix} X \\ Z \end{bmatrix} + \begin{bmatrix} B \\ 0 \end{bmatrix} V_t + \begin{bmatrix} 0 \\ 1 \end{bmatrix} V_{ref}$$

$$\begin{bmatrix} \dot{X} \\ \dot{Z} \end{bmatrix} = \begin{bmatrix} A & 0 \\ -\begin{bmatrix} 0 & H_3 \end{bmatrix} & 0 \end{bmatrix} \begin{bmatrix} X \\ Z \end{bmatrix} + \begin{bmatrix} B \\ 0 \end{bmatrix} (K_p e + K_I Z) + \begin{bmatrix} 0 \\ 1 \end{bmatrix} V_{ref} \qquad \text{equation 4.12}$$

Where

$$\dot{X} = AX + BV_t \qquad \dot{Z} = e = V_{ref} - \begin{bmatrix} 0 & H_3 \end{bmatrix} X$$

$$X = \begin{bmatrix} I \\ W \end{bmatrix}$$

$$\begin{bmatrix} \dot{I} \\ \dot{W} \\ \dot{Z} \end{bmatrix} = \left(\begin{bmatrix} -2520 & (-76.4 - (2000 K_p H_3)) & 2000 K_I \\ 4494118 & \frac{B_f}{J} & 0 \\ 0 & -H_3 & 0 \end{bmatrix} \begin{bmatrix} I \\ W \\ Z \end{bmatrix} \right) + \begin{bmatrix} 2000 K_p \\ 0 \\ 1 \end{bmatrix} V_{ref} \qquad \text{equation 4.13}$$

The parameters H_3, K_P, K_I can now be experimentally estimated.

4.6 Experimental Estimation of Encoder F/V converter Gain H_3

The value of the gain H_3, can be estimated by working out the closed loop transfer function $\frac{W(s)}{V_{ref}(s)}$. From figure (4.11) the closed loop transfer function is

$$\frac{W(s)}{V_{ref}(s)} = \frac{G_c G_p}{1 + G_c G_p H_3} \qquad \text{equation 4.14}$$

$$V_t = K_p e + K_I Z \qquad = K_p (V_{ref} - H_3 W) + \frac{K_I (V_{ref} - H_3 W)}{s}$$

$$= \frac{K_p s + K_I}{s} V_{ref} - \frac{K_p s + K_I}{s} H_3 W = \frac{K_p s + K_I}{s} e(s)$$

$\therefore$

$$G_c = \frac{K_p s + K_I}{s} \qquad \text{equation 4.15}$$

Hence

$$\frac{W(s)}{V_{ref}(s)} = \frac{(K_p s + K_I) G_p(s)}{s + (K_p s + K_I) G_p(s) H_3} \qquad \text{equation 4.16}$$

Evaluating the above transfer function at s=0 gives the DC gain of the closed loop

$$\frac{W}{V_{ref}} = \frac{K_I G_p(0)}{K_I G_p(0) H_3} = \frac{1}{H_3} \qquad \text{equation 4.17}$$

system.

Equation (4.17) indicates that for a constant input V_{ref} the corresponding motor speed W is given by $W = \frac{1}{H_3} V_{ref}$. Therefore the value of H_3 can be obtained from the gradient of the graph in figure (4.10). Also the least squares method was used giving the same value.

$$H_3 = \frac{V_{ref}}{W} = \text{Gradient of line} = 72.99 \text{ V/rad/sec}$$

$$H_3 = \frac{1}{72.99} = 0.0137 \text{ V/rad/sec} \qquad \text{equation 4.18}$$

Substituting the value of H_3 into the model derived in equation (4.13) yields the following

$$\begin{bmatrix} \dot{I} \\ \dot{W} \\ \dot{Z} \end{bmatrix} = \begin{bmatrix} -2520 & (-76.4-(27.4K_P) & 200(K_I \\ 4494118 & 2.41 & 0 \\ 0 & -0.0137 & 0 \end{bmatrix} \begin{bmatrix} I \\ W \\ Z \end{bmatrix} + \begin{bmatrix} 200(K_P \\ 0 \\ 1 \end{bmatrix} V_{ref} \qquad \text{equation 4.19}$$

Let

$$A=\begin{bmatrix} -2520 & -76.4-(27.4K_p) & 2000K_I \\ 4494118 & 2.41 & 0 \\ 0 & -0.0137 & 0 \end{bmatrix} \quad \text{and} \quad B=\begin{bmatrix} 2000K_p \\ 0 \\ 1 \end{bmatrix} \qquad \text{equation 4.20}$$

In order to evaluate the K_p and K_I gains an experiment was set up in which the practical behaviour of the motor and the driver was experimentally examined. A tachometer (Appendix E) was mounted to the motor shaft to measure the speed of the motor. The output of the tacho was connected to a first order low pass filter (figure 4.12) which had a cut of frequency of 28 Hz. When selecting the anti aliasing filter, two considerations had to be kept in mind. The filter's cut off frequency must not exceed half the sampling frequency in order to avoid aliasing. The second was the frequency of the noise to be attenuated. Using the Fast Fourier Transforms (FFT) in Matlab the data collected was analyzed to see the frequency of the noise. This clearly showed that cycle noise (50 Hz) was present. As well as connecting a 1-microfarad capacitor across the terminals of the power supply, a filter of approximately 30 Hz was chosen. Selecting the available components gave a cut of frequency of 28 Hz, which was close enough to the required, cut off frequency. The output of the filter was connected to 486 PC via a digital to analogue converter (Appendix E). The sampling time used was 0.5 milli seconds. The experimental set up shown in figure (4.13) was used.

4.7 Sensor Interface

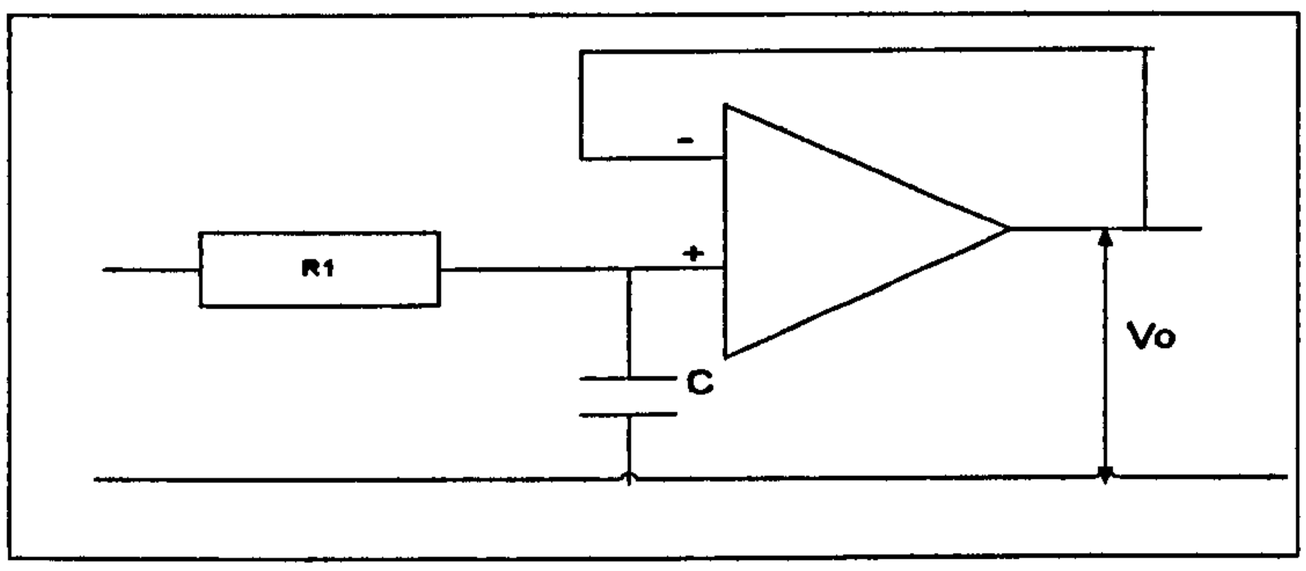

Figure 4.12 Amplifier and filter set-up

To achieve a cut of frequency of approximately 28 Hz for the filter and a gain of 1 the following calculations were carried out. The filter needed was a low pass filter.

$$f = \frac{1}{2 * piR1C}$$

let $R1 = 56k\Omega$ therefore $C = 0.1 \times 10^{-6}$ farads

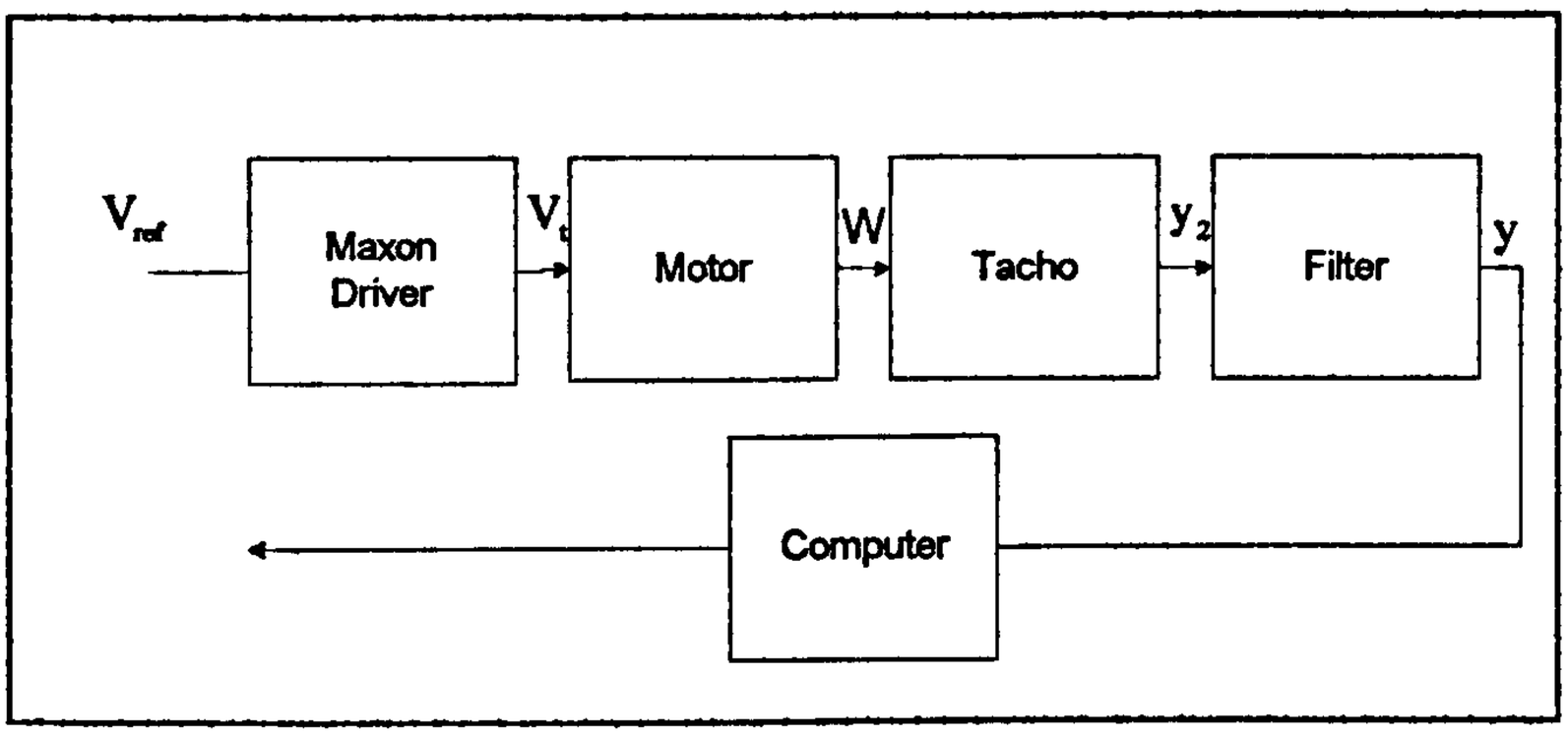

Figure 4.13 Experimental set up for data collection

4.8 Motor model with filter

Equation (4.20) gives the model for the motor and driver unit with unknown values of the proportion, integral gains. The model does not take into account the filter

Filter transfer function

$$y = \frac{y_2}{R1Cs+1} \quad \therefore \quad \dot{y} = \frac{y_2}{R1C} - \frac{y}{R1C} \qquad \text{equation 4.21}$$

Now the A matrix becomes when the filter is added as follows.

$$A = \begin{bmatrix} -2520 & [-76.4-(27.4K_p)] & 2000K_I & 0 \\ 4494.118 & 2.41 & 0 & 0 \\ 0 & -0.0137 & 0 & 0 \\ 0 & \frac{1}{R1C} & 0 & -\frac{1}{R1C} \end{bmatrix} \qquad \text{equation 4.22}$$

Looking at the output

$$Y=\begin{bmatrix}1 & 0 & 0 & 0\\ 0 & K_t & 0 & 0\end{bmatrix}\begin{bmatrix}I\\ W\\ Z\\ y\end{bmatrix}$$ After filter $$Y=\begin{bmatrix}1 & 0 & 0 & 0 & 0\\ 0 & K_t & 0 & 0 & 0\\ 0 & 0 & 0 & 0 & K_{tf}\end{bmatrix}\begin{bmatrix}I\\ W\\ Z\\ y\end{bmatrix}$$ equation 4.23

$K_t = 41.1\times10^{-3}$ v/rad/sec $\qquad$ $K_{tf} = 41.1\times10^{-3}$ v/rad/sec

Using the set up in figure (4.13) data was collected and different values for the integral gain and proportional gain were tried in simulations. The results are shown in figures (4.14-4.23). It can be seen that at certain values of proportional and integral gains, the simulated data was capable of resembling the real data. The proportional and integral gains, which gave a reasonable match between the practical data and simulated data, are 12 and 20000 respectively.

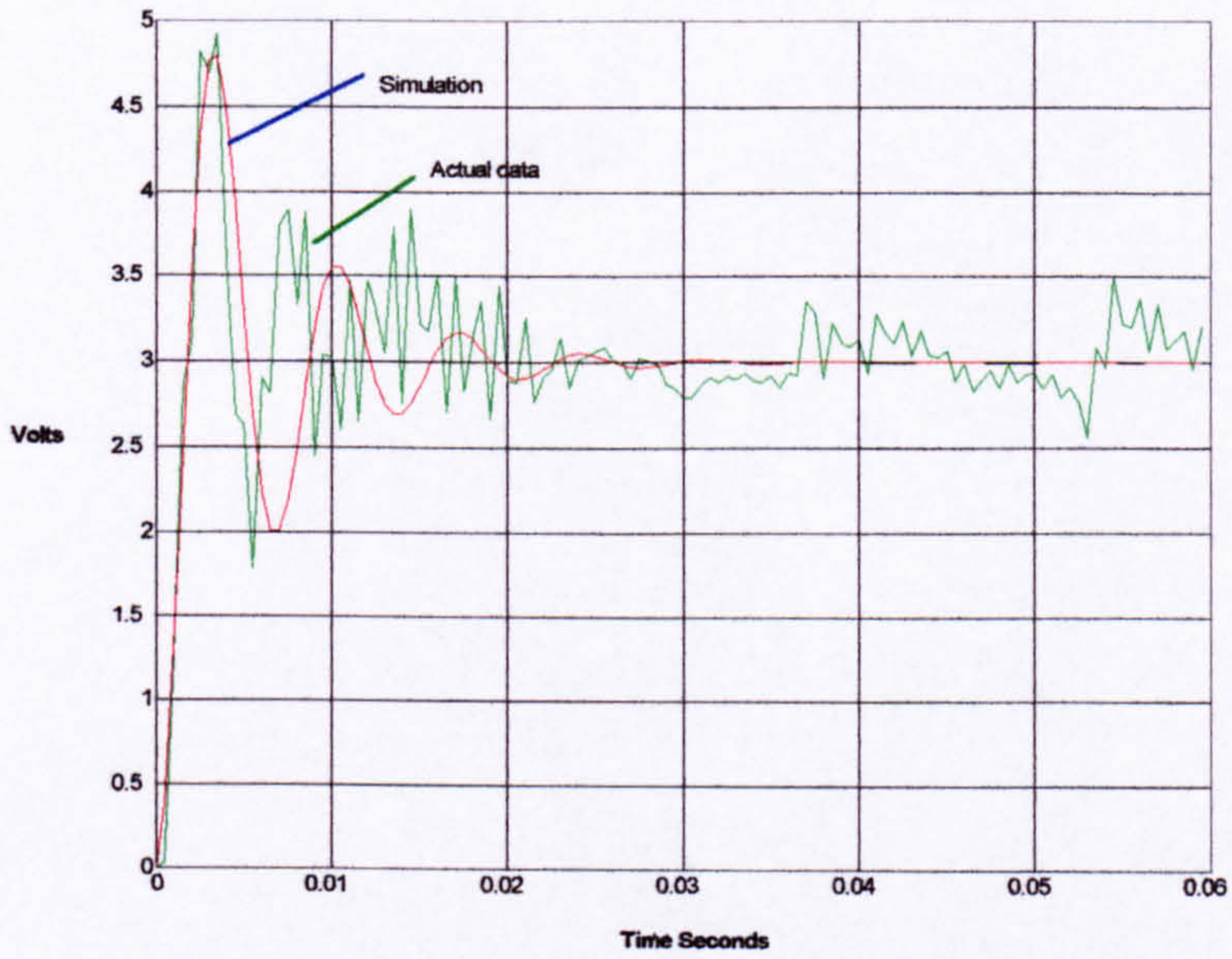

Figure 4.14 Comparison of simulated data and actual data for values of K_P=10 and K_I=15000

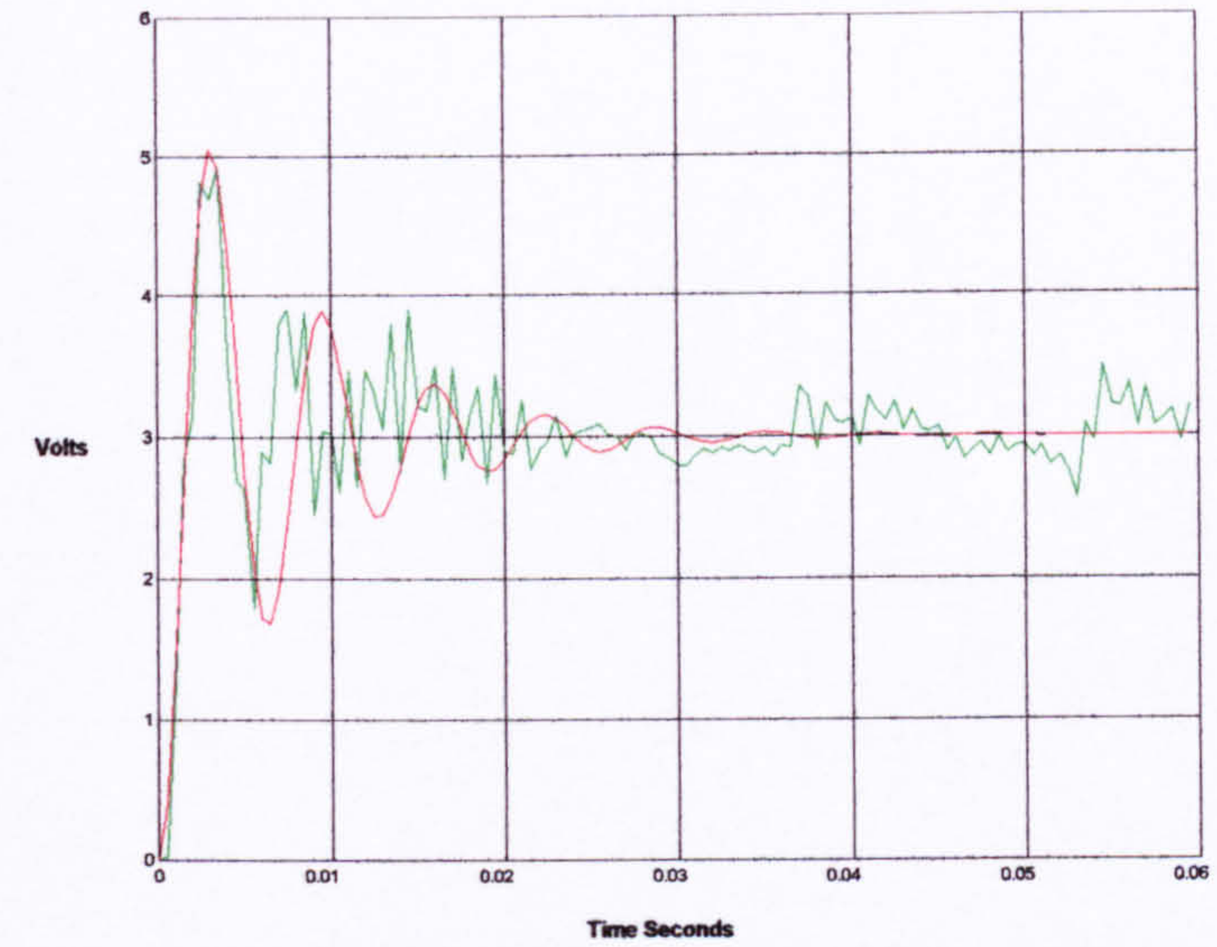

Figure 4.15 Comparison of simulated data and actual data for values of K_P=10 and K_I=18000

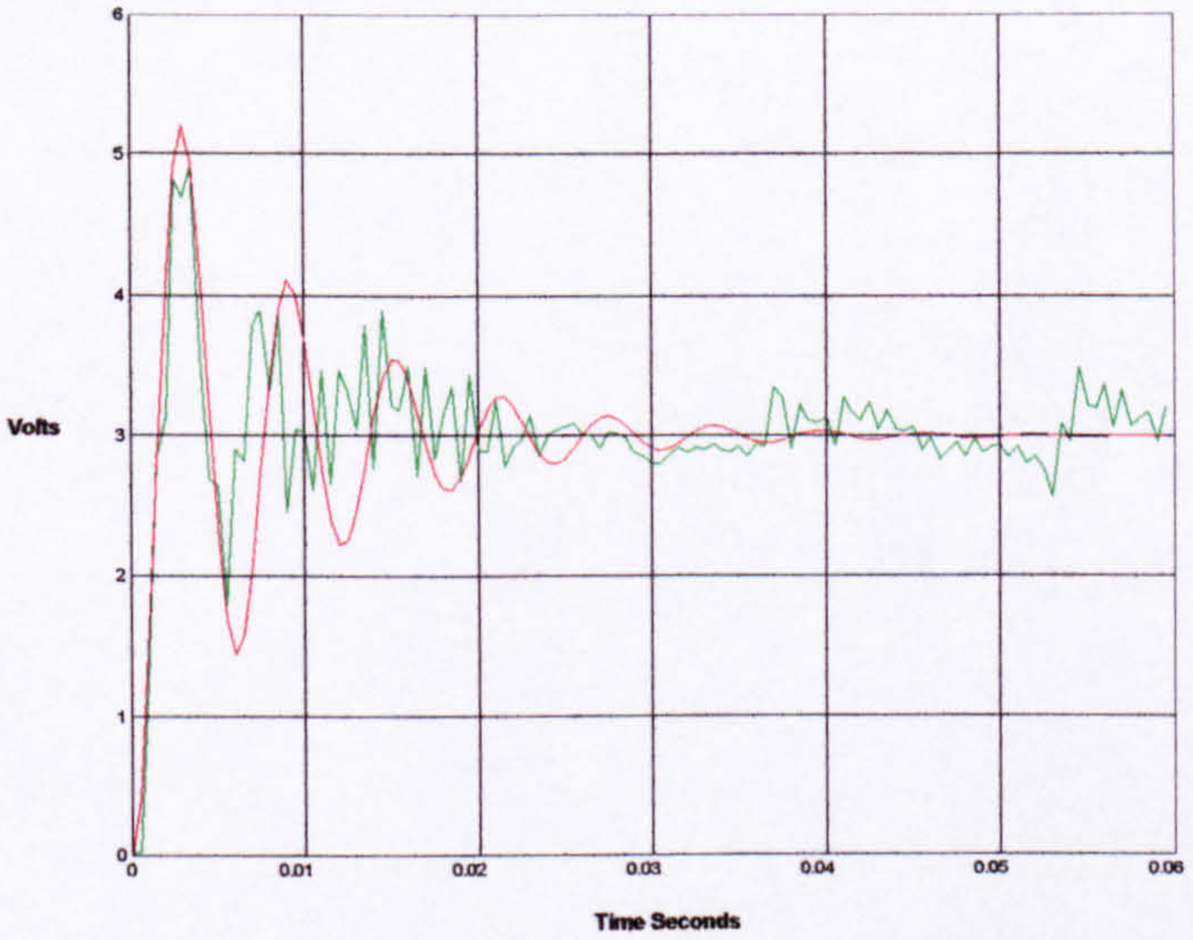

Figure 4.16 Comparison of simulated data and actual data for values of K_P=10 and K_I=20000

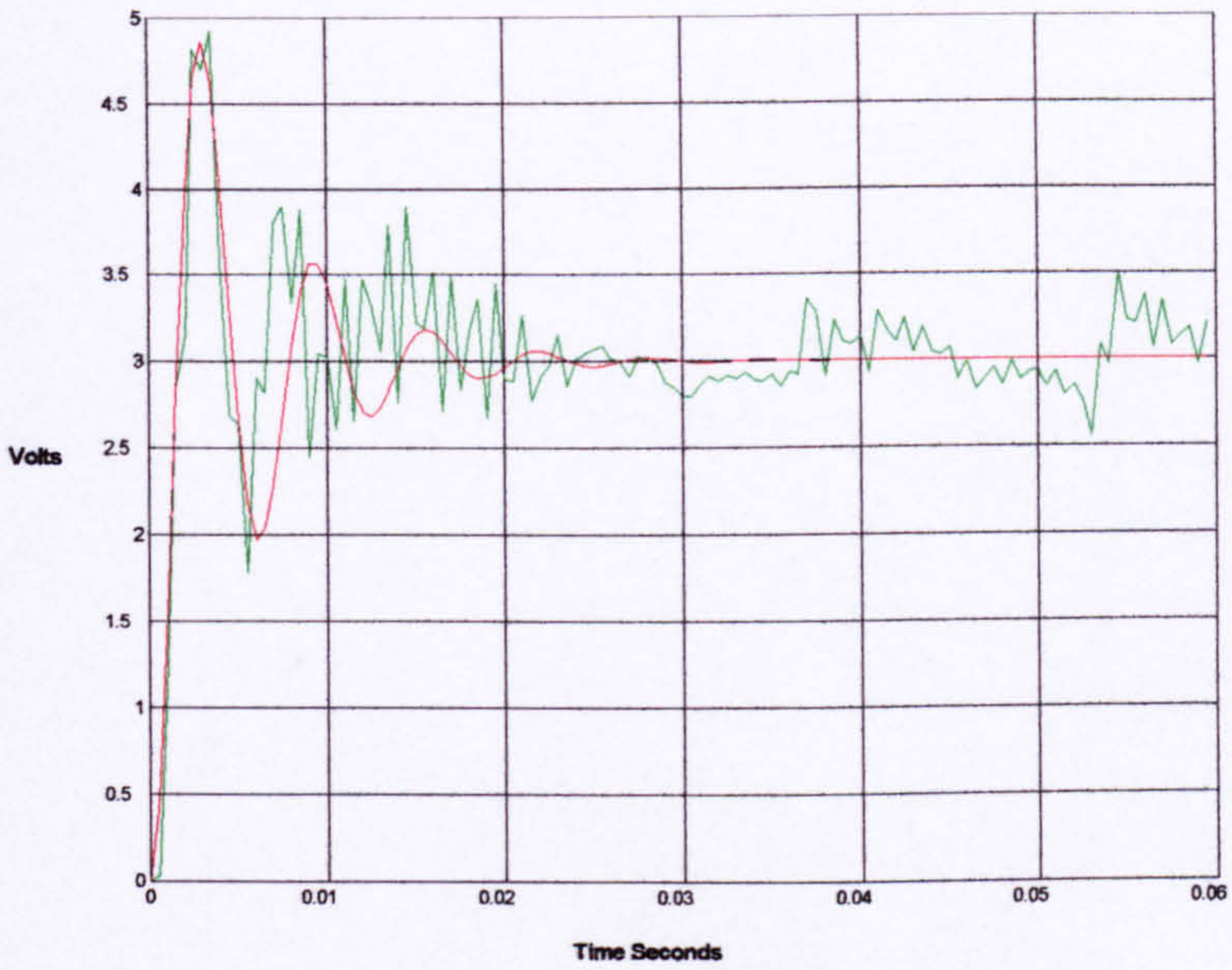

Figure 4.17 Comparison of simulated data and actual data for values of K_P=12 and K_I=18000

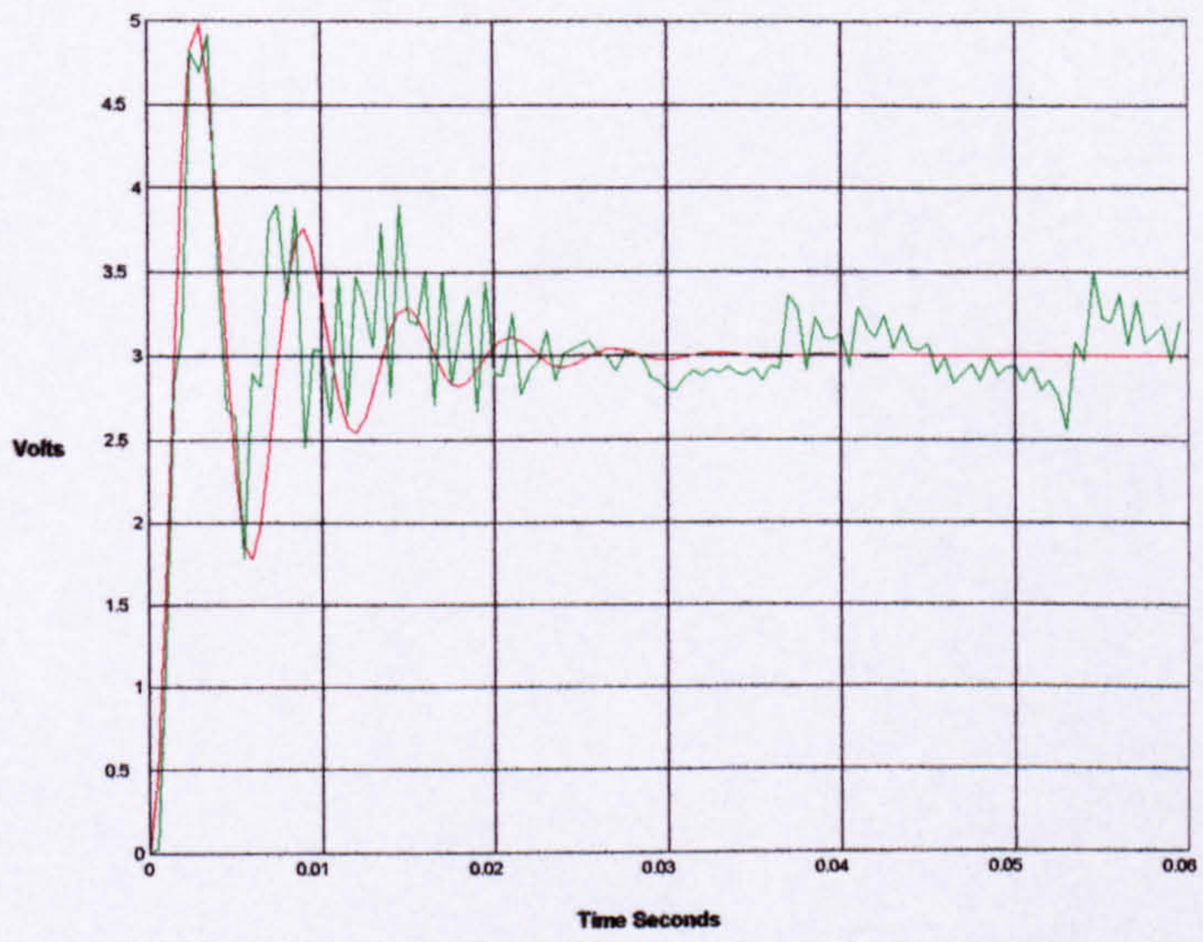

Figure 4.18 Comparison of simulated data and actual data for values of K_P=12 and K_I=20000

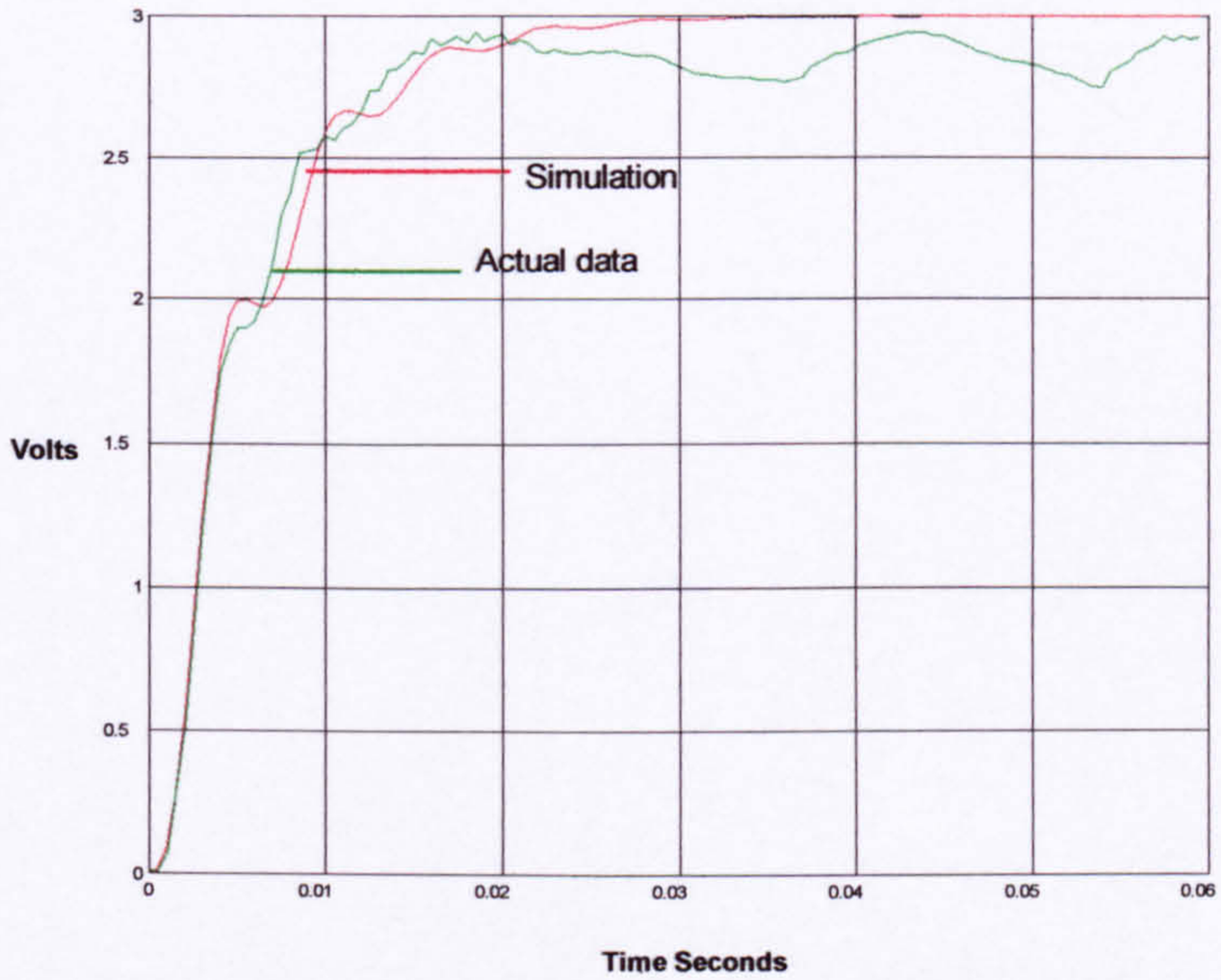

Figure 4.19 Comparison of simulated data and actual data for values of K_P=12 and K_I=20000 after filtering the signals

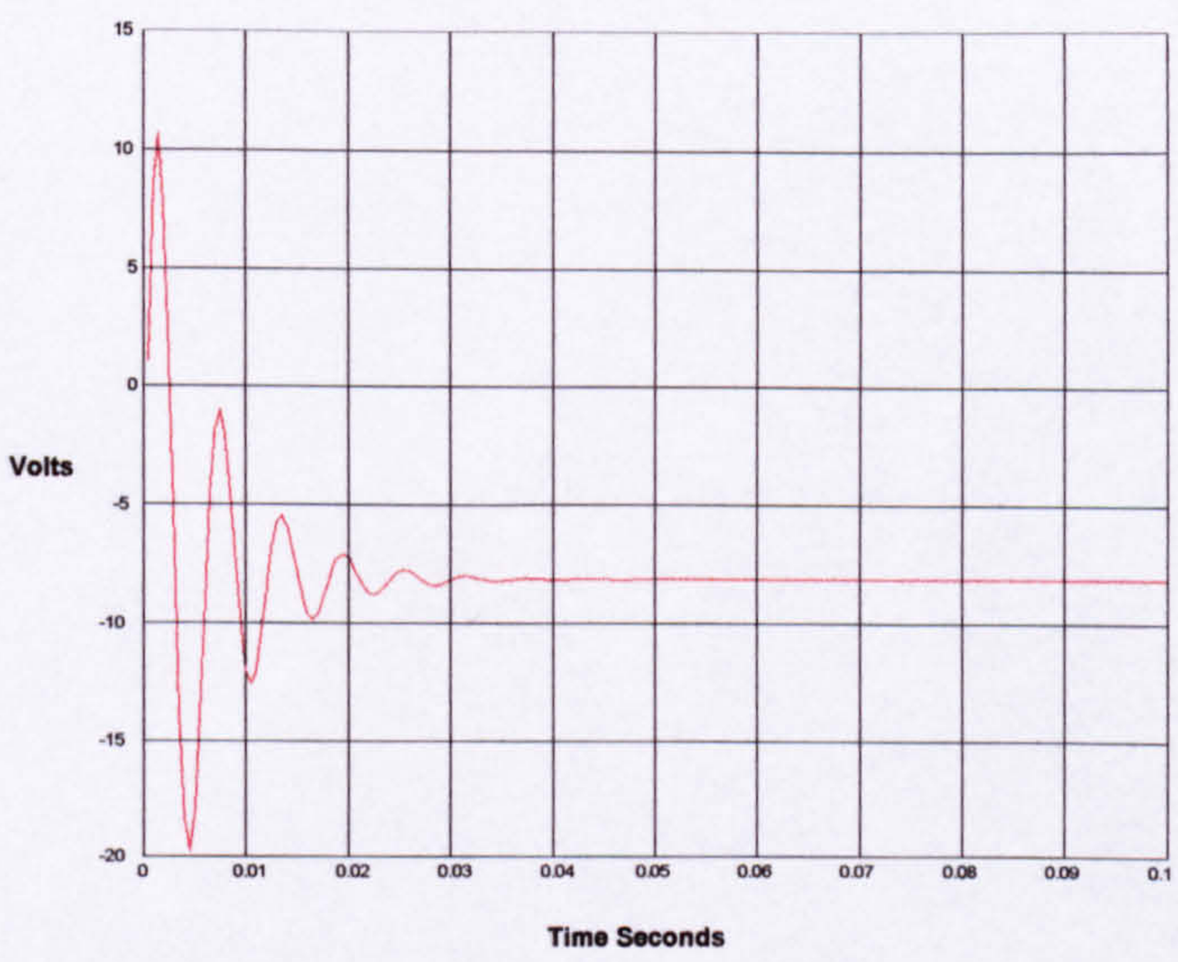

Figure 4.20 Simulated Control Signal at values of K_P=12 and K_I=20000

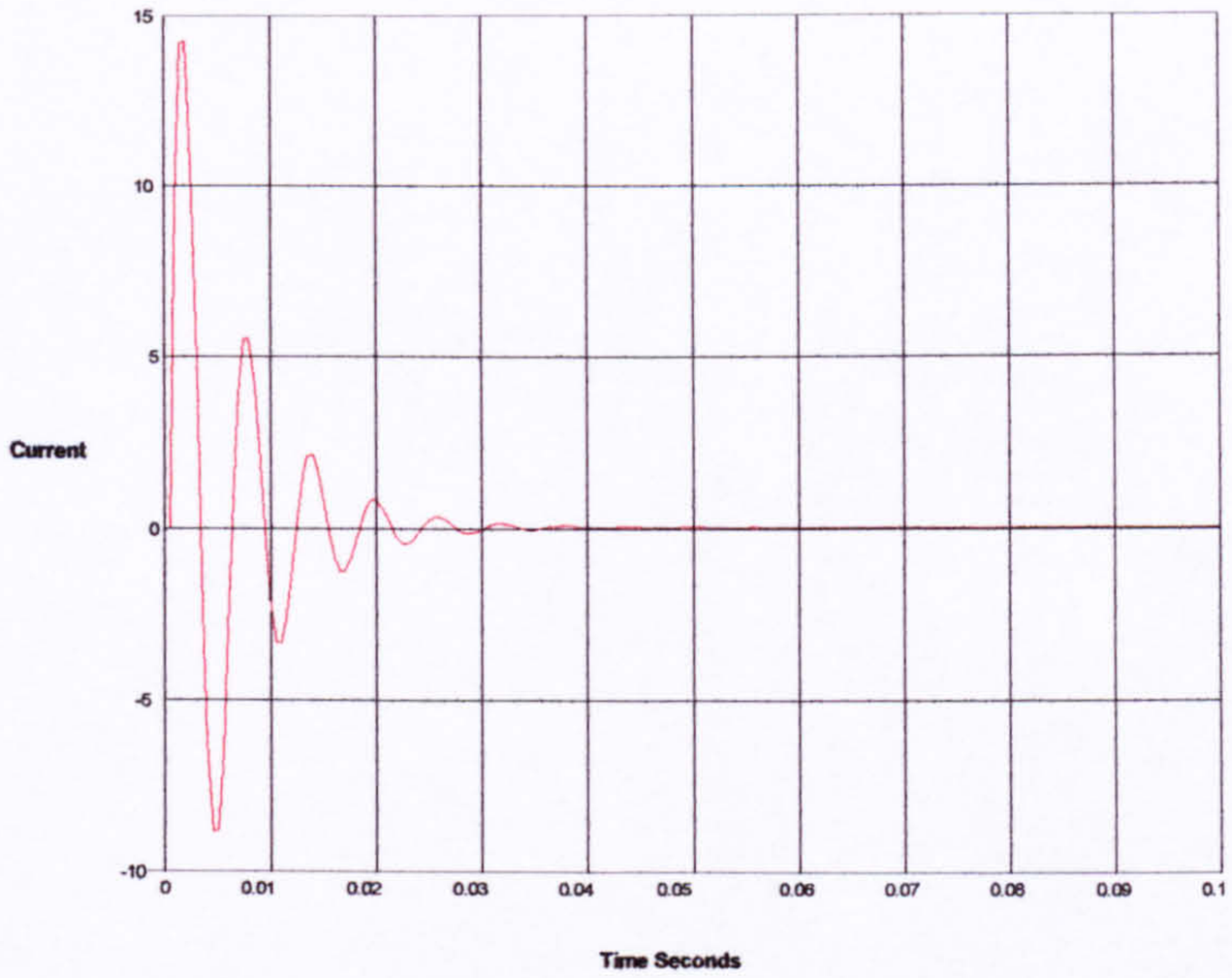

Figure 4.21 Simulated Motor Current at values of K_P=12 and K_I=20000

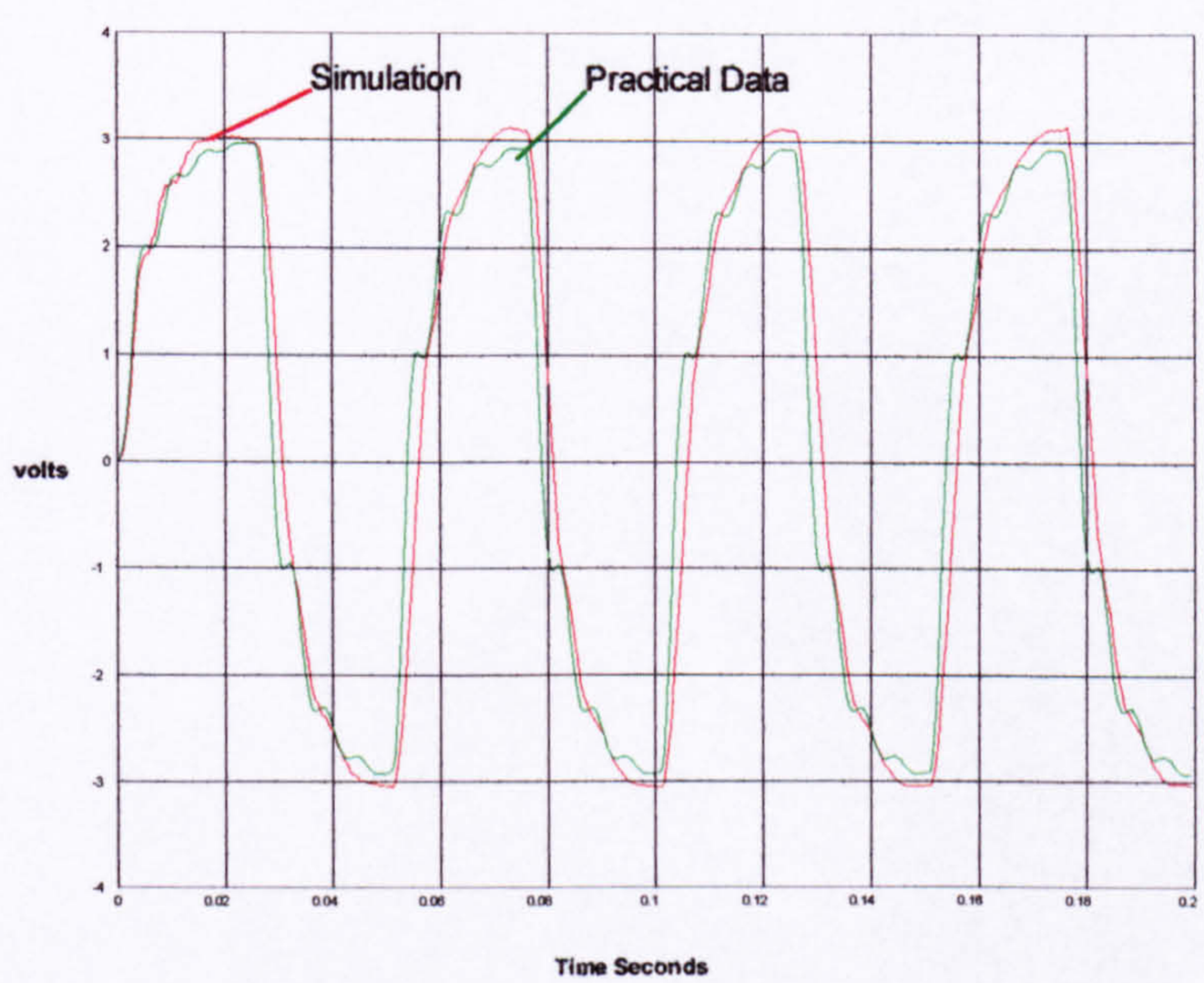

Fig 4.22 Comparing the simulated behaviour with actual behaviour at chosen values of K_P=12 and K_I=20000 of square wave at frequency of 20 Hz

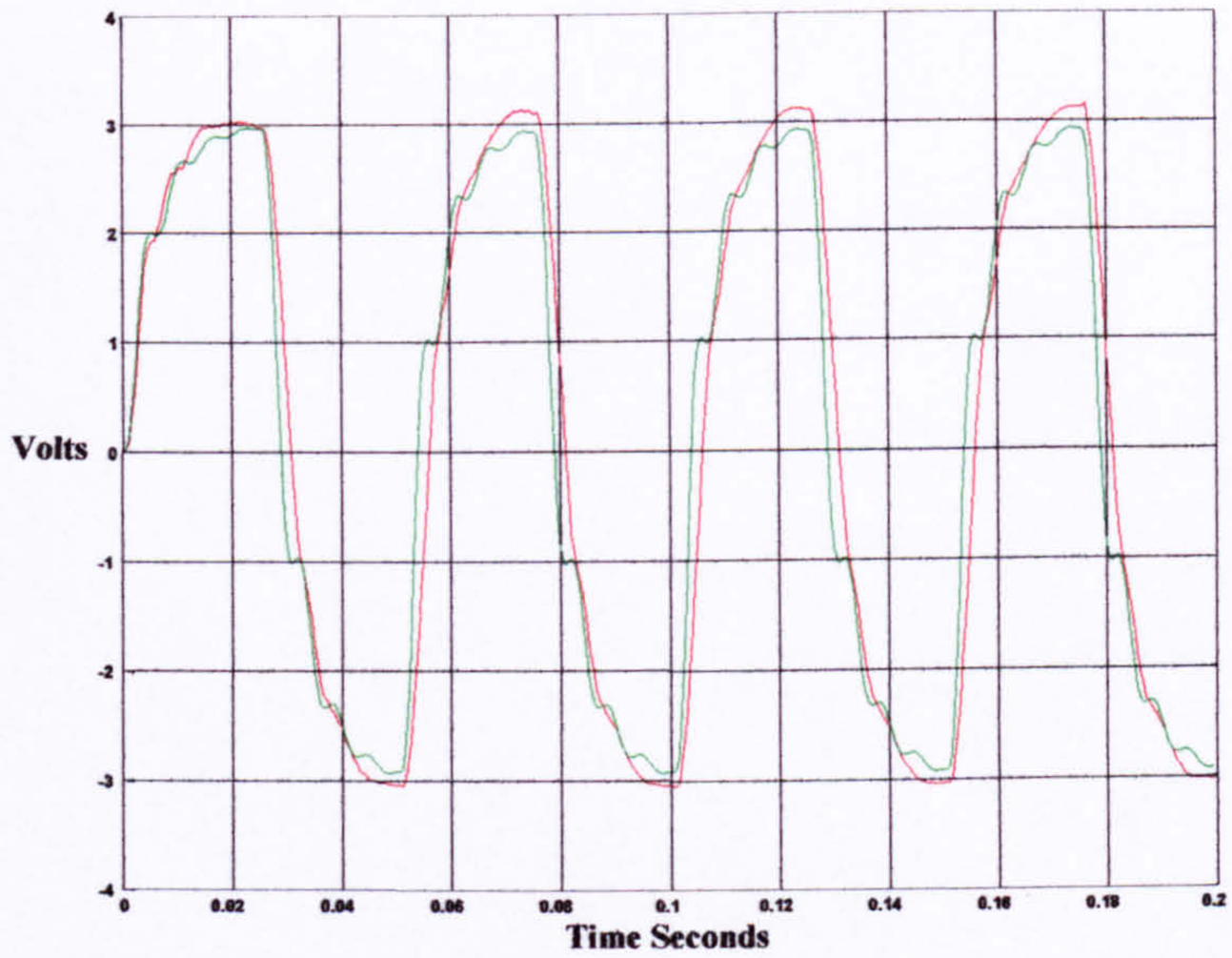

Fig 4.23 Comparing the simulated behaviour with actual behaviour at chosen values of K_P=12 and K_I=20000 of square wave at frequency of 30 Hz

Figure (4.14) shows the comparison for K_p=10 and K_I=15000. This figure shows that although these values capture the general behaviour particularly the overshoot well. However the oscillations which follow are not only out of phase but their amplitude is less than that of the real data. The decay of these oscillations was faster than indicated by the actual system behaviour.

Figure (4.15) shows a higher value of integral gain, K_p=10 K_I=18000. The transition is still captured although now the overshoot is beginning to exceed that shown by the real data. The oscillation amplitude is closer and the phase difference seems to be less than that of the figure (4.14).

Figure (4.16) shows the simulation for K_p=10 and K_I=20000. The amplitude of the simulation exceeds that of the real data while there is no real improvement in phase shift. There is however improvement in the capture of the oscillation decay.

Figure (4.17) shows the simulation when the proportional gain is increased from 10 to 12 and the integral gain is decreased from 20000 to 18000. The amplitude of the simulation dropped. The transition is still captured but the oscillation amplitude is less than that shown by the real data. Hence figure (4.18) kept the proportional gain at 12 and increased the integral gain to 20000. The transition is captured and the oscillation amplitude is also better. The time taken for the oscillations to decay seems to resemble the real data. Further tuning was attempted but no real improvement was noticed. Therefore these values of K_P=12 and K_I=20000 will be taken as the values which are the closest to the real values based on the simulations.

Figure (4.19) shows the comparison between simulation of the model when values of 12 and 20000 for the proportional and integral gains respectively are inserted and real data. The response is clearly satisfactory.

Figures (4.20) and (4.21) show the motor current response and the control signal for the selected proportional and integral values. The control signal is clearly within the capability of the power supply used (30 volts). The current however is higher than that permissible by the continuous current of ± 6 amps and the dynamic current of $\pm$ 10 amps. However the time interval it stays outside the limit is approximately 0.025 seconds.

This may cause motor saturation. If this happens the controller will initiate current limiting, but because it is for such a short time it is unlikely to have a substantial effect on the performance of the system.

To have more confidence in the values of the proportional gain and integral gain, the model derived was simulated and compared to real data for two different frequency square wave inputs. The results are shown in figures (4.22) and (4.23). They indicate that the selected values for the proportional and integral gains gave a close match between the simulation and real data.

4.9 Mathematical Model for the Motor, Motor diver and Gearbox

A model for the motor was derived earlier in this chapter. But that was a simple model which does not take into account the gearbox or load. Starting from the point where that model finished the load effects are considered. It is important to include the load effects because the final system to be modeled has a ball screw arrangement. Adding the gearbox may introduce extra friction or backlash. Therefore considering the load side yields

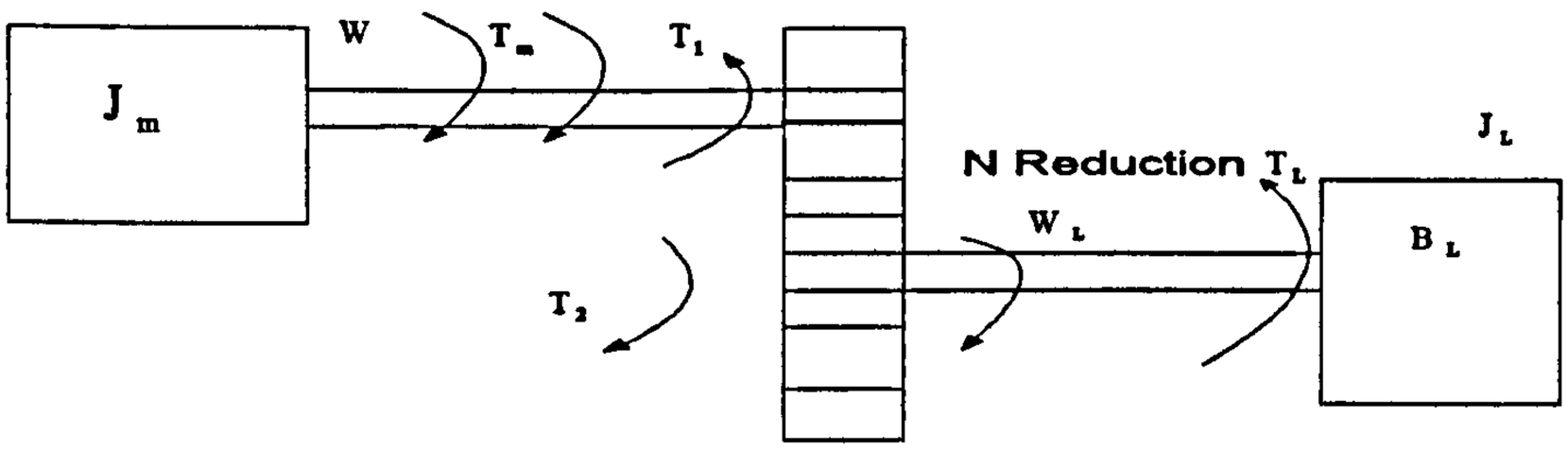

Figure 4.23 Considering the load side

$$T_m = K_t I = J_m \ddot{\theta}_m + B_f \dot{\theta}_m + T_l \qquad \text{equation 4.24}$$

$$T_l = K_t I - J_m \ddot{\theta}_m - B_f \dot{\theta}_m \qquad \text{equation 4.25}$$

$$T_2 = J_L \ddot{\theta}_L + B_L \dot{\theta}_L + T_L \qquad \text{equation 4.26}$$

Writing T_2 in terms of T_l

$$\eta N T_l = T_2 = J_L \ddot{\theta}_L + B_L \dot{\theta}_L + T_L \qquad \text{equation 4.27}$$

Where N = gearbox ratio, η = Efficiency of gearbox, J_L = load inertia, B_L = Load friction, T_L = Load Torque, $\ddot{\theta}_L$ = Angular acceleration of the load

The load inertia J_L was calculated for the gearbox by working out the volume and the density of the material of the gearbox and then using the standard formulae the inertia was calculated.

$$\left(J_m + \frac{J_L}{\eta N^2}\right)\ddot{\theta}_m + \left(B_f + \frac{B_L}{\eta N^2}\right)\dot{\theta}_m = KI - \frac{T_L}{\eta N} \qquad \text{equation 4.28}$$

Introducing the following notations :

J_{eq} = Equivalent Inertia as seen by the motor B_{eq} = Equivalent Friction as seen by the motor

Let $J_{eq} = J_m + \frac{J_L}{\eta N^2}$ $B_{eq} = B_f + \frac{B_L}{\eta N^2}$

Therefore equation (4.28) becomes

$$\dot{W} = -\frac{K_t}{J_{eq}} I - \frac{B_{eq}}{J_{eq}} W - \frac{T_L}{\eta N J_{eq}} \qquad \text{equation 4.29}$$

The next unknown parameter is the total friction in the system (Motor+Driver+Leg) B_{eq}

Input Voltage (Volts)	Motor Current With gearbox (Amps)	Speed in rad/sec With gearbox
1	0.3	70.56
2	0.4	143.56
3	0.5	214.11
4	0.6	284.67
5	0.7	362.53
6	0.8	440.38
7	0.9	506.08
8	1.0	571.78
9	1.05	642.34
10	1.1	715.32

Table 4.5 Summary of results for the motor and gearbox

Previously using the least squares method the friction was estimated for the system without the gearbox. The friction for the same system but with the gearbox added was estimated in the same way. From (table 4.5) the value of B_{eq} is $6.64*10^{-5}$ Nms/rad This clearly indicate that the amount of friction when the motor has the gearbox is approximately 3.5 times more than if the motor is unloaded.

Substituting for $\dot{W}$ in equation 4.4 yields

$$\begin{bmatrix} \dot{I} \\ \dot{W} \end{bmatrix} = \begin{bmatrix} \frac{-R}{L} & \frac{-E_a}{L} \\ \frac{-K}{J_{eq}} & \frac{-B_{eq}}{J_{eq}} \end{bmatrix} \begin{bmatrix} I \\ W \end{bmatrix} + \begin{bmatrix} \frac{1}{L} \\ 0 \end{bmatrix} V_t + \begin{bmatrix} 0 \\ \frac{-1}{\eta N J_{eq}} \end{bmatrix} T_L \qquad \text{equation 4.30}$$

Substituting the values into this equation and putting $T_L = 0$ as there is no load torque

where

$J_m = 85 * 10^{-7} \text{Kgm}^2$ $\quad J_L = 2.118 * 10^{-7} \text{Kgm}^2$ $\quad N = 50$ $\quad \eta = 50\%$

$\therefore$

$J_{eq} = 85.00169 * 10^{-7} \text{Kgm}^2$ $\quad B_{eq} = 6.64 * 10^{-5} \text{Nms/rad}$ $\quad B_f = 2.046 * 10^{-5} \text{Nms/rad}$

$$\begin{bmatrix} \dot{I} \\ \dot{W} \end{bmatrix} = \begin{bmatrix} -2520 & -76.4 \\ 4494.028 & -7.811 \end{bmatrix} \begin{bmatrix} I \\ W \end{bmatrix} + \begin{bmatrix} 2000 \\ 0 \end{bmatrix} V_t \qquad \text{equation 4.31}$$

Now Let

$$A = \begin{bmatrix} -2520 & -76.4 \\ 4494.028 & -7.811 \end{bmatrix} \qquad B = \begin{bmatrix} 2000 \\ 0 \end{bmatrix} \qquad \text{equation 4.32}$$

Now considering the effect of the motor driver unit as derived earlier equation 4.12

$$\begin{bmatrix} \dot{I} \\ \dot{W} \\ \dot{Z} \end{bmatrix} = \left(\begin{bmatrix} A & 0 \\ -[0 \quad H_3] & 0 \end{bmatrix} - \begin{bmatrix} 0 & BK_P H_3 & -BK_I \\ 0 & 0 & 0 \end{bmatrix} \begin{bmatrix} I \\ W \\ Z \end{bmatrix} + \begin{bmatrix} BK_P \\ 1 \end{bmatrix} V_{ref} \right)$$

Substituting in the values gives

$$\begin{bmatrix} \dot{I} \\ \dot{W} \\ \dot{Z} \end{bmatrix} = \begin{bmatrix} -2520 & (-76.4-(2000K_pH_3)) & 2000K_I \\ 4494.028 & -7.811 & 0 \\ 0 & -H_3 & 0 \end{bmatrix} \begin{bmatrix} I \\ W \\ Z \end{bmatrix} + \begin{bmatrix} 2000K_P \\ 0 \\ 1 \end{bmatrix} V_{ref}$$

Therefore the loaded model with all the values of the DC, Proportional and Integral gains substituted becomes.

$$\begin{bmatrix} \dot{I} \\ \dot{W} \\ \dot{Z} \end{bmatrix} = \begin{bmatrix} -2520 & -405.2 & 40*10^6 \\ 4494.028 & -7.811 & 0 \\ 0 & -0.0137 & 0 \end{bmatrix} \begin{bmatrix} I \\ W \\ Z \end{bmatrix} + \begin{bmatrix} 24000 \\ 0 \\ 1 \end{bmatrix} V_{ref} \qquad \text{equation 4.33}$$

Now let

$$A = \begin{bmatrix} -2520 & -405.2 & 40*10^6 \\ 4494.028 & -7.811 & 0 \\ 0 & -0.0137 & 0 \end{bmatrix} \qquad B = \begin{bmatrix} 24000 \\ 0 \\ 1 \end{bmatrix}$$

In order to compare the theoretical models and the real behaviour the above model has to be discretized at 10 ms and using Matlab simulation was carried out.

Let

$$X = [I\ W\ Z]^T$$

$$X((K+1)T) = e^{AT}X(KT) + \int_0^T e^{A(T-s)}B\,ds\ V_{ref}(KT)$$

$$= e^{AT}X(KT) + B\int_0^T e^{As}\,ds\ V_{ref}(KT) \qquad \text{equation 4.34}$$

Working out the integratio n part first yields

$$B\int_0^T\left(I + As + \frac{A^2s^2}{2*1} + ...\right)ds$$

$$= \left[Bs + B\frac{As^2}{2} + B\frac{A^3s^3}{3*2!}\right]_0^T$$

Therefore the whole equation yields

$$= e^{AT}X(KT) + \left[Bs + B\frac{As^2}{2} + B\frac{A^3s^3}{3*2!}\right]_0^T + ... \qquad \text{equation 4.35}$$

Where

$$Ad = e^{AT} = I + AT + \frac{A^2T^2}{2} + \frac{A^3T^3}{3*2!} \qquad Bd = \left[Bs + B\frac{As^2}{2} + B\frac{A^3s^3}{3*2!}\right] + ... \qquad \text{equation 4.36}$$

Working out the above yields

$$Ad = \begin{bmatrix} 0.0005 & 0.0004 & -20.0808 \\ -0.0022 & -0.0008 & -50.7385 \\ 0.0000 & 0.0000 & -0.0013 \end{bmatrix} \qquad Bd = \begin{bmatrix} 0.1037 \\ 73.0574 \\ 0.0001 \end{bmatrix}$$

A theoretical model has been derived. The model was discretized and simulation using Matlab was carried out in order to establish the fidelity of this model. Comparison of the theoretical model with the practical data is shown in figure (4.24).

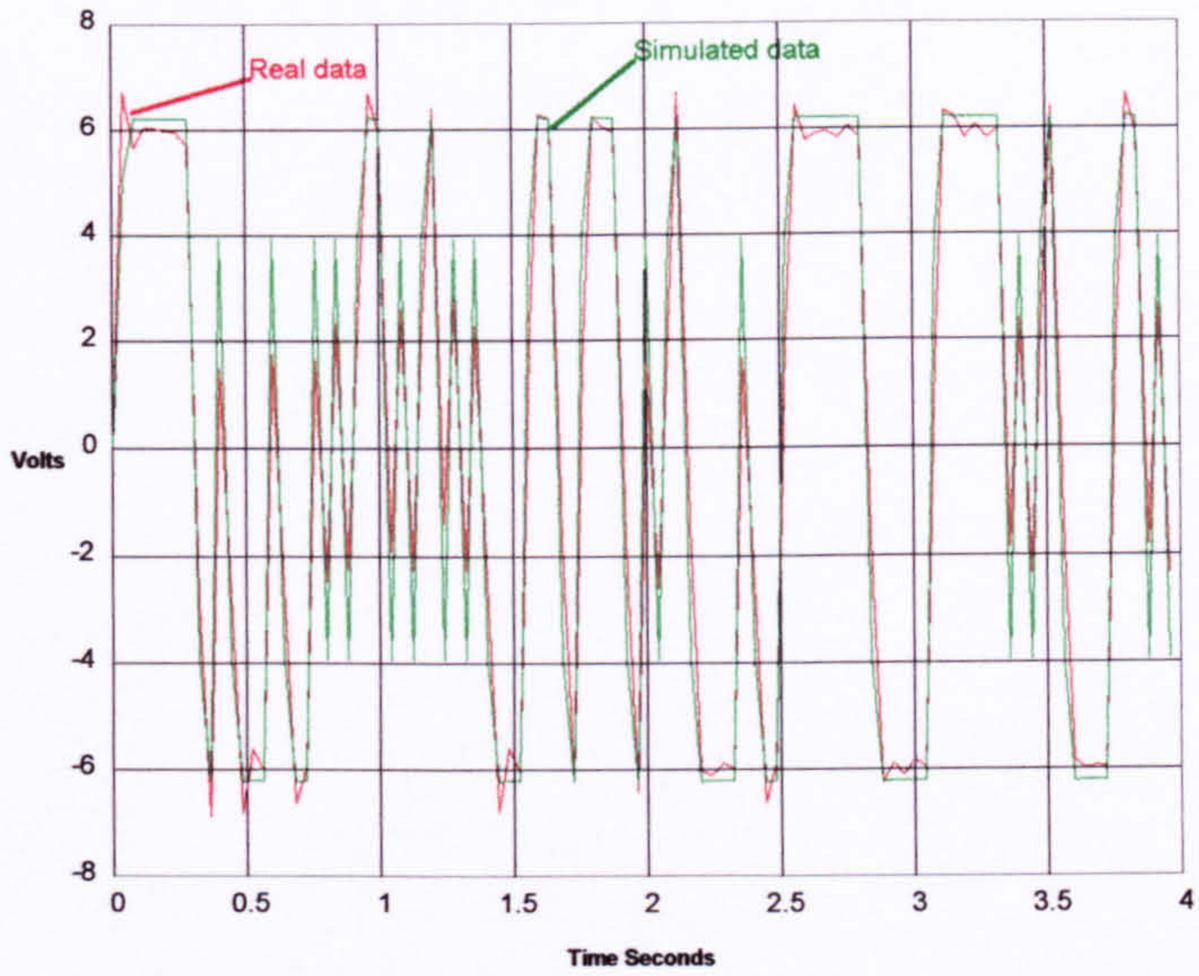

Figure 4.24 Velocity comparison between real data and simulated data for both models

The poles, zeros and DC gain of the above model are as follows

poles location → [-0.0008 + 0.0012i,-0.0008 - 0.0012i,0.000]
zeros location → [-0.0086,0.000]
DC gain → 0.90

Figure (4.24) shows that the fidelity of the theoretical model has not been completely validated. The simulated response at some instances is considerably different to that of the practical data. Between the time interval of 0.3-0.7 seconds of figure (4.24) the theoretical model predicts a larger velocity than that of the real data. The same behaviour is exhibited between 1-1.5 seconds.

4.10 Friction and Inertia Estimation

In order to estimate friction and inertia similar approach as in the derivation of the model for the motor and driver was used. First a theoretical model was obtained then experimental data was collected and finally the parameters of the model are adjusted to match simulations with the real data. The leg was allowed to swing freely by tilting the Orthosis so that the leg would be at mid point, then the leg was pulled to one side and released to swing freely. Using Matlab and the C program in appendix (A) data was collected and was used as the reference signal. The model of the leg (resembled a pendulum) was worked out and simulations were carried out until the response was close to the experimental data.

4.11 System modelling

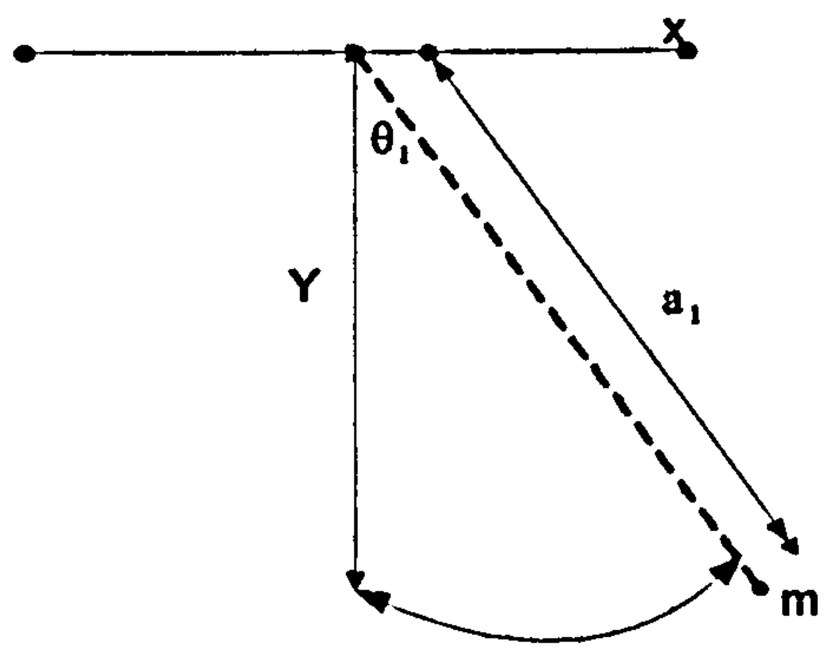

Figure 4.25 Friction estimation for the Orthosis leg

In order to analyse a dynamic system, an accurate mathemetical model that describes the system compllletely must be determined. The derivation of such models can be based on the fact that the dynamic system can be completely described by known differential

equations or by experimental methods such as input,output data based identification methods(chapt 5).

In electrical circuits Kirchofs laws are used for writing the differential equations of electrical networks and Newton's laws are used for writing the equations of motion of mechanical systems. In real applications there are complex systems which contain a combination of electrical and mechanical components. The use of Lagranges equation provides a systematic unified approach for handling a broad class of physical systems.

Lagranges equation is given by:-

$$Q_n = \frac{d}{dt}\left\{\frac{dT}{d\dot{\theta}_i}\right\} - \frac{dT}{d\theta_i} + \frac{dV}{d\theta_i} + \frac{dD}{d\dot{\theta}_i}$$

Where

Q_n = External Torques T = Kinetic energy terms V = Potential energy terms

D = Dissipated Energy terms (due to friction).

The total Kinetic energy includes all energy regardless of whether the are electrical or mechanical. The dissipation function D represents one half of the rate at which energy is dissipated as heat. This usually as a result of friction or resistance. The forcing functions applied to a system take the form of externally applied forces or torques in mechanical systems or voltages and currents in electrical ones

For the system to be modelled (figure 4.25) the kinetic energy, potential energy, dissipated energy are given by: -

$$T = \frac{1}{2} J_1 \dot{\theta}_1^2 + \frac{1}{2} m \left(a_1^2 \dot{\theta}_1^2 \right) \qquad \text{equation 4.37}$$

$$V = mg\theta_1 \qquad \text{equation 4.38}$$

$$D = \frac{1}{2} C_1 \dot{\theta}_1^2 \qquad \text{equation 4.39}$$

Applying Lagrange to the above equations yields: -

Taking the first component $\frac{d}{dt}\left\{\frac{dT}{d\dot{\theta}_i}\right\}$

$$\frac{dT}{d\dot{\theta}_1} = J_1 \dot{\theta}_1 + m\left(a_1^2 \dot{\theta}_1\right)$$

Where

a_1 = Dis tan ce to the centre of gravity J_1 = Leg Inertia m = Leg mass

θ_1 = Angle the leg moves $\dot{\theta}_1$ = angular velocity

$$\frac{d}{dt}\left\{\frac{dT}{d\dot{\theta}_i}\right\} = J_1 \ddot{\theta}_1 + m\, a_1^2 \ddot{\theta}_1 \qquad \text{equation 4.40}$$

Taking the second component $-\frac{dT}{d\theta_1}$:-

$$-\frac{dT}{d\theta_1} = 0 \text{ (As there is no } \theta_1 \text{ in T)} \qquad \text{equation 4.41}$$

Now considering the third component $\frac{dV}{d\theta_1}$

$$V = mg\,y_1 = -mg\,a_1\cos\theta_1$$

Taking the third component (Potential energy)

$$\frac{dV}{d\theta_1} = mg\,a_1\sin\theta_1$$

But for all small angles $\sin\theta_1 = \theta_1$ and taking this approximation gives

$\therefore$

$$\frac{dV}{d\theta_1} = mg\,a_1\theta_1 \qquad \text{equation 4.42}$$

Now Considering the fourth component (dissipated energy)

$$D = \frac{1}{2}C_1\dot{\theta}_1^2 \quad \Rightarrow \frac{dD}{d\dot{\theta}_1} = C_1\dot{\theta}_1 \qquad \text{equation 4.43}$$

$\therefore$

$$T_1 = J_1\ddot{\theta}_1 + ma_1{}^2\ddot{\theta}_1 + mga_1\theta_1 + C_1\dot{\theta}_1$$

$$= \left(J_1 + ma_1{}^2\right)\ddot{\theta}_1 + mga_1\theta_1 + C_1\dot{\theta}_1$$

Now let $M = (J_1 + ma_1^2)$, $N = C_1$ and $P = mga_1$

$\therefore$

$$Q_n = M[\ddot{\theta}_1] + N[\dot{\theta}_1] + P[\theta_1]$$

$$M[\ddot{\theta}_1] = Q_n - N[\dot{\theta}_1] - P[\theta_1]$$

$\therefore$

$$[\ddot{\theta}_1] = -M^{-1}N[\dot{\theta}_1] - M^{-1}P[\theta_1] + M^{-1}Q_n$$

Putting in state space representation

$$\begin{bmatrix}\dot{\theta}_1 \\ \ddot{\theta}_1\end{bmatrix} = \begin{bmatrix}0 & 1 \\ -M^{-1}P & -M^{-1}N\end{bmatrix}\begin{bmatrix}\theta_1 \\ \dot{\theta}_1\end{bmatrix} + \begin{bmatrix}0 \\ M^{-1}\end{bmatrix}Q_n \qquad \text{equation 4.44}$$

Substituting in the Parameters

$m = 3Kg + \text{weight of artificial leg}(10Kg) = 13Kg$

$a_1 = \text{distance from reference to centre of gravity} = 0.73m$

$g = \text{gravity} = 9.81\,m/sec^2$

$J_1 = 0.849Kgm^2$ (estimated, taking the leg as a cylinder)

$C_1 = \text{Unknown Nms/rad}$

$M = [0.849 + 6.94]$ $M = [7.79]$ $M^{-1} = [0.128]$

$N = [0.283]$ $P = [93.10]$

$$\therefore$$

$$\begin{bmatrix}\dot{\theta}_1\\ \ddot{\theta}_1\end{bmatrix}=\begin{bmatrix}0 & 1\\ -11.90 & -0.05\end{bmatrix}\begin{bmatrix}\theta_1\\ \dot{\theta}_1\end{bmatrix}+\begin{bmatrix}0\\ 0.128\end{bmatrix}Q_n \qquad \text{equation 4.45}$$

Now let our model for simulation be

$$a_m=\begin{bmatrix}0 & 1\\ -11.9 & -0.05\end{bmatrix} \quad b_m=\begin{bmatrix}0\\ 0.128\end{bmatrix} \qquad \text{equation 4.46}$$

There are two initial conditions for this system. That is the angular velocity and the angular position. The angular velocity in this case is zero as the test will be starting from a stationary position. However the angular position is not zero as the test is starting at an angle. There are two ways in calculating this parameter, the first is by reading the value of the potentiometer (RS, $\pm 20\,K\Omega$) which is located at the hip joint of the Orthosis when it is upright. That is there is no real angle but the pot reading may not be zero. The pot is then read again when the leg is pulled back to the starting position. These two values are then subtracted from each other and divided by the pot gain yielding angular position.

The second method is to use MATLAB. That is done by collecting experimental data i.e. collecting data when swinging the leg. Then finding the point from the graph where the swing begins. Subtract from that the mean of the signal then divide by the pot gain.

Once all the parameters are found the simulation was carried out and the values of inertia and friction were varied till the simulation matched the practical data as shown in figure (4.26)

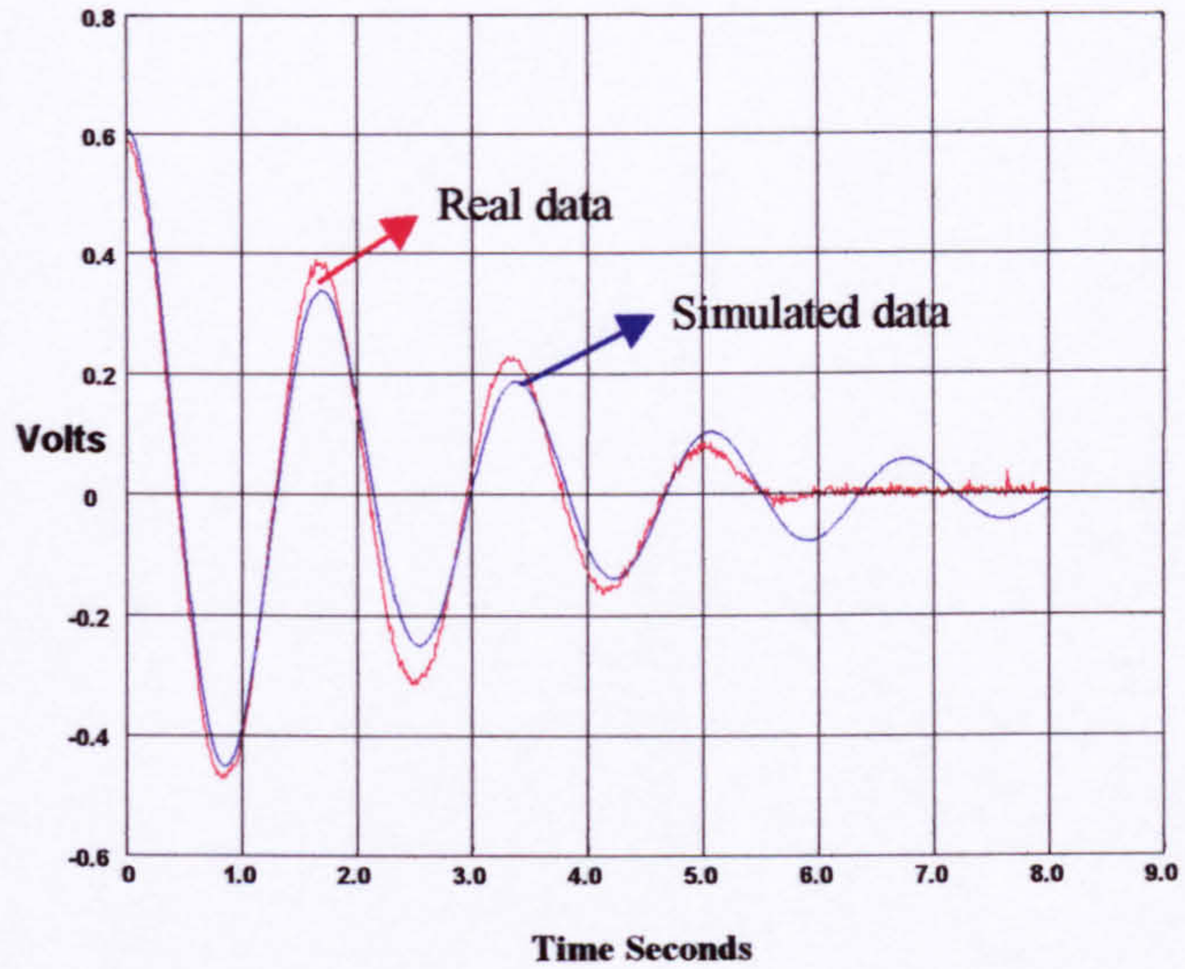

Figure 4.26 Comparison of theoretical simulations with real data of the leg motion after model parameters were adjusted

For consistency the sampling time used was 10 milliseconds. This sampling time is the same as the sampling time used when the integral and proportional gains were derived. Simulation and practical data were compared to see if they were in phase or not. The parameters of the model were varied till the envelope corresponding to the decay of the sine wave was approximately the same as the practical data for the first five seconds. After that time interval non-linear effects (Stiction) become important. Varying the inertia value effects the frequency of the oscillation. This value was varied till a match with the practical data was obtained. Varying the friction effects the amplitude of the signal and the rate it decays. This was also done by varying the value till there was a match between the simulation and practical data as shown in figure (4.26). Closer

inspection of the graph shows the decay of practical data is not linear towards the end. This indicates that there is some non linear friction in the system (Stiction).

Figure (4.26) shows a good comparison of the simulated inertia and friction values and the actual friction value. The model, which gave the simulations in figure (4.26), was

$$a_m = \begin{bmatrix} 0 & 1 \\ -14.5 & -0.7 \end{bmatrix} \qquad b_m = \begin{bmatrix} 0 \\ 0.12 \end{bmatrix} \qquad \text{equation 4.47}$$

This model which gave a good estimation of the friction is considerably different than the theoretical model. This shows that the friction and inertia of the system have been greatly underestimated. The inertia and friction coefficients derived by this estimation will now be used for any further work. From the identified model we can now find the true values of friction and inertia. The experimental response also shows that non linear friction (Stiction) actually exists. This is shown by the sudden decay of the collected data at the

$$\left(J_1 + ma_1^2\right)^{-1} P = 14.5 \qquad \text{equation 4.48}$$

This expression gives a value of $1.77\ \text{Kgm}^2$ for the inertia

$$\left(J_1 + ma_1^2\right)^{-1} C_1 = 0.7\text{Nms/rad} \qquad \text{equation 4.49}$$

This expression gives avalue of 4.73 for friction
end.

Because of the linearization carried out the model would be accurate for small angles approximately up to 30 degrees

4.12 Evaluating the Motor Performance

Before the motor can be mounted to the Orthosis and software developed to control the motor, the performance of the motor has to be evaluated. The practical characteristics have to be compared to the theoretical characteristics and to confirm the manufacturer's claims that it behaves like a Permanent magnet Dc motor.

The first test was to verify the torque capability of the motor when it is loaded and when there is no load. An experiment was set up where the unloaded and loaded (with the gearbox) motor was run at various speeds and the corresponding currents were recorded. These values are shown in tables (4.4) and (4.5). From that data the motor torque is calculated by multiplying the currents with the torque constant and the estimated torque which was calculated by multiplying the viscous friction values with the speed, were recorded and compared with the practical ones. The results are shown in table (4.6)

Reference Voltage	loaded Motor Torque Nm	Estimated Torque arising from Viscous friction (loaded) Nm	Unloaded Motor Torque Nm	Estimated Torque arising from Viscous friction (Unloaded) Nm
1	0.0115	0.0047	0.0053	0.0014
2	0.0153	0.0095	0.0061	0.0029
3	0.0191	0.0142	0.0073	0.0044
4	0.0229	0.0189	0.0076	0.0059
5	0.0267	0.0241	0.0080	0.0074
6	0.0306	0.0292	0.0092	0.0089
7	0.0344	0.0336	0.0103	0.0105
8	0.0382	0.380	0.0115	0.0118
9	0.0401	0.0427	0.0122	0.0133
10	0.0420	0.0475	0.0130	0.0147

Table 4.6 Summary of Results for Unloaded and Loaded Motor

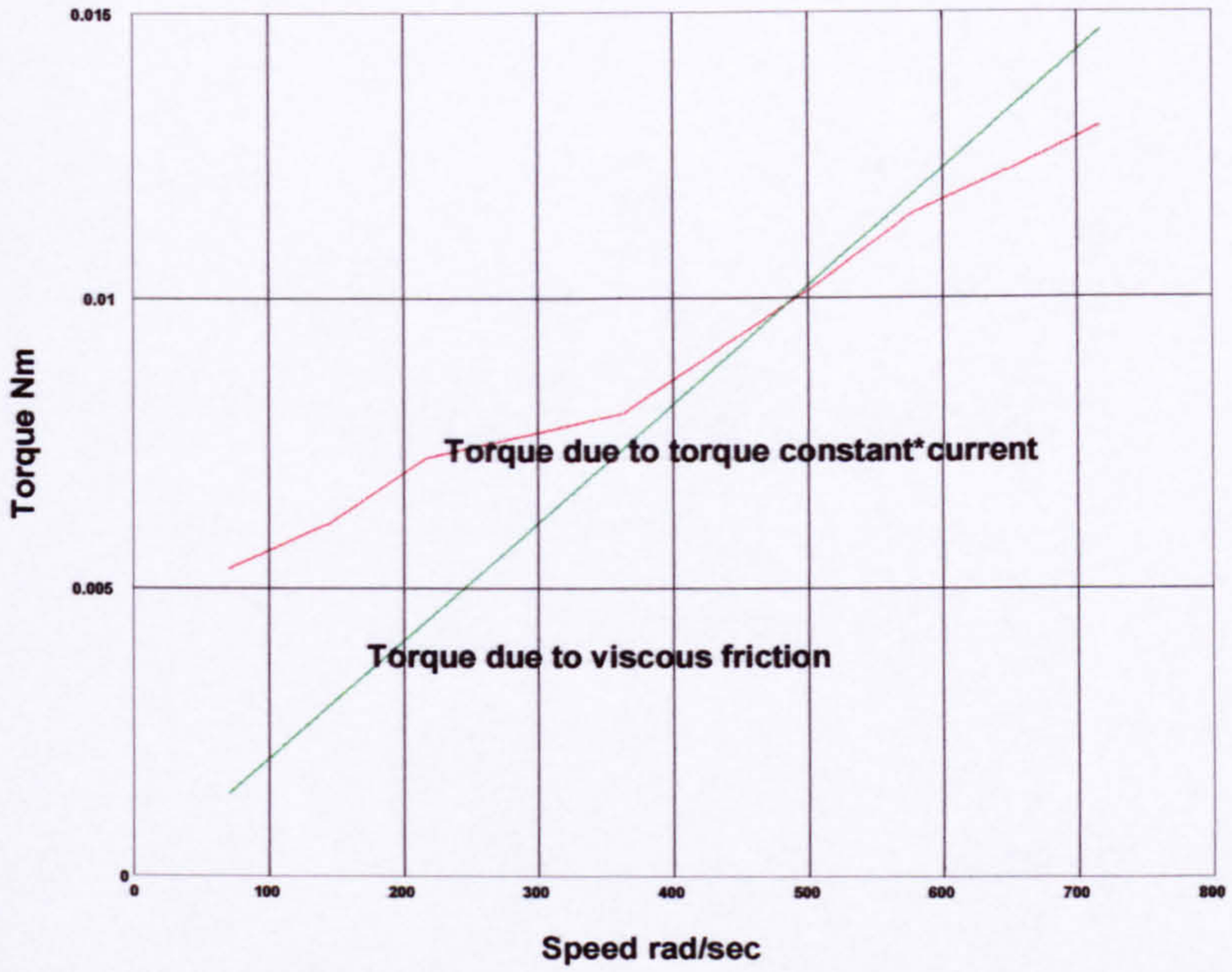

Figure 4.27 Viscous Torque and Torque (torque constant*current) Speed characteristics for unloaded motor

Figure 4.27b Viscous Torque and Torque (torque constant*current) Speed characteristics for motor with gearbox

Table (4.6) shows a good comparison between the theoretical and practical values of torque giving us confidence in the value of friction when the motor is unloaded. Closer inspection of table (4.6) and figure (4.27) shows clearly that at low values of reference voltages or speeds the torque calculated using the torque constant is not close to the torque calculated using estimated viscous friction values. In fact at the lowest speed the torque due to viscous friction is three times less than that of the torque using the torque constant.

An experiment was set up to evaluate the speed of the motor at various torques.

A tacho was mounted at one end of the motor shaft and the end coupled to the Dynamometer through a 50:1 gearbox as shown below. Details of equipment are given in appendix (F)

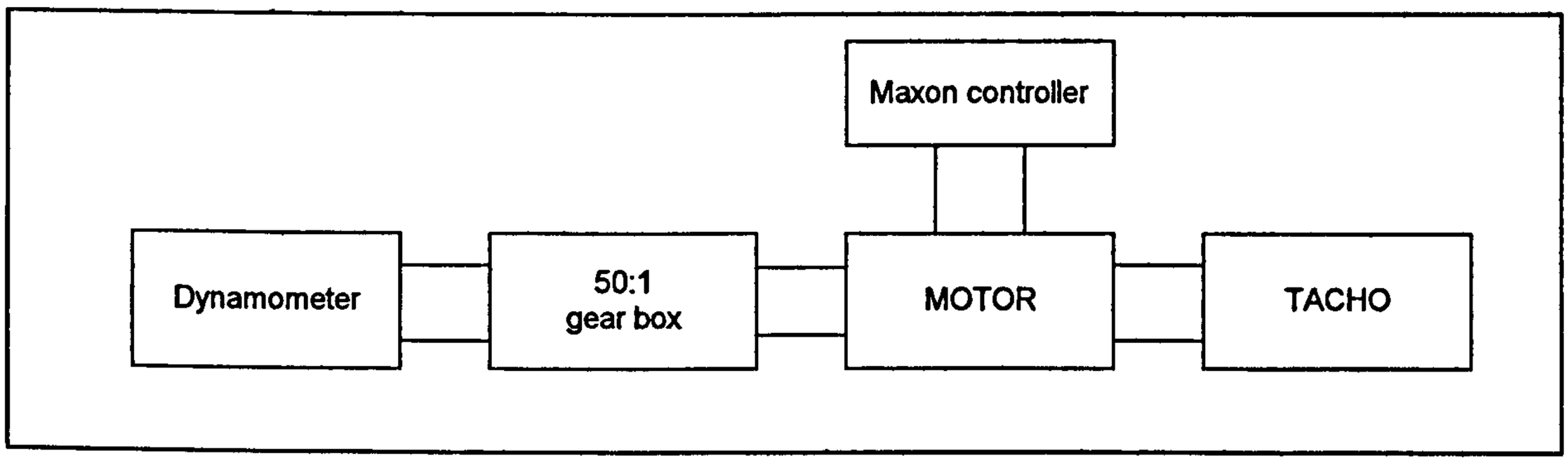

Figure 4.28 Experimental set up for Current, Torque and Speed Evaluation

This set up enabled us to measure the speed and torque simultaneously. The gearbox was used because this would provide information that is more relevant to the real set up on the Orthosis, which uses a ball screw arrangement. The current was also monitored to insure the motor was operating within the safe limit. The torque was gradually increased noting down the corresponding currents and speeds. This experiment was repeated for several different input voltages. The results were recorded and corresponding graphs drawn. The experiment was carried out using the 4-Q driver. So the results are for the motor with the driver (PI controller).

All the following results were recorded for the four-quadrant driver.

Experiment1: input voltage=10volts (4-Q Driver)

TORQUES Nm	Tacho Output (Volts) Speed*gearbox ratio	CURRENTS amps	W=Vt/Kt rad/sec
0	0.59*50=29.5	0.85	718
0.1	0.59*50=29.5	0.9	718
0.2	0.59*50=29.5	1.45	718
0.3	0.59*50=29.5	2.00	718
0.4	0.59*50=29.5	2.6	718
0.5	0.59*50=29.5	3.0	718

Table 4.7 Summary of results at 10 volts

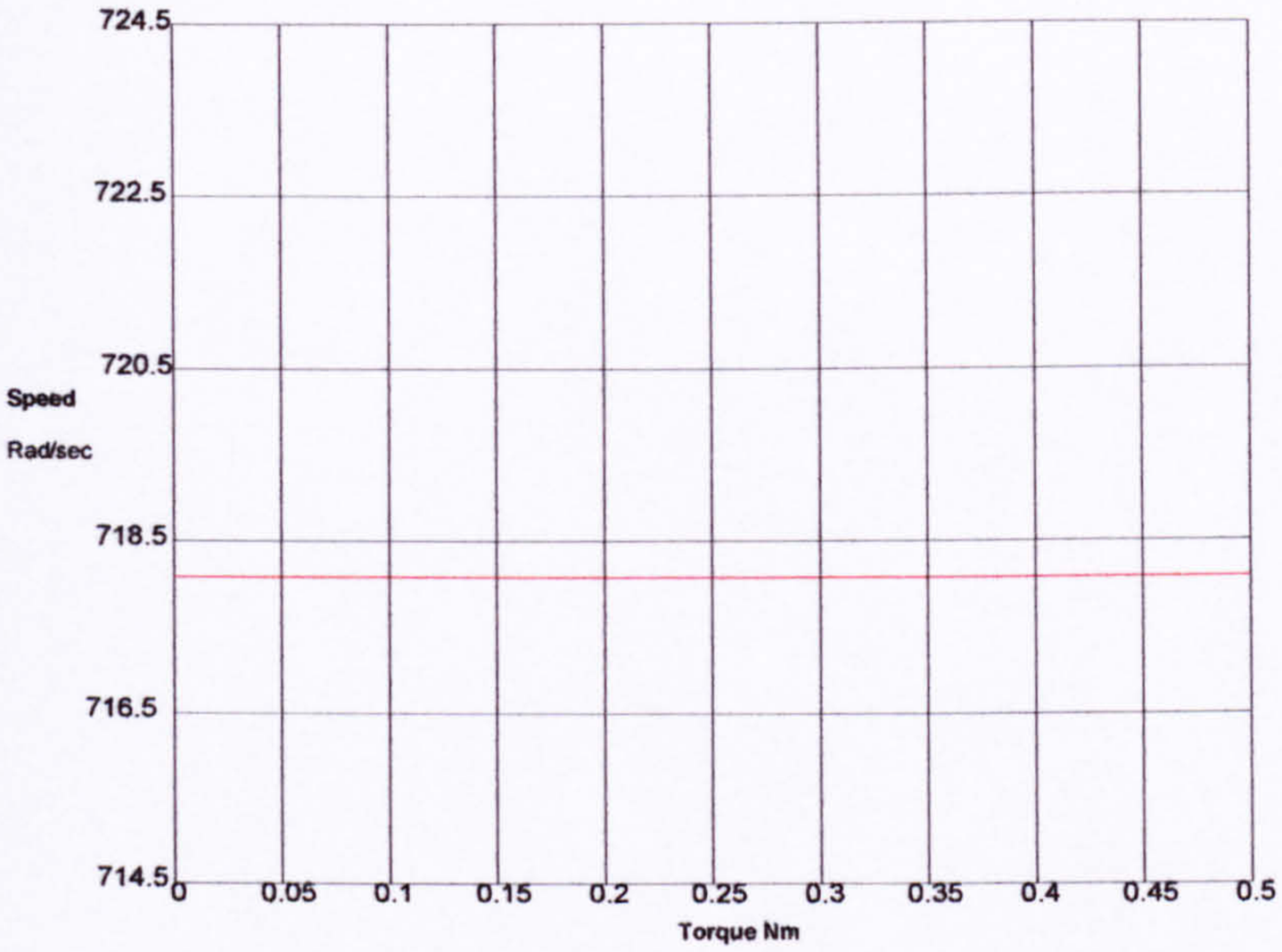

Figure 4.29 Effect on speed when torque is increased

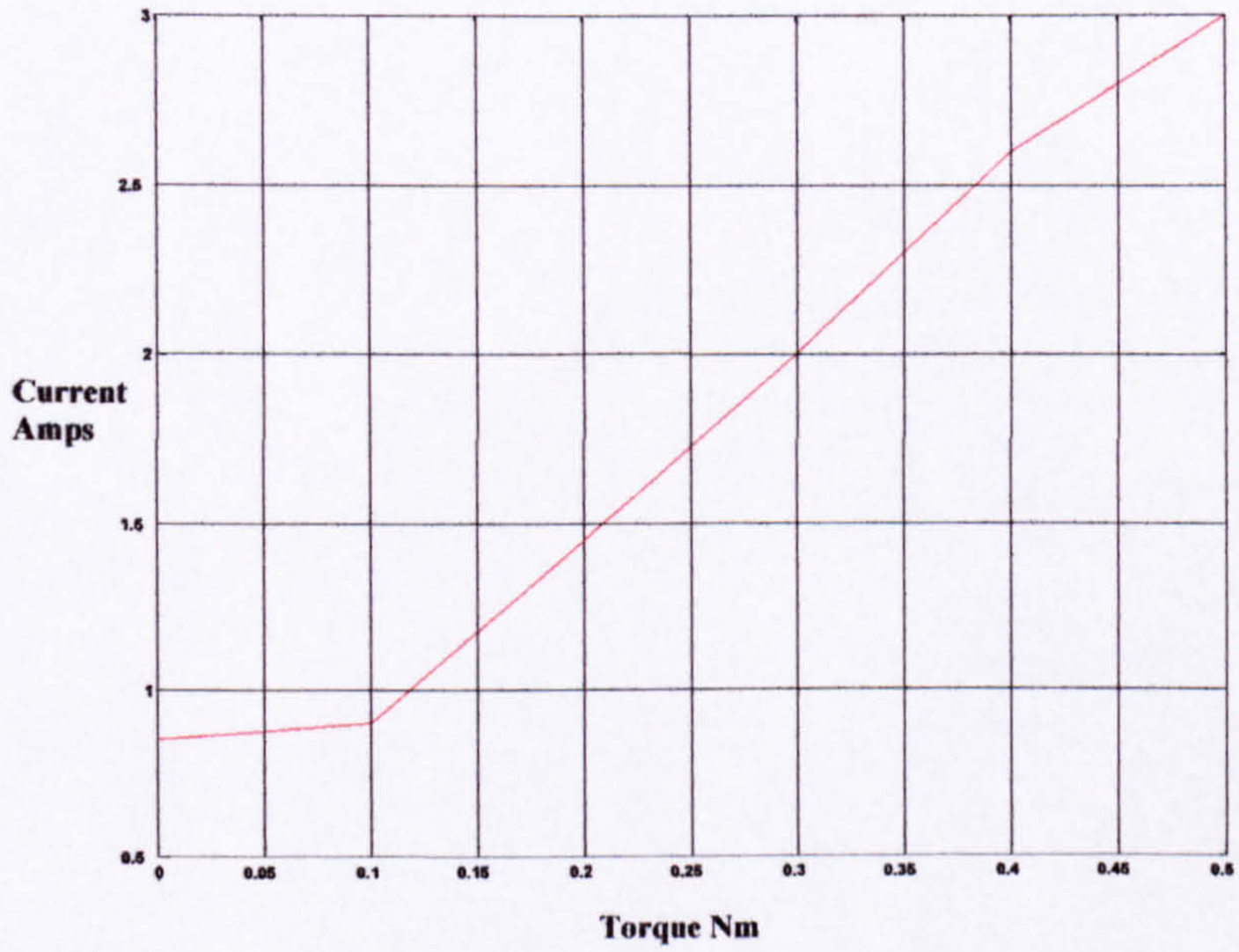

Figure 4.30 Effect on current when torque is increased

Experiment 2: input voltage = 5volts

TORQUE N/m	TACHO OUTPUT VOLTS	CURRENTS Amps	W =Vt/Kt Rad/sec
0	0.30*50=15.0	0.6	364.9
0.2	0.30*50=15.0	0.96	364.9
0.3	0.30*50=15.0	1.25	364.9
0.5	0.30*50=15.0	1.7	364.9
0.7	0.30*50=15.0	1.92	364.9

Table 4.8 Summary of all results at 5 volts

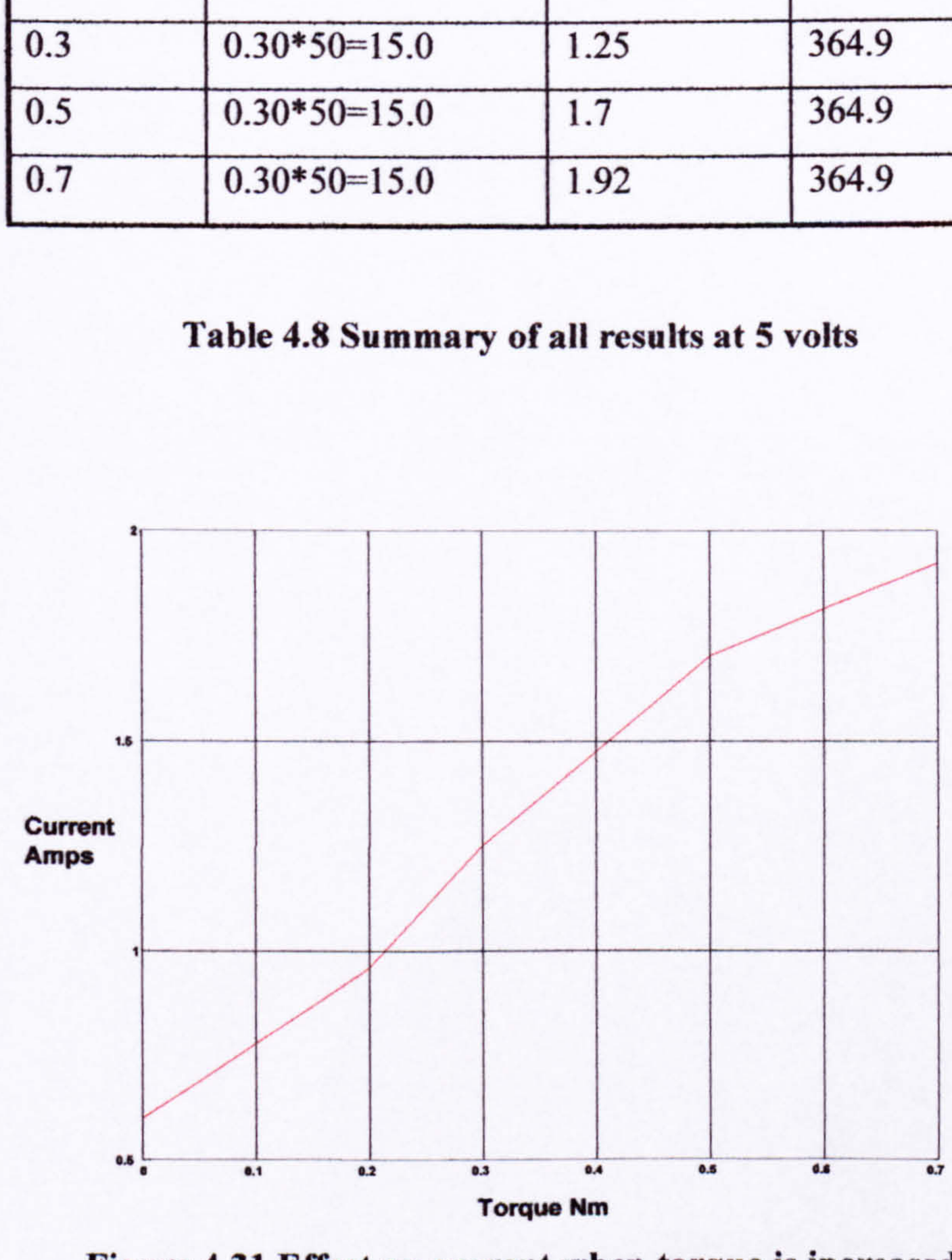

Figure 4.31 Effect on current when torque is increased

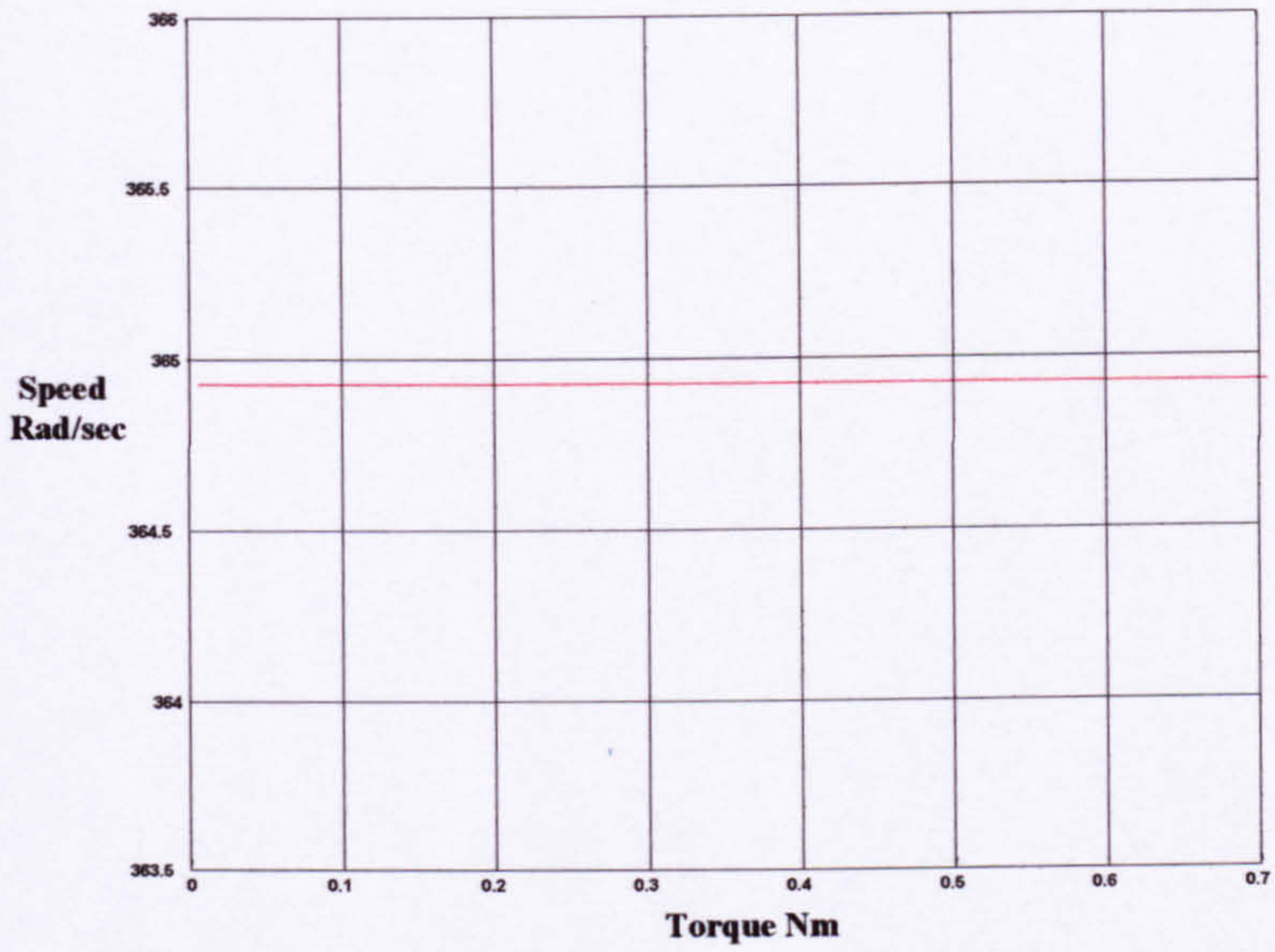

Figure 4.32 Effect on speed when torque is increased

Experiment3: input voltage = 2volts

TORQUE N/m	TACHO OUT PUT VOLTS	CURRENTS Amps	W=Vt/Kt Rad/sec
0	0.12*50=6	0.38	146.0
0.1	0.12*50=6	0.4	146.0
0.2	0.12*50=6	0.68	146.0
0.3	0.12*50=6	0.88	146.0
0.4	0.12*50=6	1.0	146.0
0.5	0.12*50=6	1.2	146.0

Table 4.9 Summary of results at 2 volt

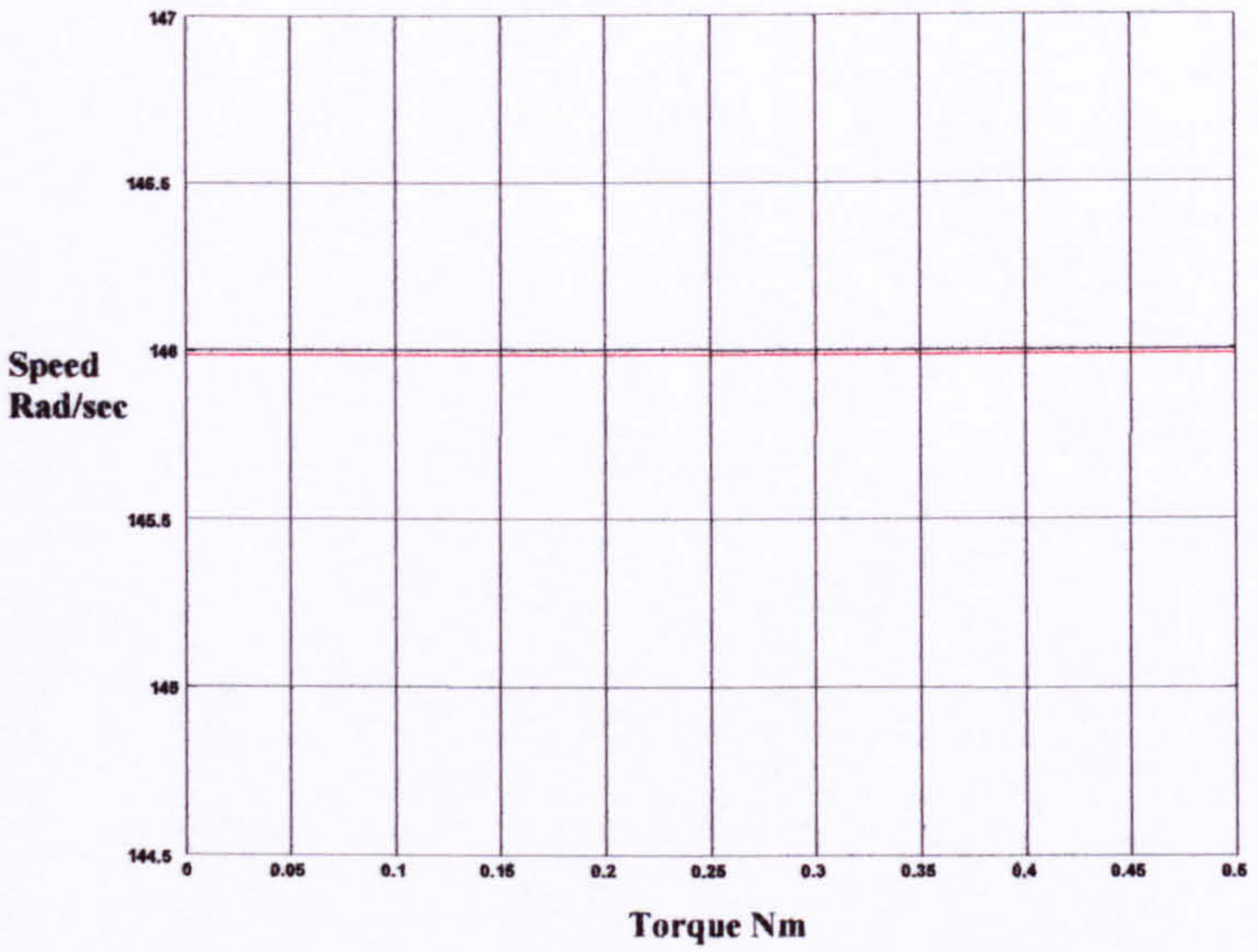

Figure 4.33 Effect on speed when torque is increased

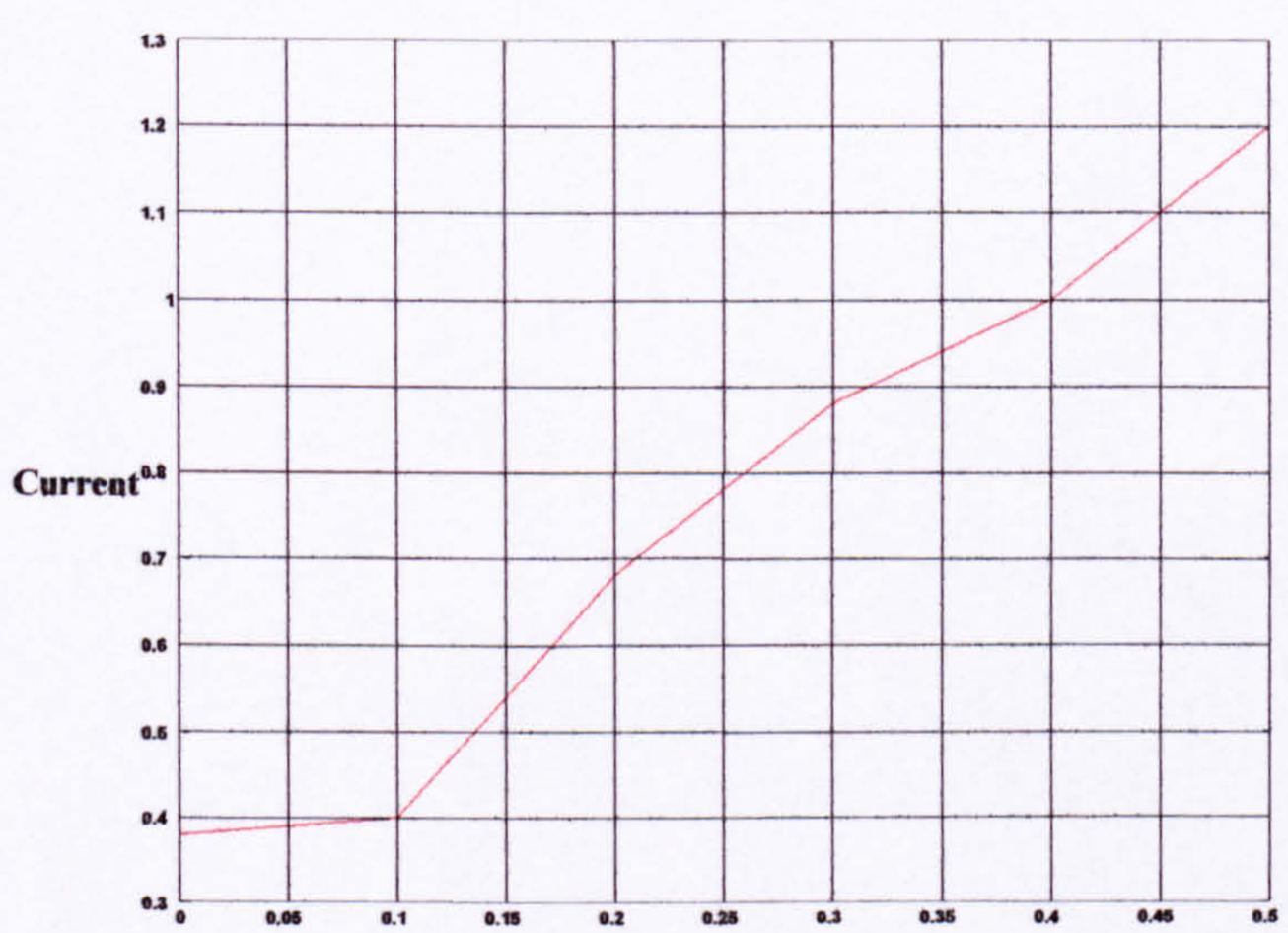

Figure 4.34 Effect on current as torque is increased

Figures (4.29)-(4.34) show the speed-torque, current torque and tacho voltage-torque characteristics of the motor at the gearbox output shaft. The gearbox used has a ratio of 50:1.

Looking at tables (4.7)-(4.9) and figures (4.29)-(4.34), it could be seen that the Maxon 4-quadrant controller with integral and proportional gain is a very good speed controller. Despite increasing the load resistance in the dynamometer i.e. increasing the load torque, the speed is maintained exactly. The current is slowly increasing as the torque is increased. This was expected as the Maxon motor driver use a PI controller which means that the integral gain produces a current increase in order to compensate for the increase in load thus maintaining a relatively constant speed.

Closer inspection of the first value in tables (4.7)-(4.9) shows that the current for unloaded motor seems to be higher than expected. The theoretical value for unloaded current is approximately 150 mA. This is an indication that before even applying a load torque or just by adding the gearbox and the coupling to the system extra friction has been introduced. Comparing the currents at 10 volts, 5 volts and 2 volts from table (4.4) and the first values from tables (4.7)-(4.9) clearly shows an increase in current. These values are compared because these are the points with no load torque applied but with the gearbox and dynamometer coupled to the motor.

Figures (4.29), (4.32) and (4.33) clearly show how well the speed control is maintained for a range of input voltages. Figures (4.30), (4.31) and (4.34) show a linear increase of

current as the load torque is increased. The corresponding tables and figures show that the current required does not exceed the current limit. Closer inspection of the torque, current characteristics figures (4.30), (4.31), (4.34) clearly show that for torque's up to 0.1 Nm the increase in current is not as steep as those for higher values. The low torque readings are not reliable because the dynamometer was not stable hence making it extremely difficult to get an accurate reading.

4.13 Conclusion

The results indicate that the motor driver unit is a good speed controller. Even when loaded the current increases sufficiently to overcome the load thus maintaining speed. While it worked perfectly maintaining the speed exactly at lower voltages and higher voltages it was clear that at low reference voltages the torques derived using the torque constant are more than the torques using the viscous friction. However both values become very close as the reference voltage is increased.

The values of the proportional gain and the integral gain were successfully evaluated and simulations supported the use of these values. Friction for the motor and driver unit was estimated using least squares then the same procedure was repeated with the addition of a load (gearbox). These two values were not close indicating the addition of the gearbox would increase the friction.

A theoretical model for the motor, driver and gearbox was derived using the estimated proportional, integral gains and the estimated friction values and encoder sensor gain.

The model derived was a third order model. The sampling time used for data collection and for the simulation was 10ms. This model was discretized and velocity simulation was compared with practical data figure (4.24). The results were not completely satisfactory. At time intervals between (0.3-0.7) seconds and (1-1.5) seconds the theoretical model exceeded the practical data. The other difference is that the real data indicate that the system initially overshoots. This behaviour is not captured by the simulated data. Figure (4.26) shows the comparison between the experimental data and the simulated data for the leg motion. It clearly shows that there is stiction in the system.

Also the initial values of friction and inertia were not close to those derived using simulations. All these problems and the fact that different people will eventually be using the Orthosis means that the mass, inertia and friction will be changing. These reasons give motivation in the use of system identification, as will be shown in chapter 5. Although in this thesis off line identification is used it would not be too difficult to implement on line identification in the future.

CHAPTER 5

System Identification

5.0 INTRODUCTION

The existence of cheap and powerful computers and microcontrollers has enabled engineers to replace analogue controllers with computer based digital controllers. The performance of these controllers is enhanced by the better technology available leading to faster speeds of computer processors and better conversion times of the analogue-to-digital and digital-to-analogue converters. The control algorithm and the programming language used further enhance performance. The requirement for more complex and high performance control systems has been the impulse for the development of a systematic control theory. Even with the development of such theory there is still a problem in the sense that a good knowledge of the dynamic characteristics of the controlled plant is not always available.

The need for effective modelling tools becomes apparent when an attempt is made to represent real systems by mathematical models. This need stimulated a lot of research into techniques for obtaining models directly from plant data [Astrom K.J., 1990, pp 19].

The most simple off line identification procedure employs the least squares technique for parameter estimation. For the off line identification of the process

Matlab facilities are used. Matlab is an interactive software package with, graphic facilities, data import/ export capabilities and together with the system identification toolbox can be used to implement the most common and useful parametric and non-parametric identification algorithms [Riadi I.C., 1990, pp3].

This chapter is split in two problems. The first involves the identification procedure for the motor, driver and the gearbox. That is the same experimental set-up for which a theoretical model was derived in chapter 4. This would enable us to compare the accuracy of the theoretical model and the identified model with real data. The second problem is to use the identification procedure on the full system (Orthosis).

5.1 System Identification

System identification is the experimental approach to process modelling, it includes the following.

1) Estimation methods.

2) Experimental planning.

3) Selection of model structure.

4) Model Validation.

In reality system identification is iterative. Usually a priori knowledge of the process being investigated is poor. A good starting point would be to consider the transient or frequency response analysis, which would yield crude dynamical models. Then using these results further experimental work can be planned to refine the models.

5.1.1 Estimation methods or schemes

A criterion, which will give a measure of how well a model fits the experimental data, is introduced when carrying out identification problems. The least squares method can be used to fulfill this criteria i.e. minimization of the sum of the squares of the error. This method is restricted to model structures that are linear in the unknown parameters. There are other methods available such as instrumental variables, prediction error, generalized least squares. However these other alternatives are usually more complex to implement, particularly for on line identification and therefore are not considered in this thesis.

The result of the estimation problem depends of course on how the problem is formulated, For instance, the obtained model depends on the amplitude and frequency content of the input signal. There are two main ways to organise the computation method, on-line and off-line. The method used for this thesis is the off line method.

The on-line method give estimates recursively as the measurements are obtained and are the only alternative if the identification is going to be used in an adaptive

controller or if the process is time varying. However in many cases the off-line methods give estimates with higher precision and are more reliable, for instance in terms of convergence [Mustafa M.M., 1989].

5.1.2 Experimental planning

It is desirable to have identification methods that do not require special input signals, that is the signals do not have to be sinusoid or impulses. This is because it is difficult sometimes and costly to experiment with industrial processes. An ideal identification method should thus be insensitive to the characteristics of the input signal. But this is not the case in most applications.

One requirement of the input signal is that it should excite all the modes of the process sufficiently. This means that the input signal frequency content must be large enough to excite all dynamics of the process. [Ljung L., 1987] and [Goodwin G.C., 1977] discuss methods for optimal input design. For simplicity in this project the input signal was chosen to be a Pseudorandom-binary-sequence which has a zero mean. The amplitude of the signal was limited by the mechanical constraints on the leg travel. To overcome stiction the amplitude should not be selected to be too small. Using a random generator in a PC produces Pseudorandom - binary sequence. The data signals are then converted into analogue signals in order to excite the motor driver. Software for generating this random data and for collecting the data is written in C (appendix A). The data is then stored in a Matlab file ready to be analysed by Matlab.

It is possible to base system identification on data obtained under closed loop control of the process. Adaptive controllers are based mostly on closed loop identification, however the main difficulty with data obtained from a process under feedback is that it may be impossible to determine individual parameters in the desired model i.e. the system may not be identifiable. Identifiability can be recovered if the feedback is sufficiently complex. The identification to be carried out is closed loop since the speed controller driver is a closed loop driver. This limits the identification to deriving an overall model but not individual parameters like the proportional and integral gains (K_P,K_I). The identification is an off-line identification.

For the identification of discrete-time models the sampling has to be selected properly before any experiments are carried out. Once the sampling time is selected all related work is carried out at the same sampling time. The sampling time can be increased or decreased by simply changing corresponding data from the C program. The sampling time selection depends primarily on: -

1) The sampling time for final application of the model (e.g. desired bandwidth of the closed loop system).

2) Accuracy of the resulting model.

3) Numerical problems if the sampling time is too small, such as round off errors, overflows, under flows, quantization noise.

Originally the maximum bandwidth of the closed loop system was not to exceed 10 Hz so the sampling time was chosen to be 10 milliseconds giving a frequency of 100 Hz. The usual rule of thumb indicates that the maximum closed loop bandwidth should be around one tenth of the sampling frequency. [Isermann R., 1980] has given an example, which illustrates that the sampling time should not be selected too small or too large because of accuracy problems in the resulting model.

After many attempts at 10 milliseconds it was decided to increase the sampling time interval to 40 milliseconds giving a possible closed loop bandwidth of 2.5Hz. This was sufficient as it was not anticipated that higher closed loop bandwidth would be needed. In fact it would not be needed to go higher than 0.5 Hz (see chapter 6 bandwidth selection section 6.8).

This decision was taken after two months of trials. At no time it was possible to derive a model while sampling at 10ms. During identification the Orthosis was suspended in the air to allow the legs to freely move. However due to the vibrations and shaking of the legs no model derived would match the real data. Repeating the experiment minutes later gave us completely different results. No consistency in the models derived was possible. Not only the parameters of the models were not consistent, but also the order and structure of the models were all different. The experiments were repeated at various amplitude input signals but with the same results.

In an attempt to reduce the vibrations the Orthosis was loaded with an artificial load (10kg-plaster leg). Signal conditioning using different filters (1^{st} and 2^{nd} order) with different cut off frequencies but with no success. Identification was only successful only when the sampling time was dropped to 40ms. This effectively improved the signal-noise ratio. The models were consistent and the results repeatable at this sampling rate.

5.1.3 Selection of Model Structure

When a model is identified using the least squares method it is in the following format.

$$A(q^{-1})y(t) = B(q^{-1})u(t) + e(t)$$

Where

$$A(q^{-1}) = 1 + a_1 q^{-1} + ... + a_{na} q^{-na}$$

$$B(q^{-1}) = b_1 + b_2 q^{-1} + ... + b_{nb} q^{-nb}$$

q^{-1} is the backward shift operator

$\{y(t), t = 1,2,.....n\}$ = Output signal

$\{u(t), t = 1,2,.....n\}$ = Inputs

$\{e(t), t = 1,2,.....n\}$ = White noise disturbance

The model structures are derived from prior knowledge of the process and the disturbances. In some cases the only a priori knowledge is that the process can be described as a linear system in a particular operating range. It is then desirable to use natural representation of a linear system, such representations are called black-box models. The choice of model structure (order and delays) are chosen by the designer. MATLAB makes the process semiautomatic. MATLAB does all the calculations and then displays the data in the form of a graph. Minimum cost (least squares) versus the number of parameters used. The least squares cost is calculated by (Ay – Bu = error) $\rightarrow \sum(\text{error})^2$) where A and B are the model derived and y,u are the output and input signals. The designer chooses the number of parameters, which he thinks gives the minimum cost with out making the model too complicated. That is although the minimum cost could be further decreased by choosing a higher order model but this increase in complexity is not justified by the slight improvement. A typical example is the difference equation model. The unknown parameters are the model parameters and the order of the model

5.1.4 Model Validation

When a model has been obtained from experimental data, it is necessary to check the model in order to reveal its inadequacies. For model validation it is useful to determine such factors as step response, Autocorrelation of residuals, Simulations, poles-zeros and apply other inputs which were not used for identification. It is also

useful to look for quantities that are sensitive to model changes. A model can never be accepted as a final and true description of a system. Rather it can at best be regarded as a good enough description of the process that is of a particular interest to us.

5.2 Practical Identification (Bench test)

The system to be identified consists of a controller driving an EC motor with a 50:1 gearbox connected to one end of the motor while a tachometer is mounted to the output shaft of the gearbox. The theoretical model for this system has already been worked out in the previous section, which gives us an opportunity to compare both models. The identified model is in the format shown in section 5.1. 3 where A, B are polynomial in q^{-1}.

Before system identification could be applied on the full system (Orthosis) a bench test to estimate a model for the motor and driver unit with a gearbox was carried out. This exercise was carried out for the simpler set-up (motor, motor driver, gearbox) in order to evaluate this approach and test the feasibility of its use in the full system identification and to test the fidelity of the theoretical model.

Three pseudo random binary signals with different amplitudes were used as inputs in order to obtain three different models. This would give the opportunity to see if the models change considerably with different amplitude input signals.

TEST 1 input signal amplitude 1 volt

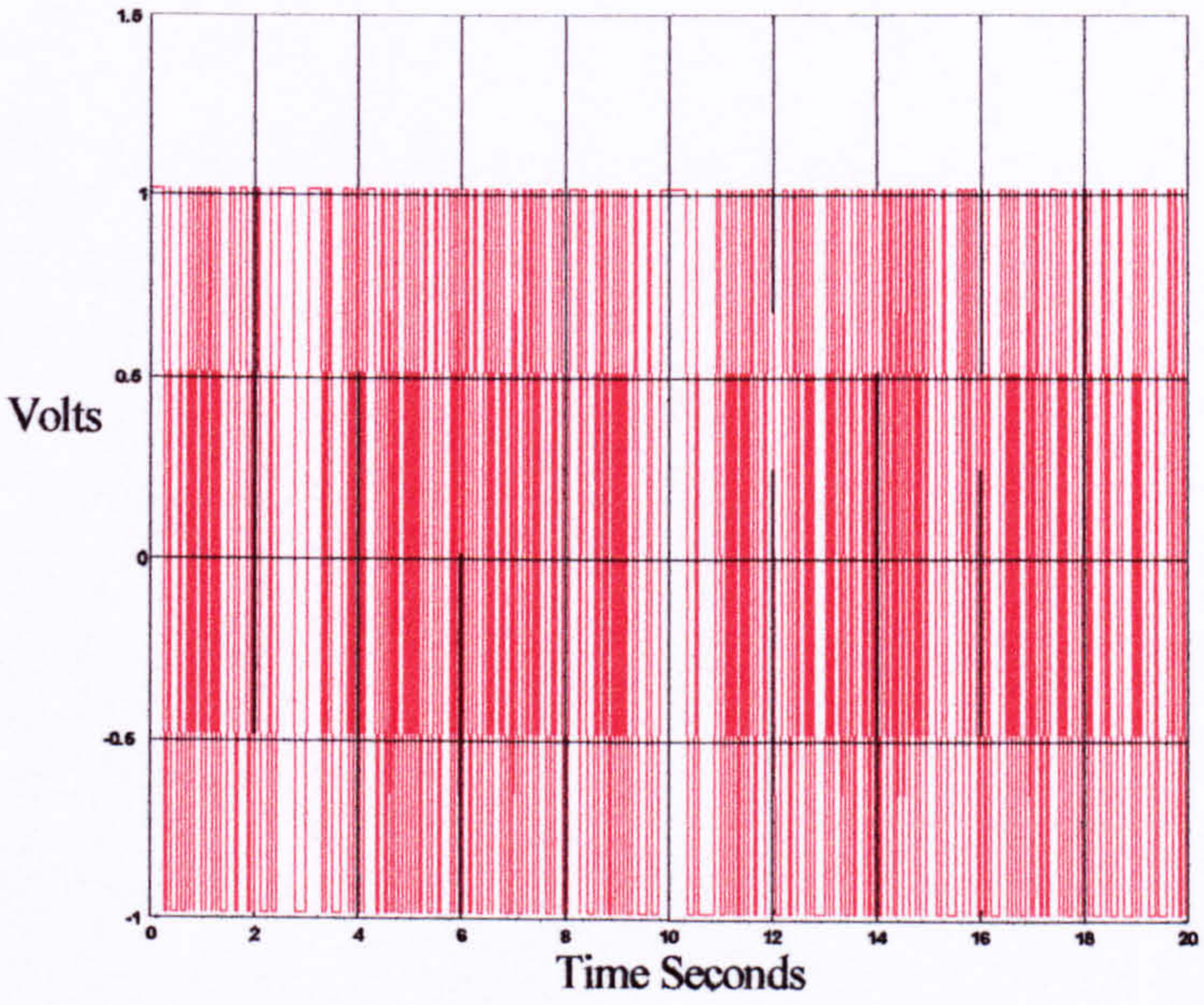

Figure 5.1 Input signal for test 1

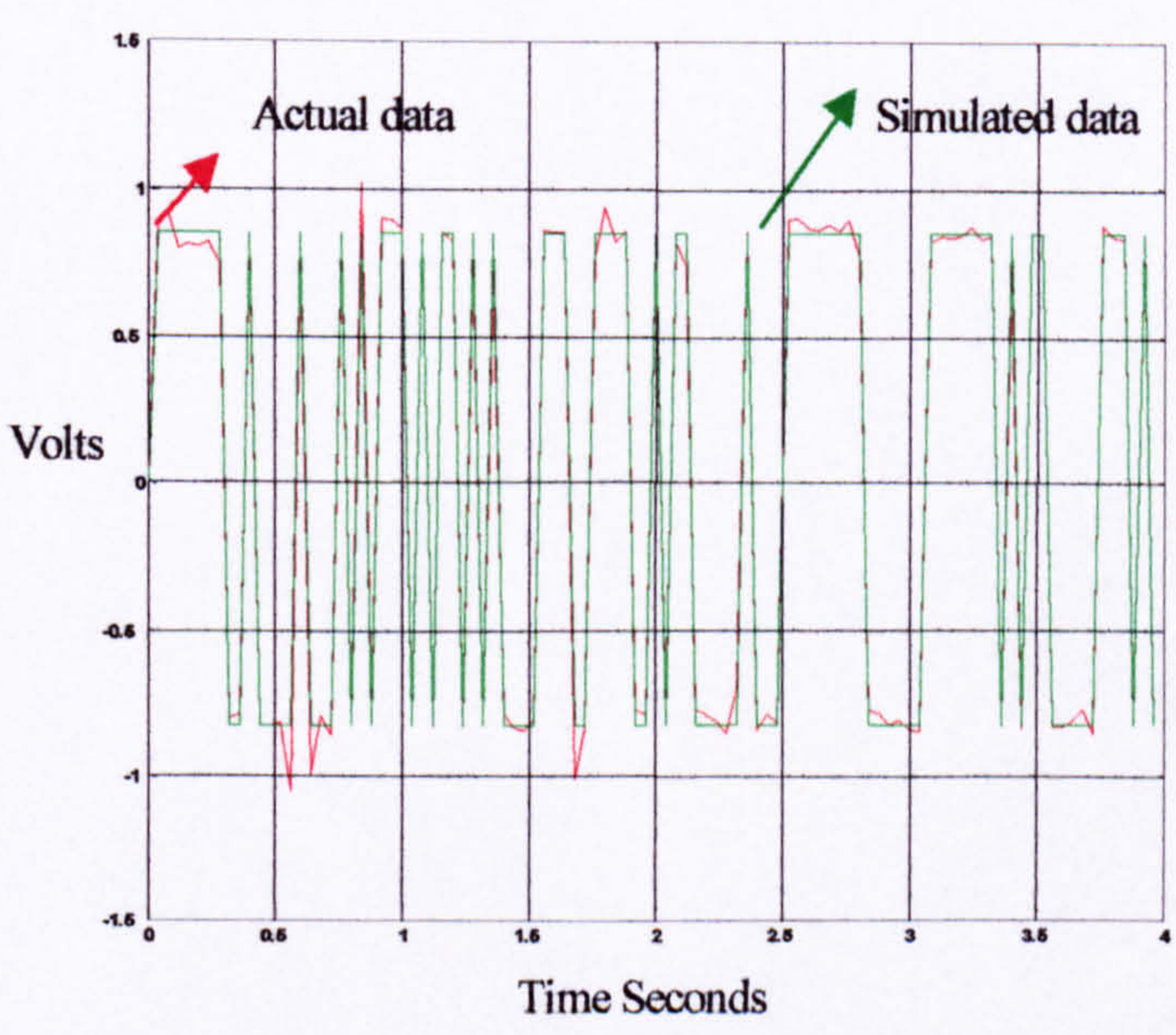

Figure 5.2 Comparison of actual data and simulated data for test 1

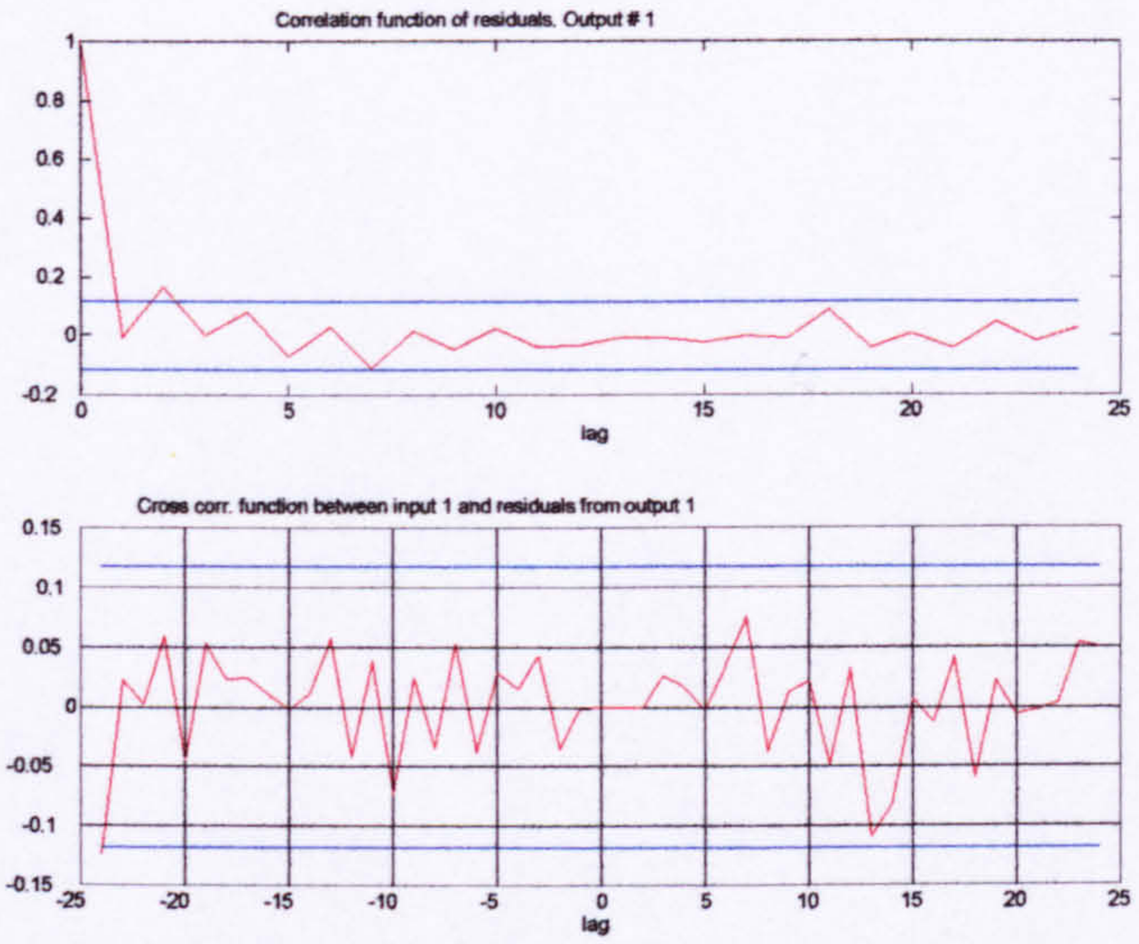

Figure 5.3 Residuals tests for data in test 1

TEST 2 input signal amplitude 4 volts

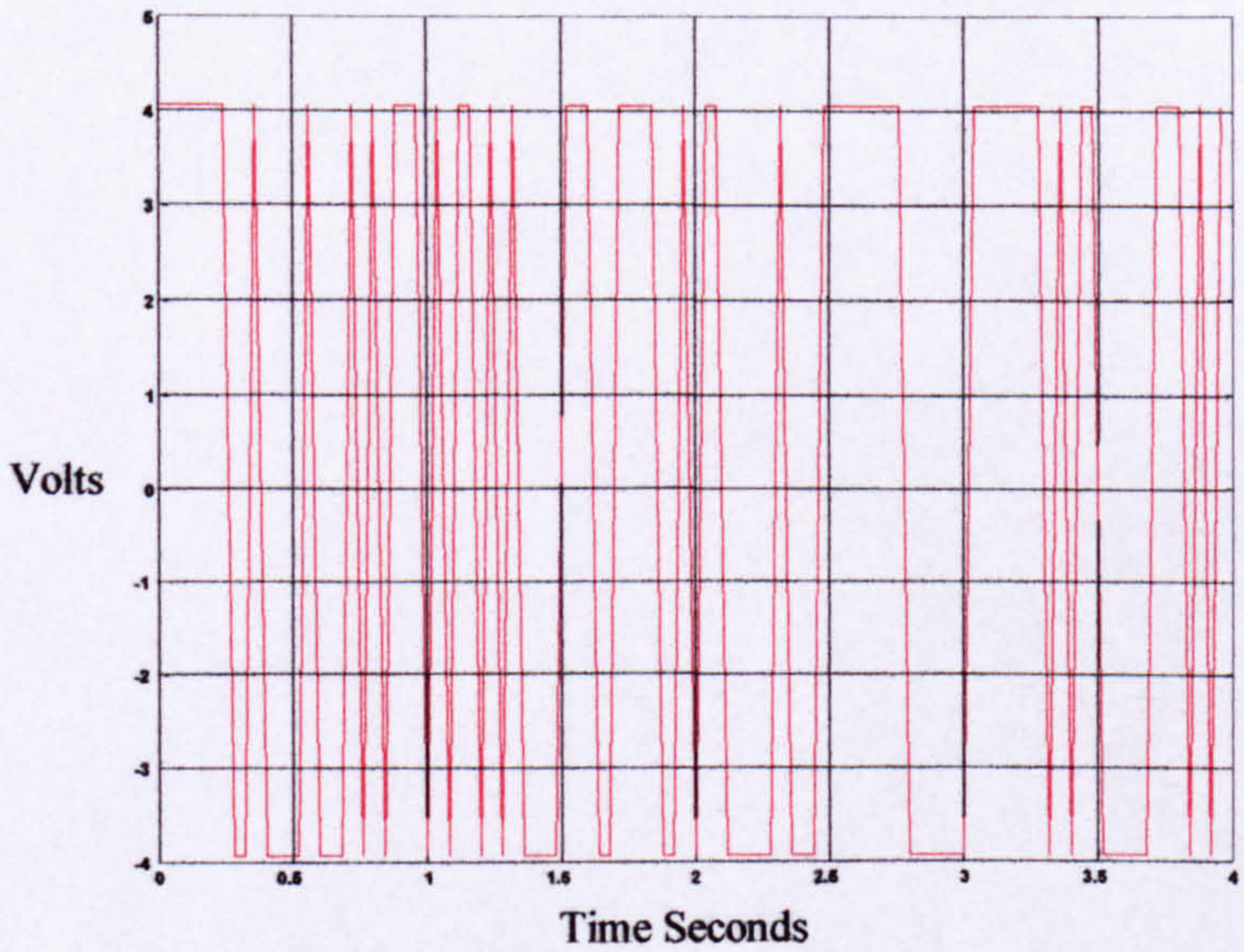

Figure 5.4 Input signal for test 2

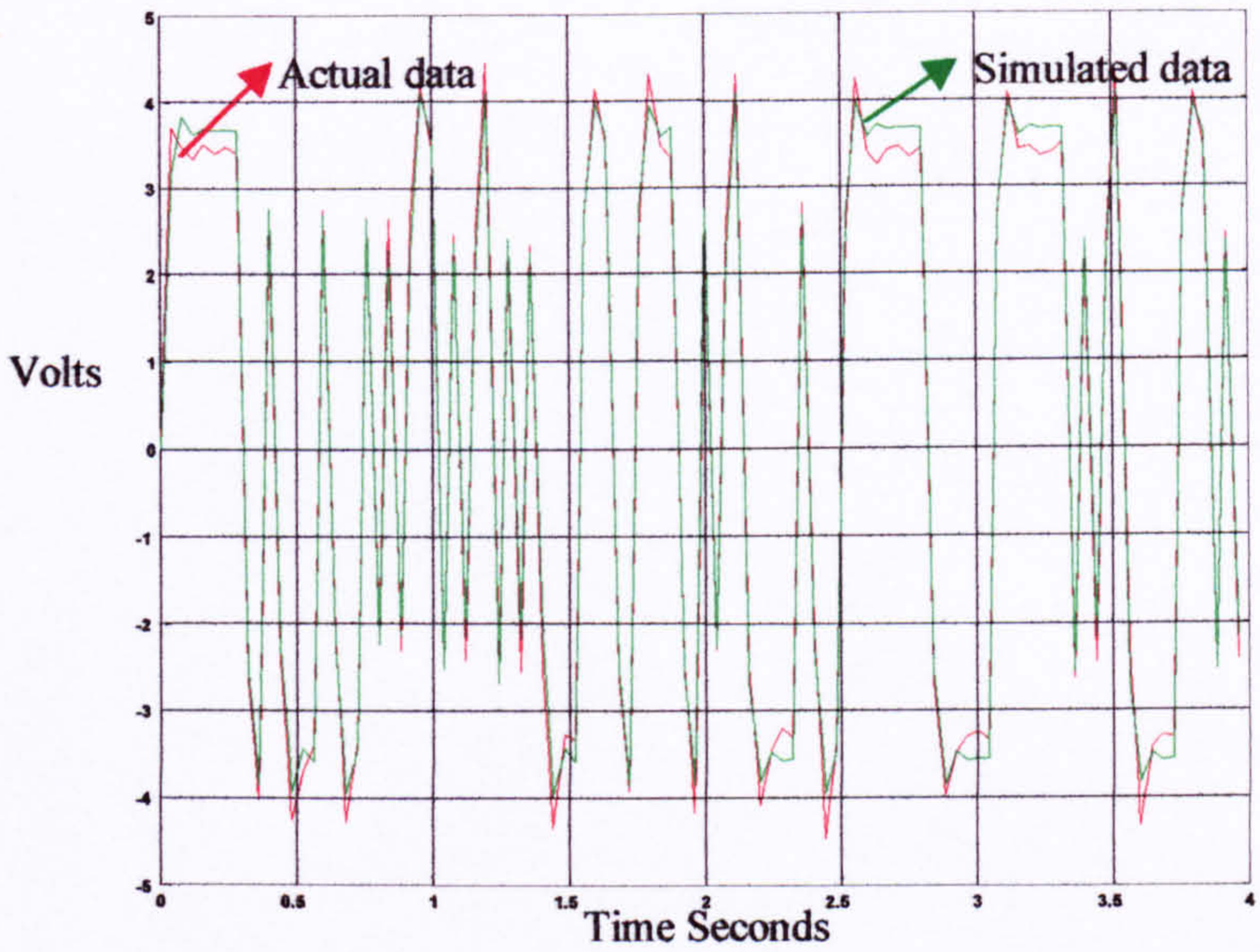

Figure 5.5 Comparison of Actual data and simulated data for test 2

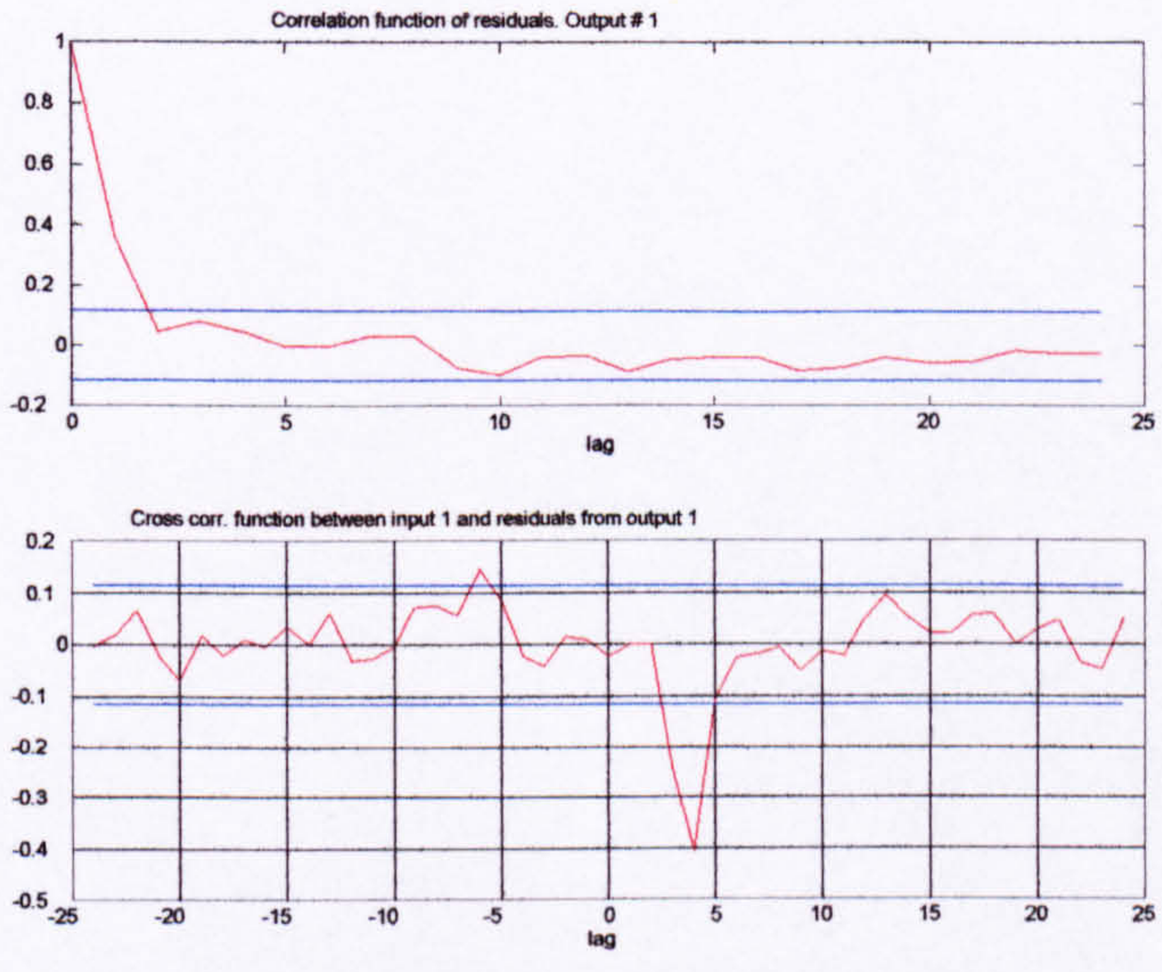

Figure 5.6 Residuals tests for data in test 2

TEST 3 Input signal amplitude 7 volts

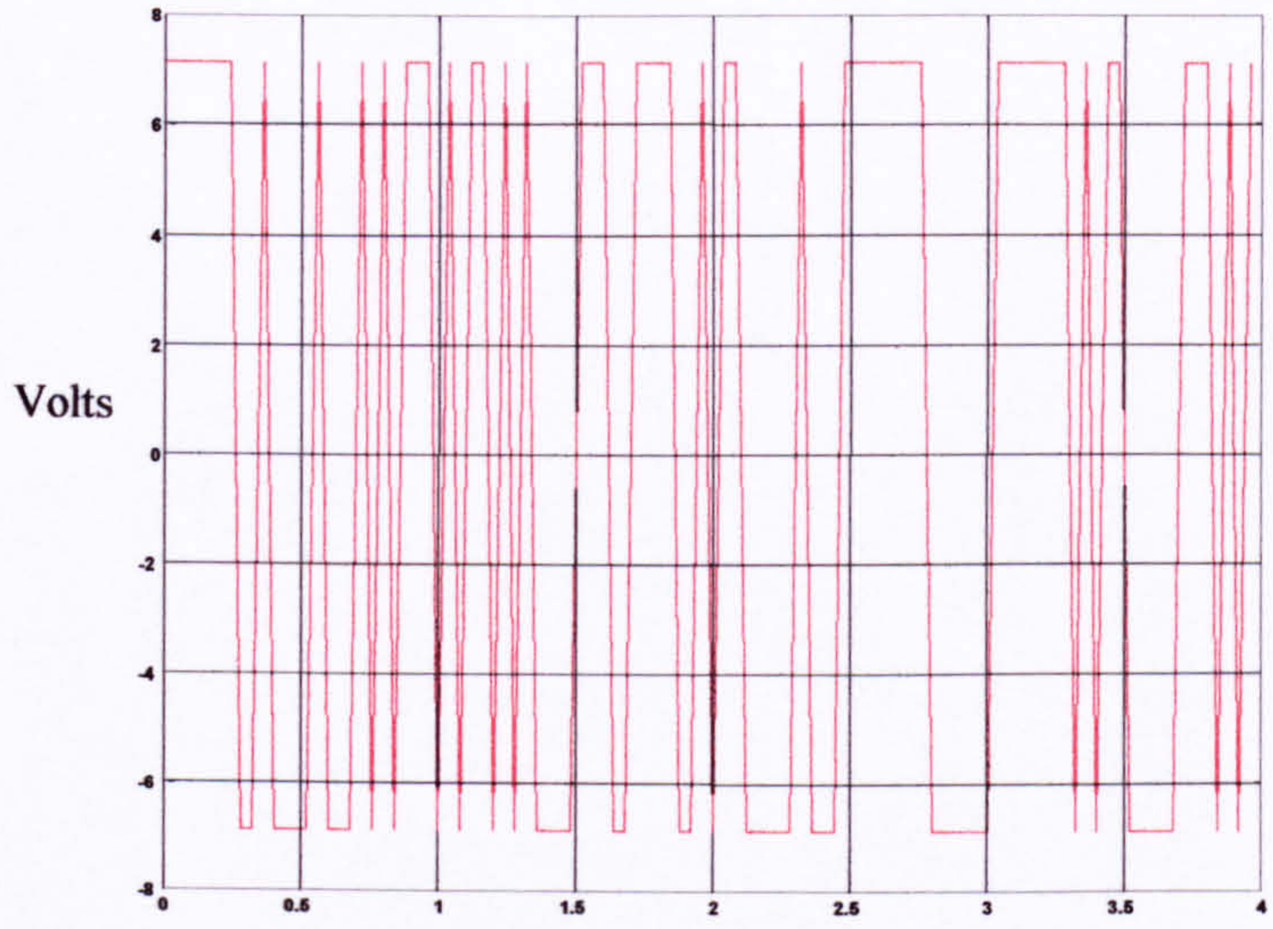

Figure 5.7 Input Signal for test 3

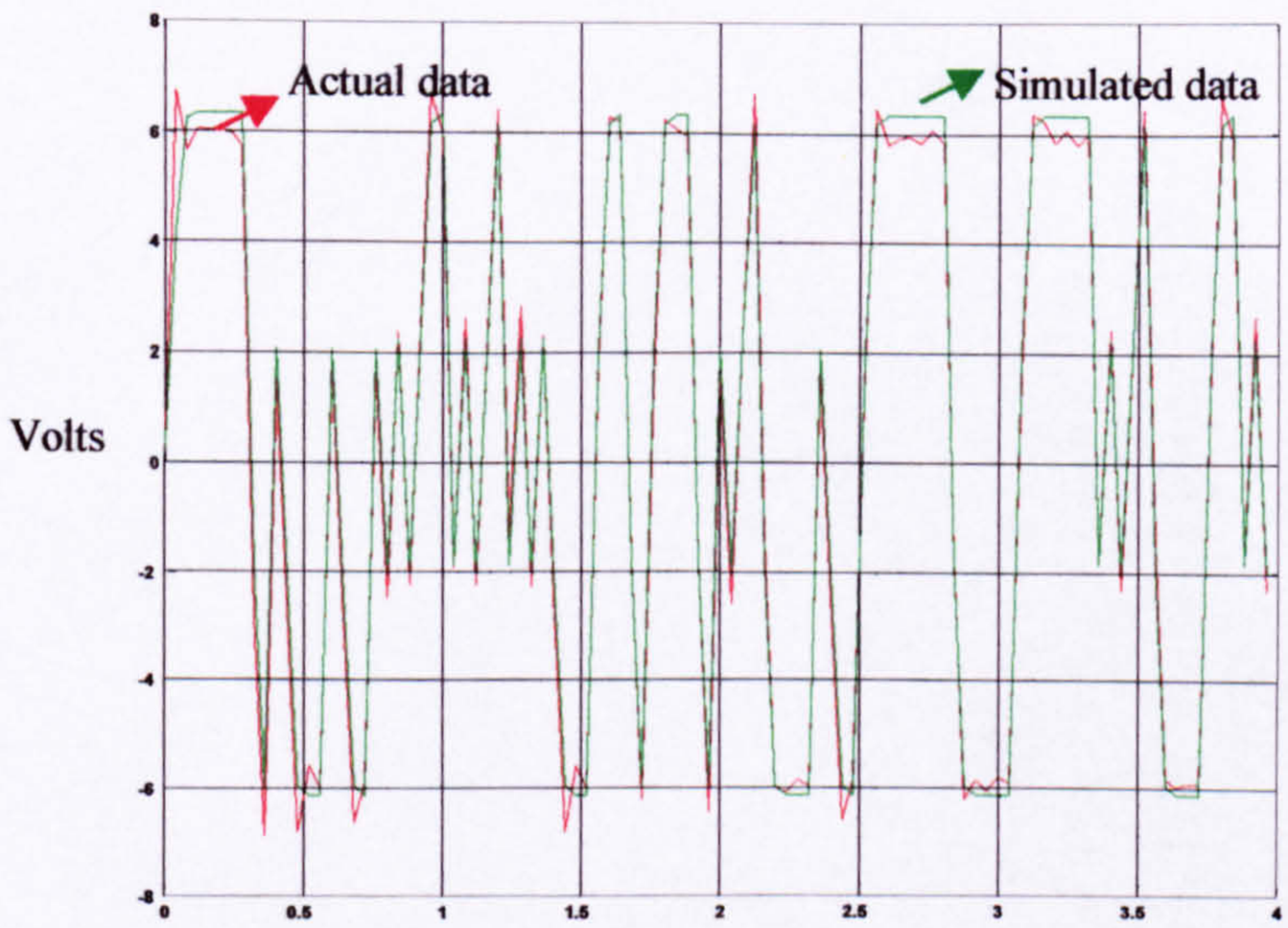

Figure 5.8 Comparison of actual data and simulated data for test 3

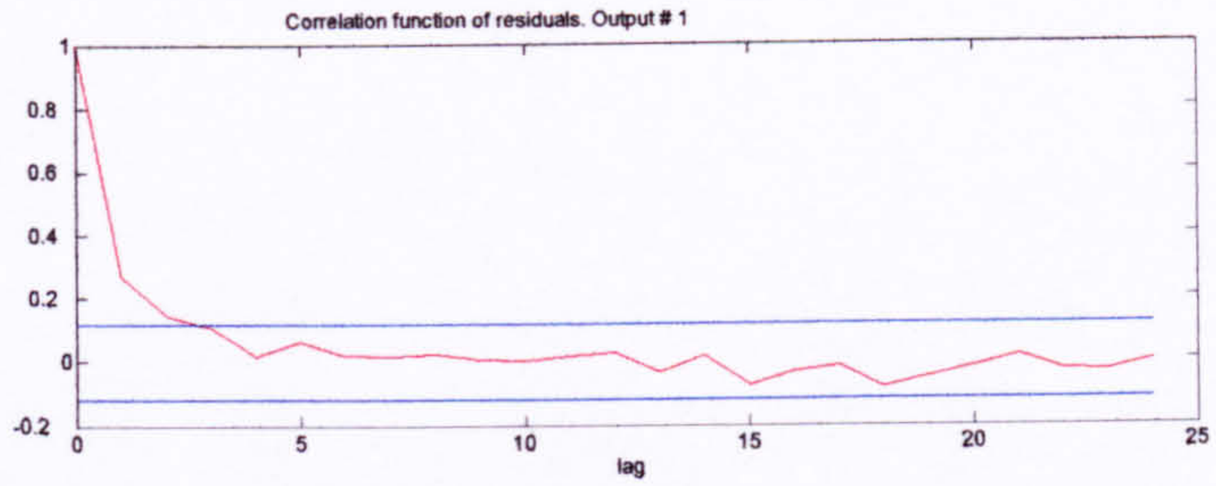

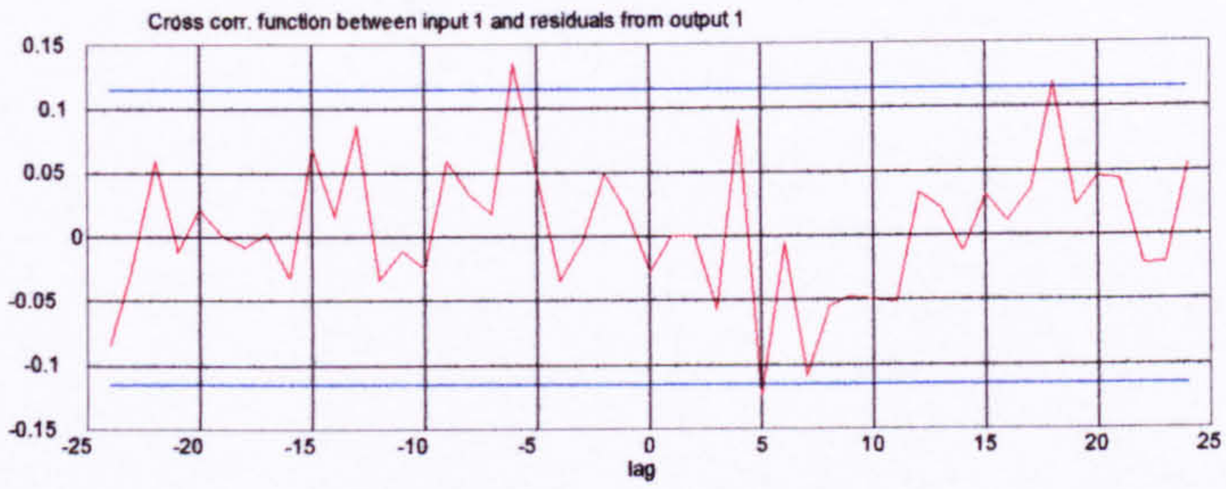

Figure 5.9 Residuals tests for data in test 3

5.3 Results Analysis

The models which were identified are as follows:

Test 1 model.

$$B = [0 \quad 0.8387 \quad -0.0412] \qquad A = [1.000 \quad -0.0495]$$

Test 2 model

$$B = [0 \quad 0.7791 \quad 0.3973] \qquad A = [1.0000 \quad 0.3013]$$

Test 3 model

$$B = [0 \quad 0.5856 \quad 0.2678] \qquad A = [1.000 \quad -0.0428]$$

Test 1		Test 2		Test 3	
1 volt input		4 volts input		7 volts input	
Poles	DC Gain	Poles	DC Gain	Poles	DC Gain
0.0495	1.19	-0.3013	1.11	0.0428	1.12
0.000		0.000		0.000	

Table 5.1 Summary of the model analysis

Test 1	Test 2	Test 3
1 volt input	4 volts input	7 volts input
Zeroes location	Zeroes location	Zeroes location
0.0492	- 0.5100	-0.457

Table 5.2 Location of the zeros of different models

Figures (5.2), (5.5) and (5.8) show comparison of the actual behaviour and the simulated behaviour of all the models. The response is similar and accurately follows the actual data. The order of the models is exactly the same. Further analysis of the DC gain, the location of the poles clearly indicate that all the models are stable and have similar DC gain value. For this simple set up this was not surprising as higher amplitude of signals do not excite the system in any way, which may cause

vibration or non linear behaviour. However the poles and zeros location is not consistent. Going to more complex models with higher order does bring the poles and zeros location closer but in terms of simulation the improvement does not justify using more complex models.

5.4 Practical Model Validation

Now that a theoretical model and an identified model were derived, the next step is to compare and validate both, this is done by seeing how the models respond to the same input then compare it to the actual behaviour of the set-up with the same input. If the response is similar then the model can be accepted and used as a substitute to any model, which was derived from theoretical set of equations. The simulation of the model is compared with the practical data in figure (5.10).

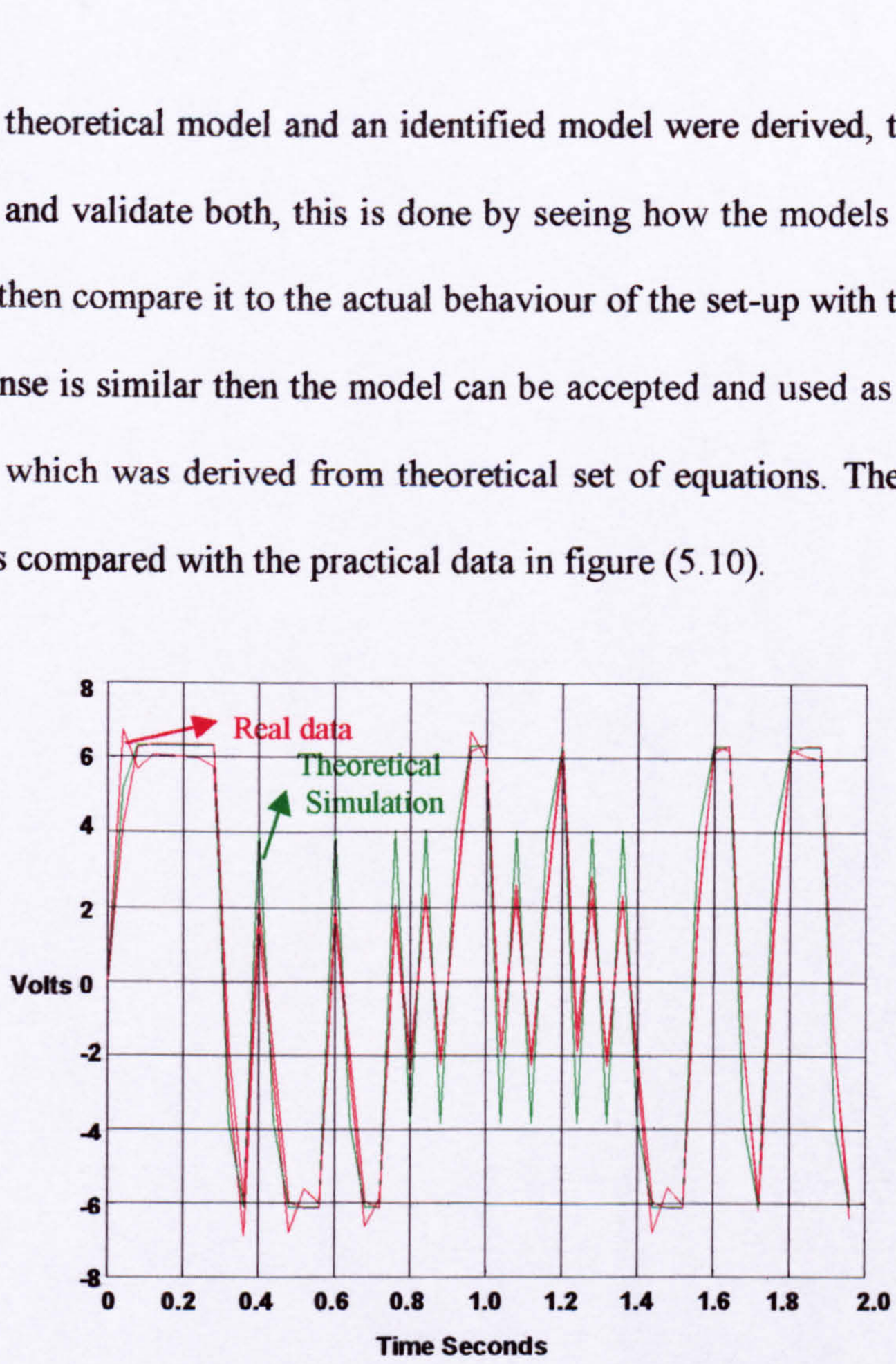

Figure 5.10 Velocity comparison between real data and simulated data for both models

Although the comparison shown here is for the model with 7 volts input, that is because when the identification was carried out the 7 volts input gave the worst results. Simulations were also carried out for the 4 volts and 1 volt input with similar results.

The comparison between the models is shown in figure (5.10). This clearly shows that the output of the identified model follows the actual data, better than the theoretical model. In particular the theoretical model predicts amplitudes for fast transients that are almost twice the amplitudes of the experimental data. Not only the identified model provides a better match, also it is a lower order (second order) than the corresponding theoretical model (third order model) derived in chapter 4.

5.5 Full system Identification

The process to be identified consists of an EC motor (EC040-070-38EAA200A), a motor drive unit, a potentiometer and a ball screw arrangement, which connects the motor shaft to the leg. The process was interfaced to a 486 PC by using the (PC30GA) plug in board. Signal conditioning was done through an amplifier and a first order filter. The overall system configuration is shown below. Details of equipment are shown in appendix (F).

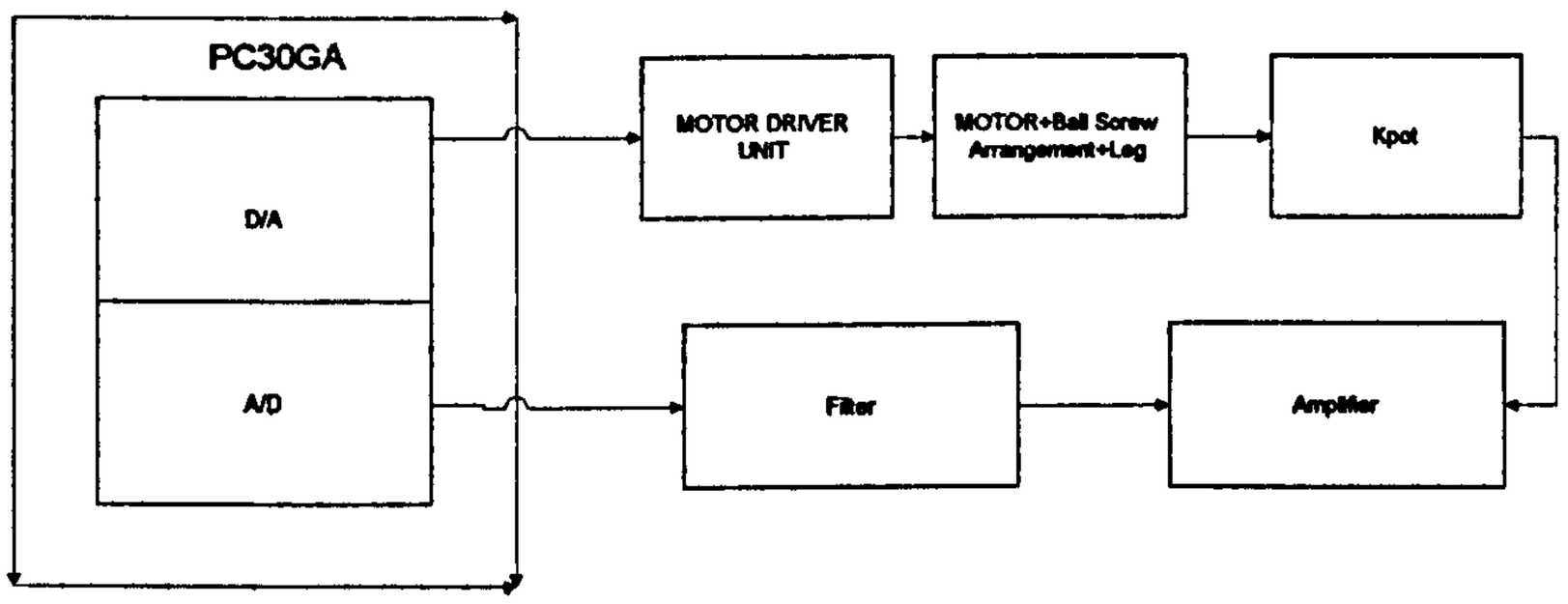

Figure 5.11 The overall system configuration

5.13 Identification results

Five experiments were carried out, three when the Orthosis was unloaded. In all the experiment pseudo random input signals were used with different amplitudes and the fourth and fifth experiments were carried out with the Orthosis loaded with a person. Thus five models were derived and cross-checked with each other. Table (5.3) displays the parameter estimates of the five models.

Exp	b2	b3	b4	b5	a1	a2	a3	a4	a5
1	0.0743	0.0285	0.0291	0.0432	1.000	-1.7167	0.7520	0.3061	-0.3341
2	0.0634	0.0233	0.0276	0.0260	1.000	-1.7383	0.6808	0.4440	-0.3802
3	0.0511	0.0304	0.0328	0.0191	1.000	-1.7533	0.7460	0.2973	-0.2884
4	0.1162	0.1020	0.0710	0.0231	1.000	-0.8755	0.0220	-0.1763	0.0362
5	0.1209	0.0649	0.0400	0.0282	1.000	-1.0412	0.1343	-0.1374	0.0386

Table 5.3 Parameter Estimation using ARMA model with 2 delays

It can be seen that the first three experiments gave very similar results to each other. The fourth and fifth experiments show the parameter estimates when the Orthosis was loaded. Although these two experiments show different parameter estimates when compared to the first three experiments they all have the same structure and order as the first three. This indicates that the model for the unloaded may be good enough to describe the system both unloaded and loaded. In order to be satisfied with this statement further tests were carried out. The frequency response of the five models is shown in figures (5.12)-(5.16). These show that all the models derived have approximately a cross over frequency of 1.2 Hz, a nyquist frequency of 12.5 Hz, and a sampling frequency of 25 Hz

The response of the model as compared with real data collected was also investigated and the results shown in figures (5.18), (5.21), (5.24), (5.27), (5.29), (5.32). These show that several models were derived. 3 models with the Orthosis unloaded and the other two were with a volunteer in the Orthosis. It is clear that all

the models derived are validated and can be described as good enough to describe the system. However model 1 was derived at 4 volts input which was the highest input voltage used for model derivation when the Orthosis was unloaded. This model was cross-checked with other models derived and was validated. This model also managed to capture the behaviour of the Orthosis when it was loaded. This gave us confidence in the use of this model for designing the controller.

The cross correlation function between residuals and inputs and the residual tests figures (5.19), (5.22), (5.25), (5.28), (5.30) confirm that the models can be accepted. For model validation the model chosen was the model in experiment one. The reason for that is that although the other two unloaded models were similar the input signal for model one was higher than those of the other two models. It was decided to take that model and see if it can reproduce the response of the system at different amplitude of random input signal.

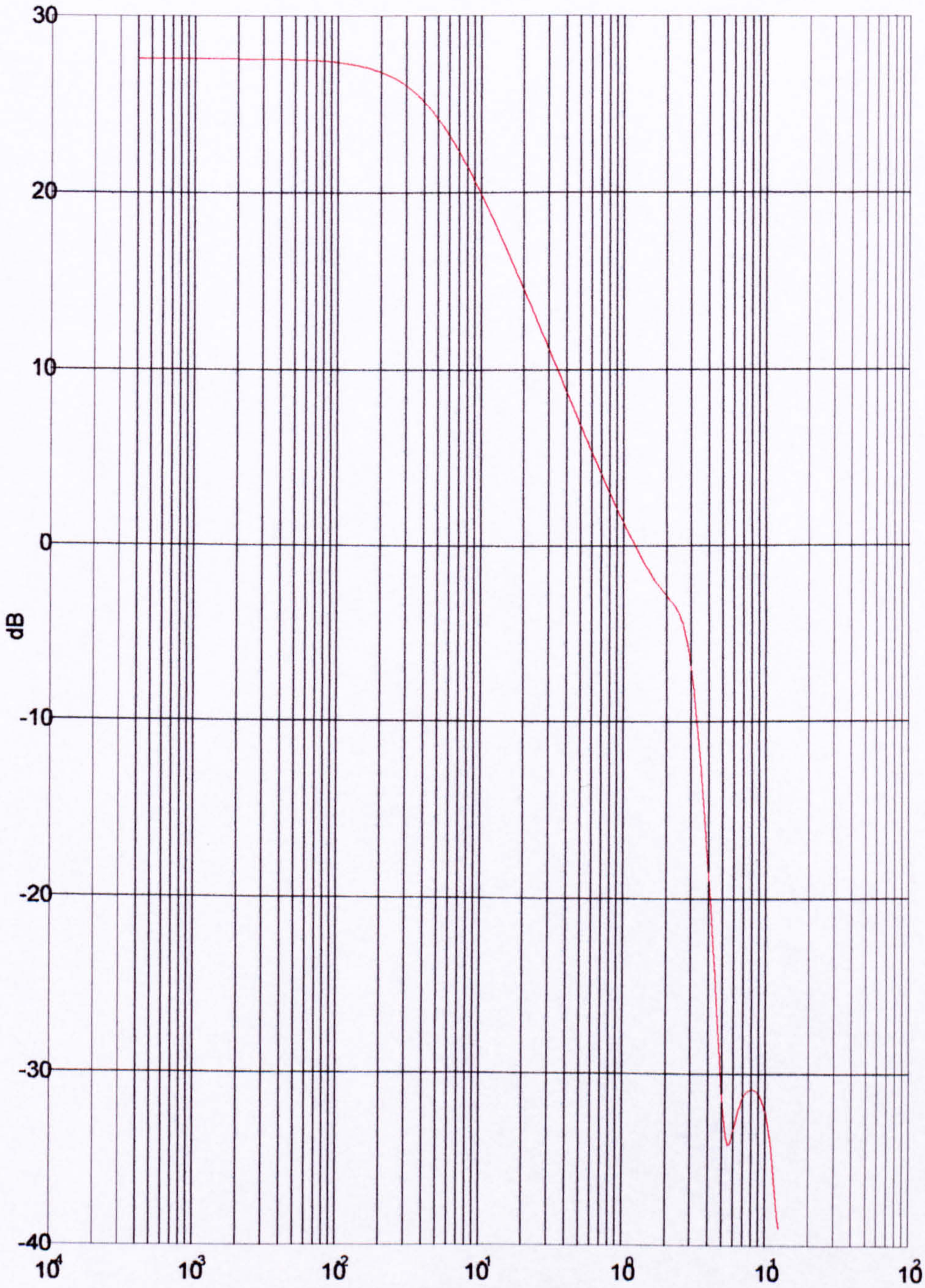

Figure 5.12 The frequency response of model 1

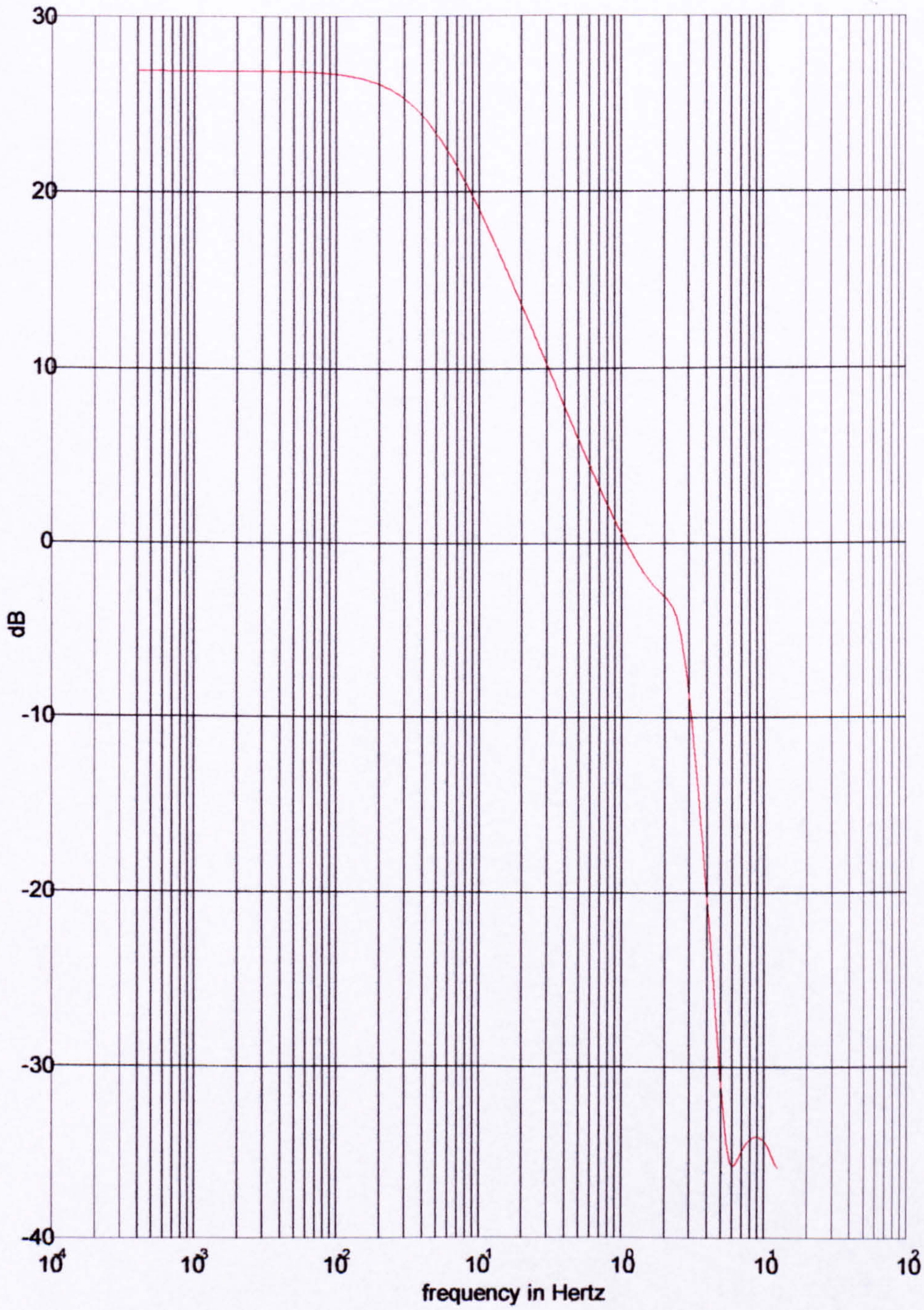

Figure 5.13 frequency response of model 2

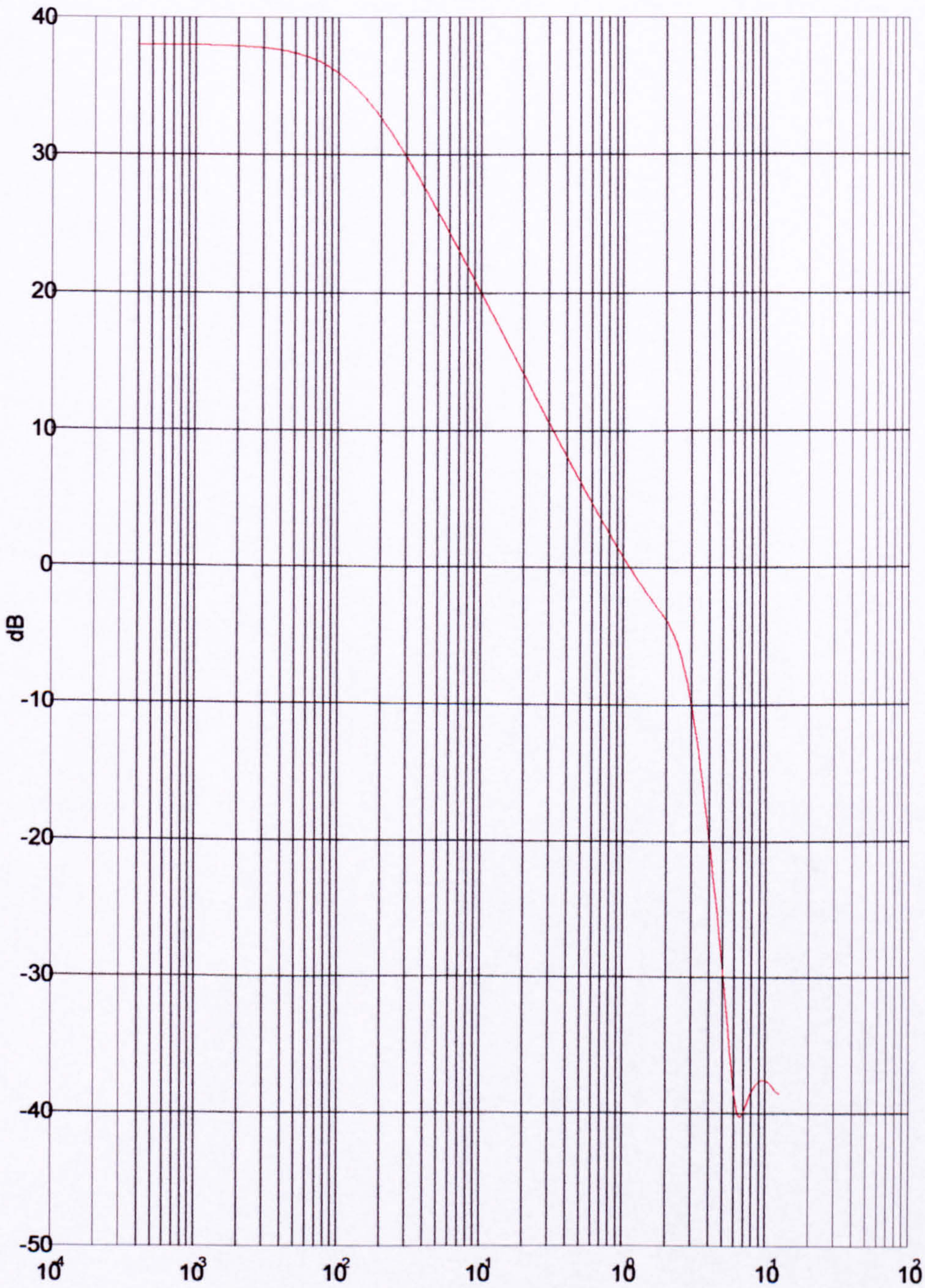

Figure 5.14 frequency response of model 3

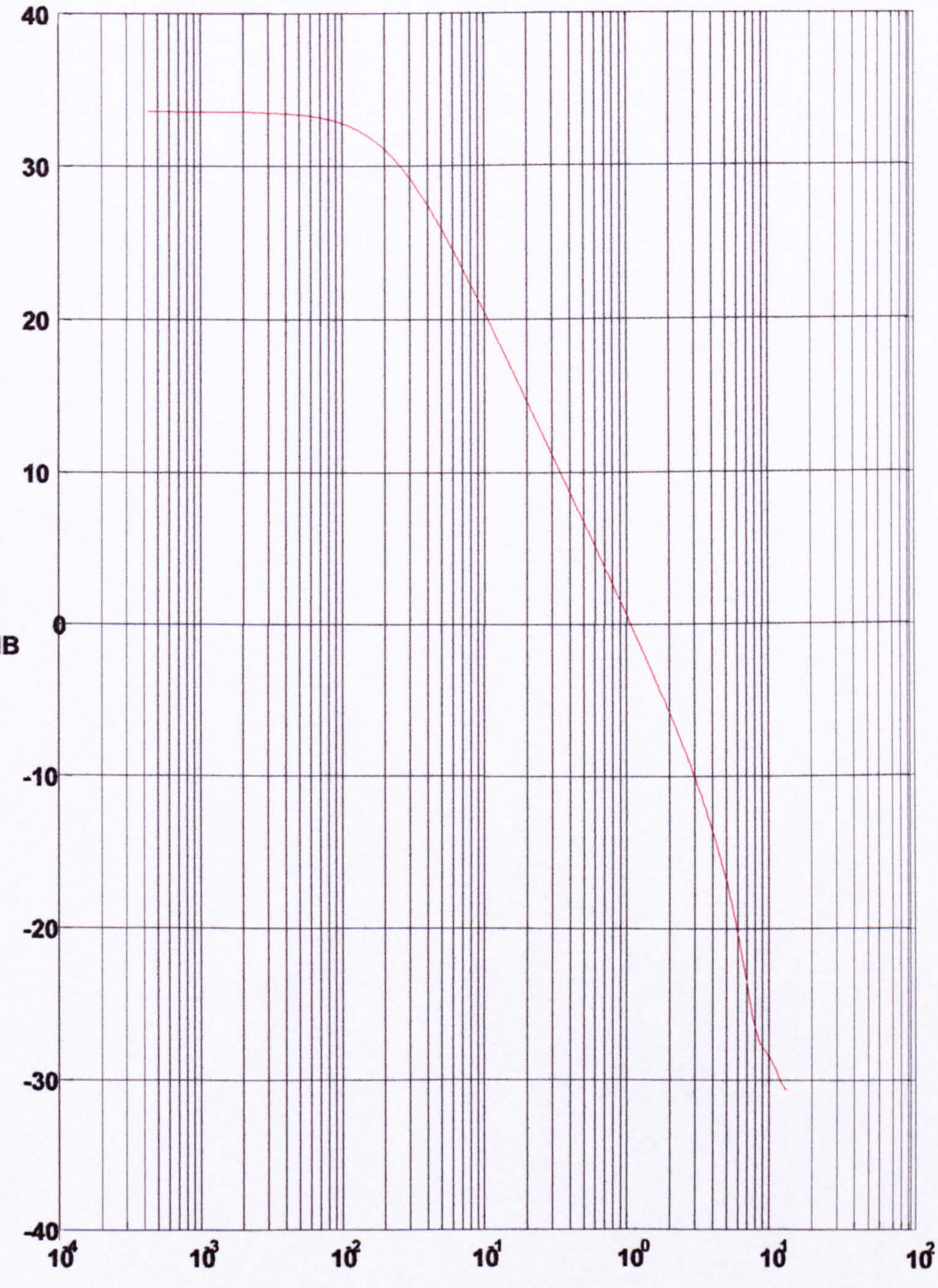

Figure 5.15 The frequency response of model 4

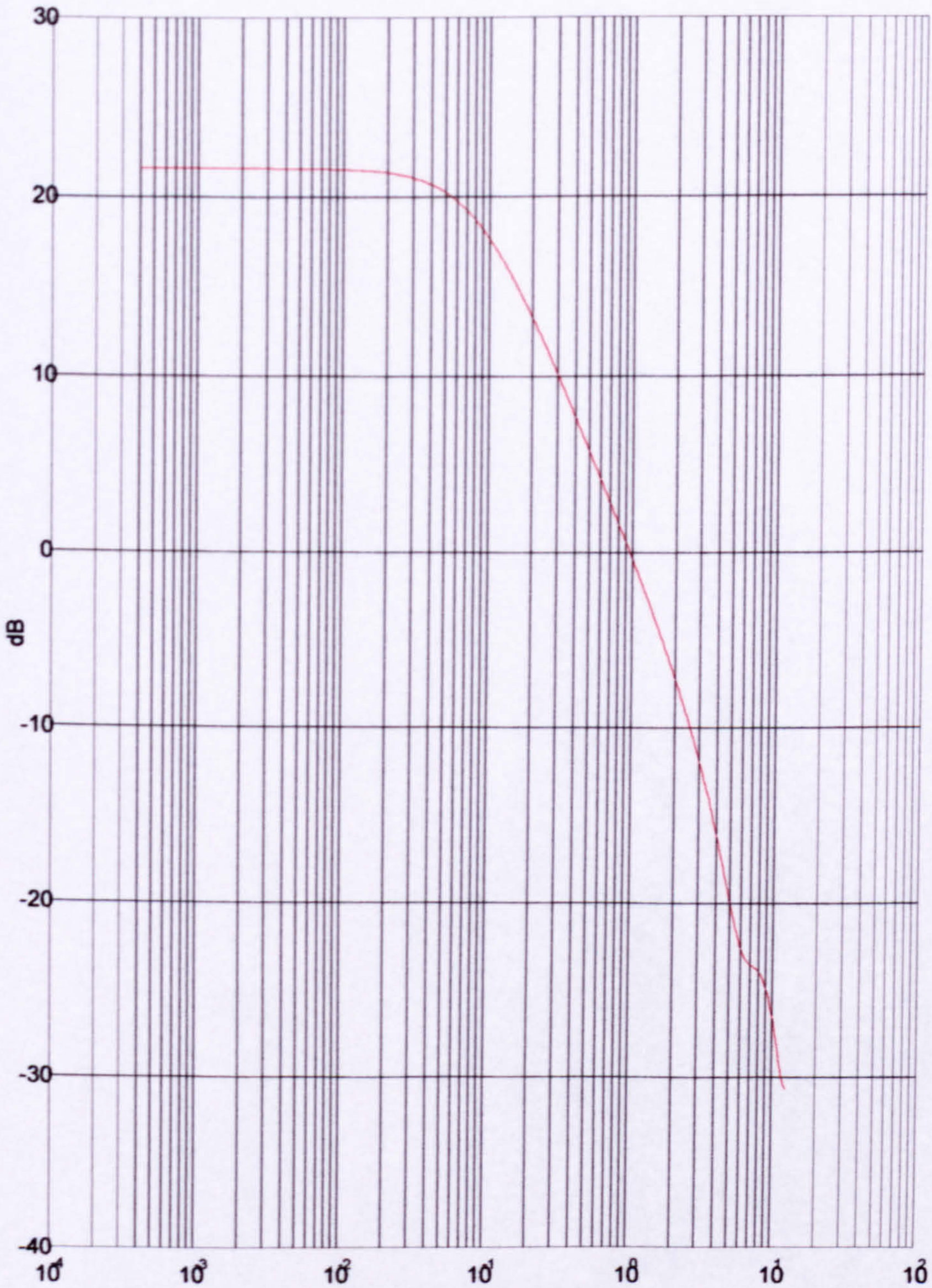

Figure 5.16 The frequency response of model 5

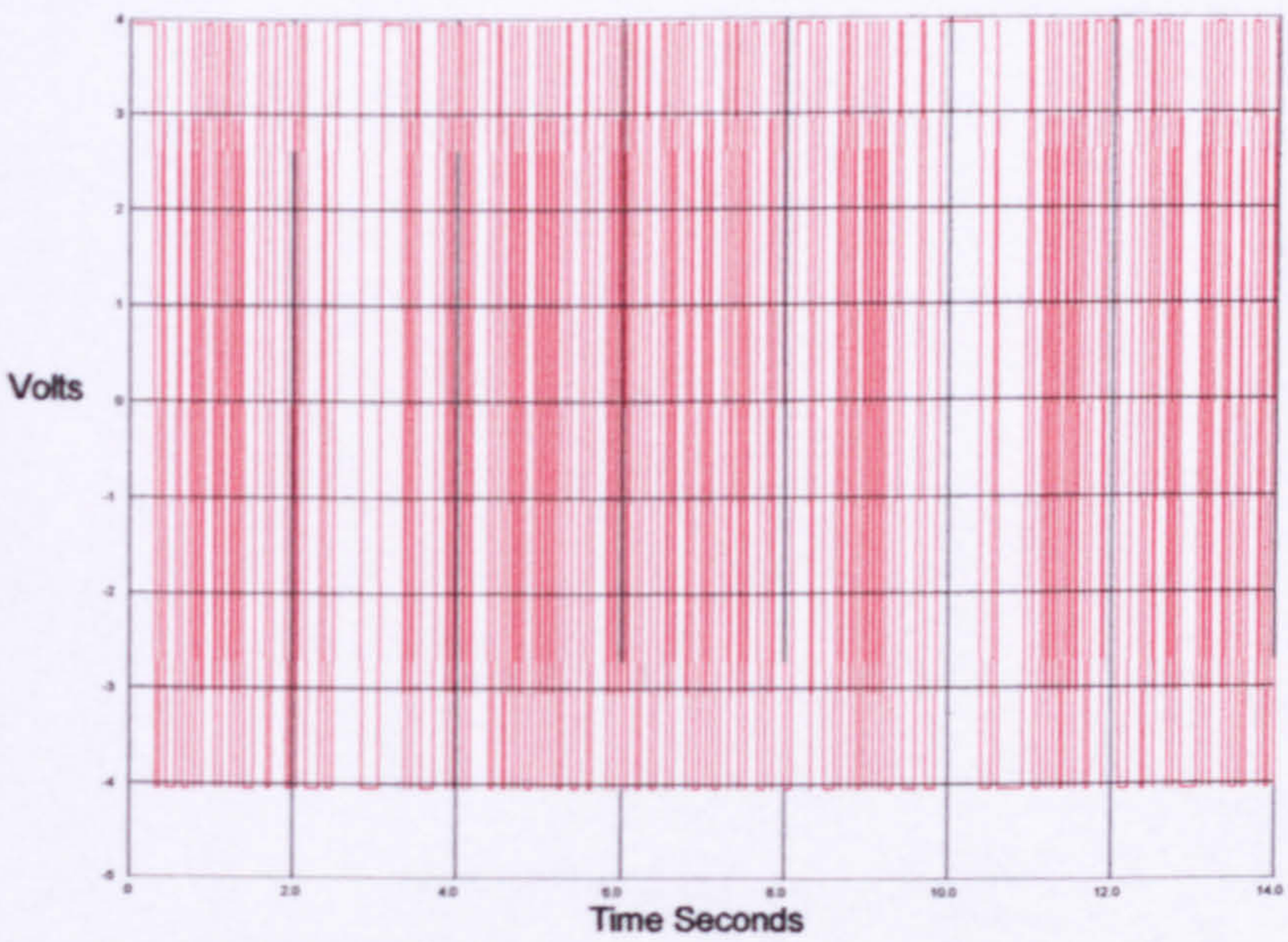

Figure 5.17 Input signal for exp1

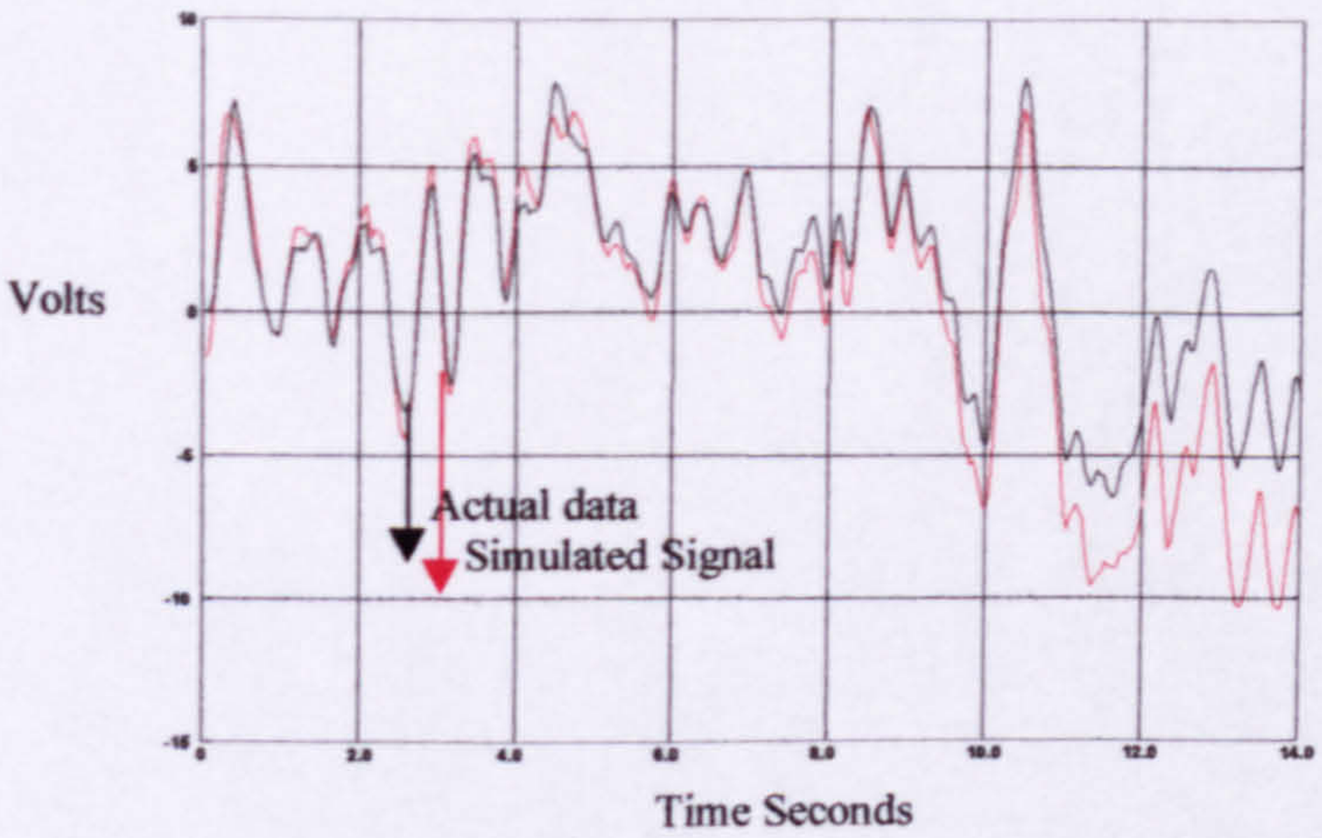

Figure 5.18 Comparison of actual data with simulated data for model 1

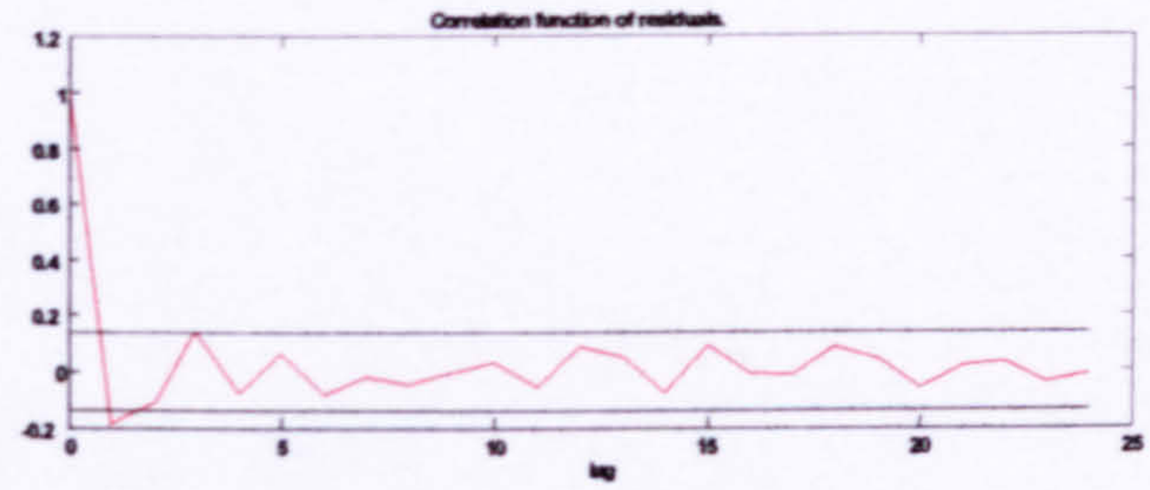

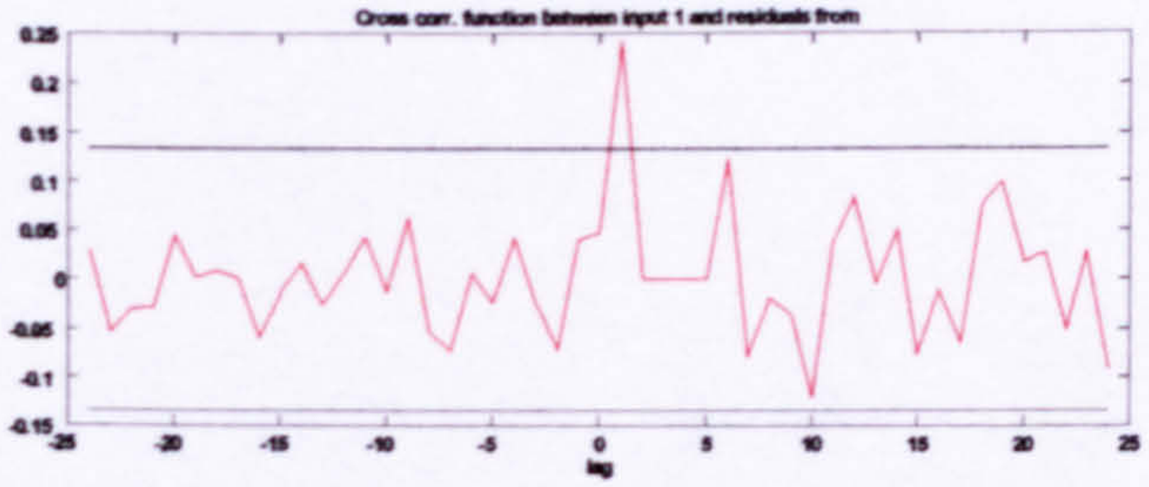

Figure 5.19 Residuals tests for the data of experiment 1 horizontal bars indicate 95 percent confidence levels

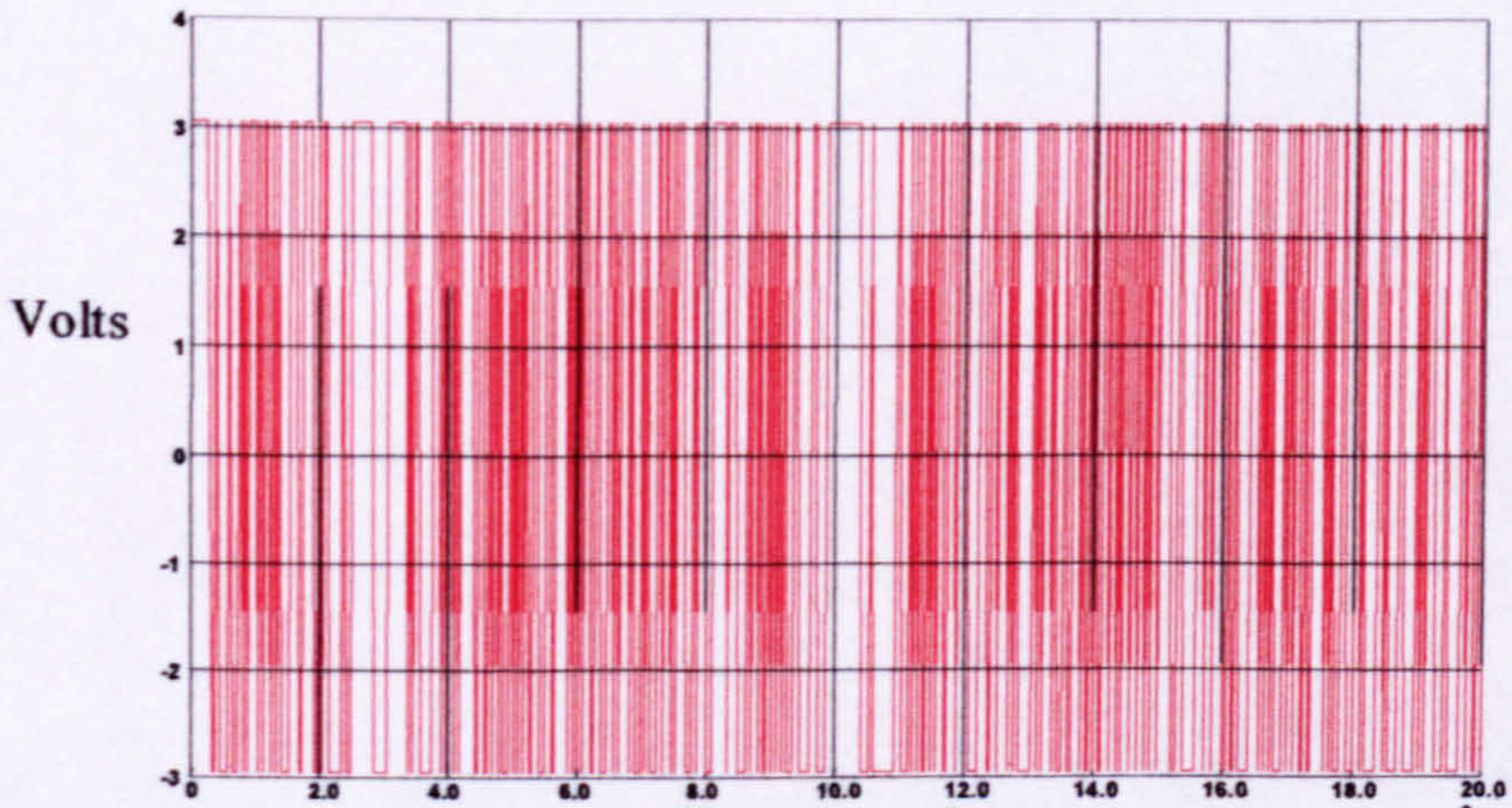

Figure 5.20 Input signal for exp2

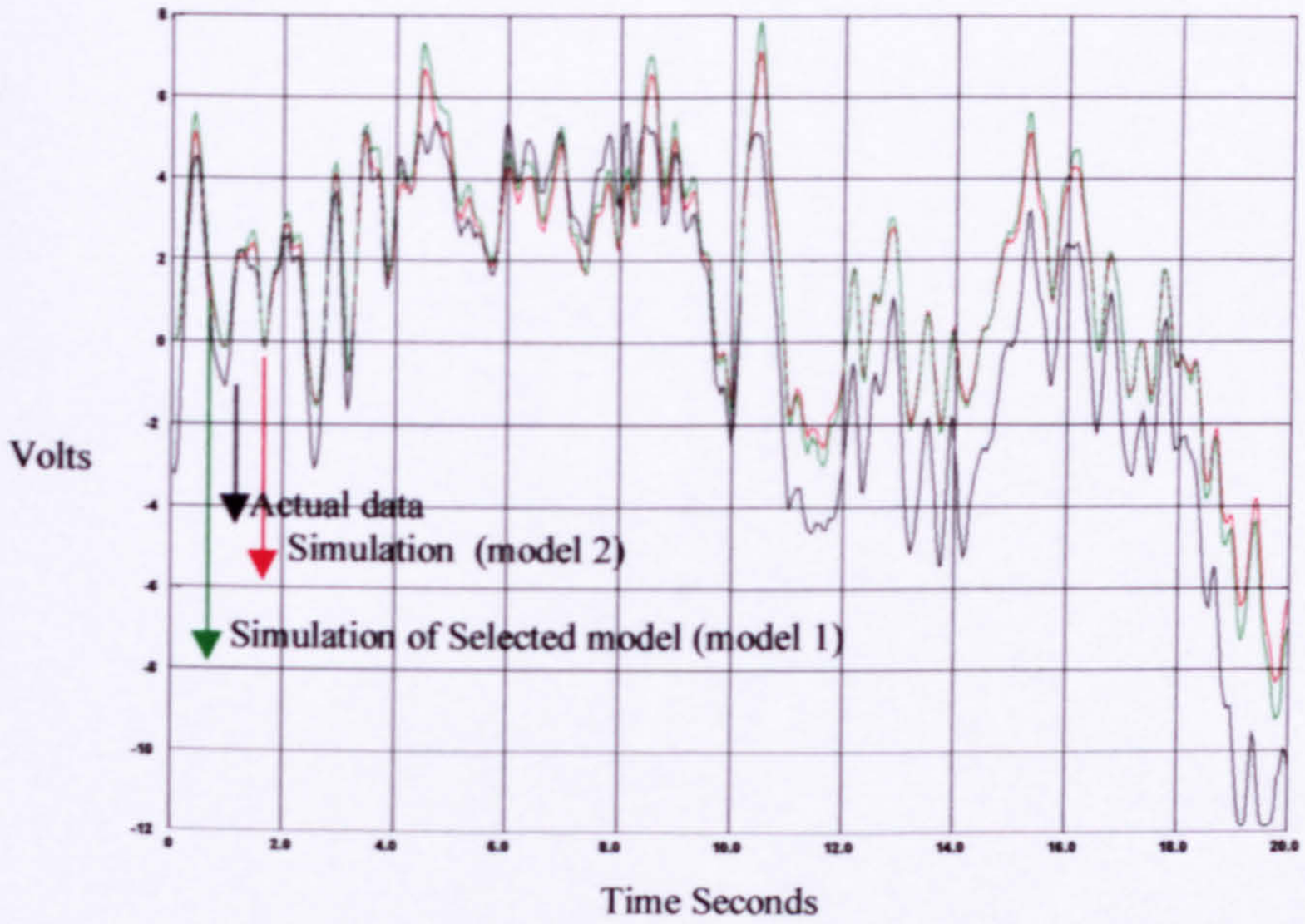

Figure 5.21 Comparison of actual data with simulated data for model 2 and model 1

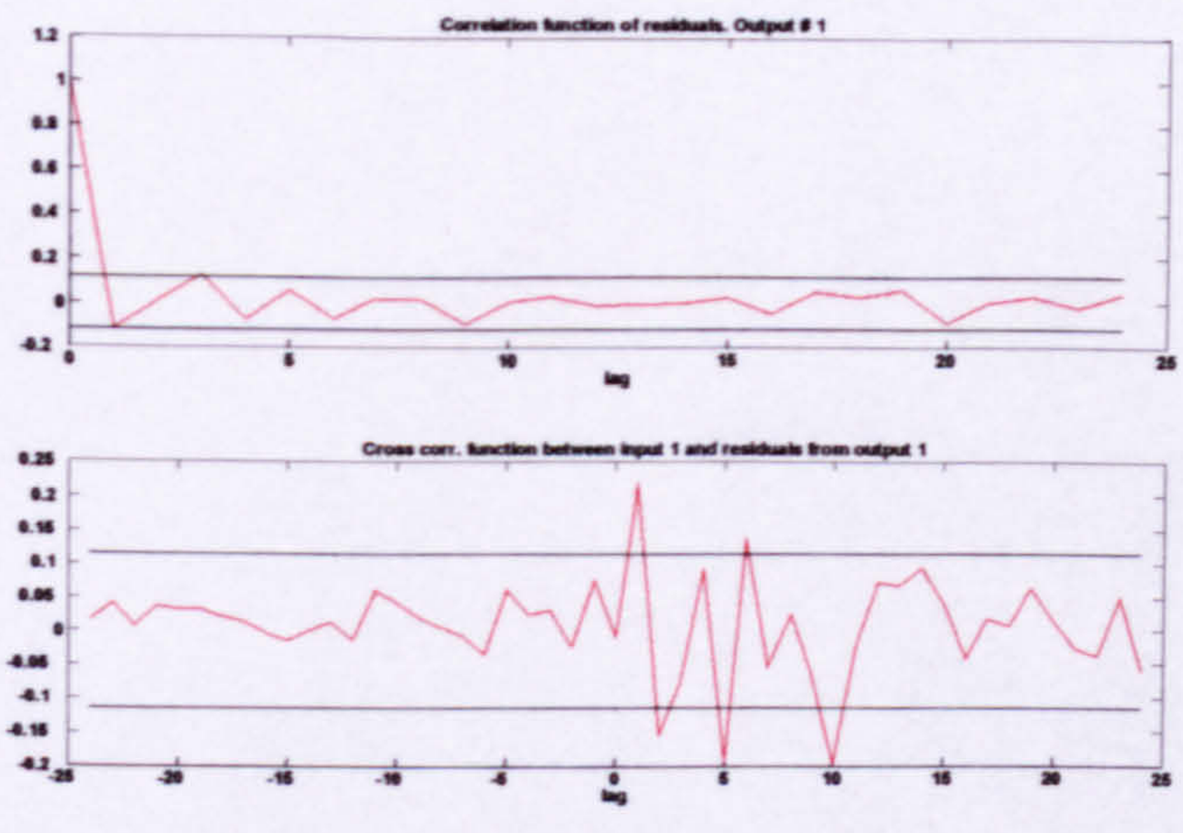

Figure 5.22 Residuals tests for the data of experiment 2 horizontal bars indicate 95 percent confidence levels

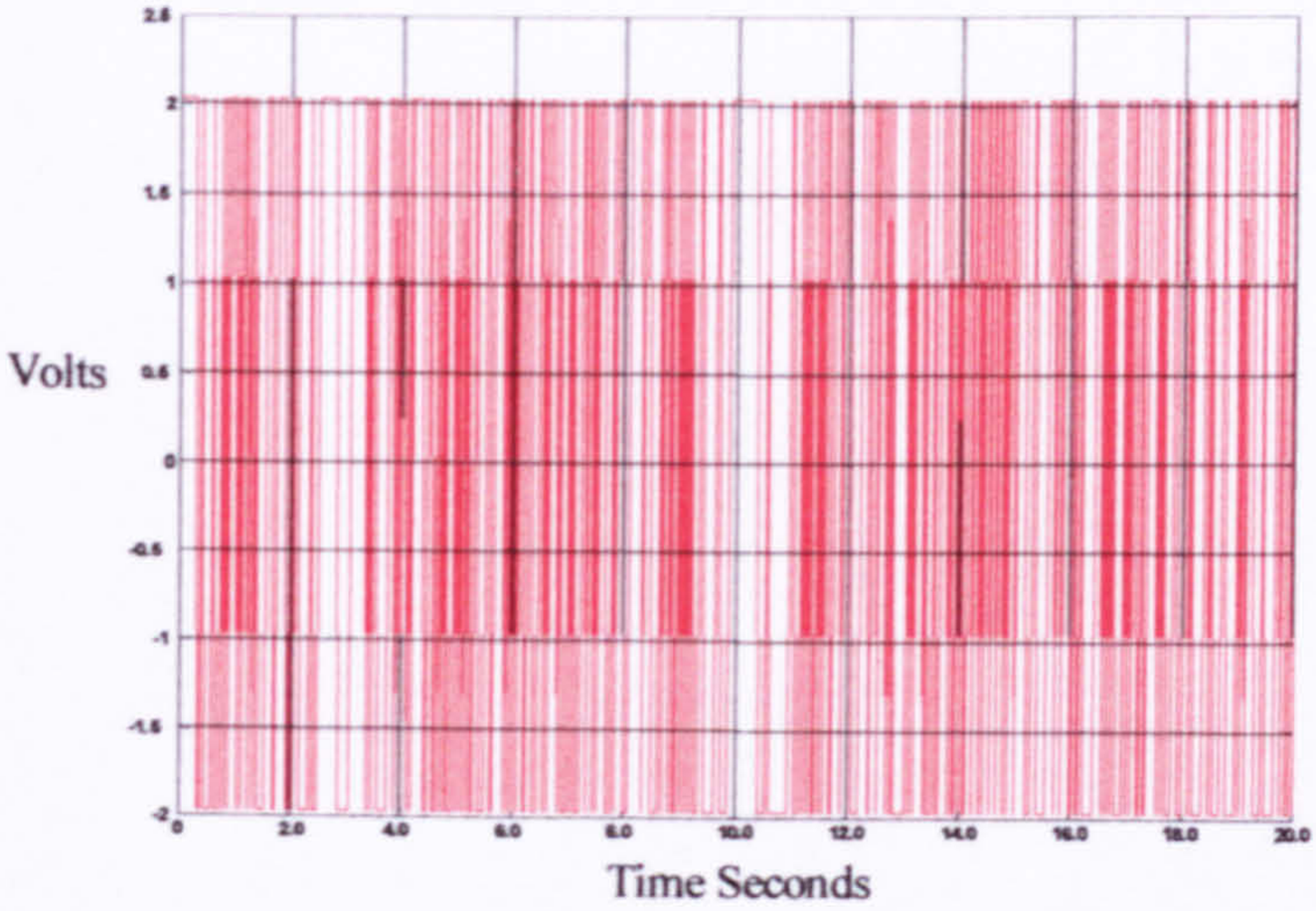

Figure 5.23 Input signal for exp3

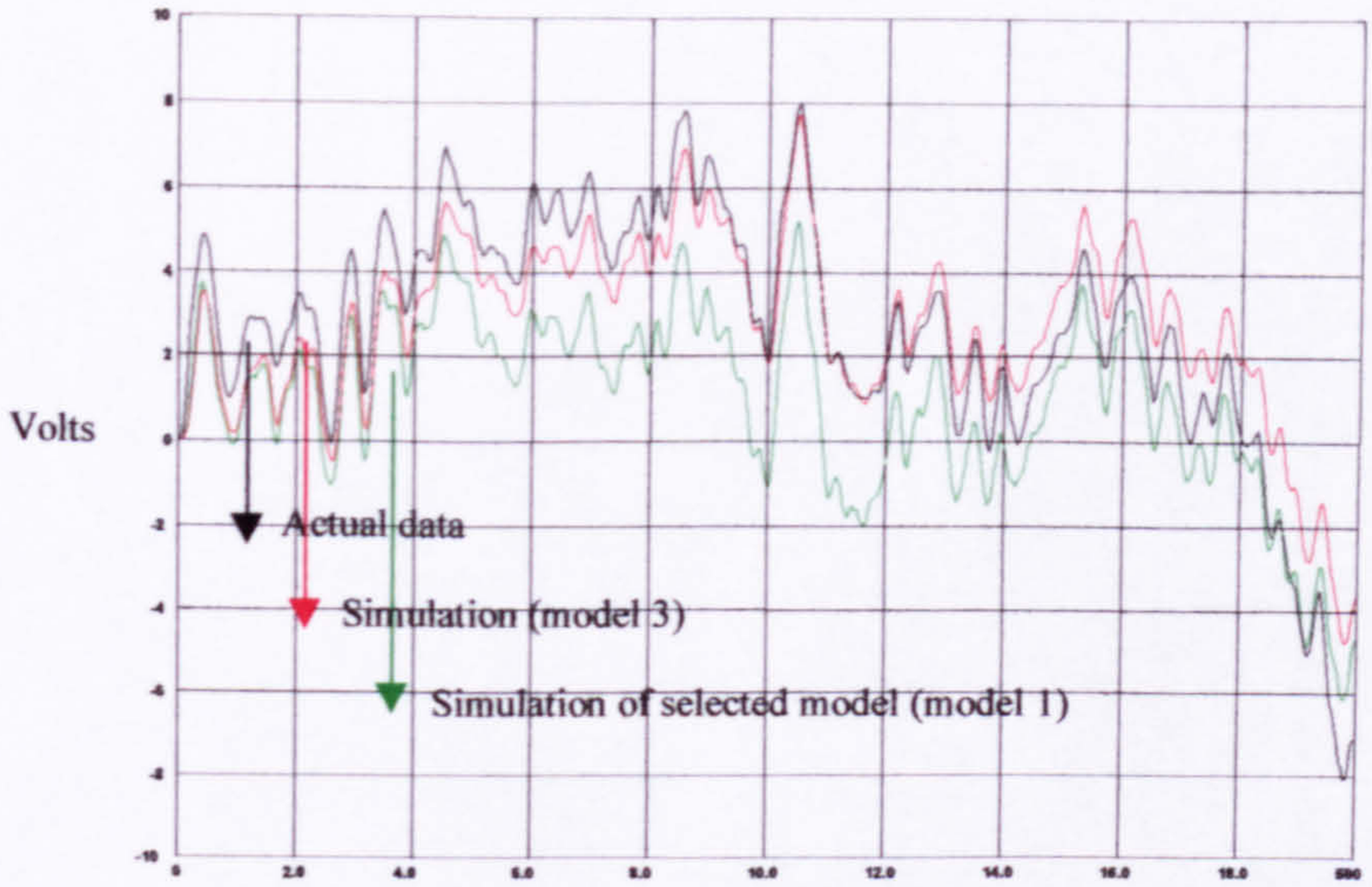

Figure 5.24 Comparison of Actual data with Simulated data for model 3 and model 1

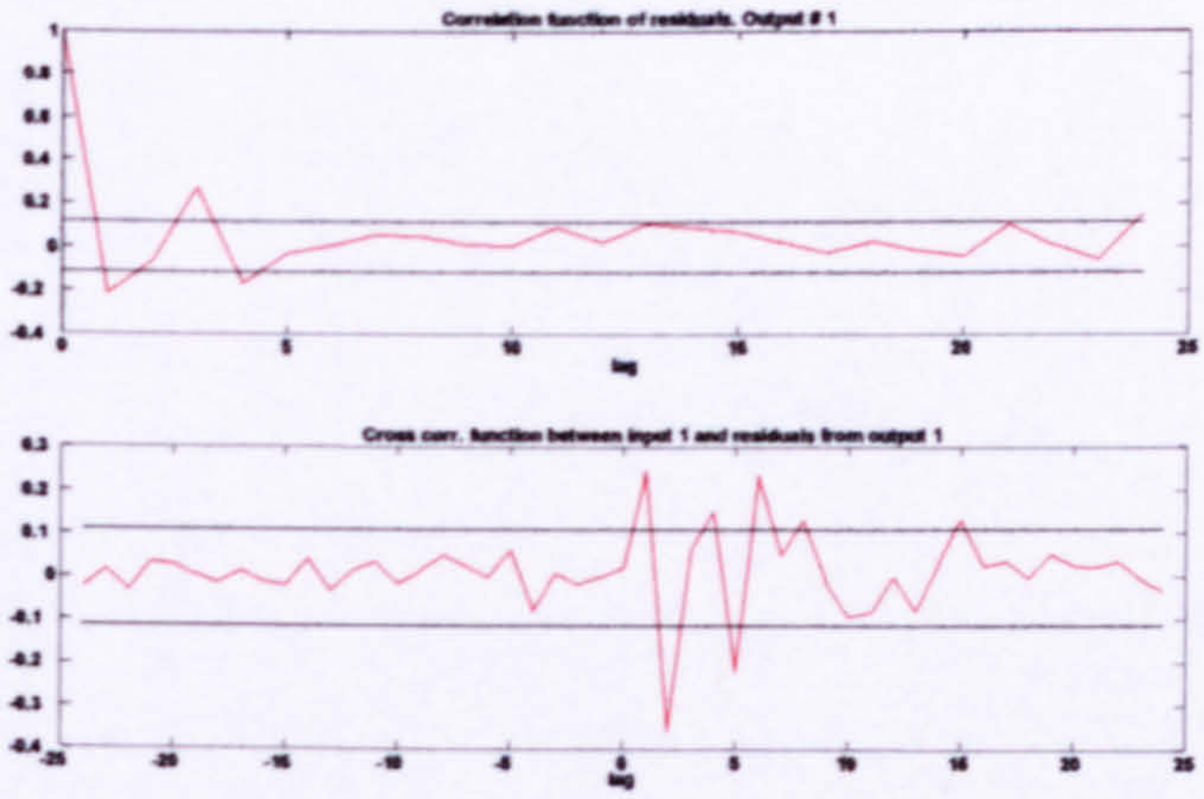

Figure 5.25 Residuals tests for the data of experiment 3 horizontal bars indicate 95 percent confidence levels

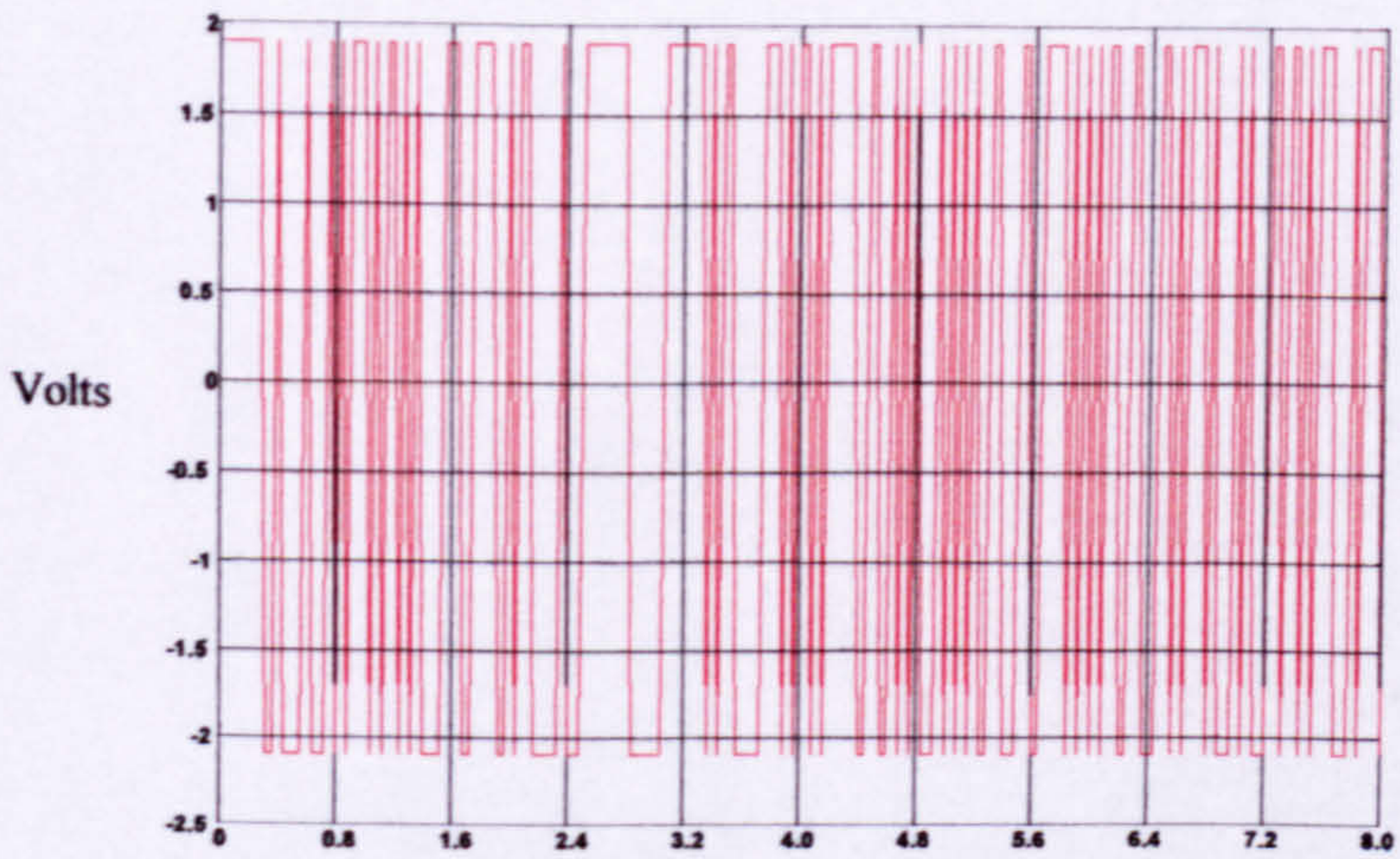

Figure 5.26 Input signal for exp4

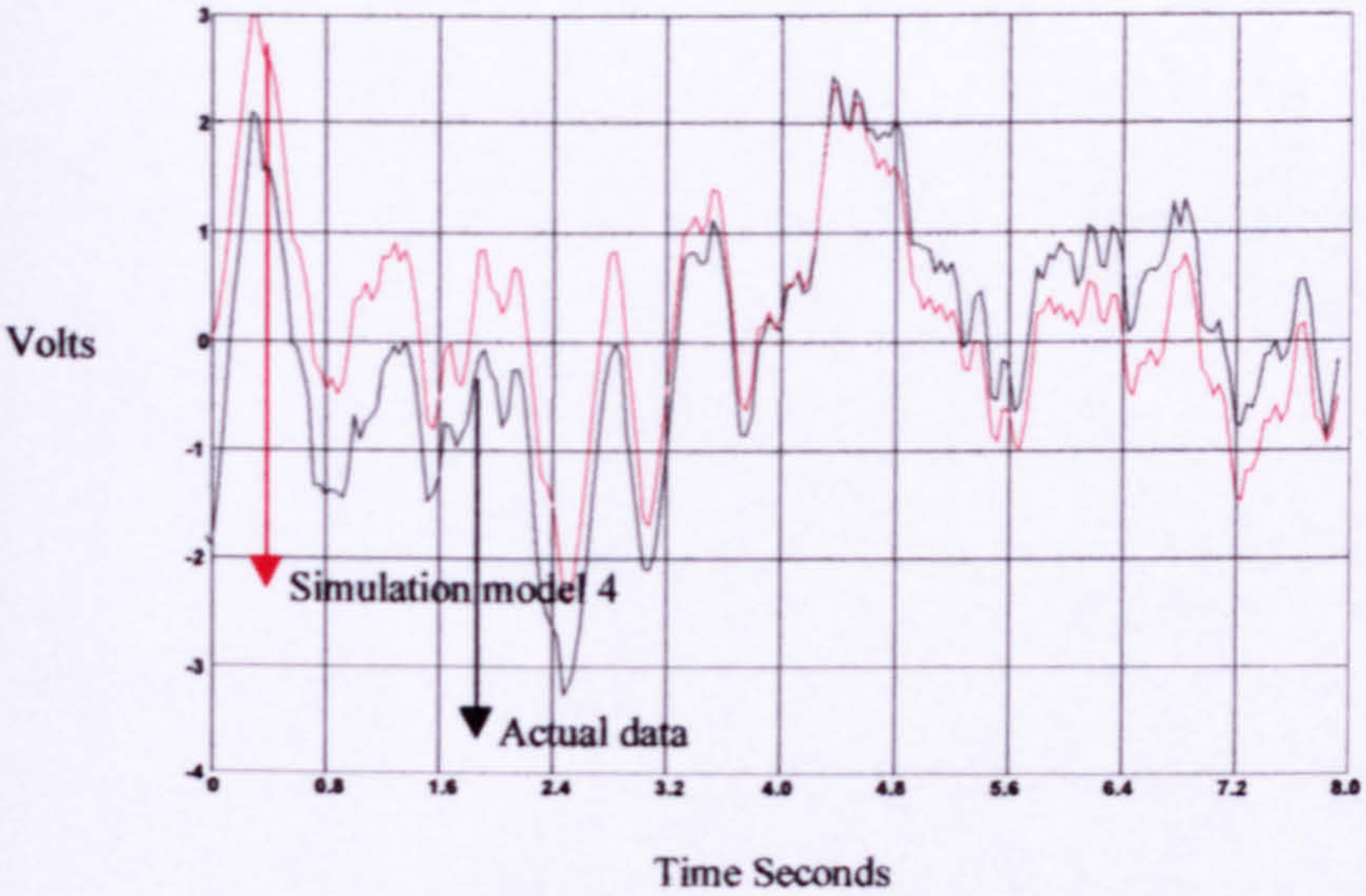

Figure 5.27 Comparison of actual data with simulated data for model 4

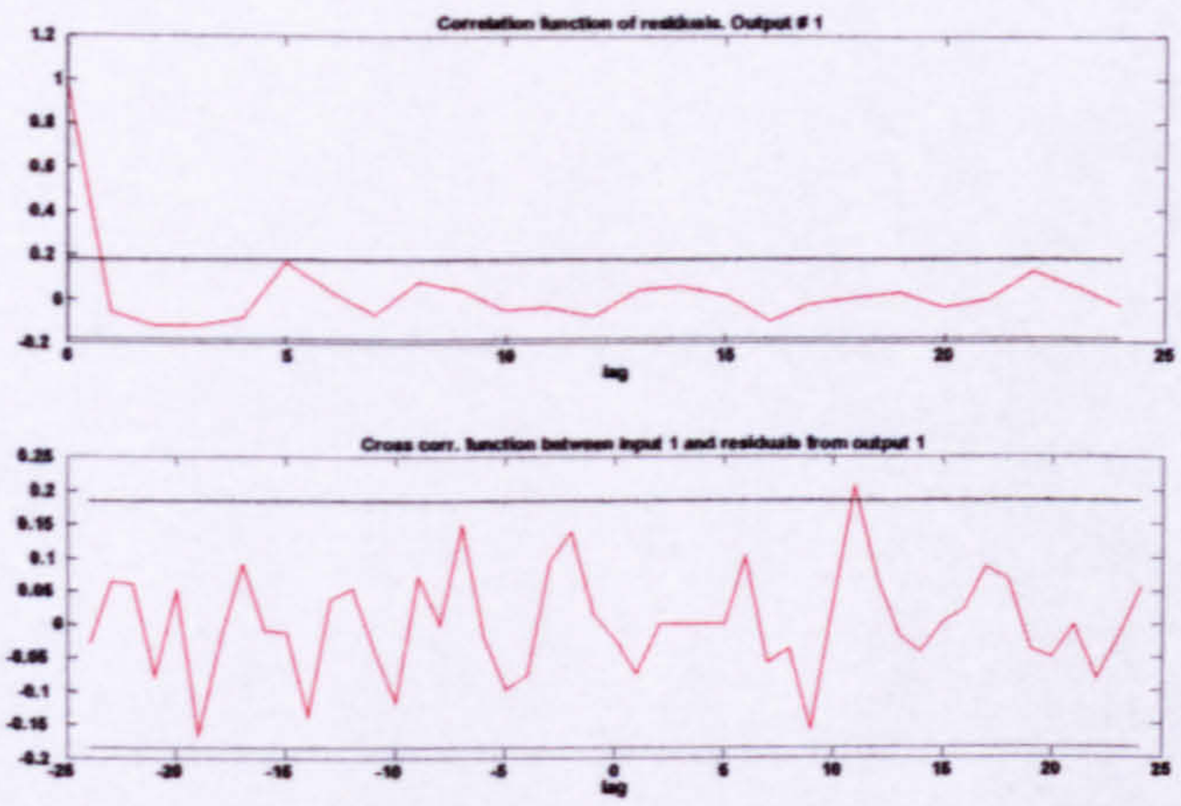

Figure 5.28 Residuals tests for the data of experiment 4 horizontal bars indicate 95 percent confidence levels

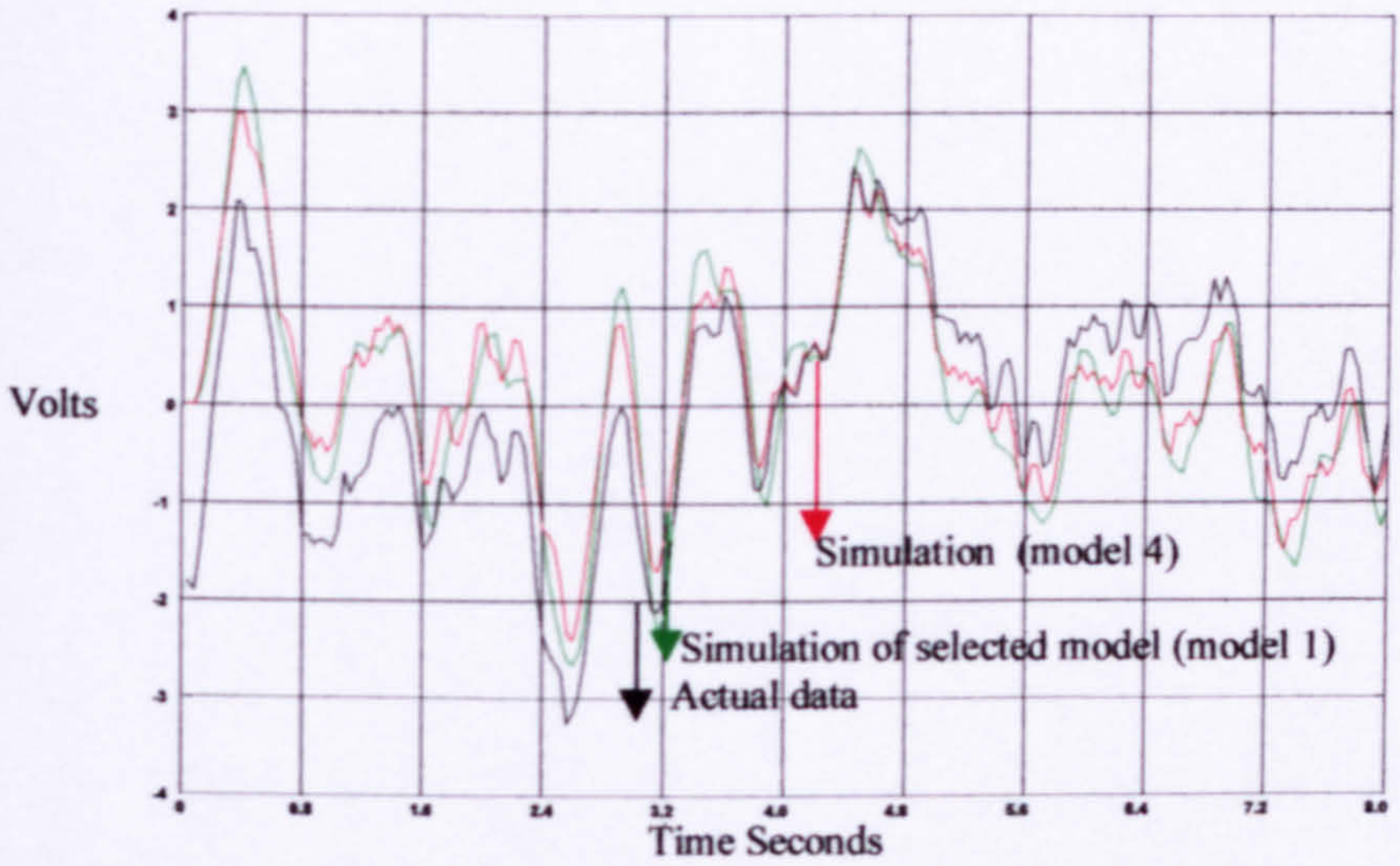

Figure 5.29 Comparison of acual data and simulated data for model 4 and model 1

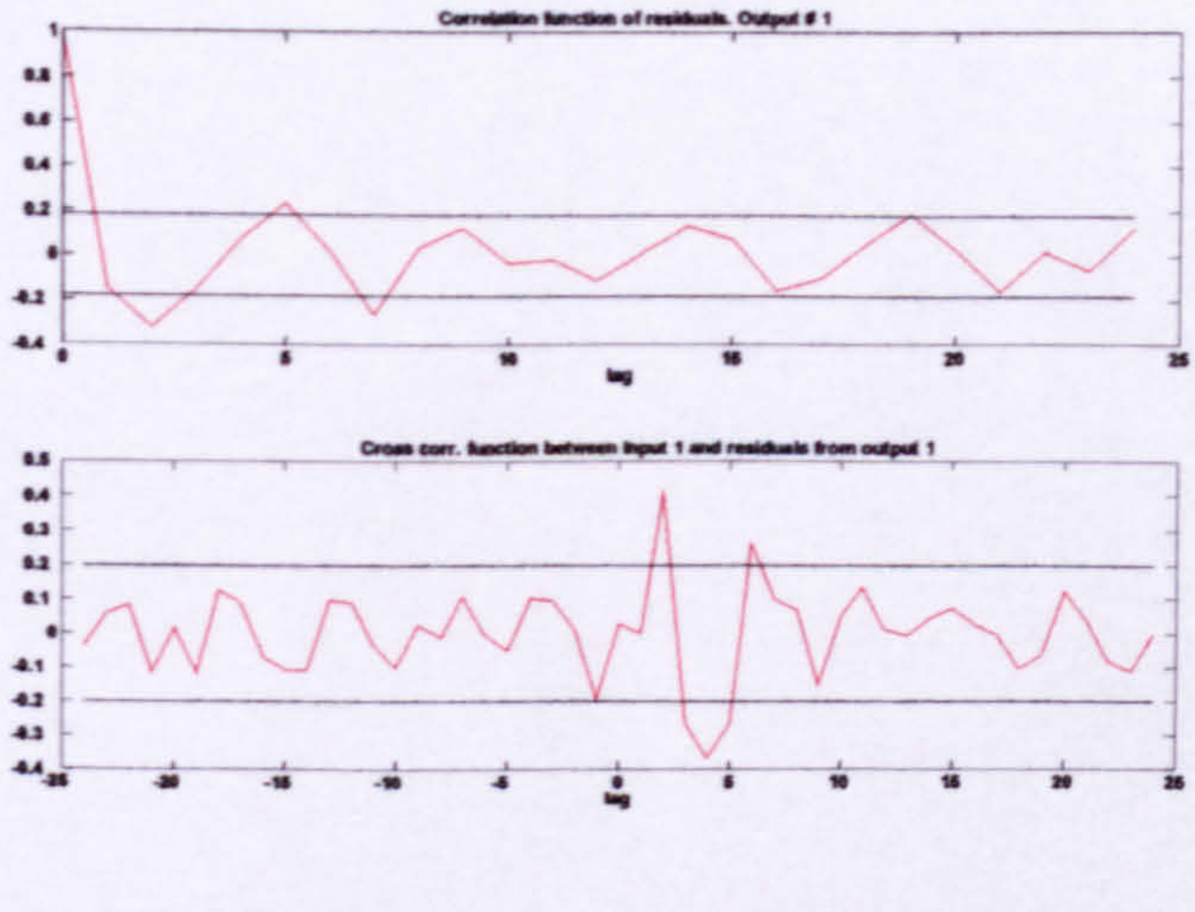

Figure 5.30 Residuals tests for data of experiment 4 horizontal bars indicate 95 percent confidence levels

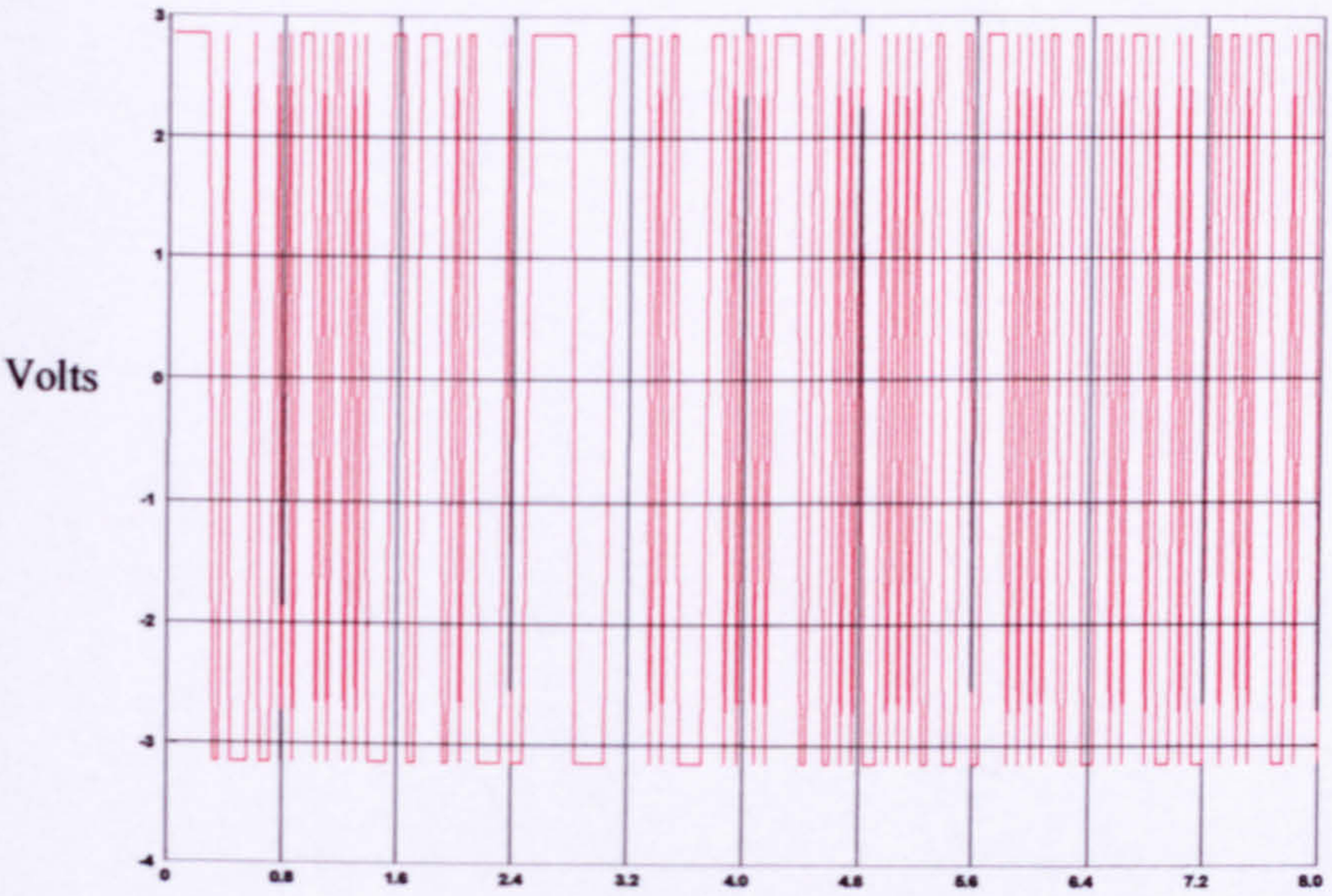

Figure 5.31 Input signal for experiment 5

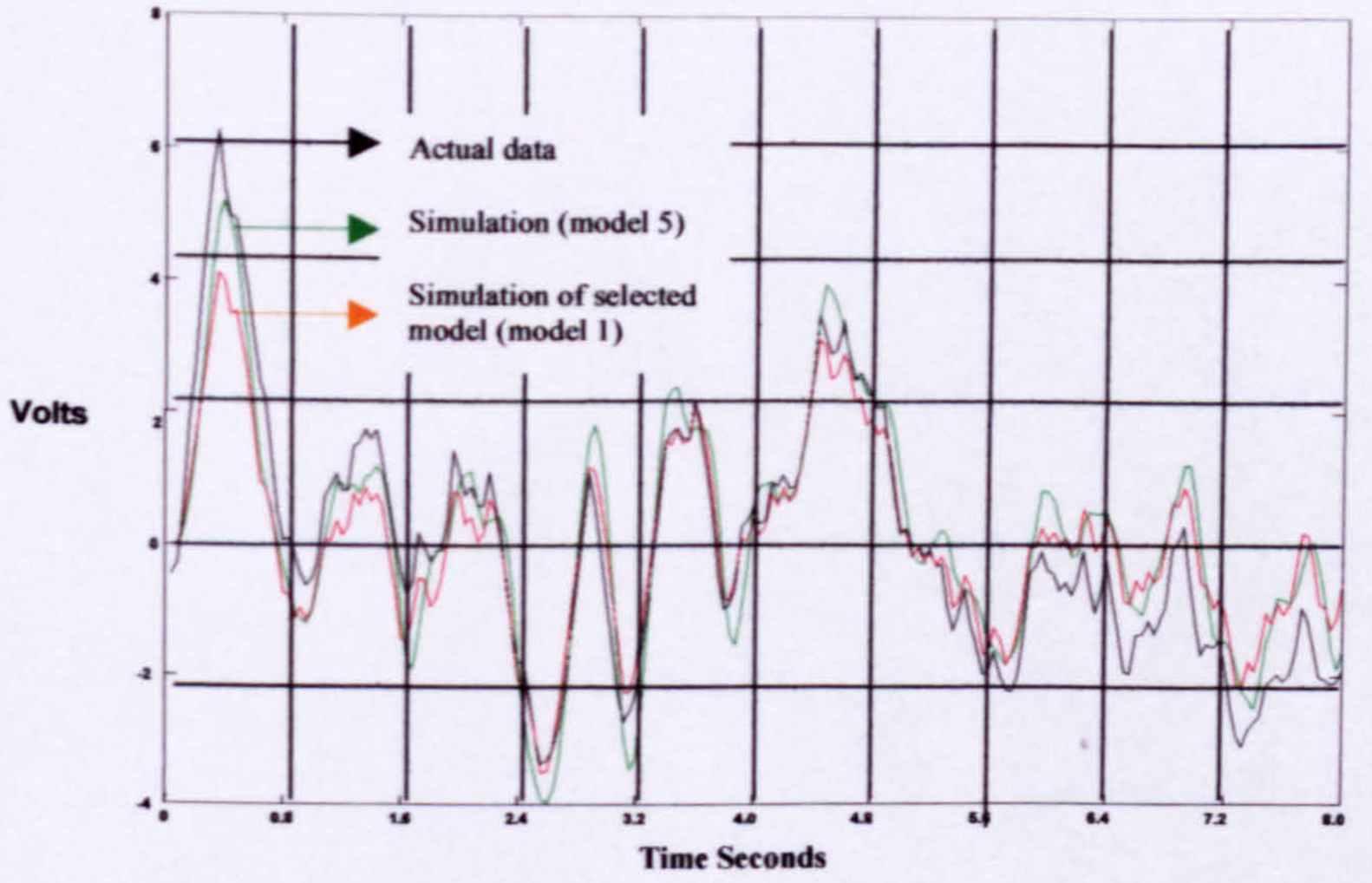

Figure 5.32 Comparison of actual data with simulated data for model 5 and model 1

5.7 DC gain and poles location of the five models

Further comparisons can be made of the five models by comparing the poles location and the DC gain of the system. For experiment 1 from table (5.3)

This gives the transfer function

$$\frac{0.0743z^{-2}+0.0285z^{-3}+0.0291z^{-4}+0.04322z^{-5}}{1-1.7167z^{-1}+0.7520z^{-2}+0.3061z^{-3}-0.3341z^{-4}}$$

The above equation is in the z inverse in order to convert to z we have to multiply by the highest power of z. This allows us to find the poles and zeros of the transfer function.

$$\frac{0.0743z^{3}+0.0285z^{2}+0.0291z+0.0432z}{z^{5}-1.7167z^{4}+0.7520z^{3}+0.3061z^{2}-0.33412z}$$

Using Matlab the magnitude of the poles of this system can be found

[0.00,0.9887,0.8143, 0.8143,0.5097]

Since the system is stable, to determine the DC gain we set z to 1 in the above equation. This yields a DC gain of 22.3. The same procedure was carried out for all the experiments with the following results.

Exp1 4 volts input	Exp2 3 volts input	Exp3 2 volts input	Exp4(loaded) 2 volts input	Exp5(loaded) 3 volts input
|Zeroes location|	|Zeroes location|	|Zeroes location|	|Zeroes location|	|Zeroes location|
0.8520	0.7906	0.8095	0.6482	0.6153
0.8520	0.7906	0.8095	0.6482	0.6157
0.8007	0.6558	0.5577	0.4729	0.6157

Table 5.4 Location of the zeros of different models

Exp1 4 volts input		Exp2 3 volts input		Exp3 2 volts input		Exp4(loaded) 2 volts input		Exp5(loaded) 3 volts input	
|Poles|	DC Gain	|Poles|	DC Gain	|Poles|	DC Gain	|Poles|	DC Gain	|Poles|	DC Gain
0.9887	22.30	0.9890	23.82	0.9881	25.4	0.9948	47.59	0.9793	11.97
0.8143		0.8253		0.7009		0.4437		0.3943	
0.8143		0.8253		0.7009		0.4437		0.3943	
0.5097		0.5644		0.4775		0.1849		0.2535	
0.00		0.00		0.00		0.00		0.00	

Table 5.5 Summary of the model analysis

Looking at tables (5.4-5.5) the first three tests were carried out at three separate input signals of different amplitudes. This enabled us to compare the models at different input signals. It was desirable to see if changing the amplitude of the input signal would change the order and the structure of the models. The first amplitude

was selected to be 2 volts. This was the smallest amplitude input signal which would excite the system enough for identification. Also the 2 volts was enough to overcome any friction or stiction in the system. Then the voltage was increased to 3 and 4 volts while observing the effect on the system. Over exciting the system would mean that the travel of the leg would be stopped by the mechanical constraints.

The fourth and fifth experiments were for the Orthosis with a person strapped to it. Therefore when choosing the input signal the response and acceptance of the person in the Orthosis into account. The 2 and 3 volts were the amplitudes accepted by our volunteers.

All the poles indicate that the system is stable as they are all inside the unit circle. All the zeroes are also inside the unit circle indicating that all models will yield a minimum phase system.

5.8 Conclusion

These results show that the model is capable of describing the system quite well. Furthermore figures (5.29), (5.32) show the model derived for the unloaded system can actually fit the data collected when the model is loaded. This would indicate that only one model is needed whether the system is loaded or not. The order, the structure and the delays were the same for the unloaded model and the loaded one. In deriving the loaded models volunteers were used. From their reaction it was clear that they were not happy if large amplitude input signals were used. The experiment

with volunteers lasted for approximately 15 minutes. This included strapping time and training in the posture the volunteer was expected to take. Because these volunteers were able bodied it would be uncertain how they would react to Pseudo random input signal. That is to say it would be unknown if they will fight the system movement or not. This problem will not occur with paraplegics and can be minimised with further training for able-bodied volunteers.

From the figures and data shown in this chapter it is clear that the model derived is good enough to be used for the pole placement controller. It matched the data collected at several different amplitudes of the pseudo-random-binary signals.

It also became apparent the importance of selecting the sampling time interval. Due to the shaking and vibration which corrupted the output signal, it was not possible to derive a consistent model when the sampling rate was 10 milliseconds. However when the sampling rate was dropped to 40ms these problems were not encountered. It is necessary to have a "clean" signal for the orthosis identification. To cope with cases of low signal to noise ratio, more advanced techniques are available such as the Generalised Least Squares.

CHAPTER 6

Robust Pole Placement controller

6.0 Introduction

The design of a control system requires a mathematical model, which represents as accurately as possible the actual system. The model has to represent the system with fidelity but it is also desirable to have it as simple as possible. This step is crucial in the controller design. An accurate model gives us confidence in the resulting controller as all the information for the controller is based on the system model then a good model actually implies a good controller.

The effect of parameter perturbations or un-modelled dynamics on stability and performance of systems is a crucial point in the design of control systems. Usually such perturbations are not amenable to exact modelling. These may be as a result of changing environmental conditions, calibration errors, noise or even neglected dynamics such as friction. Under these conditions it is desirable to have what is termed 'Robust Control'. That is a controller that at least maintains the stability of the system.

Modern robust control involves the development of synthesis techniques for robust performance stabilization, using H_∞ norm and H_2 norm. These techniques may involve intricate calculations. Furthermore H_∞ methods may yield unstable controllers even

when the open loop system is stable. This is undesirable from a practical point of view since excessive actuator saturation can occur.

Among the more traditional methods for controller design, we have **PID, Lag Lead** and **Pole-Assignment** controllers. The Pole-Assignment method is particularly appealing since the designer can completely specify the closed-loop poles of the system. For any given set of closed loop poles the controller computation is a straightforward task of solving a set of simultaneous linear equations. The main problem in designing a pole placement controller involves the selection of the closed loop poles to achieve good performance and a reasonable degree of robustness.

Once a controller has been designed we can obtain a family of stabilizing controllers using Youla's Parameterisation [Mustafa M.M., 1989a, 1989b]. The main advantage of this technique is that it can be applied to any system despite its poles and zeros locations. Moreover, using Youla's parameterisation we have additional degrees of freedom for tuning the controller to improve performance and robustness of the closed loop system. However the resulting controller will become more complex

The system considered in this thesis is a single input single output system. It is assumed that the single input single output process to be controlled is linearizable at some operating point so that it can be described by a linear stochastic difference equation. From the previous chapter it was found that the ARMAX model can represent our system quite satisfactorily. Generally the ARMAX model is given by: -

$$A(q^{-1})y(t) = B(q^{-1})u(t) + e(t) \qquad \text{equation 6.1}$$

Where

$$A(q^{-1}) = 1 + a_1 q^{-1} + \ldots\ldots\ldots + a_{na} q^{-na} \qquad \text{equation 6.2}$$

$$B(q^{-1}) = b_1 q^{-1} + b_2 q^{-2} + \ldots\ldots\ldots + b_{nb} q^{-nb} \qquad \text{equation 6.3}$$

Where

q^{-1} is the backward shift operator

The signals y(t) and u(t) are uniformly sampled values of the system output and input respectively. The signal e(t) represents modelling errors, noise and disturbances that cannot be measured directly. The feedback scheme for the model given by equation 6.1 is shown in figure (6.1). The controller polynomials $F(z^{-1}), G(z^{-1})$ and $H(z^{-1})$ are to be determined according to the pole assignment. The signal r(t) denotes the reference or set point for the controller.

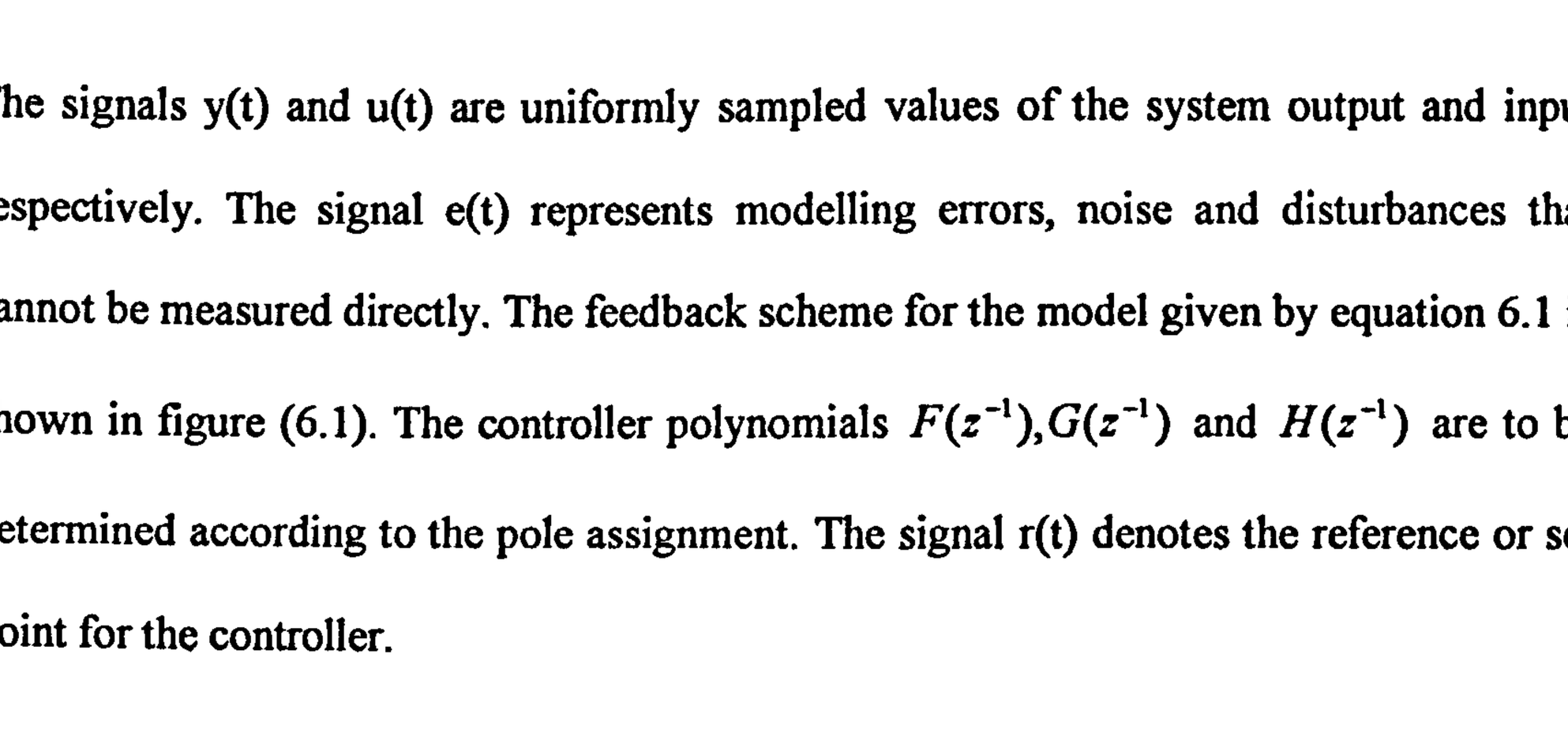

Figure 6.1 Pole Assignment Controller Configuration

From the block diagram in figure (6.1) the controller equation is given by

$$F(z^{-1})u(t) = -G(z^{-1})y(t) + H(z^{-1})r(t) \qquad \text{equation 6.5}$$

Where

$$F(z^{-1}) = 1 + f_1 z^{-1} + \ldots\ldots\ldots\ldots + f_{nf} z^{-nf} \qquad \text{equation 6.6}$$

$$G(z^{-1}) = g_0 + g_1 z^{-1} + \ldots\ldots\ldots\ldots + g_{ng} z^{-ng} \qquad \text{equation 6.7}$$

The closed loop description can be obtained by combining the controller and system equation in (6.1)

$$\left[A(z^{-1})F(z^{-1}) + B(z^{-1})G(z^{-1})\right]y(t) = \left[B(z^{-1})H(z^{-1})\right]r(t) + F(z^{-1})e(t) \qquad \text{equation 6.8}$$

The closed loop dynamics are designed by specifying the location of the closed loop poles as specified by the zeros of $T(z^{-1})$ i.e. by selecting $F(z^{-1})$ and $G(z^{-1})$ according to

$$A(z^{-1})F(z^{-1}) + B(z^{-1})G(z^{-1}) = T(z^{-1}) \qquad \text{equation 6.9}$$

where

$$T(z^{-1}) = 1 + t_1 z^{-1} + \ldots\ldots\ldots\ldots + t_{nt} z^{-nt}$$

The resulting closed loop system is given by

$$y(t) = \frac{B(z^{-1})H(z^{-1})}{T(z^{-1})}r(t) + \frac{F(z^{-1})}{T(z^{-1})}e(t) \qquad \text{equation 6.10}$$

$$u(t) = \frac{A(z^{-1})H(z^{-1})}{T(z^{-1})}r(t) - \frac{G(z^{-1})}{T(z^{-1})}e(t) \qquad \text{equation 6.11}$$

The pre-compensator $H(z^{-1})$ is chosen as a constant, so that the closed loop system $r(t) \rightarrow y(t)$ has unity gain.

$$H = \frac{T(z^{-1})}{B(z^{-1})}\bigg|_{z=1} \qquad \text{equation 6.12}$$

It is worth noting at this point that if $A(z^{-1})$ or $F(z^{-1})$ has a root at z=1 i.e. system or controller has an integrator then $H = G(z^{-1})\big|_{z=1}$ and hence H does not depend on the system parameters

The polynomial $T(z^{-1})$ influences both the response to r (t) and the noise e(t) It is generally difficult to get good transient response and noise rejection simultaneously.

6.1 Analysis of the pole assignment solutions

Equation (6.9) is solved by equating the coefficients of the power-like of z^{-1} to yield a set of simultaneous linear equations. The number of unknowns is $n_f + n_g + 1$ and the number of equations is $\max(n_a + n_f, n_b + n_g)$ the solution depends on the degrees of $F(z^{-1}), G(z^{-1})$, and $T(z^{-1})$. We can have the following cases

Case 1: Approximate solutions

In general if

$$n_f + n_g + 1 < \max(n_a + n_f, n_b + n_g)$$

$$\text{Or} \quad n_t > \max(n_a + n_f, n_b + n_g)$$

Then an exact solution does not exist, however approximate solutions such as least squares solutions can be found.

Case 2: An exact and unique solution with minimum order

If $A(z^{-1})$ and $B(z^{-1})$ are relatively prime i.e. do not have common roots and

$$n_f = n_b - 1, n_g = n_a - 1$$

then

$$n_f + n_g + 1 = \max(n_a + n_f, n_b + n_g) = n_a + n_b - 1 \qquad \text{equation 6.13}$$

i.e. the number of unknowns equals the number of equations.

and $nt \leq \max(n_a + n_f, n_b + n_g) = n_a + n_b - 1$ equation 6.14

Case 3: Infinite number of exact solutions

An infinite number of exact solutions exist when

A, B are relatively prime and

$n_f + n_g + 1 \rangle \max(n_a + n_f, n_b + n_g)$ equation 6.15

and

$n_t \leq \max(n_a + n_f, n_b + n_a)$ equation 6.16

A controller that satisfies equations (6.9), (6.13) and (6.14) is referred to as a minimal order controller. A controller which satisfies equations (6.9), (6.15) and (6.16), is known as a high order controller. The design of the high order and minimal order controllers and the resulting input output behaviour of the system will be evaluated later however an example of solving equation (6.9) for minimal order controller is given below

6.2 Minimal order Example

Let our model be

$$A(z^{-1}) = 1 - 2.5757z^{-1} + 2.5753z^{-2} - 1.2444z^{-3} + 0.2446z^{-4}$$

$$B(z^{-1}) = 1.177 \times 10^{-3} z^{-4} + 1.5332 \times 10^{-3} z^{-5}$$

These model parameters were selected from models, which were derived for the motor during experimentation. They do not represent the final models for the motor or Orthosis but were chosen for simplicity.

The minimal order controller polynomials $F_o(z^{-1})$ and $G_o(z^{-1})$ are parameterised according to the following equation.

$$A(z^{-1})F_o(z^{-1}) + B(z^{-1})G_o(z^{-1}) = T(z^{-1})$$

In this example.

$n_b = 5$	The degree of the B polynomial
$n_a = 4$	The degree of the A polynomial

Hence equations (6.13) and (6.14) yield

$n_f = 5 - 1 = 4$	The degree of the F_o polynomial
$n_g = 4 - 1 = 3$	The degree of the G_o polynomial
$n_t \leq 4 + 5 - 1 = 8$	The degree of the closed loop polynomial $T(z^{-1})$

Substituting for $A(z^{-1})$ and $B(z^{-1})$ yields

$$\left(1-2.5757z^{-1}+2.5753z^{-2}-1.2444z^{-3}+0.2448z^{-4}\right)\times\left(1+f_1z^{-1}+f_2z^{-2}+f_3z^{-3}+f_4z^{-4}\right)+$$

$$\left(1.177e-3z^{-4}+1.5332e-3z^{-5}\right)\times\left(g_o+g_1z^{-1}+g_2z^{-2}+g_3z^{-3}\right)=T(z^{-1})$$

Putting the above equation in matrix form

$$\begin{bmatrix} 1 & 0 & 0 & 0 & 0 & 0 & 0 & 0 \\ -2.5757 & 1 & 0 & 0 & 0 & 0 & 0 & 0 \\ 2.5753 & -2.5757 & 1 & 0 & 0 & 0 & 0 & 0 \\ 2.5753 & -2.5757 & 1 & 0 & 0 & 0 & 0 & 0 \\ -1.2444 & 2.5753 & -2.5757 & 1 & 1.177e-3 & 0 & 0 & 0 \\ 0.2448 & -1.2444 & 2.5753 & -2.5757 & 1.5332e-3 & 1.177e-3 & 0 & 0 \\ 0 & 0 & 0.2448 & -1.244 & 0 & 0 & 1.5332e-3 & 1.77e-3 \\ 0 & 0 & 0 & 0.2448 & 0 & 0 & 0 & 1.5332e-3 \end{bmatrix} \begin{bmatrix} f_1 \\ f_2 \\ f_3 \\ f_4 \\ g_0 \\ g_1 \\ g_2 \\ g_3 \end{bmatrix} + \begin{bmatrix} -2.5757 \\ 2.5753 \\ -1.2444 \\ 0.2448 \\ 0 \\ 0 \\ 0 \\ 0 \end{bmatrix} = \begin{bmatrix} t_1 \\ t_2 \\ t_3 \\ t_4 \\ t_5 \\ t_6 \\ t_7 \\ t_8 \end{bmatrix}$$

Once $t_1, t_2, \ldots\ldots, t_8$ are chosen the above expression is used to compute

$$f_1, f_2, f_3, f_4, g_o, g_1, g_2 \text{ and } g_3$$

6.3 Computation of Higher order controllers using Youlas Parameterisation

In section (6.2) we established that under suitable assumptions the pole assignment equation (6.9) has an infinite number of solutions. We now consider a parameterization of all controllers that will yield the same closed loop polynomial $T(z^{-1})$ in terms of the minimal order controller $F_o(z^{-1})$ and $G_o(z^{-1})$. This parameterisation was essentially introduced by [Youla et al, 1974, 1976a, 1976b,1985]. Let $F_o(z^{-1})$ and $G_o(z^{-1})$ be the

minimum order controller satisfying equation (6.9). Then any other F and G are given by

$$F(z^{-1}) = F_o(z^{-1}) + B(z^{-1})P(z^{-1}) \qquad \text{equation 6.17}$$

$$G(z^{-1}) = G_o(z^{-1}) - A(z^{-1})P(z^{-1}) \qquad \text{equation 6.18}$$

Where $P(z^{-1})$ is a stable transfer function. The stability of $P(z^{-1})$ is imposed to prevent internal instability due to unstable pole-zero cancellations. In this dissertation P will be chosen as a finite polynomial to insure stability and simplify calculations.

$$P(z^{-1}) = p_o + p_1 z^{-1} + \ldots\ldots\ldots + p_{np} z^{-np} \qquad \text{equation 6.19}$$

For such polynomials the degrees of F and G are increased by the same amount $n_p + 1$.

Equations (6.17) and (6.18) provide additional freedom to design the controller F, G. There are some important questions. How do we select P to achieve good results? Can we choose P to prevent the closed loop system becoming unstable under model mismatch? Can P be chosen to prevent actuator saturation or fast variations in control signals? Can P be chosen to reduce the effect of noise in y and u? What is a suitable order np of $P(z^{-1})$ [Zarrop B., 1985]? These issues will be discussed in the following sections.

6.4 Closed Loop Stability in presence of model mismatch

Consider the closed loop in figure (6.2) below

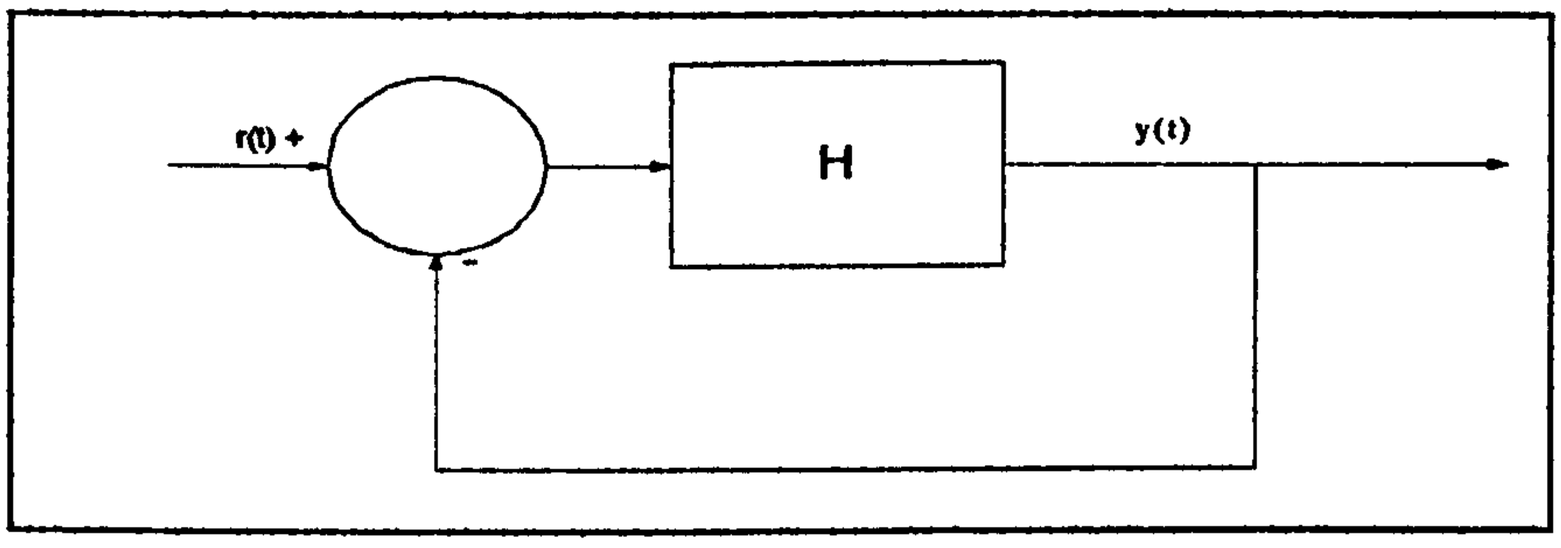

Figure 6.2 Closed loop unity feedback system

Let the true open loop system be H and let $\hat{H}$ be a model of H. Let S and $\hat{S}$ be the corresponding closed loop systems. Since H and $\hat{H}$ are in general different, it is not at all evident that the real system is closed loop stable just because $\hat{S}$ is stable. The following theorem [Astrom&Wittenmark, 1984] gives conditions to ensure the stability of S

THEOREM

Let H and $\hat{H}$ be represented as a ratio of polynomials in z, such that both H and $\hat{H}$ are strictly proper. The closed loop system S is stable if the following conditions hold.

1) $\hat{S}$ is stable

2) H and $\hat{H}$ Have the same number of unstable poles.

3) The following inequality is fulfilled for $|z| = 1$

$$\left|H - \hat{H}\right| < \left|1 + \hat{H}\right|$$

Proof is shown in Appendix B [Mustaffa M.M, 1989].

The essence of this result is that it is possible to draw conclusions about closed loop stability properties for two systems with similar frequency responses if they have the same number of unstable open loop poles.

The above theorem gives only a sufficient condition for the closed loop stability. In other words if the inequality is satisfied then the closed loop system is stable, but if the inequality is violated we cannot conclude anything. There are systems H that violate the inequality and S is stable, while other systems H violating the inequality result in an unstable closed loop system.

For our specific case the previous theorem takes the following form

Corollary

Let the actual system $\frac{B(z^{-1})}{A(z^{-1})}$ be modelled as $\frac{\hat{B}(z^{-1})}{\hat{A}(z^{-1})}$ where $A(z^{-1})$ and $\hat{A}(z^{-1})$ are stable.

Based on the model $\hat{B}(z^{-1}), \hat{A}(z^{-1})$ a pole placement controller $F(z^{-1})$ and $G(z^{-1})$ is designed with closed loop poles given by the roots of $T(z^{-1})$ The closed loop system will be stable if

$$\left|\frac{\hat{B}(z^{-1})}{\hat{A}(z^{-1})} - \frac{B(z^{-1})}{A(z^{-1})}\right| < \left|\frac{T(z^{-1})}{\hat{A}(z^{-1})G(z^{-1})}\right| \quad \text{for all } |z| = 1 \qquad \text{equation 6.20}$$

If $A(z^{-1})$ and $\hat{A}(z^{-1})$ are not stable but have the same number of unstable poles it can still be concluded that closed loop stability can be achieved if (6.20) is satisfied

PROOF

For stability analysis the block diagram in figure (6.1) is equivalent to the system shown in figure (6.2)

Let

$$H = \frac{BG}{AF} \quad \text{and} \quad \hat{H} = \frac{\hat{B}G}{\hat{A}F}$$

Then from the previous theorem the sufficient condition for closed loop stability is

$$\left|\frac{BG}{AF}-\frac{\hat{B}G}{\hat{A}F}\right| < \left|1+\frac{\hat{B}G}{\hat{A}F}\right| \quad \text{for all } |z|=1 \qquad \text{equation 6.21}$$

This expression is equivalent to

$$\left|\frac{G}{F}\right|\left|\frac{B}{A}-\frac{\hat{B}}{\hat{A}}\right| < \left|\frac{\hat{A}F+\hat{B}G}{\hat{A}F}\right| \quad \text{for all } |z|=1 \qquad \text{equation 6.22}$$

Since $\hat{A}F+\hat{B}G=T$, equation (6.22) reduces to equation (6.20)

Note that the inequality (6.20) can be expressed in different formats, for example

$$\left|\frac{\hat{A}G}{T}\right| < \frac{1}{\left|\frac{B}{A}-\frac{\hat{B}}{\hat{A}}\right|}, \quad \text{for all } |z|=1$$

Or

$$|G| < \left|\frac{T}{\hat{A}}\right| \frac{1}{\left|\frac{B}{A}-\frac{\hat{B}}{\hat{A}}\right|}, \quad \text{for all } |z|=1 \qquad \text{equation 6.23}$$

Equation (6.23) indicates that when there are large errors between the model and the actual plant the term $\frac{1}{\left|\frac{B}{A}-\frac{\hat{B}}{\hat{A}}\right|}$ becomes very small. This effectively means that in order to satisfy the inequality (6.23), it would be of interest to make $\left|\frac{T}{\hat{A}}\right|$ large and/or $|G|$ small. If

the error is small then $\frac{1}{\left|\frac{B}{A}-\frac{\hat{B}}{\hat{A}}\right|}$ becomes large. In this case we only need to make sure that $\left|\frac{T}{\hat{A}}\right|$ does not become too small and/or $|G|$ is not excessively large.

Knowing that usually we have model mismatch, which is more significant at high frequencies, then $\left|\frac{T}{\hat{A}}\right|$ can be chosen to make the R.H.S of the inequality (6.23) large at those frequencies.

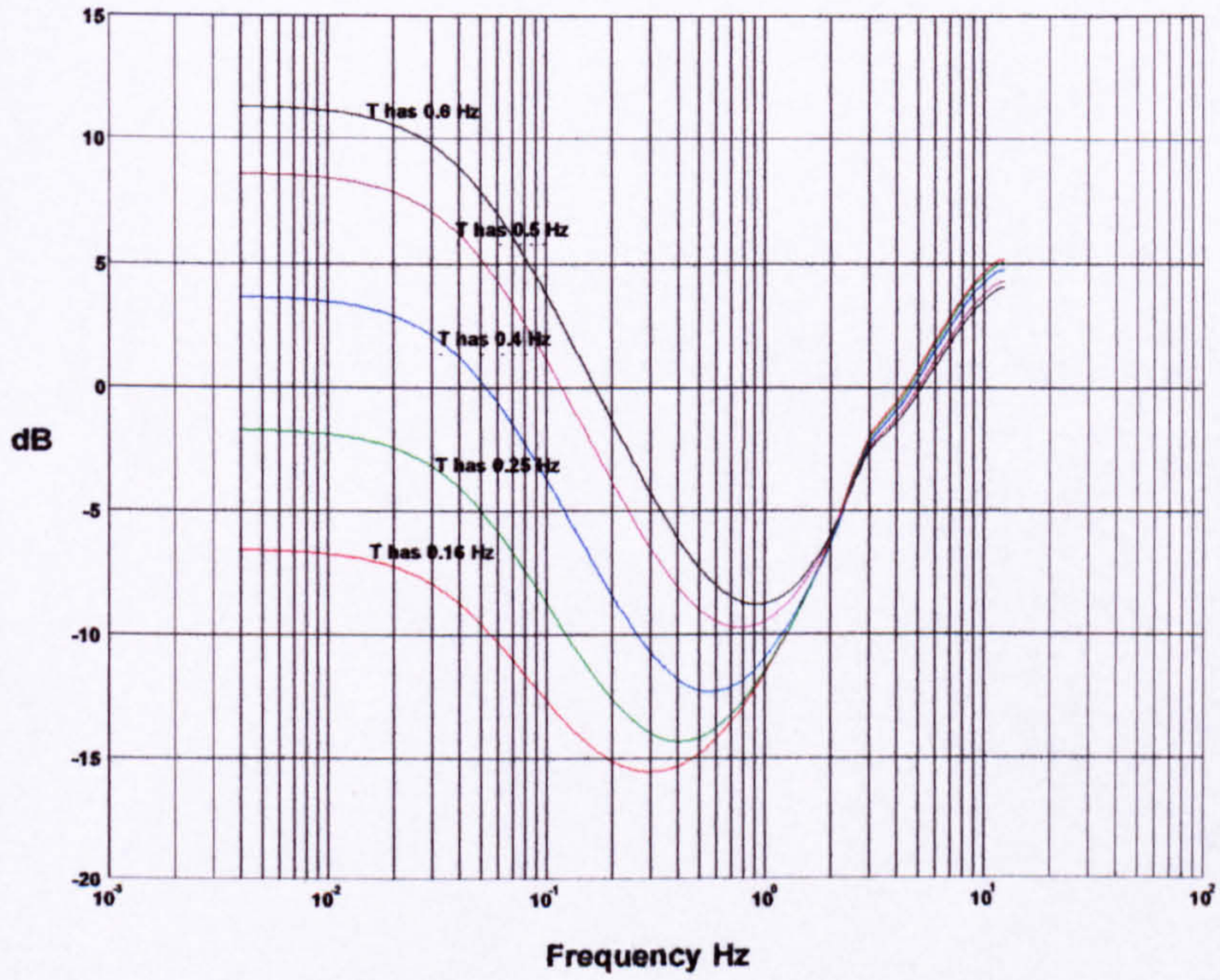

Figure 6.3 Frequency response of $\left|\frac{T}{\hat{A}}\right|$ for different polynomials T

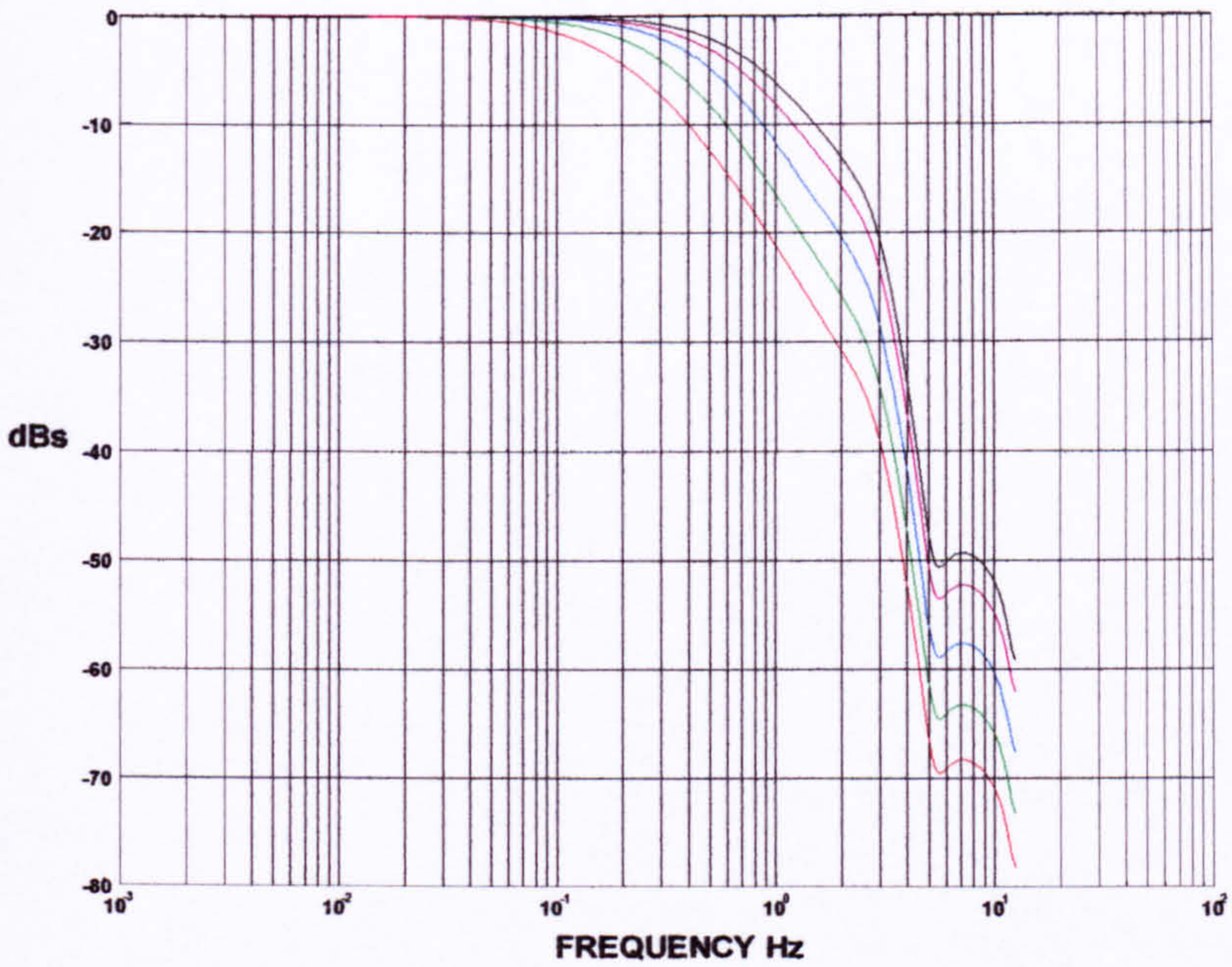

Figure 6.4 Frequency response $\frac{\hat{B}}{T}H$ for different closed loop polynomials

Figure (6.3) shows different plots of $\left|\frac{T}{\hat{A}}\right|$ where $\hat{A}$ is the model for the Orthosis (chapter 4 model 1) and different closed loop poles polynomial T with different bandwidth figure (6.4). It is clear that the selection of T has an effect in terms of the magnitude of $\frac{T}{\hat{A}}$ at low and mid frequencies. This gives us freedom in tuning T to give the desired shapes at these frequency regions. As stated before our options are to make the term $\left|\frac{T}{\hat{A}}\right|$ as large as possible or $|G|$ as small as possible in order to satisfy the inequality (6.23). To show how

this is achieved the following analysis is based on figures (6.3) and (6.4) where the frequency regions are split into three. The low, middle and high frequency regions

Figure (6.3) shows that the selection of T plays a big part in giving large values for $\left|\frac{T}{\hat{A}}\right|$ in the low frequency region. In the middle frequency region selection of T plays a significant part but may not be enough. This is where the second option of minimizing $|G|$ can play a big part, since it is not possible to make $\left|\frac{T}{\hat{A}}\right|$ large over the whole frequency range.

From equation (6.23) it follows then that given any two controllers say G1 and G2 which give the same closed loop polynomial $T(z^{-1})$, then we can say that G1 is a better controller than G2 from a stability robustness point of view if

$$\left|\frac{\hat{A}G1}{T}\right| < \left|\frac{\hat{A}G2}{T}\right| \quad \text{for } |z| = 1 \qquad \text{equation 6.24}$$

Or in other words

$$|G_1| < |G_2| \quad \text{for all } |z| = 1 \qquad \text{equation 6.25}$$

According to equation (6.25) we need to minimize G over the whole frequency range.

This is what the H_∞ does. However in order to decrease the computational complexity

we will minimize using the L_2 norm of $|G|$. This has he effect of minimizing $|G|$ in the high frequency region. Further more since G is a polynomial the L_2 norm becomes very easy to compute.

L_2 and Euclidean norms

Let $Q(z^{-1})$ be a complex function defined on the unit circle such that $\left|Q(e^{-jw})\right|$ is integrable on $w \in [0,2\pi]$.

The L_2 norm of $Q(z^{-1})$ is then defined as

$$\left\|Q(z^{-1})\right\|_{L_2}^2 = \frac{1}{2\pi}\int_{-\pi}^{\pi}\left|Q(e^{-jw})\right|^2 dw \qquad \text{equation 6.26}$$

To evaluate the L_2 norm either we can use the residuals technique or the algorithm given in [Astrom K.J., 1970], which is suitable for numerical computation.

In the case where $Q(z^{-1})$ is a polynomial, the L_2 norm reduces to $\sqrt{\sum q_i^2}$ (see appendix B) where q_i are the coefficients of $Q(z^{-1})$, and by a slight abuse of language this will be referred to as the Euclidean norm of a polynomial.

Figure (6.5) shows the plots of $|G|$ for different controller's $G_o, G_1, G_2, \ldots$, that produce the same closed loop polynomial T for the model $\hat{B}, \hat{A}$. This is very useful in order to satisfy the inequality (6.23). Figure (6.5) shows that the general trend in the high frequency region is a reduction in gain as the order of the controller is increased. In fact for a minimum order and two above the minimum order there is amplification in the high frequency region.

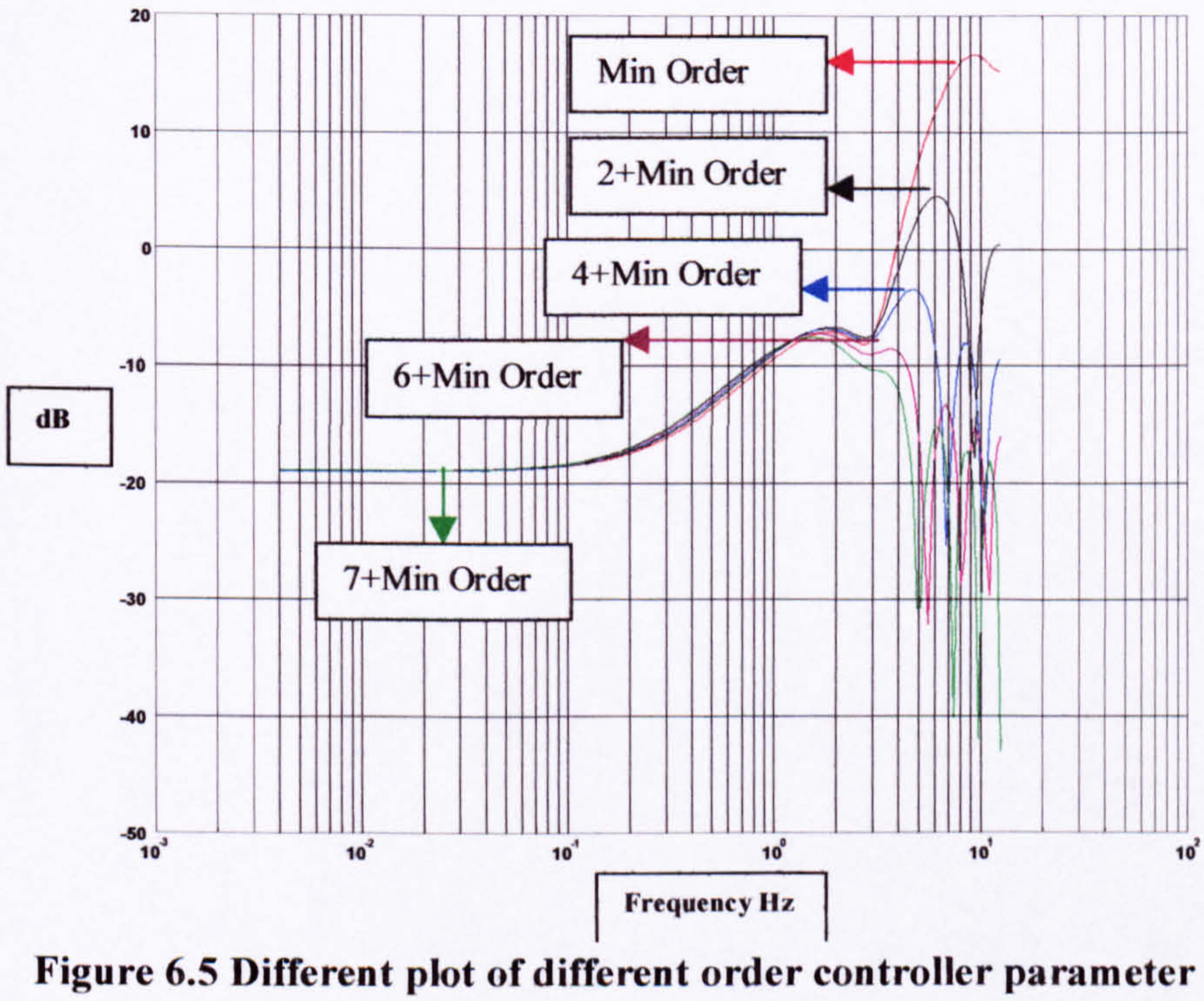

Figure 6.5 Different plot of different order controller parameter $|G|$

6.5 Calculation of the $P(z^{-1})$

The L_2 norm of G in terms of Youlas Parameterisation, equation 6.18 is

$$\|G\|_{L_2} = \|G_o - \hat{A}P\|_{L_2} \qquad \text{equation 6.28}$$

The following example illustrates the calculation of high order controllers minimizing (6.28).

The model to be used is

$$\frac{\hat{B}}{\hat{A}} = \frac{z^{-1} - 0.1z^{-2}}{1 - 1.065z^{-1} + 0.0833z^{-2}}$$

The chosen closed loop polynomials $T(z^{-1}) = 0.8, 0.6 \pm j0.4$

And the minimum order controller is

$F_o(z^{-1}) = 1 + 21.64z^{-1}$ and $G_o(z^{-1}) = -222.577 + 22.1881z^{-1}$

Equations 6.17 and 6.18 must be solved to obtain a high order controller

$F(z^{-1}) = F_o(z^{-1}) + \hat{B}(z^{-1})P(z^{-1})$ and $G(z^{-1}) = G_o(z^{-1}) - \hat{A}(z^{-1})P(z^{-1})$

As we are minimizing $\|G\|_{L_2}$ first write G in terms of the free polynomial

$P(z^{-1}) = p_o + p_1(z^{-1})$

$$G(z^{-1}) = \left(-222.577 + 22.188z^{-1)}\right) - \left(1 - 1.065z^{-1} + 0.0833z^{-2}\right)\left(P_o + P_1 z^{-1}\right)$$

$$= \left(-222.577 + 22.1881z^{-1}\right) - \left(P_o + P_1 z^{-1} - 1.065z^{-1}P_o - 1.065z^{-1}P_1 z^{-1} + 0.0833z^{-2}P_o + 0.0833z^{-2}P_1 z^{-2}\right)$$

$$= -222.577 + 22.18881z^{-1} - [P_o - 1.065z^{-1}P_o + o.0833z^{-2}P_o + P_1 z^{-1} - 1.065z^{-1}P_1 z^{-1} + 0.0833z^{-2}P_1 z^{-1}]$$

$$= \left(-222.577 - P_o\right) + \left(22.1881 + 1.065P_o + P_1 + 1.065P_1\right)z^{-1} - \left(0.0833P_o + 0.0833P_1\right)z^{-2}$$

Now taking the L_2 norm.

$$\|G\|_{L_2} = \left(-222.577 - P_o\right)^2 + \left(22.1881 + 1.065P_o + P_1 + 1.065P_1\right)^2 + \left(0.0833P_o + 0.0833P_1\right)^2$$

$$=$$

$$50032.8 + 492.4P_o + 92.7P_1 + 2.137P_o^2 + 3.20P_1^2 + 4.40P_oP_1$$

Now differentiating with respect to P_o and P_1

$$\frac{dJ}{dP_o} = 492.4 + 4.26P_0 + 4.40P_1 \qquad \frac{d^2J}{dP_o^2} = 4.26$$

$$\frac{dJ}{dP_1} = 92.7 + 6.4P_1 + 4.40P_o \qquad \frac{d^2J}{dP_1^2} = 6.4$$

$$\frac{dJ}{dP_o dP_1} = 4.40$$

$$\begin{pmatrix} 4.26 & 4.4 \\ 4.4 & 6.4 \end{pmatrix} \rangle\ 0$$

Knowing that the $\begin{pmatrix} 4.26 & 4.4 \\ 4.4 & 6.4 \end{pmatrix} \rangle 0$ is satisfied then the solution of $\frac{dJ}{dP_o} = \frac{dJ}{dP_1} = 0$ will give a minimum solution for P_o and P_1.

6.6 Pole Zero cancellation in the closed loop

The closed loop input output transfer function will not be effected if we chose the high order controller according to the methods described above. However by using a high order controller we introduce extra poles and zeros in the open loop transfer function $\frac{BG}{AF}$, therefore exact pole zero cancellation will occur because these extra poles and zeros do not appear in the input output closed loop transfer function. Two questions are worth asking at this point. Is the closed loop system internally stable? What happens to these cancellations in the presence of modelling errors? [Mustafa M.M., 1989] has shown that there are pole zero cancellations at the origin. Since these cancellations are in the stable region there is no problem of internal stability. In the presence of small model mismatch, some of the poles at the origin will change position but will remain inside the unit circle. For details see [Mustafa M.M., 1989].

Using the example (model) in section (6.8), we can clarify these questions.

Let our model as derived be

$$\text{Model: } \frac{\hat{B}(z^{-1})}{\hat{A}(z^{-1})} = \frac{z^{-1} - 0.1z^{-2}}{1 - 1.065z^{-1} + 0.0833z^{-2}} \qquad \text{equation 6.29}$$

The following controllers will place the closed loop poles of this model at $0.8, 0.6 \pm j0.4$

$$F_0(z^{-1}) = 1 + 21.64z^{-1}$$ equation 6.30

$$G_0(z^{-1}) = -222.577 + 22.1881z^{-1}$$ equation 6,31

and

$$F_2(z^{-1}) = 1 - 0.87z^{-1} + 0.521z^{-2} + 0.173z^{-3}$$ equation 6.32

$$G_2(z^{-1}) = -0.067 - 0.0551z^{-1} + 0.0326z^{-2} + 0.1441z^{-3}$$ equation 6.33

If the model is exact both these controllers will lead to the same input-output transfer function

$$\frac{\hat{B}(z^{-1})}{F(z^{-1})\hat{A}(z^{-1}) + \hat{B}(z^{-1})G(z^{-1})} = \frac{z^{-1} - 0.1z^{-2}}{1 - 2z^{-1} + 1.48z^{-2} - 0.416z^{-3}}$$

$$= \frac{z(z-0.1)}{z^3 - 2z^2 + 1.482z - 0.416}$$ equation 6.34

However let us assume that the model described in equation (6.29) does not exactly describe the true plant for example the true plant has a slightly higher gain.

$$\frac{B(z^{-1})}{A(z^{-1})} = \frac{1.1(z^{-1} - 0.1z^{-2})}{1 - 1.065z^{-1} + 0.0833z^{-2}}$$ equation 6.35

The closed loop transfer function for the controller F_o, G_o is.

$$\frac{z(z-0.1)}{(z-3.03)(z-1.02)(z-0.21)} \qquad \text{equation 6.36}$$

and for F_2, G_2

$$\frac{z^3(z-0.1)}{(z-0.63\pm j0.34)(z-0.72)(z-0.012\pm j0.061)} \qquad \text{equation 6.37}$$

The fact that the resulting transfer function (6.34) is the same when the model and plant are exact means that the extra zeros and poles introduced by increasing the order of the controller are cancelled. Some simple calculations show that these pole-zero cancellations occur at the origin. The transfer function (6.34) has two zeros and three poles. However when the minimum order controller is applied it should have 4 poles and three zeros. Two poles from model (6.29) and two from controller parameters. When the high order controller is applied it should have 8 poles and seven zeros. This shows that even when minimum order controller is used there is pole-zero cancellation. There are obviously more pole-zero cancellations with the high order controller.

The transfer function (6.36) has three poles and two zeros. However the plant model (6.35) has two poles and there is one pole from G_o and another from $\frac{1}{F_o}$. Therefore there should be a total of four poles. This means that even under model mismatch for the minimum order controller there is a pole zero cancellation at the origin.

The transfer function (6.37) has five poles. However there should be eight poles, two from the plant model (6.35), three from the controller $\frac{1}{F_2}$ and another three from G_2. This means that there are 3 poles, which have been cancelled at the origin.

This example also suggests another potential advantage of high order controllers. The minimum order controller (6.30) resulted in unstable closed loop system (6.36). However in the presence of model mismatch the high order controller gives a stable closed loop system. Whereas the minimum order controller results in an unstable closed loop system.

A closer look at (6.37) shows that the two poles at $0.012 \pm j0.061$ are nearly cancelled by the two zeros at origin hence the input-output behaviour will not be significantly different from (6.36) also $F_0(z^{-1})$ is unstable while $F_2(z^{-1})$ is stable. In practice stability of the controller is important when the plant is open loop stable. For instance use of unstable controller will result in conditionally stable system, small changes in gain due to component malfunction or temporary signal saturation can easily result in instability, Since large classes of systems are inherently stable, it is desirable to design for stable controllers from practical point of view

6.7 Bandwidth Selection.

In order to know what bandwidth for the controller is needed it is necessary to analyse the gait cycle. The analysis will be interms of maximum step length and maximum speeds. That is we need to know the time interval it takes to move one step (half a cycle) when travelling at maximum speed.

The largest possible step length the Orthosis can take in terms of voltages as measured from the pot is 2.4 volts. That is the size of the step from the furthest point backwards to the furthest point forward. This corresponds to the length of the Orthosis foot, which will be taken as the length of the step. This is 27 cm. This measurement was taken by pushing the left leg back till its toes were in line with the heel of the right leg. The pot reading was noted down. Then the left leg was moved forward till the heel of the left leg was in line with the toes of the right leg. The n the pot reading was noted and both values were subtracted from each other.

The Pot Gain: -

$$\text{Supply Voltage} = 22 \text{ volts}$$

$$\frac{22}{340 * \frac{\pi}{180}} = 3.71 \quad \text{volts/rad}$$

Converting voltage reading of the potentiometer into radians.

$$\frac{2.4}{3.37} = 0.71 \text{ rads}$$

Taking into account maximum normal walking speed is 1.3 - 1.8 rads/sec

$\therefore$

$$\frac{0.71}{1.8} = 0.394 \text{ seconds}$$

That is the time taken to move one step forward but the same time would be needed to move the step backwards.

$$0.394 \times 2 = 0.788 \text{ seconds}$$

$\therefore$ $$\text{the frequency} = \frac{1}{0.788} = 1.3 \text{ Hz}$$

From the above it can be seen that for normal walking a model with a bandwidth of higher than 1.3 hertz would be required. However we are looking for about a third of normal walking speed. Therefore a controller which has a bandwidth of 0.5 Hz will be designed.

6.8 Selection of Closed Loop Poles.

Once an identified model was derived an integrator was added to the model to ensure zero steady state error for a step input. Then the roots of the open loop model were calculated in order to give us a starting point when selecting the closed loop poles. The integrator will in fact become part of the controller.

The selection of the polynomial $T(z^{-1})$ was based on several criteria. The location of the roots was chosen so that the controller would have a bandwidth of 0.5 hertz as discussed in the previous section. The closed loop system polynomial $T(z^{-1}) = [0.86, 0.77, -0.5, 0.6 + 0.5i, 0.6 - 0.5i]$. The selection of the closed loop polynomial was discussed in terms of the inequality (6.23). Another criterion is the response desired to step input. Whether overshoots, oscillations or just smooth transition to the steady state is required

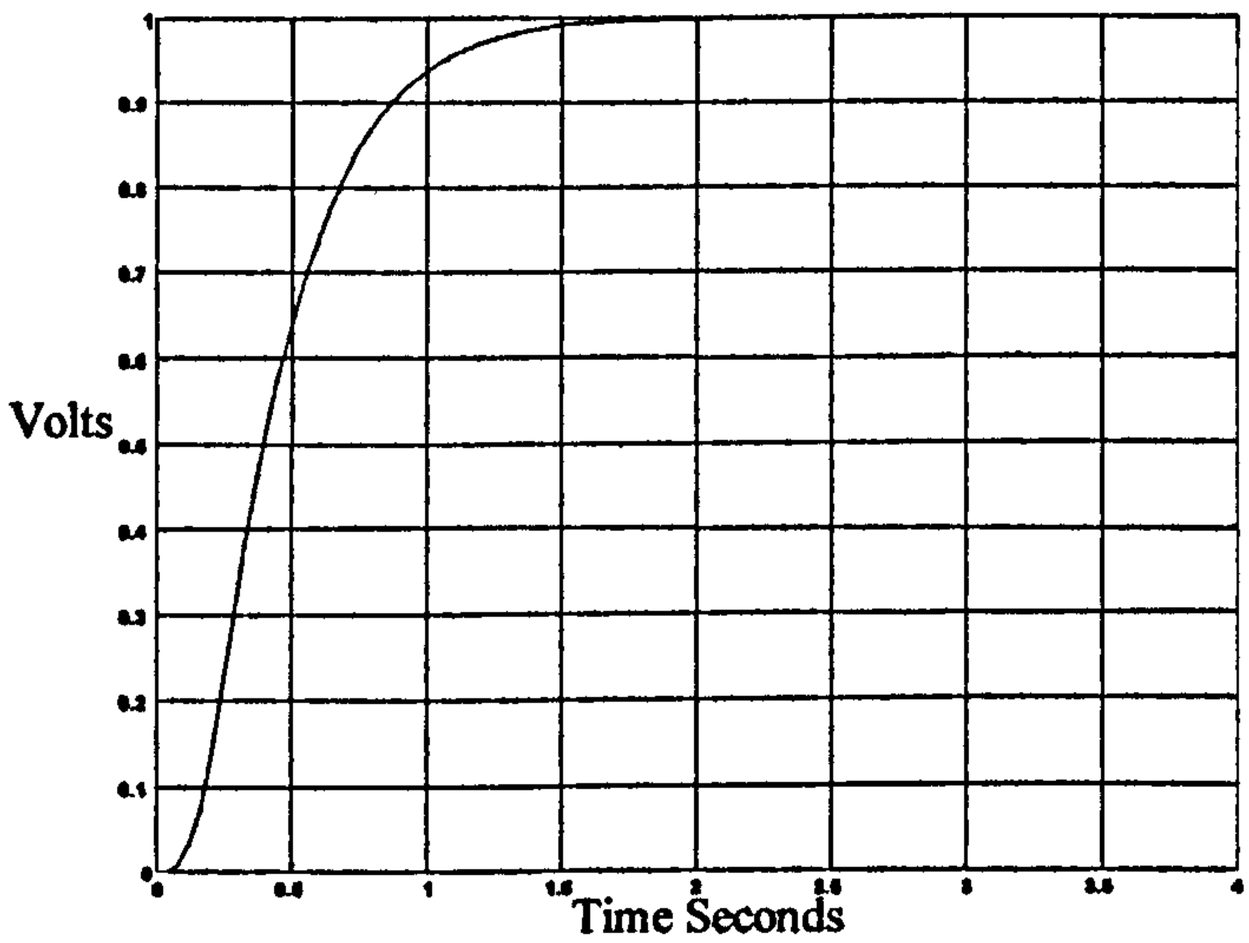

Figure 6.6 Response of the closed loop polynomial to step input

Figure (6.6) shows that after a time interval of 1.7 seconds the output reaches the steady state. There is a smooth transition from the transient to the steady state. There are no overshoots. This response to a step input corresponds to the 0.5 Hz bandwidth closed loop poles polynomial which was selected for our controller design. The next step is to work out the control parameters for different order controllers.

Results of the controller parameter are obtained explicitly and their values are shown in tables (6.1)-(6.3) for different order controller.

Degree of $p(z^{-1})$	$P_o, P_1, P_2, --$	$F(z^{-1})$	$G(z^{-1})$	$\|G\|_{L_2}$
Minimal Order Controller		$1+0.3867z^{-1}+$ $0.2367z^{-2}+$ $0.1606z^{-3}+$ $0.0957z^{-4}$	$2.1293 -$ $3.5214z^{-1}+$ $1.5709z^{-2}+$ $0.6740z^{-3}-$ $0.7398z^{-4}$	4.5170
$n_p = 0$	1.0363	$1+0.3867z^{-1}+$ $0.3138z^{-2}+$ $0.1902z^{-3}+$ $0.1258z^{-4}+$ $0.0448z^{-5}$	$1.0930-$ $0.7060z^{-1}-$ $0.9874z^{-2}+$ $1.1361z^{-3}-$ $0.0764z^{-4}-$ $0.3462z^{-5}$	2.0210
$n_p = 1$	1.4691 0.6292	$1+0.3867z^{-1}+$ $0.3459z^{-2}+$ $0.2493z^{-3}+$ $0.1564z^{-4}+$ $0.0818z^{-5}+$	$0.6602-$ $0.1594z^{-1}-$ $0.3466z^{-2}-$ $0.2243z^{-3}+$ $0.4813z^{-4}-$	0.9567

		$0.0272z^{-6}$	$0.0880z^{-5}$ - $0.2102z^{-6}$	
$n_p = 2$	1.7016 1.0334 0.3551	$1+0.3867z^{-1}+$ $0.3632z^{-2}+$ $0.2859z^{-3}+$ $0.2011z^{-4}+$ $0.1137z^{-5}+$ $0.0550z^{-6}+$ $0.0153z^{-7}$	$0.4277+$ $0.0679z^{-1}$ - $0.1775z^{-2}$ - $0.1537z^{-3}$ - $0.0663z^{-4}+$ $0.2514z^{-5}$ - $0.1179z^{-6}$ - $0.1186z^{-7}$	0.5816

Table 6.1 Controller parameter with the polynomial $T(z^{-1})$

Degree of $p(z^{-1})$	$P_o, P_1, P_2, ---$	$F(z^{-1})$	$G(z^{-1})$	$\|G\|_{L_2}$
$n_p = 3$	1.8340 1.3424 0.7172 0.2420	$1+0.3867z^{-1}+$ $0.3731z^{-2}+$ $0.3127z^{-3}+$ $0.2406z^{-4}+$ $0.1567z^{-5}+$ $0.0858z^{-6}+$ $0.0380z^{-7}+$ $0.0105z^{-8}$	0.2953 - $0.1185z^{-1}$ - $0.0268z^{-2}$ - $0.1160z^{-3}$ - $0.0802z^{-4}$ - $0.0309z^{-5}+$ $0.1185z^{-6}$ - $0.0847z^{-7}$ - $0.0808z^{-8}$	0.3880
$n_p = 4$	1.9145	$1+0.3867z^{-1}+$ $0.3790z^{-2}+$	0.2148- $0.1289z^{-1}$ -	

	1.5508 1.0252 0.5265 0.1607	$0.3305z^{-3}+$ $0.2718z^{-4}+$ $0.1962z^{-5}+$ $0.1238z^{-6}+$ $0.0642z^{-7}+$ $0.0274z^{-8}+$ $0.0069z^{-9}$	$0.0325z^{-2}-$ $0.0421z^{-3}-$ $0.0841z^{-4}-$ $0.0527z^{-5}-$ $0.0237z^{-6}+$ $0.0662z^{-7}-$ $0.0730z^{-8}-$ $0.0537z^{-9}$	0.2976
$n_p=5$	1.9692 1.7102 1.2919 0.8366 0.4090 0.1248	$1+0.3867z^{-1}+$ $0.3831z^{-2}+$ $0.3439z^{-3}+$ $0.2978z^{-4}+$ $0.2339z^{-5}+$ $0.1657z^{-6}+$ $0.1011z^{-7}+$ $0.0516z^{-8}+$ $0.0213z^{-9}+$ $0.0054z^{-10}$	$0.1601+$ $0.1181z^{-1}+$ $0.0637z^{-2}+$ $0.0032z^{-3}-$ $0.0421z^{-4}-$ $0.0660z^{-5}-$ $0.0419z^{-6}-$ $0.0216z^{-7}+$ $0.0379z^{-8}-$ $0.0568z^{-9}-$ $0.0417z^{-10}$	0.2417

Table 6.2 Controller parameter with the polynomial $T(z^{-1})$

Degree of $p(z^{-1})$	$P_o, P_1, P_2, ---$	$F(z^{-1})$	$G(z^{-1})$	$\|G\|_{L_2}$
$n_p=6$		$1+0.3867z^{-1}+$ $0.3859z^{-2}+$ $0.3538z^{-3}+$	$0.1222+$ $0.1025z^{-1}+$ $0.0724z^{-2}+$	

	2.0071 1.8289 1.5120 1.1282 0.7022 0.3373 0.0984	$0.3186z^{-4}+$ $0.2669z^{-5}+$ $0.2074z^{-6}+$ $0.1433z^{-7}+$ $0.0861z^{-8}+$ $0.0430z^{-9}+$ $0.0174z^{-10}+$ $0.0043z^{-11}$	$0.0335z^{-3}-$ $0.0094z^{-4}-$ $0.0403z^{-5}-$ $0.0555z^{-6}-$ $0.0351z^{-7}-$ $0.0200z^{-8}+$ $0.0253z^{-9}-$ $0.0497z^{-10}-$ $0.0329zz^{-11}$	0.2059
$n_p=7$	2.0342 1.9199 1.6943 1.3968 1.0124 0.6210 0.2909 0.0843	$1+0.3867z^{-1}+$ $0.3879z^{-2}+$ $0.3613z^{-3}+$ $0.3355z^{-4}+$ $0.2959z^{-5}+$ $0.2473z^{-6}+$ $0.1889z^{-7}+$ $0.1291z^{-8}+$ $0.0764z^{-9}+$ $0.0377z^{-10}+$ $0.0150z^{-11}+$ $0.0036z^{-12}$	$0.0951+$ $0.0851z^{-1}-$ $0.0704z^{-2}-$ $0.0476z^{-3}-$ $0.0182z^{-4}-$ $0.0141z^{-5}-$ $0.0369z^{-6}+$ $0.0475z^{-7}-$ $0.0307z^{-8}-$ $0.0190z^{-9}+$ $0.0163z^{-10}-$ $0.0432z^{-11}-$ $0.0282z^{-12}$	0.1786

Table 6.3 Controller parameter with the polynomial $T(z^{-1})$

6.9 Conclusion

Now that the closed loop poles have been chosen to meet the required criteria. The controller parameters were all calculated as shown in the tables (6.1)-(6.3). The next step is to practically test the Orthosis with different order controllers to see which one would be more appropriate to use. All results are shown in chapter 7.

CHAPTER 7

Evaluation of controller

7.0 Introduction

In this section the different order controllers are evaluated in terms of the following: -

a) Relative Stability.

b) Noise Transmission Properties.

c) Modelling Errors.

d) Experimental Input-Output behaviour.

e) Experimental Input-output behaviour of different order controllers.

f) Experimental Comparison of both Legs.

7.1 Relative stability Evaluation

Figure (7.1) shows the frequency response of the loop gain as the order of the controller is increased. At low frequencies there is a small gain increase. However the real improvement is in the high frequency region. With the minimum order controller there is attenuation of approximately –20 dB, with the selected controller which was 7 above the minimum order the attenuation reaches –80 dB. Figure (7.2) shows the phase plots of the different order controllers. Working out the gain and phase margins from these two figures yields the following.

Controller	Gain Margin dBs	Frequency Hz	Phase Margin degrees	Frequency Hz
Min order controller	11.74 dBs	2.6 Hz	47.7 degrees	0.89 Hz
2+Min order controller	8.29 dBs	2.1 Hz	44.17 degrees	0.81 Hz
4+Min Order Controller	7.3 dBs	1.82 Hz	41.99 degrees	0.74 Hz
6+ Min Order Controller	6.78 dBs	1.62 Hz	40.41 degrees	0.68 Hz
7+Min Order Controller	6.59 dBs	1.53 Hz	39.73 degrees	0.65 Hz

From equation (6.25) and the statement which was made that in terms of robustness controller G_1 is better than controller G_2 if the inequality was satisfied. In terms of these plots figure (7.3) this means that as the order of the controller is increased the plots should be moving down. Improvement really occurs in the high frequency region. Lower order controllers have an amplification factor in the high frequency region while higher order controllers give an attenuation factor, which is increasing as the order is increased. The improvement is not always in the right direction, namely looking at the green and purple plots indicates that in some regions of the high frequency one is better than the other, but in another region it is the other way round. However the general trend is

improvement as the order is increased. Some small degradation occurs in the mid frequency region.

Looking at figure (7.4) shows a clear degradation in relative stability between the minimum order and 7+minimum order controllers. Taking these figures at face value seems to indicate that these results contradict our statement that " stability is improved as the order of the controller is increased.

Figure (7.6) shows the frequency range where the degradation occurs. This figure shows that the degradation occurs in the middle frequency region. As we stated before in chapter 6 , the L_2 norm will be used to minimize G in the high frequency region. This indicates that the improvement in relative stability occurs in the high frequency region, which means that this data verifies the statement made in chapter 6.

Comparison of both graphs at the same frequency clearly indicates improvement in relative stability at the 3.0 Hz point by the high order controller. Also zooming in at higher frequency clearly shows that the high order controller has higher attenuation.

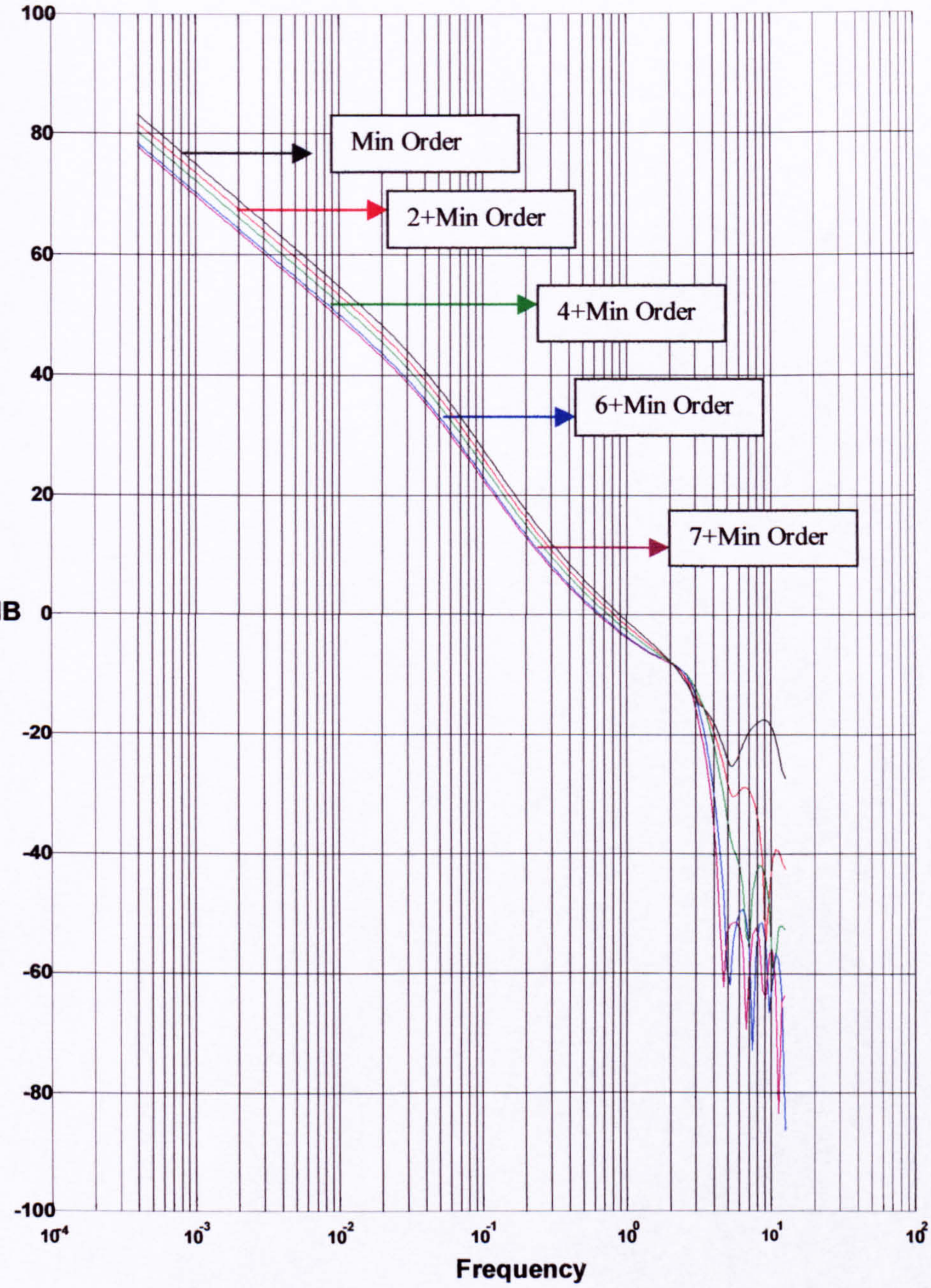

Figure 7.1 Bode plot of the loop gain $\hat{B}G/\hat{A}F$ for different order controllers

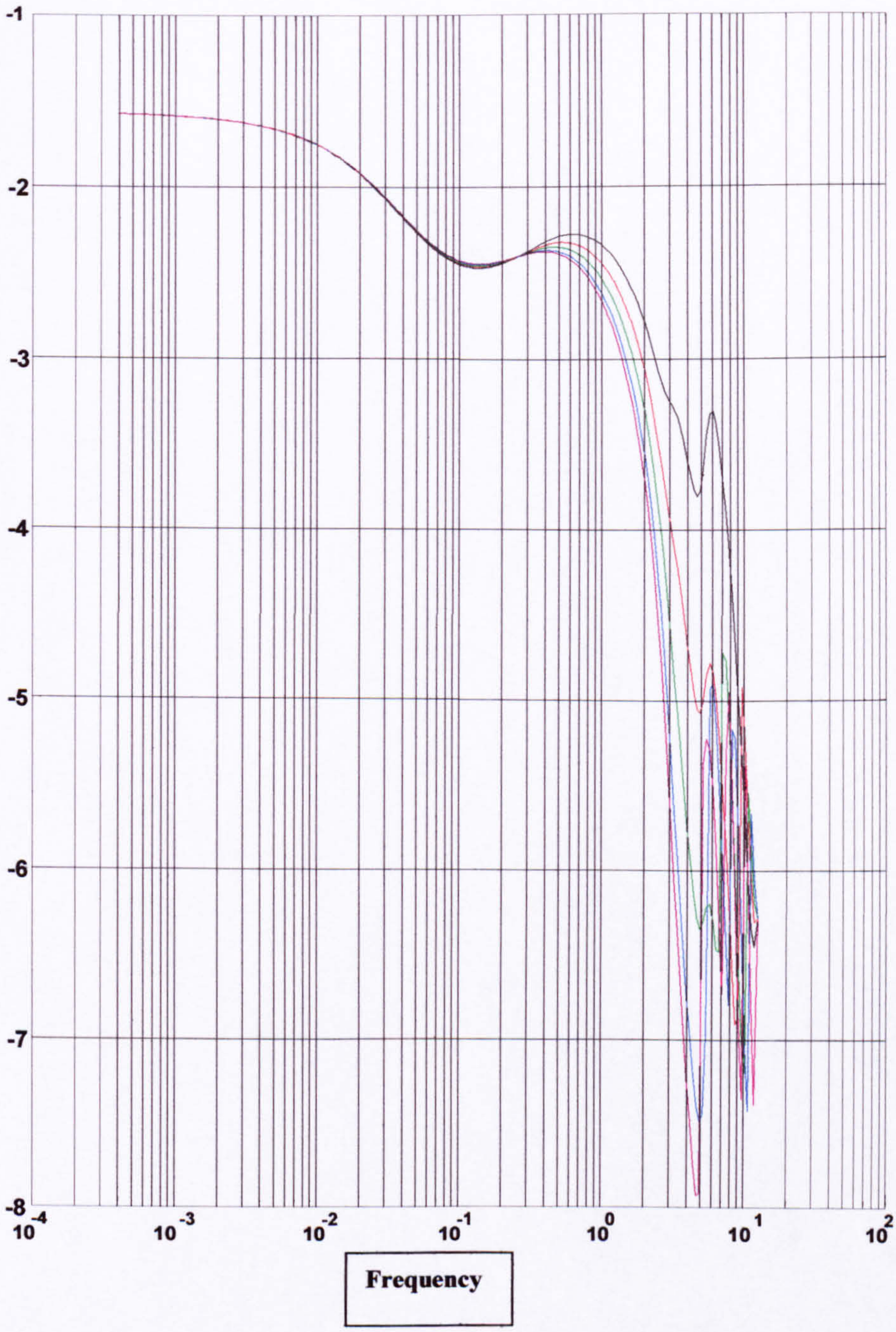

Figure 7.2 phase plot of the loop gain $\hat{B}G/\hat{A}F$ for different order controller

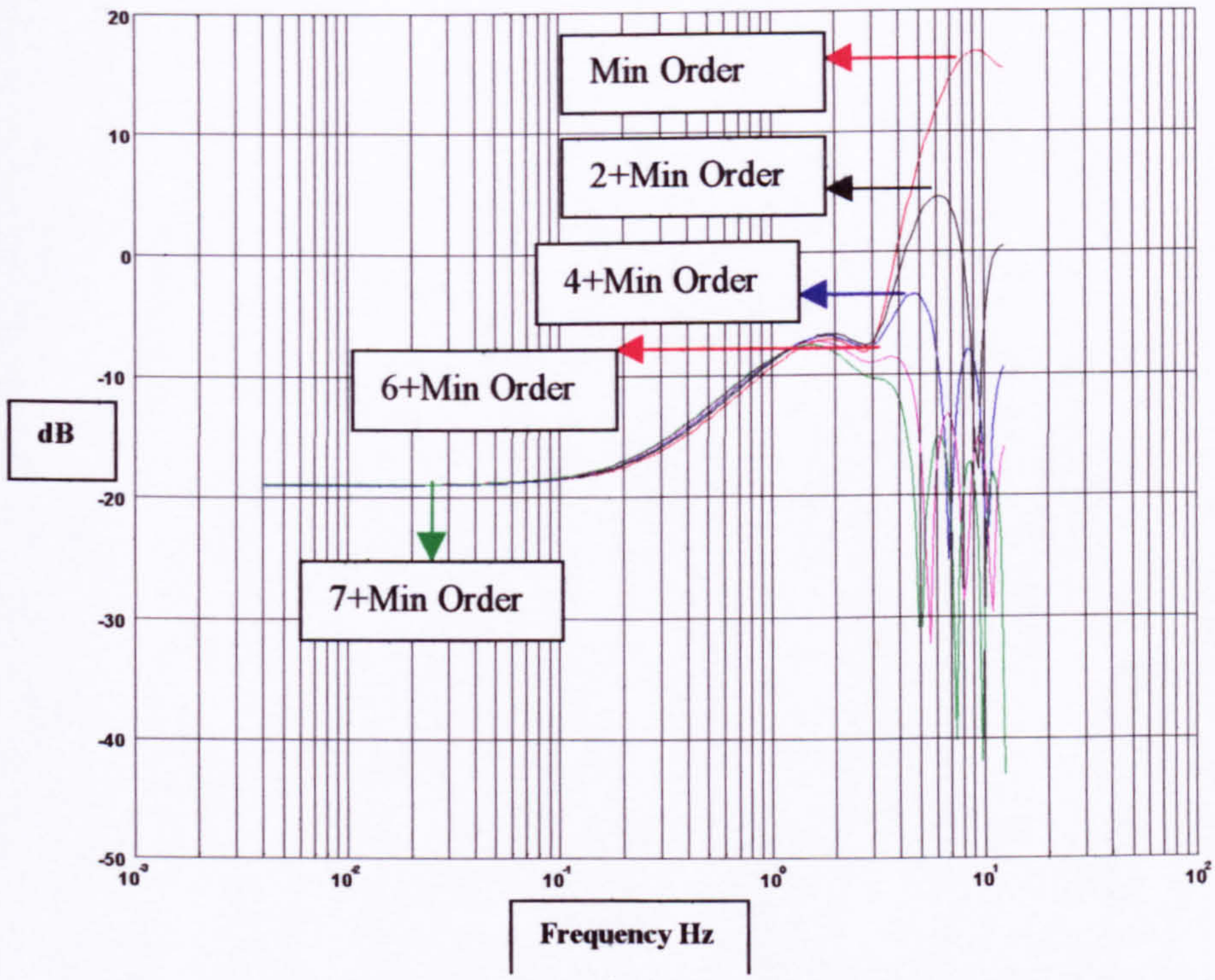

Figure 7.3 Magnitude plot of $|G|$ for different order controllers

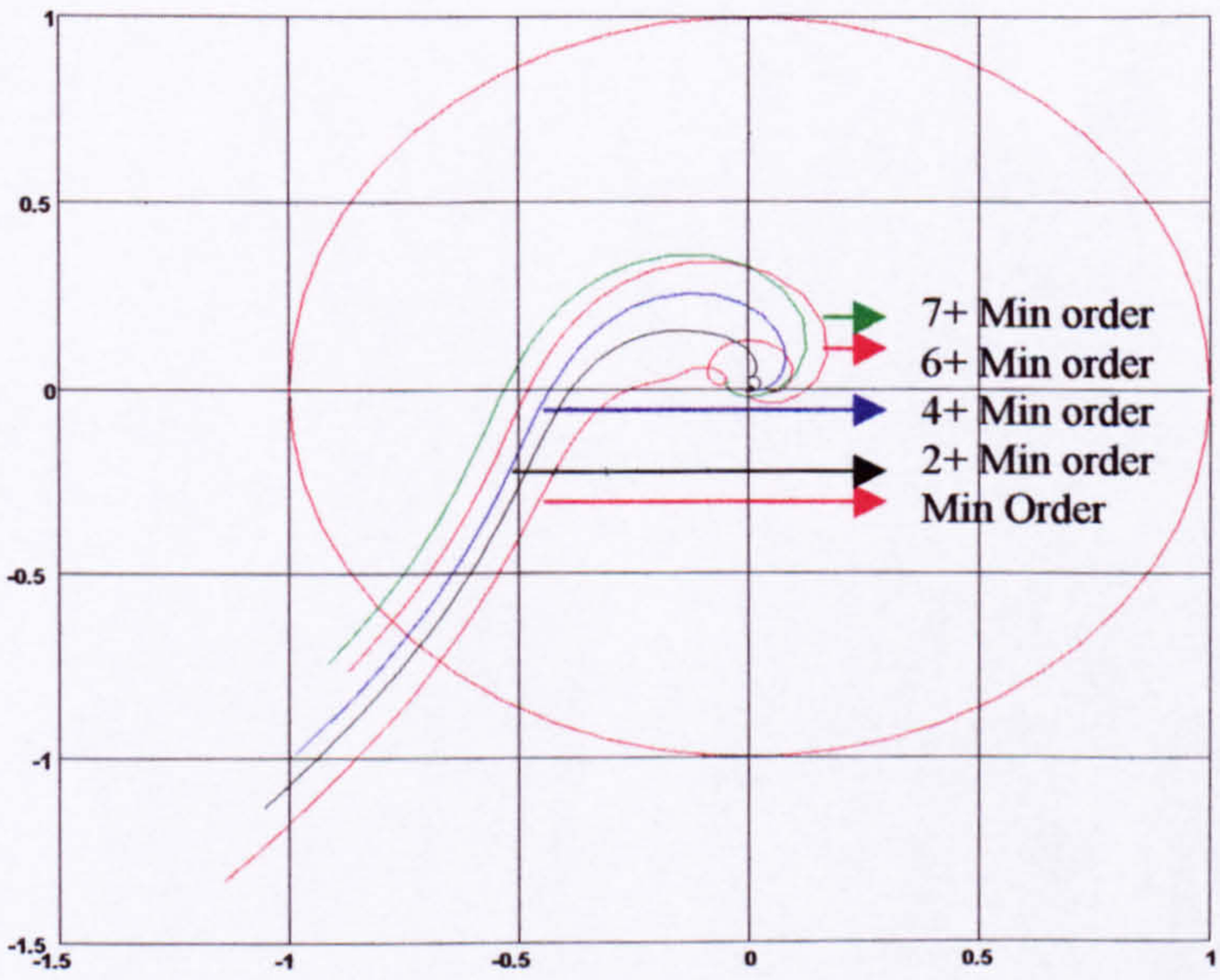

Figure 7.4 Nyquist plot of the loop gain for different order controllers

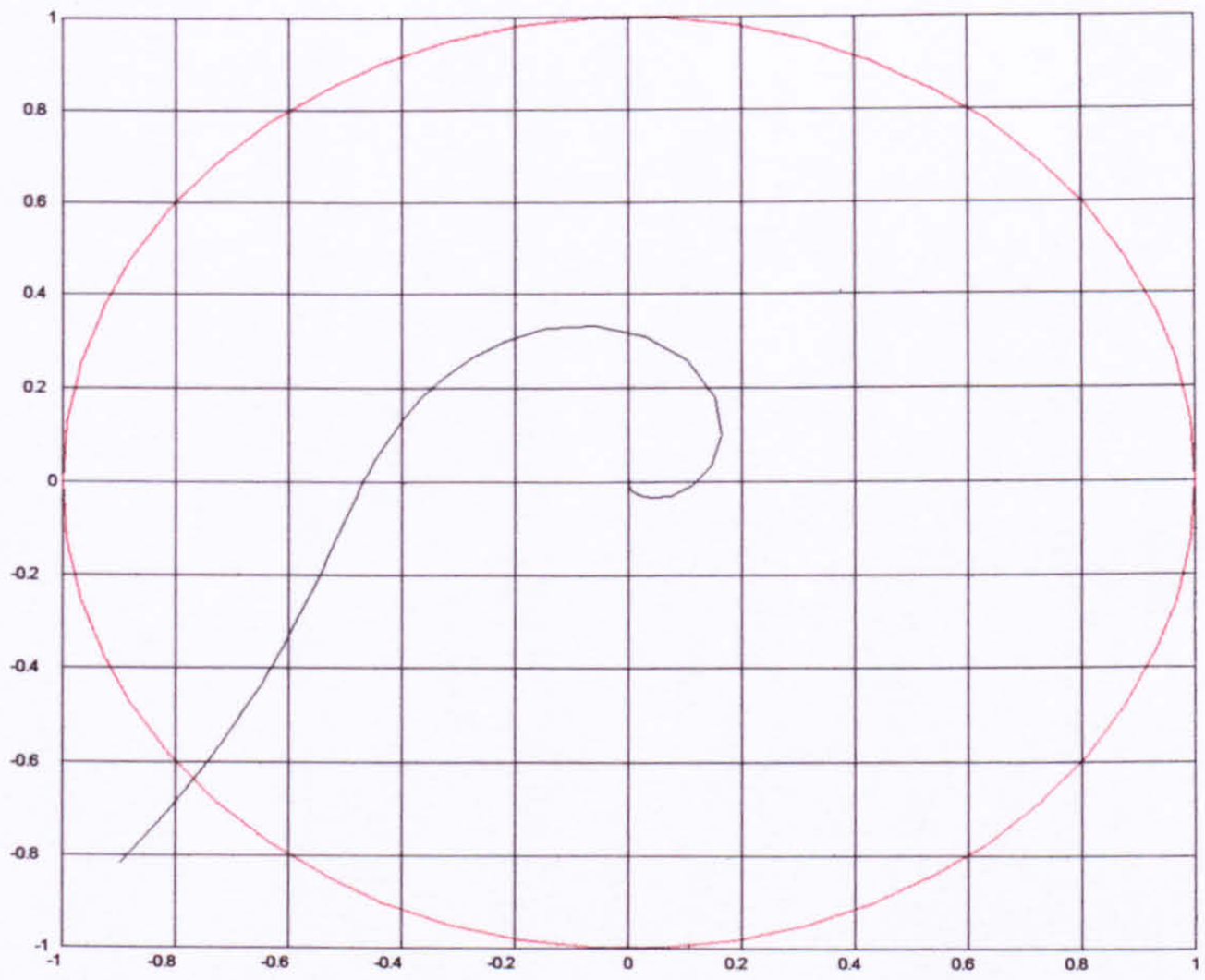

Figure 7.5 Nyquist plot of the loop gain for the chosen controller

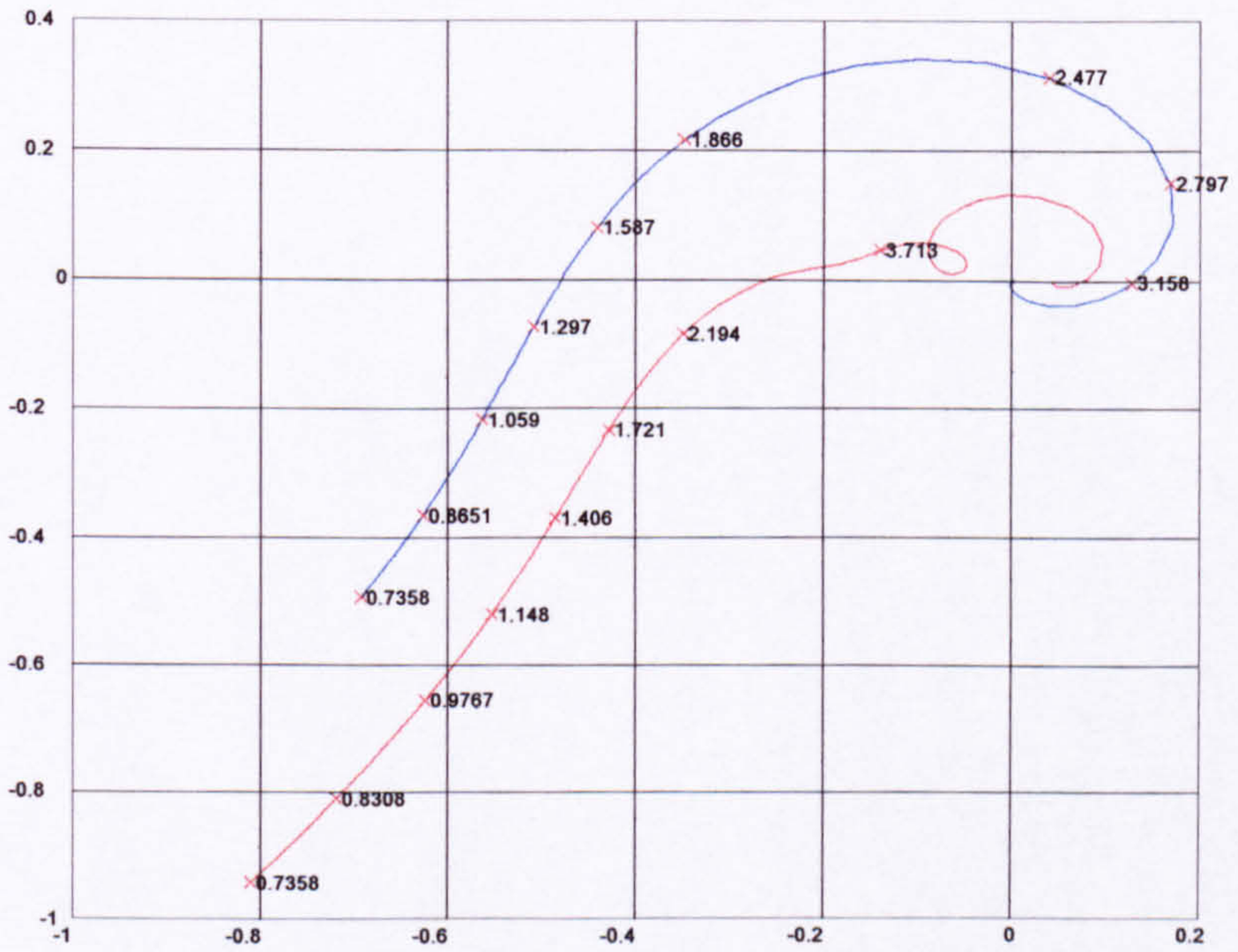

Figure 7.6 Comparison of relative stability for minimum order and selected high order controller

7.2 Noise Transmission Properties

Figure (7.7) shows the effect of noise on the control signal u (t) as the order of the controller is increased. Looking at the minimum order controller it is clear that noise is amplified throughout the entire frequency spectrum. On the other hand the high order controller attenuates noise in the high frequency region. However it is actually better at low frequency although the difference between the different order controllers is very small. The difference is very prominent at high frequency. The general trend is a faster roll off as the order is increased.

Figure (7.8) shows the effect of noise on the output signal y (t). As was said previously in control sometimes we work on the basis of trade off. That is the choice of $T(z^{-1})$ could be to have noise rejection or optimal performance. This figure clearly shows that the higher the controller the more the noise seems to effect the output signal. This is more prominent in the middle frequency range and not so obvious at high frequency. This degradation is not uniform over all frequency ranges. In the frequencies in the middle range the high order controllers seem to be better. At high frequency there is no real difference between them. It is worth noting when the simulation is carried out, by default. Matlab simulates for an input sine wave of amplitude of one volt. It is unrealistic to assume that the system will contain noise levels of this amplitude, for example quantization noise may have an amplitude of 5 milli volts. The frequency response for a signal of this amplitude for the highest order controller is shown in figure (7.9). This

clearly shows that the amplification of noise or mechanical vibration is not going to be very large.

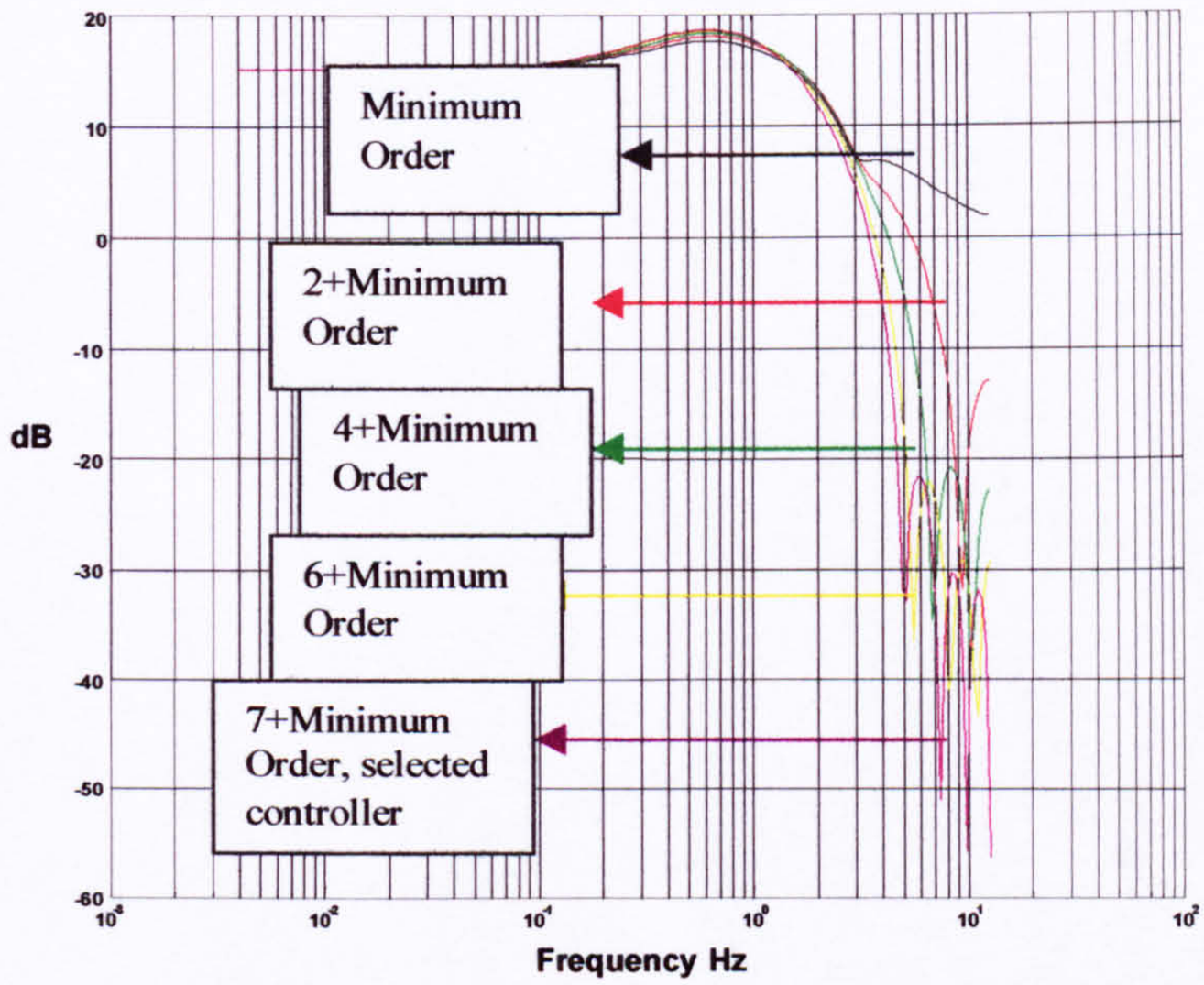

Figure 7.7 Effect of noise on the control signal u (t) as the order of the controller is increased

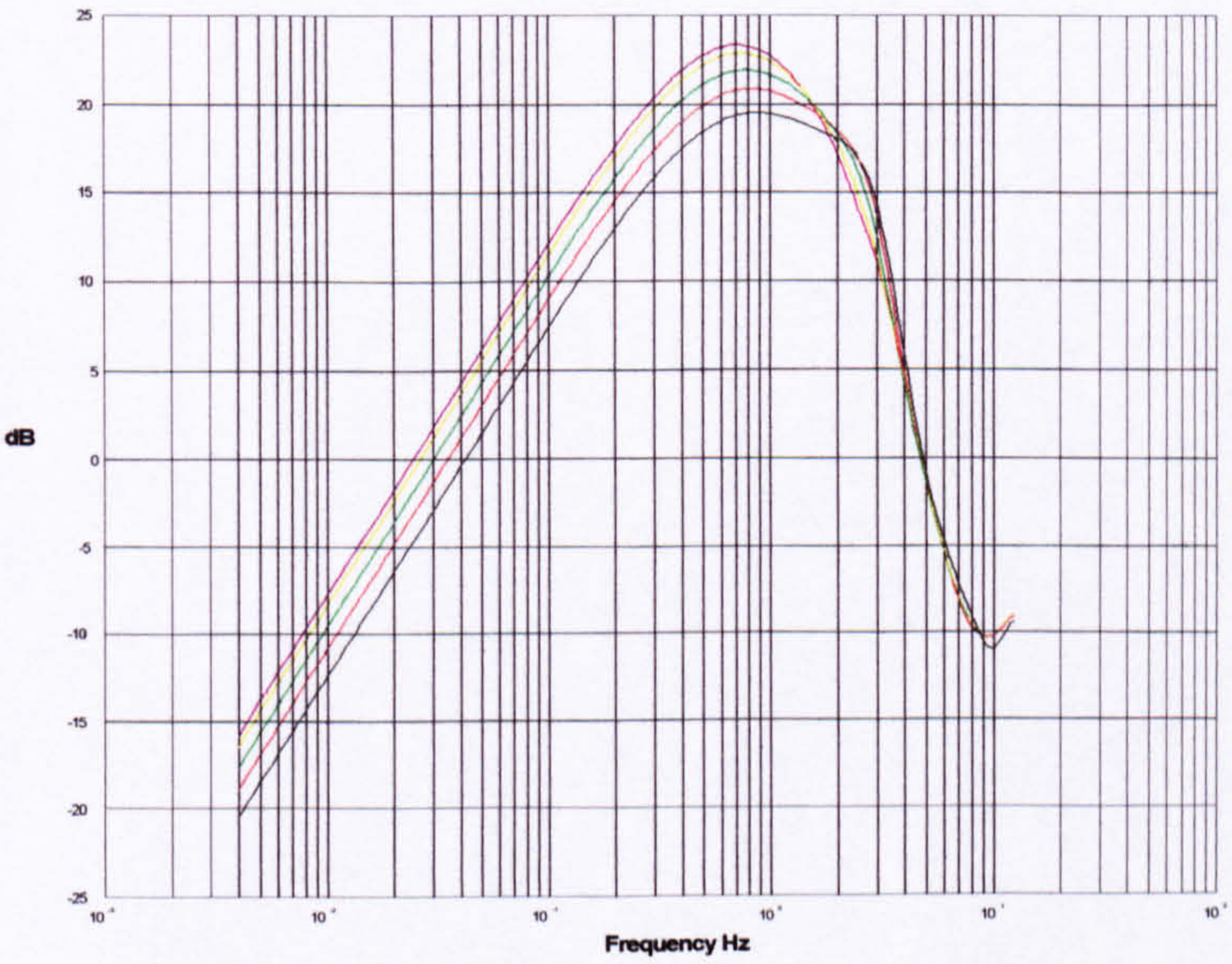

Figure 7.8 Effect of noise on the output signal y(t) $\frac{F_I}{T}$

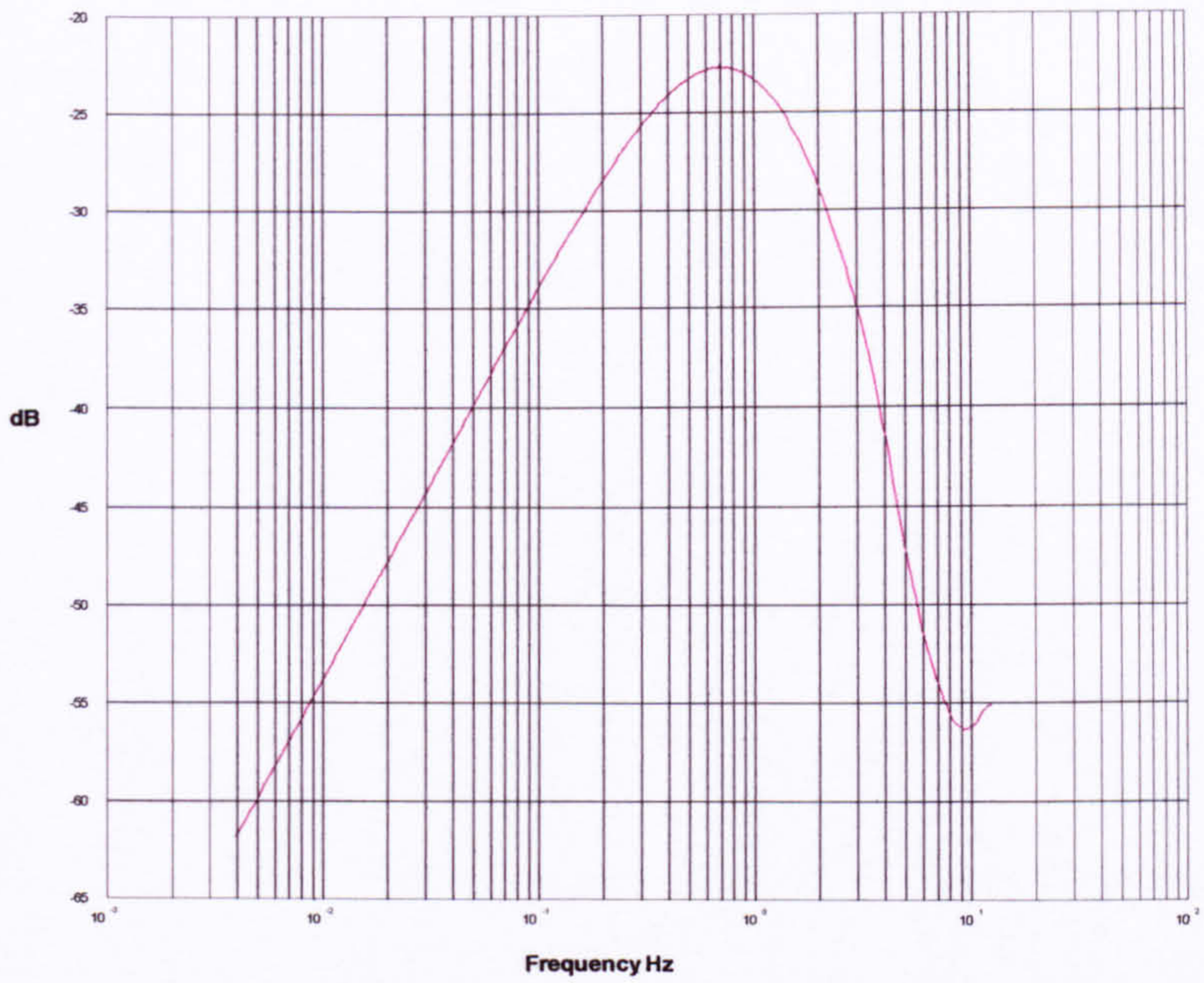

Figure 7.9 Effect of quantization noise on the output signal for 5 milli volts noise

7.3 Modelling Errors

For the benefit of this section $\frac{\hat{B}}{\hat{A}}$ is taken as the model for the Orthosis and $\frac{B}{A}$ is the plant. $\frac{B}{A}$ is one of the models derived for the Orthosis during identification. It is not used anywhere else in the thesis.

Figure (7.10) shows the plot of $\left|\frac{T}{\hat{A}}\right| \frac{1}{\left|\frac{B}{A}-\frac{\hat{B}}{\hat{A}}\right|}$ in black, $|G|$ for minimum order in green and $|G|$ for 7+minimum order in red. Looking at inequality (6.23) clearly shows that it is always desirable to have $|G|$ smaller than that of $\left|\frac{T}{\hat{A}}\right| \frac{1}{\left|\frac{B}{A}-\frac{\hat{B}}{\hat{A}}\right|}$ especially at high

frequency. Looking at figure (7.10) clearly shows that for the selected controller (red plot) this is achieved in the high frequency region. There is however a region between approximately 0.8 Hz and 1.7Hz that the inequality is not satisfied. This is the region where in the relative stability analysis it was shown that there is degradation in relative stability. Remembering that inequality (6.23) is just a sufficient condition means that we cannot conclude anything in this region. Also knowing that our technique using the L_2 norm minimizes $|G|$ in the high frequency region which is where usually the model plant mismatch is most prominent we can see that the inequality is satisfied in that region.

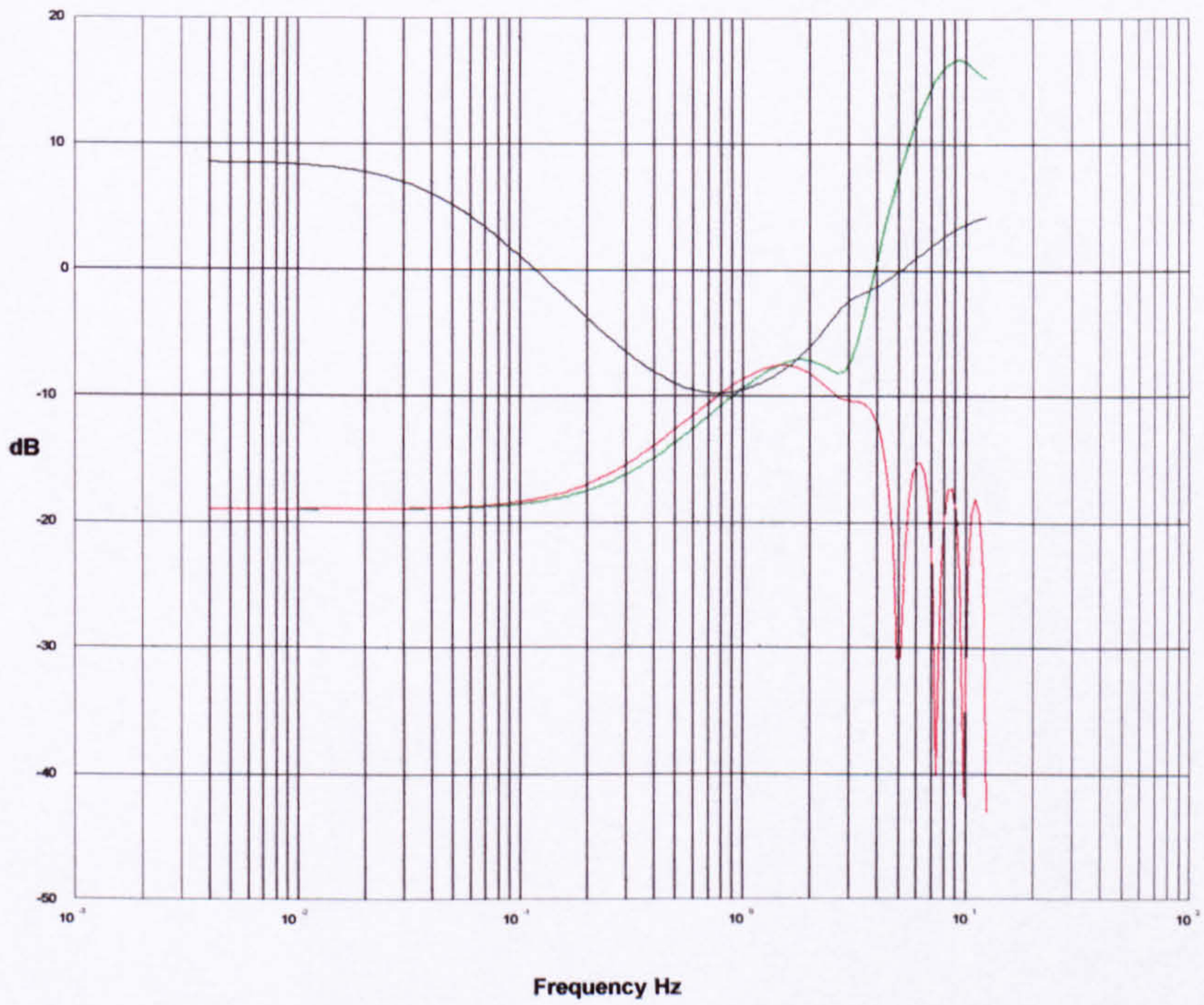

Figure 7.10 Comparison of $|G|$ with $\left|\frac{T}{\hat{A}}\right| \frac{1}{\left|\frac{B}{A} - \frac{\hat{B}}{\hat{A}}\right|}$

As we cannot conclude anything because Inequality (6.23) is not satisfied. To see if the system $\frac{B}{A}$ is stable we can apply our controller (minimum and high order) to $\frac{B}{A}$ thus yielding AF+BG=T. Then the roots are calculated to see if the system is stable or not.

7.4 Experimental Input-Output behaviour

Apart from preserving stability, we are also interested in the input-output behaviour of the closed loop system. This criterion enters explicitly in the original defined objective of this project. As the aim of this project is to control the Orthosis so that it follows a preset trajectory (input signal). It is important that the input-output performance is robust with respect to modelling errors, noise.

Figure (7.11 (a)) shows the response of the Orthosis to filtered square wave input. It is clear that the controller follows the preset reference signal closely. There are two glitches namely at 5 seconds and 11 seconds. These could be due to external disturbances such as noise or mechanical vibration. However looking at the control effort, it is clear that as soon as the response moves away from the reference signal the control efforts compensate for this deviation thus insuring the response is following the reference signal.

Figure (7.11 (b)) shows the control effort for figure (7.11). The first observation is that the maximum change in amplitude does not exceed ± 1.5 volts. Considering that it is capable of changing between ± 10 volts, the change is relatively small. This is

encouraging because it is not getting close to saturation which means it has room to increase or decrease the control effort should it become necessary.

Figure (7.12 (a)) shows the response to a higher frequency reference signal. Again this shows a good comparison. At time interval 15 seconds the Orthosis overshoots but then the control effort sends the appropriate correction signal (figure 7.12 (b)) bringing the leg in line with the reference signal.

Figures (7.13 (a))-(7.14 (a)) are at higher frequency than the previous two. These figures show the response to a filtered 0.25 Hz square wave and 0.33 Hz filtered square wave. These figures show some stiction in the system exists particularly with low frequency part of the signal (filtered section). The figures show clearly that the response seems to stick every time the reference signal starts to decelerate due to the filter. This is consistent over the whole time interval for this test in both directions. The stiction is also evident in the other plots.

The previous results show that the system has some difficulty in tracking low frequency components of the signal, figure (7.15 (a)) shows the response to a low frequency sine wave. It clearly shows that the system is struggling to follow the signal smoothly. In terms of amplitude the control effort swings between 0.6 volt and –1.0 volt. However the signal has fast variations in comparison with the previous ones. This effectively means that the control system is working all the time to track the specified trajectory. As the frequency of the reference sine wave is increased the Orthosis follows the reference

signal better but again near the peaks, as the system decelerates it struggles. All other results exhibit similar behaviour as described above

Figures (7.16 (a)), (7.17 (a)) and (7.18 (a)) show the response to filtered sine waves which have frequencies of 0.13 Hz, 0.25 Hz and 0.33 Hz respectively. These figures clearly confirm that the Orthosis manages to track the preset trajectory at these higher frequencies. However these figures also show that stiction is still prominent at these frequencies. The corresponding control efforts clearly show that the system is not driven very hard as the amplitudes of these do not exceed 1.5 volts.

Figure 7.11 Response to a filtered 0.04 Hz square wave

a) Output-Input behaviour **b)Control Effort**

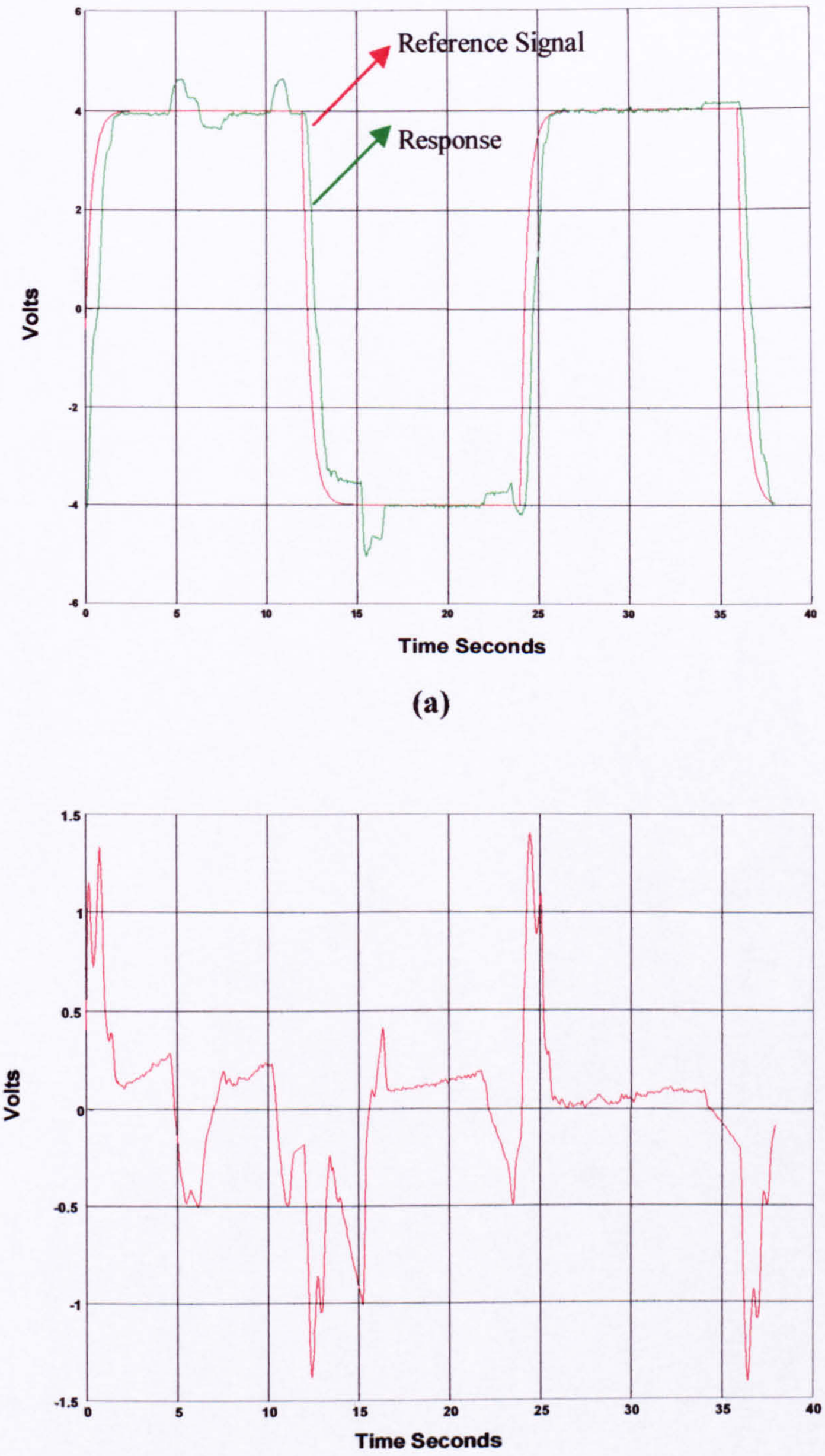

(a)

(b)

Figure 7.12 Response to a filtered 0.13 Hz square wave

a) Output-Input behaviour **b)Control Effort**

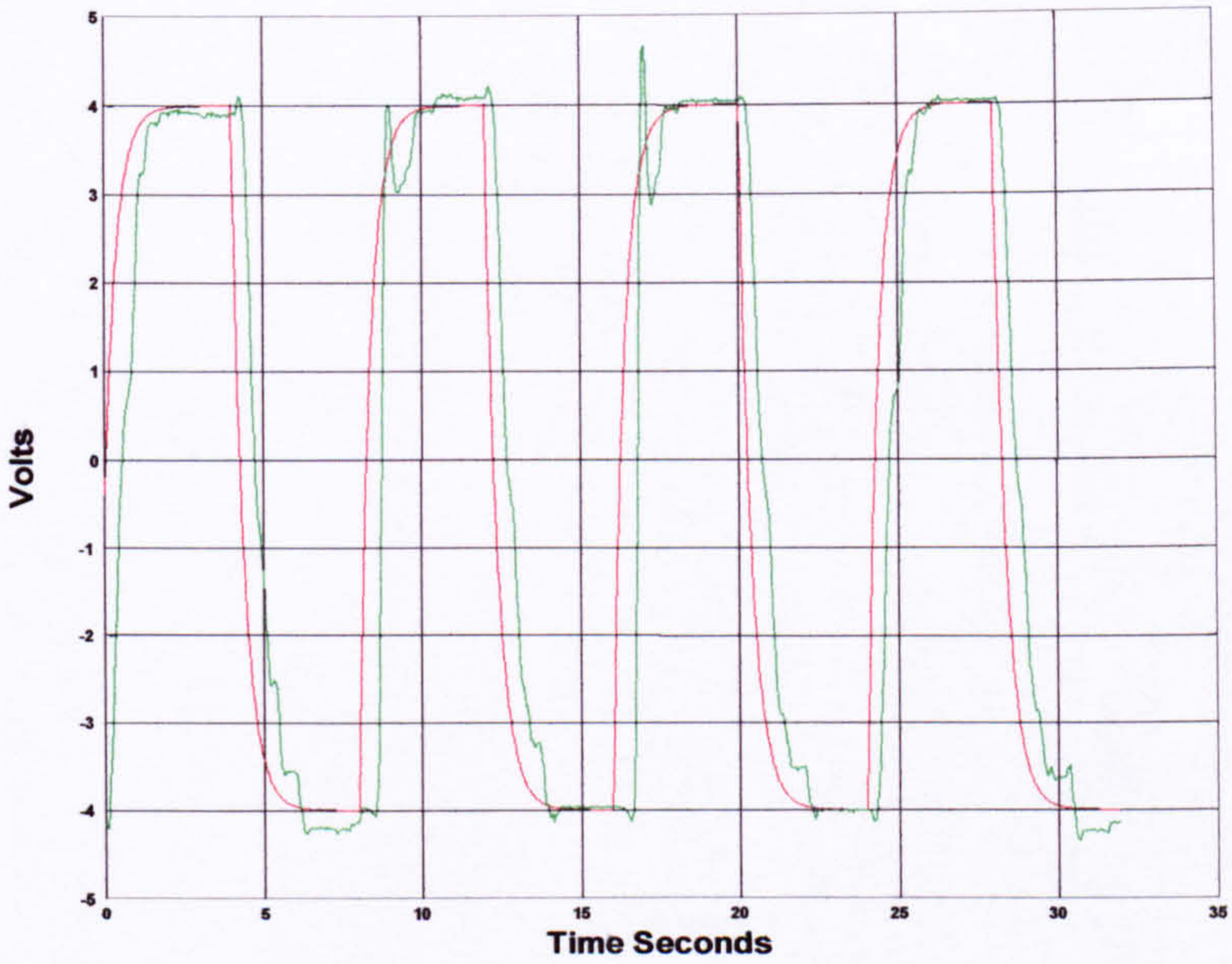

(a)

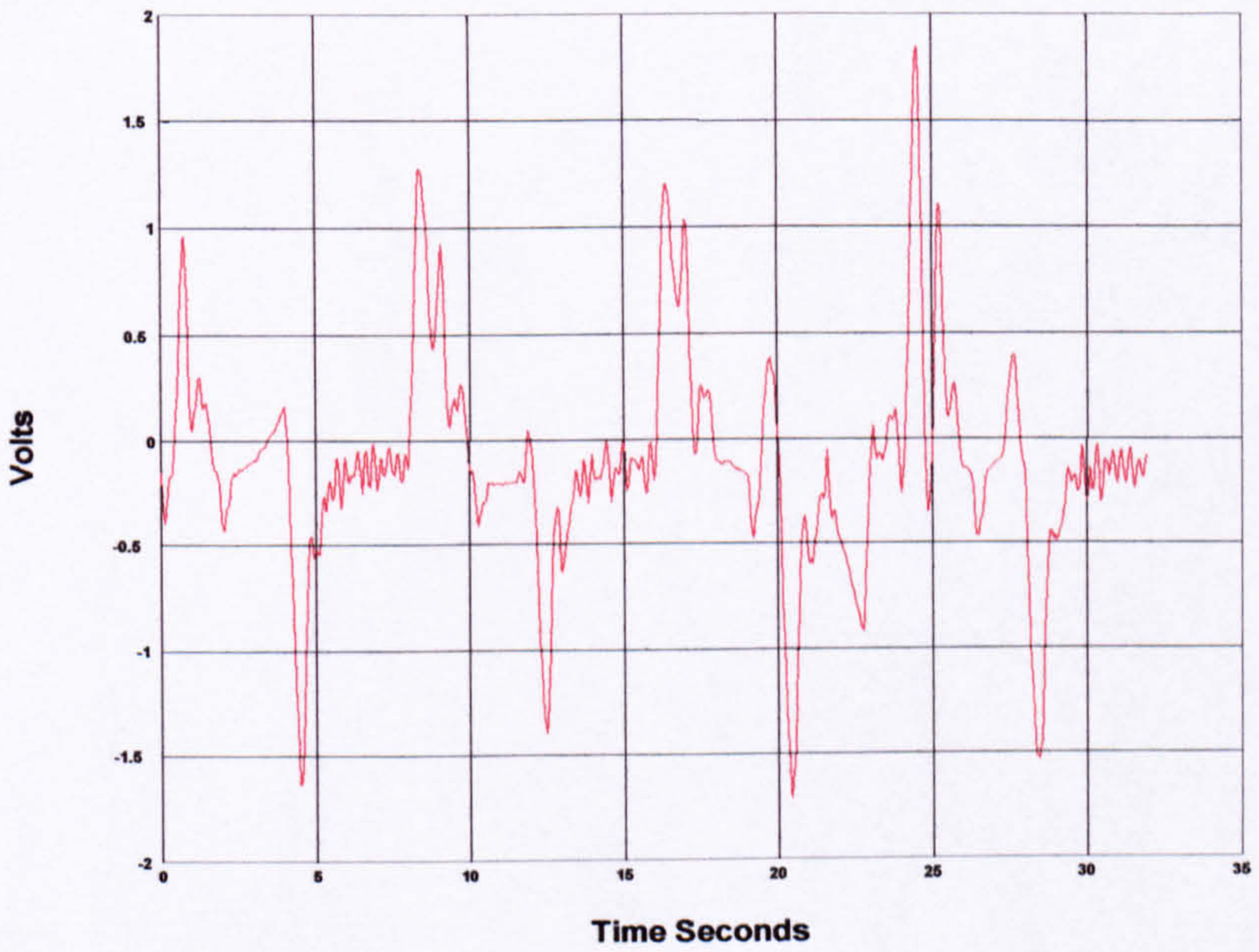

(b)

Figure 7.13 Response to a filtered 0.25 Hz square wave

a) Output-Input behaviour **b)Control Effort**

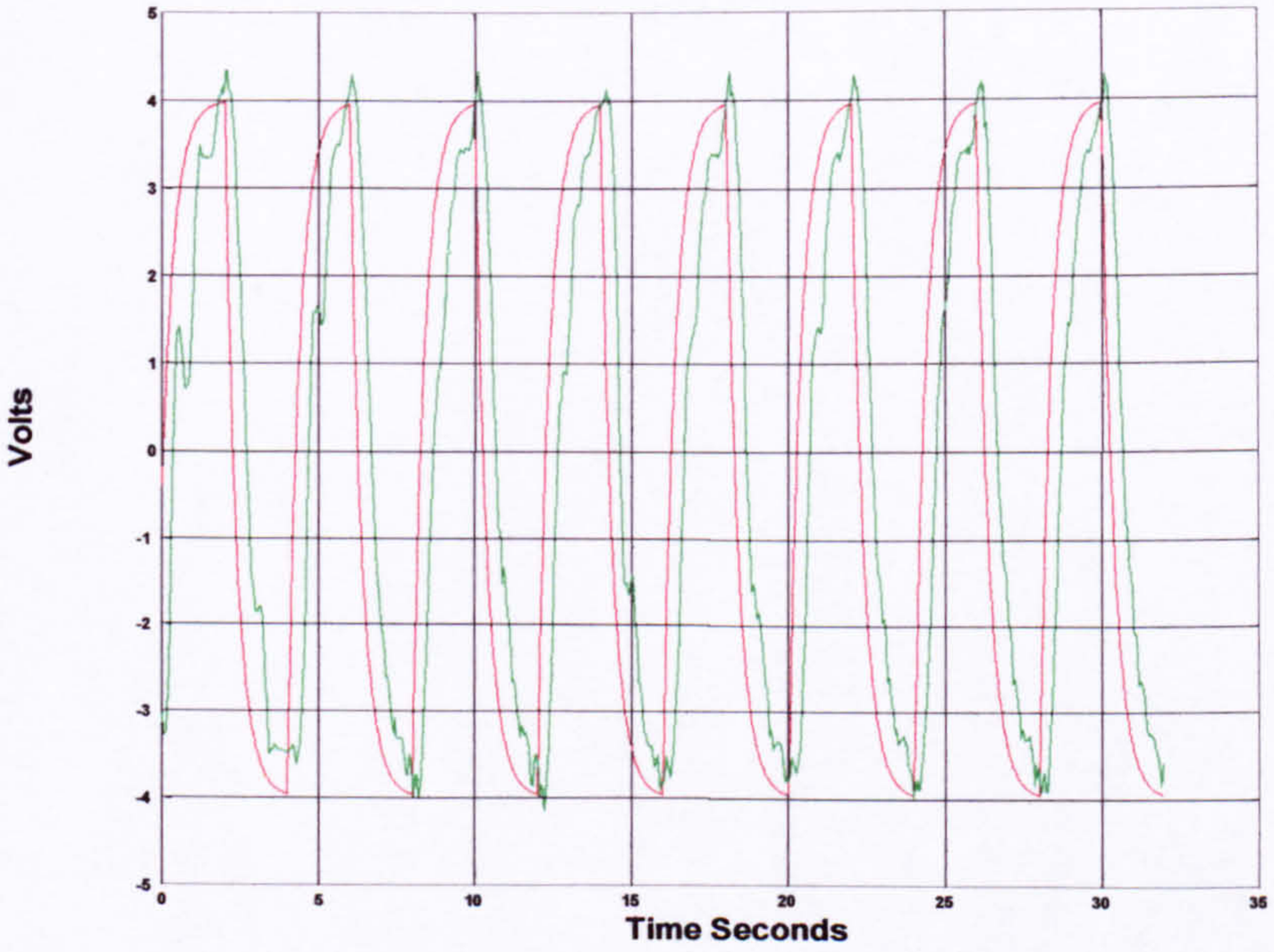

(a)

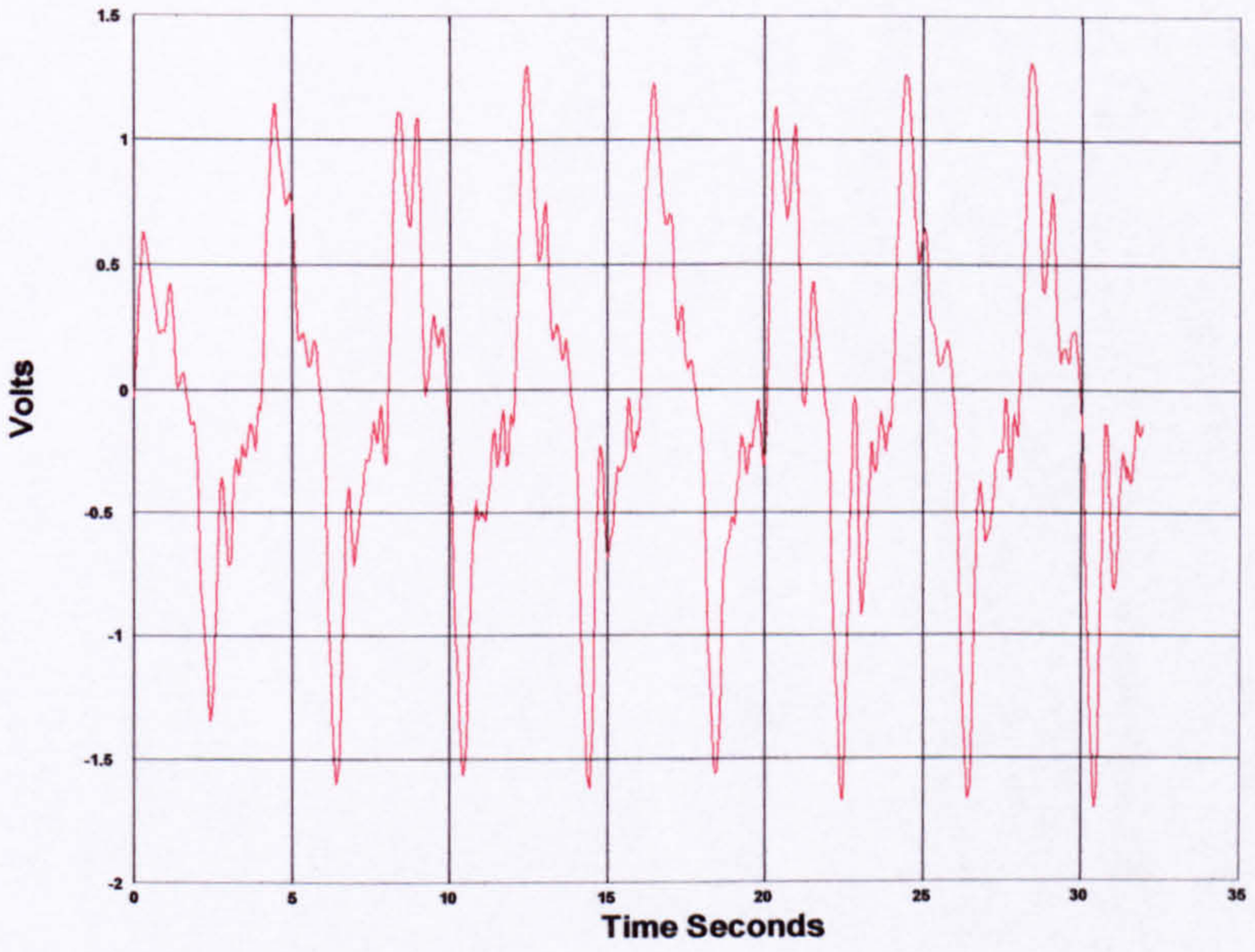

(b)

Figure 7.14 Response to a filtered 0.33 Hz square wave

a) Output-Input behaviour **b)Control Effort**

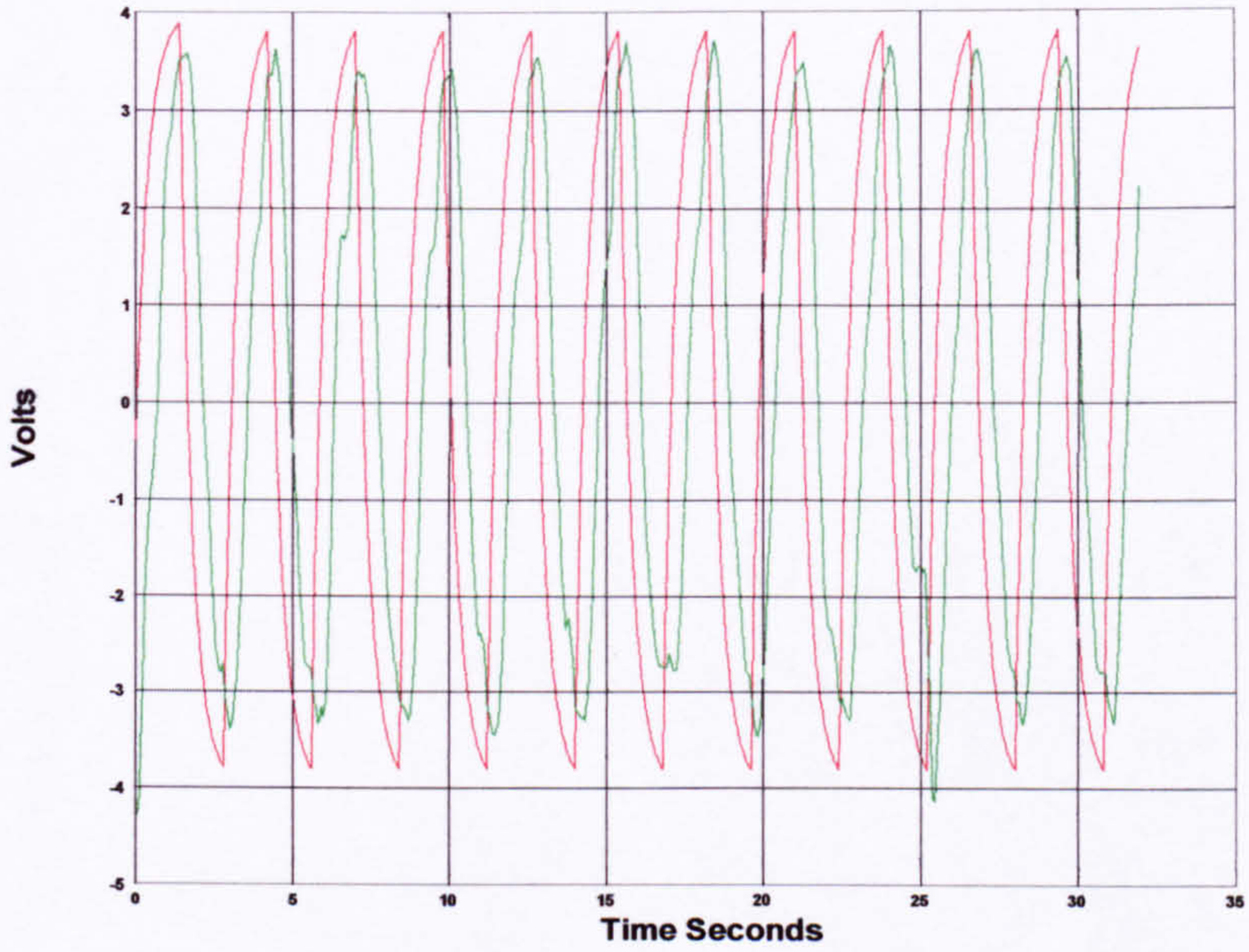

(a)

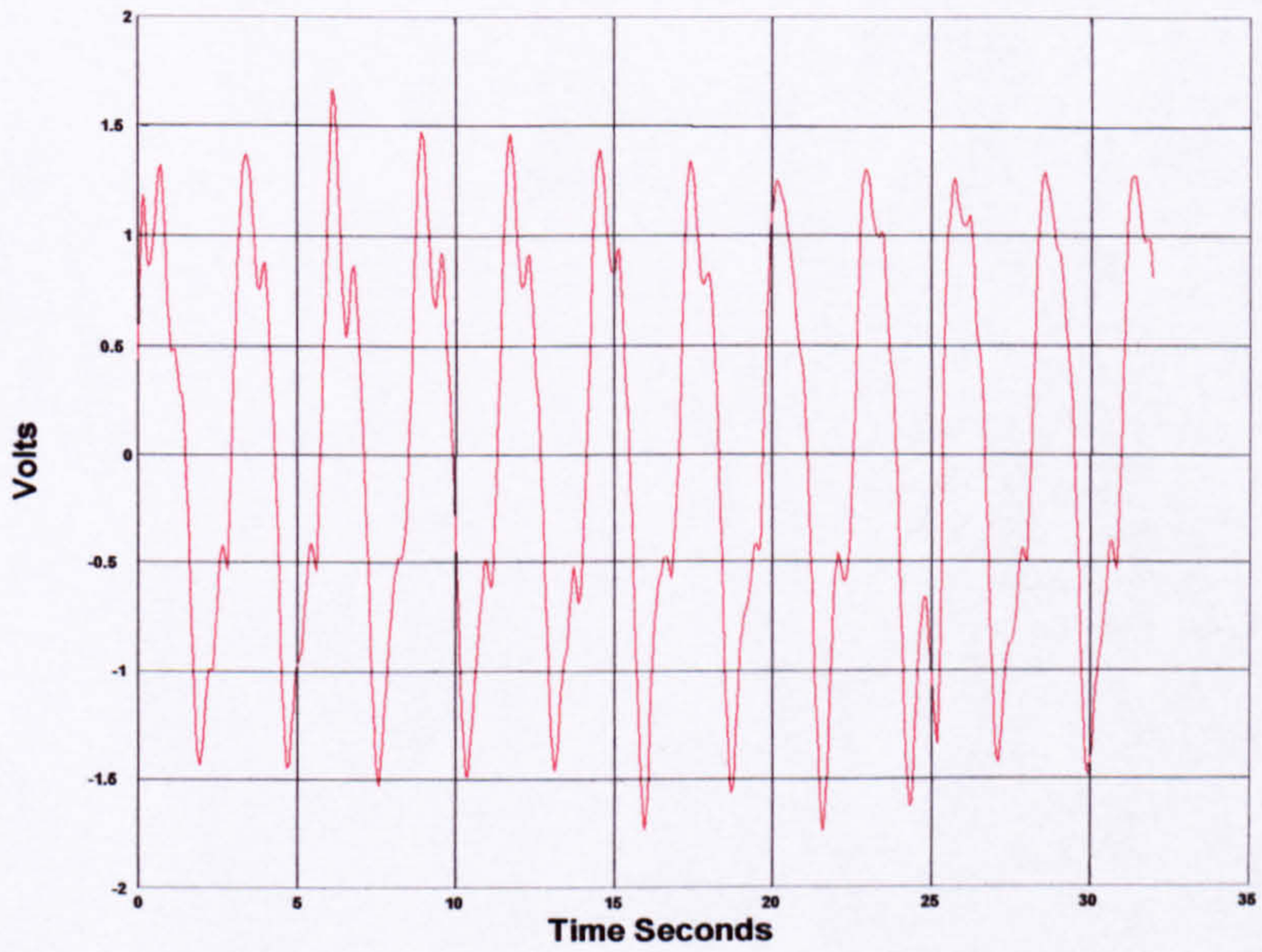

(b)

Figure 7.15 Response to a filtered 0.04 Hz sine wave

a) Output-Input behaviour **b)Control Effort**

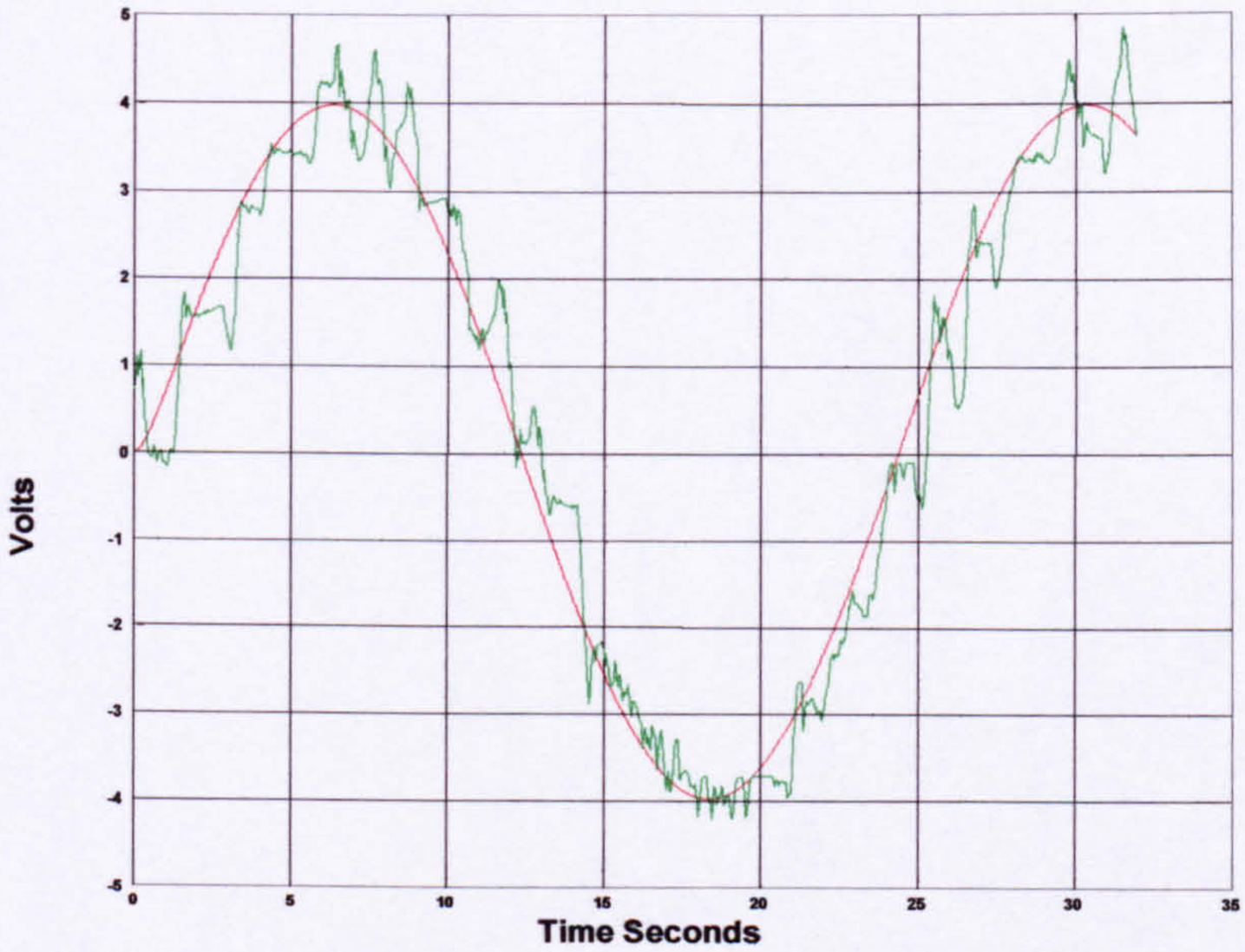

(a)

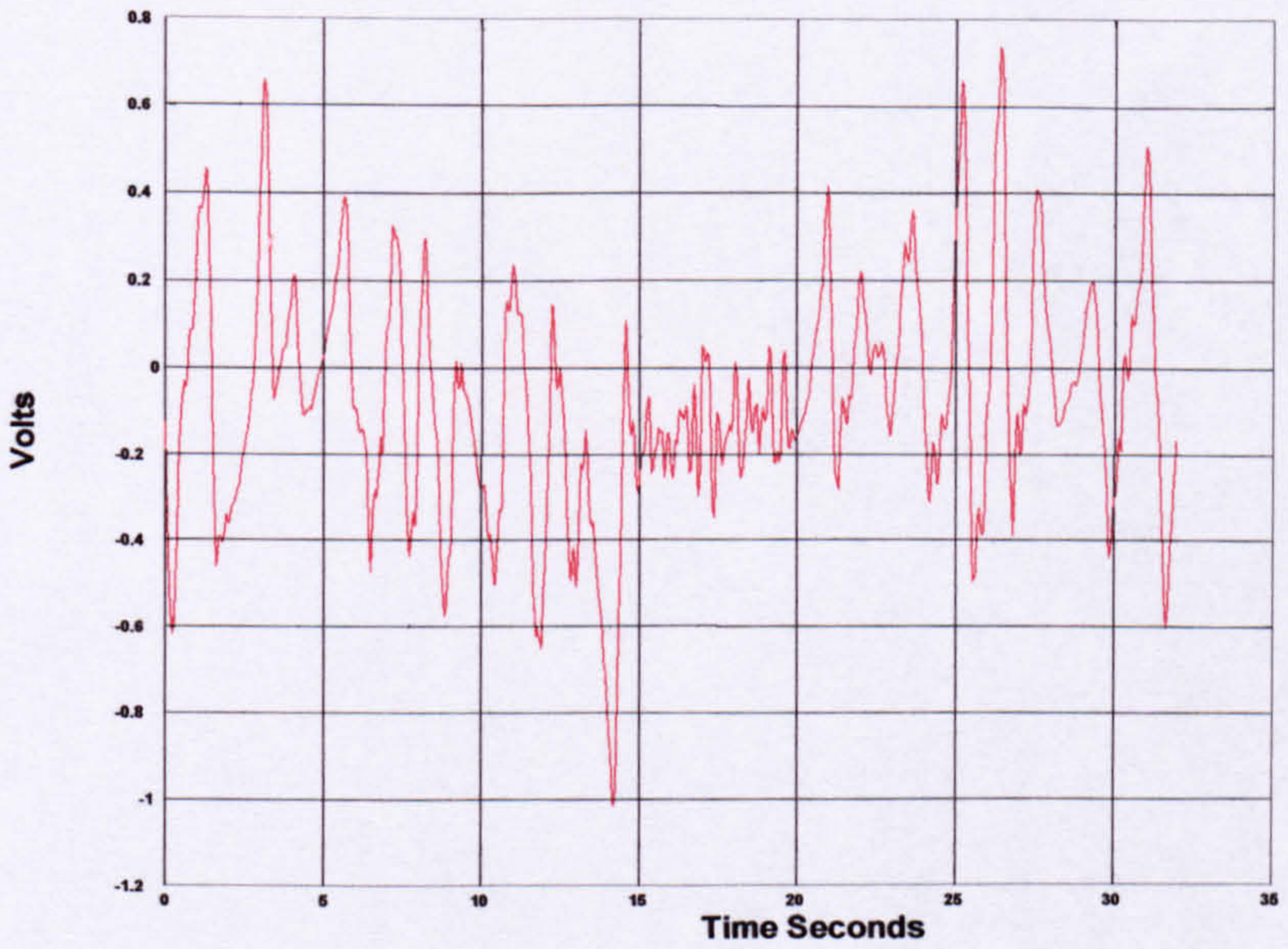

(b)

Figure 7.16 Response to a filtered 0.13 Hz sine wave

a) Output-Input behaviour **b) Control Effort**

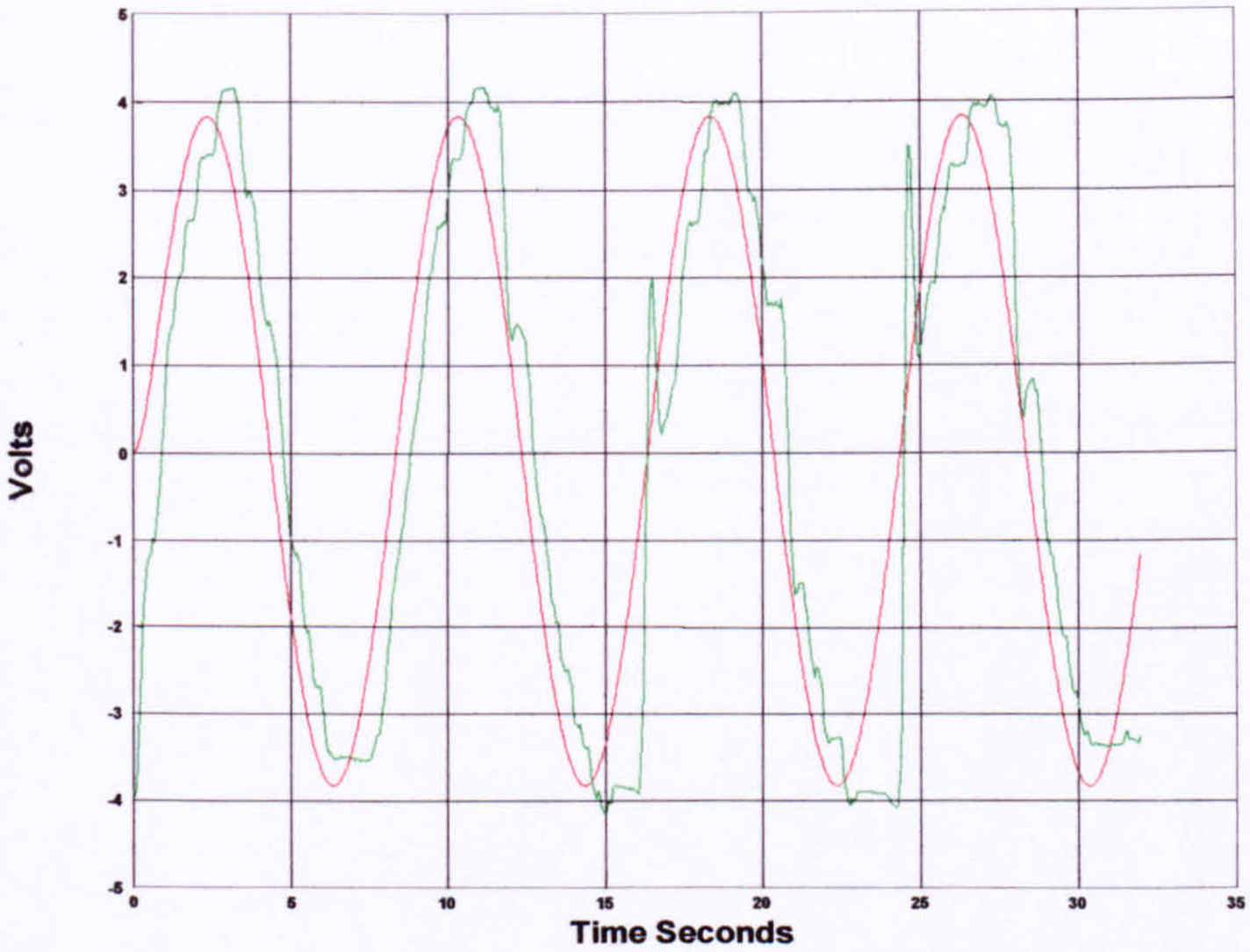

(a)

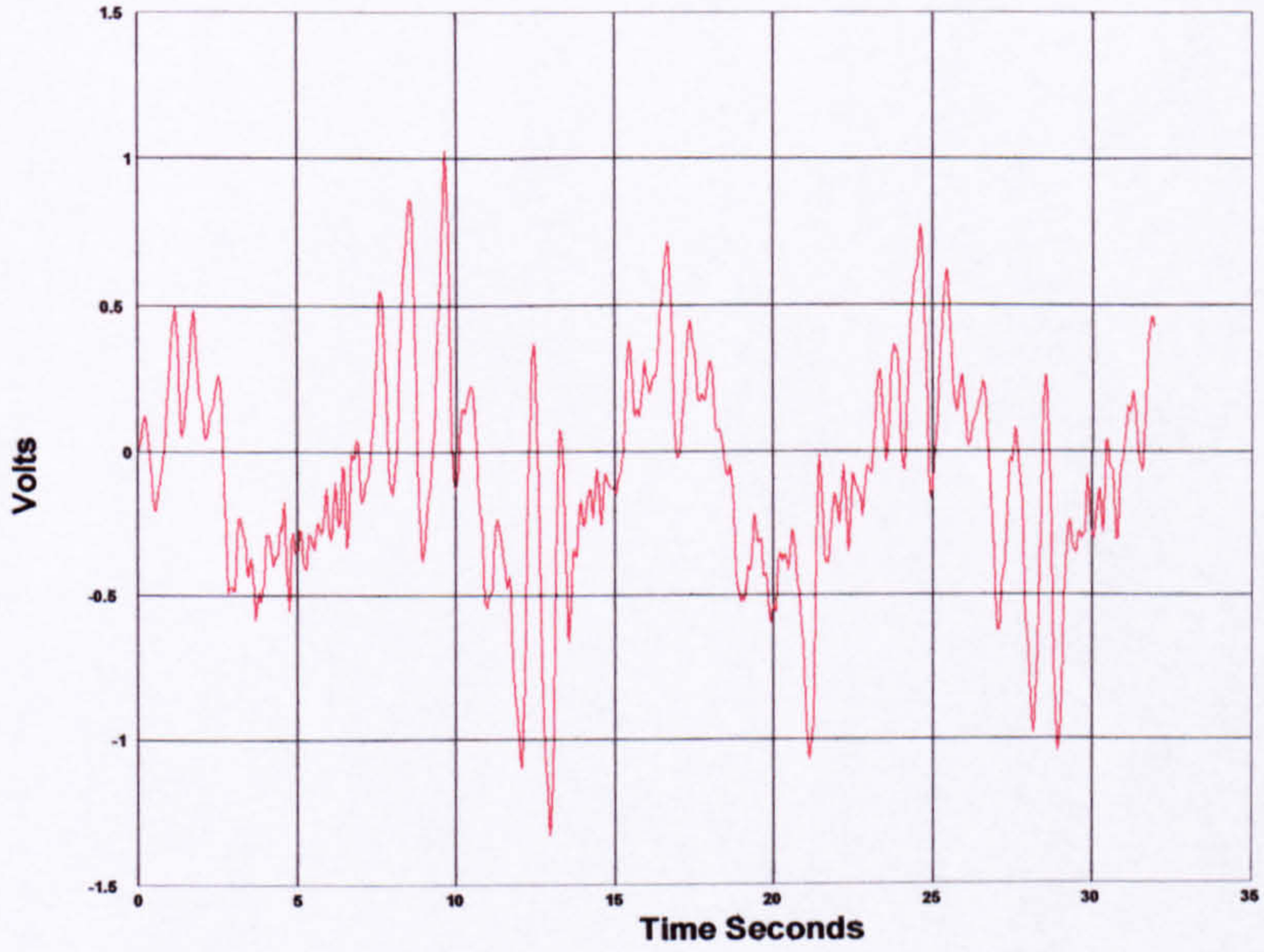

(b)

Figure 7.17 Response to a filtered 0.25 Hz sine wave

a) Output-Input behaviour **b)Control Effort**

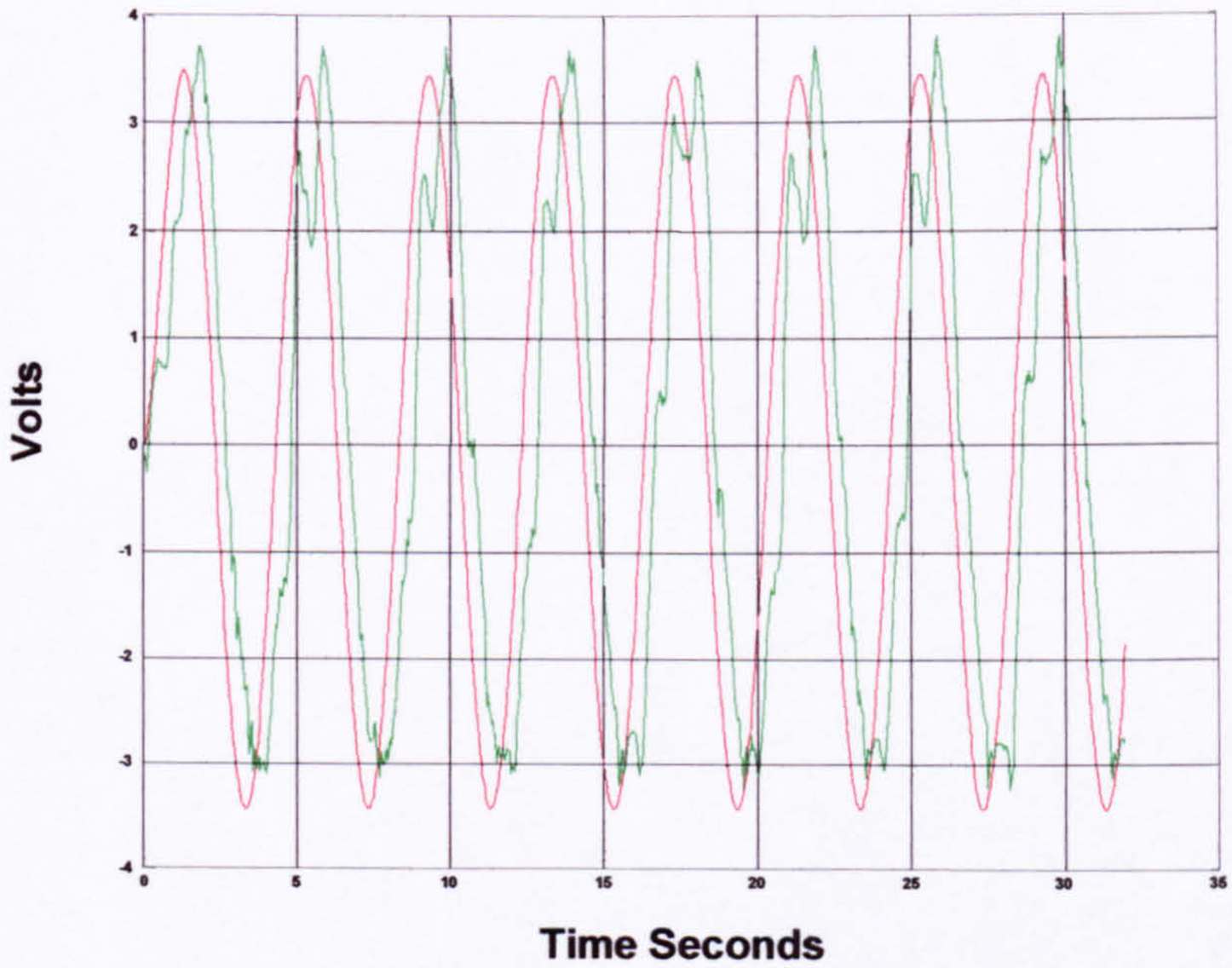

(a)

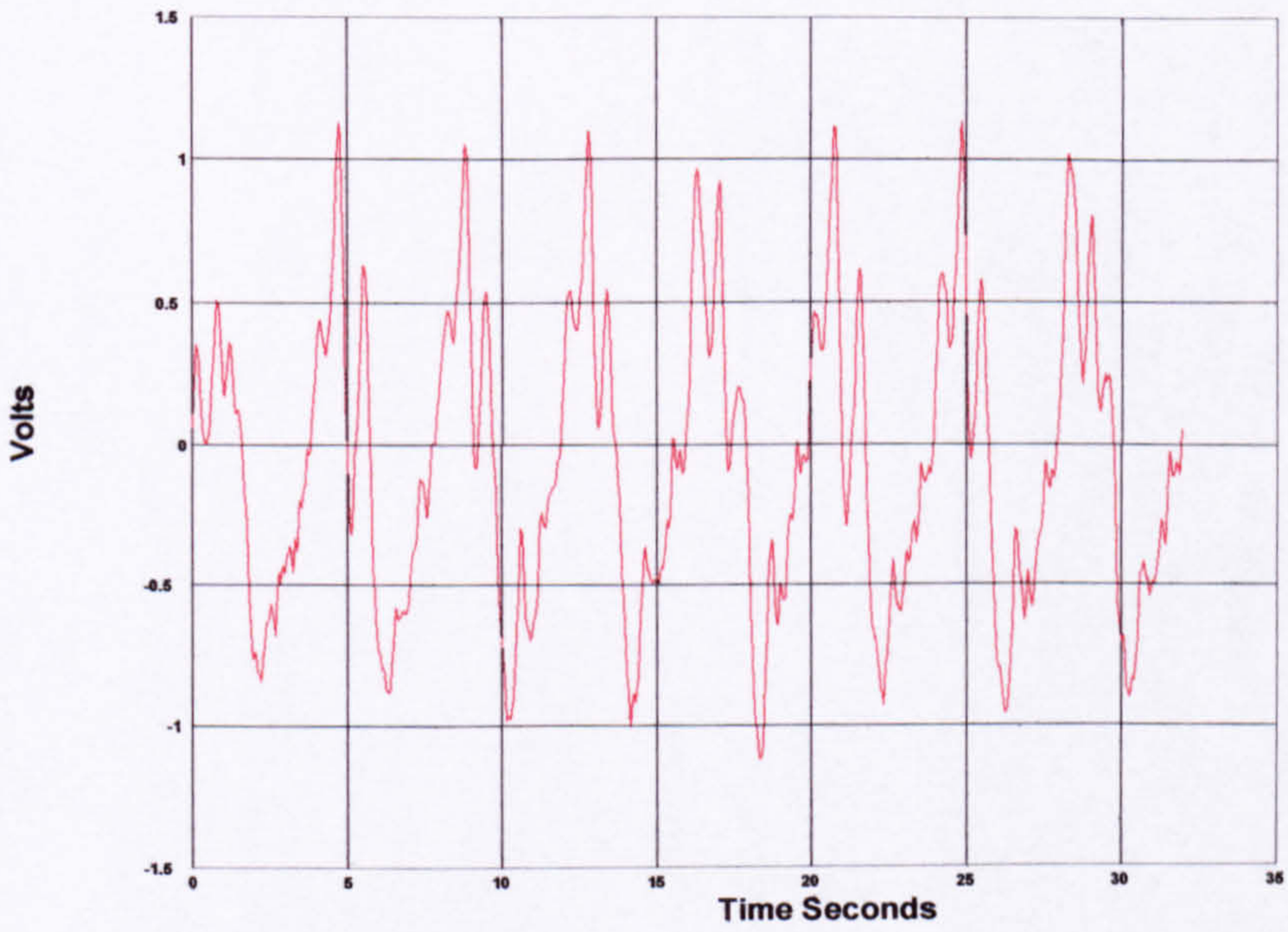

(b)

Figure 7.18 Response to a filtered 0.33 Hz sine wave

a) Output-Input behaviour **b)Control Effort**

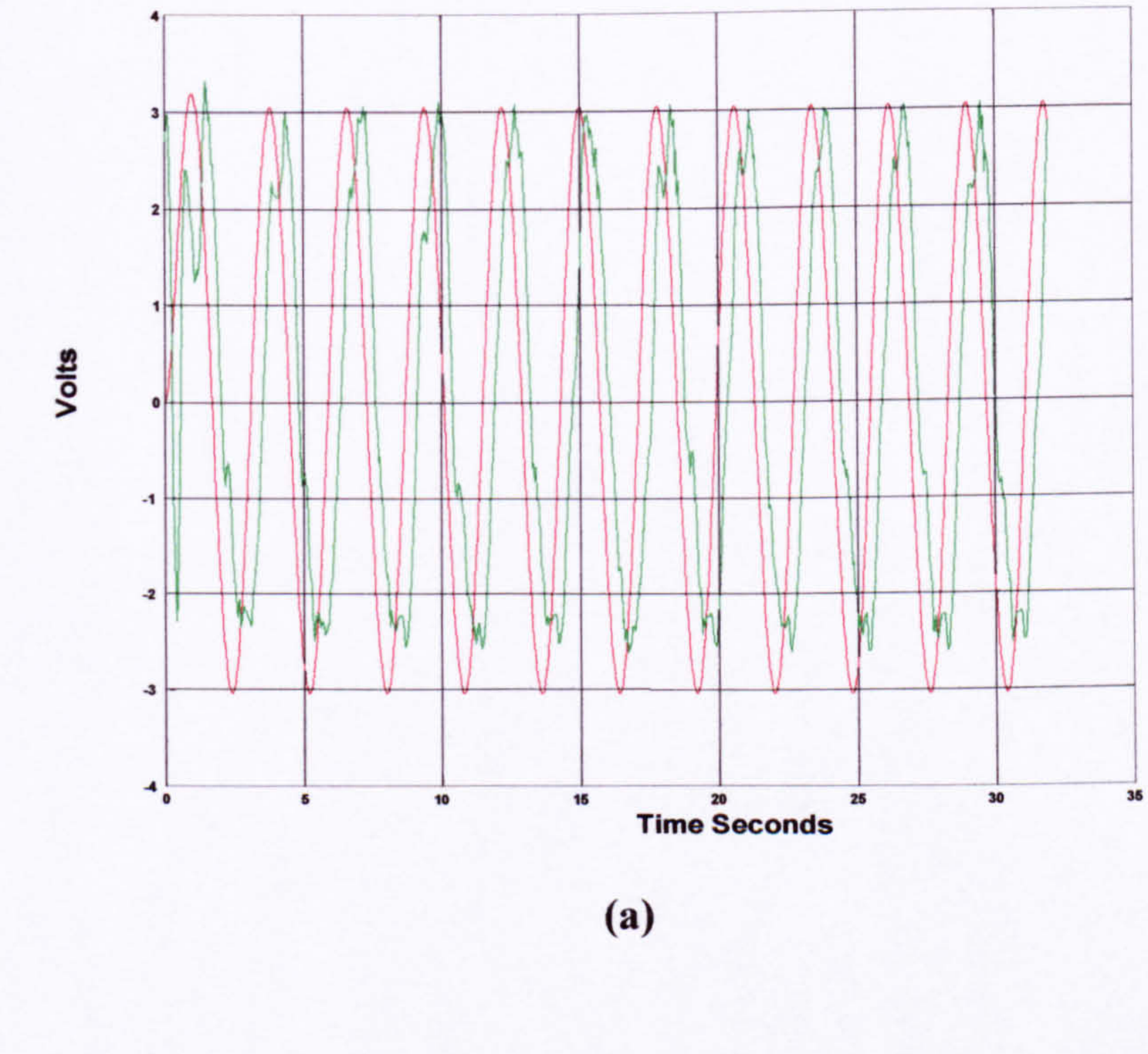

(a)

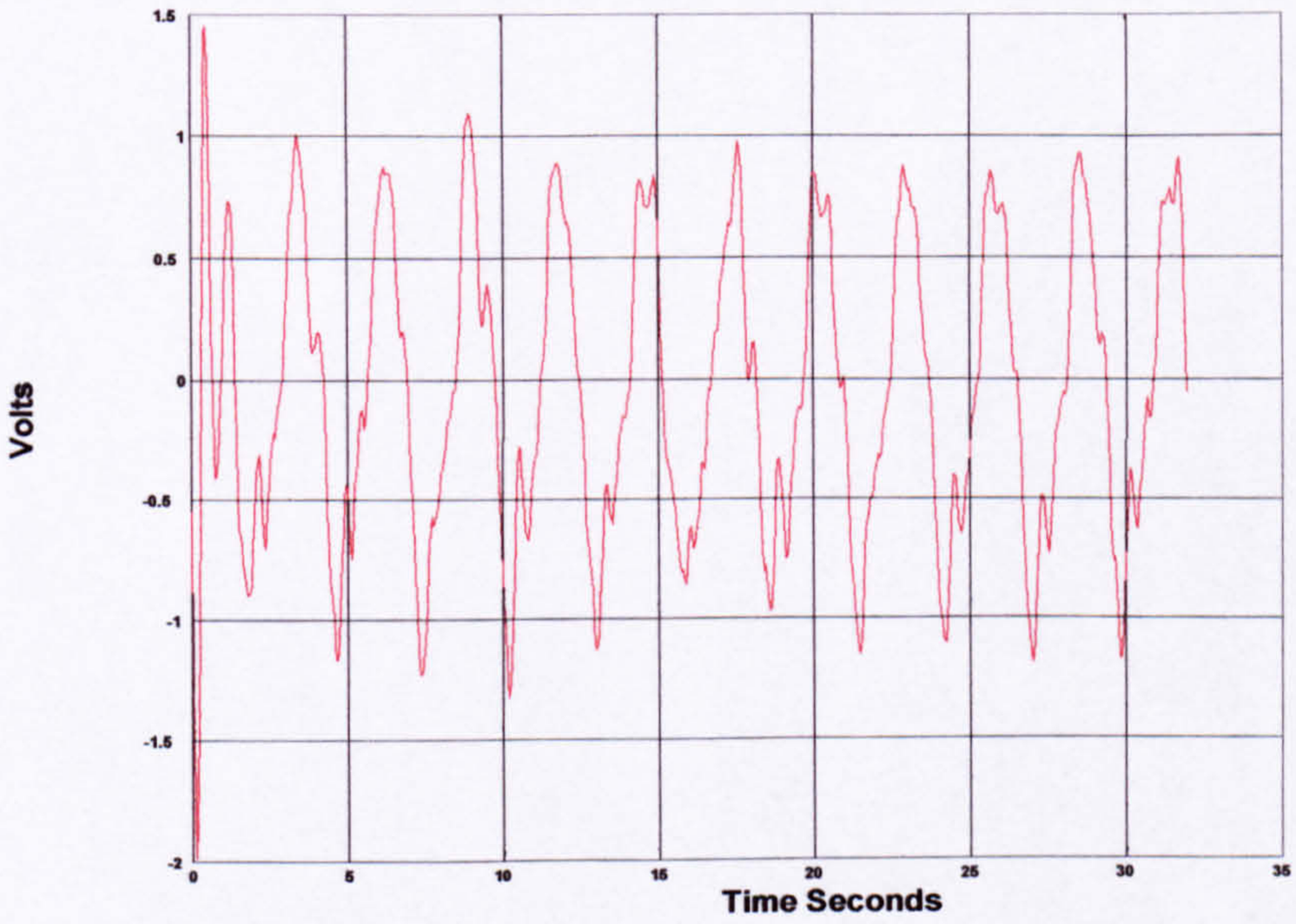

(b)

7.5 Conclusion of Controller input output behaviour

Figures (7.11) to (7.18) show the response of the selected controller to different input signals and the corresponding control effort. They show that the controller follows the pre set trajectory as set by the input signal well. However at low frequency components of the reference signal (effect of the filter in the square wave) the controller struggles. This is more prominent in figure (7.15) when a low frequency reference sine wave was used. The controller attempts to follow the shape but the system seems to get stuck thus increasing the corresponding control efforts which in turn makes the controller overshoot. The control effort is then decreased to get back onto track. It is clear from observing the Orthosis that the mechanical assembly was slightly sticking due to miss alignment.

7.6 Experimental Input-Output behaviour of different Order Controllers.

Figures (7.19)-(7.22) show a comparison of different order controllers for the same reference signal. These results were obtained with an artificial leg (approximately 10Kg) strapped to each leg. Looking at figure (7.19) for minimum order it can be seen that the Orthosis follows the general shape of the reference signal closely, but problems occur when the Orthosis is attempting to hold a certain position. That is the transition from one position to another is done perfectly but when holding is required the Orthosis seems to be staggering all the time, resulting in small deviations (oscillation) from the reference signal. As the order of the controller is increased (figures (7.20), (7.21) and (7.22)) show

improvement from the minimum order in terms of holding. However the Orthosis seems to overshoot at some point, tries to correct but over corrects resulting in slight movement when it is supposed to hold. Figure (7.22) clearly shows that the Orthosis follows the reference signal very closely and is also capable of holding, only at one instant it overshoots but quickly corrects and holds.

Another comparison is the control effort for different order controllers. These are shown in figures (7.23)-(7.26). The control effort for the minimum order controller has clearly more variations than any of the others. That is the controller has to send a signal very quickly all the time to maintain the preset trajectory. In terms of amplitude the different order controllers do not show very different behaviour (approximate peaks of 1.5 volts). The control effort intensity decreases as the order of the controller is increased. The control effort for the selected controller is much smoother than any of the others.

Figures (7.27)-(7.30) show a comparison of the different order controllers to sine wave input. These results exhibit the same behaviour as discussed above. The corresponding control efforts are shown in figures (7.31)-(7.34). The results for the sine wave show that the Orthosis struggles with low frequency signals.

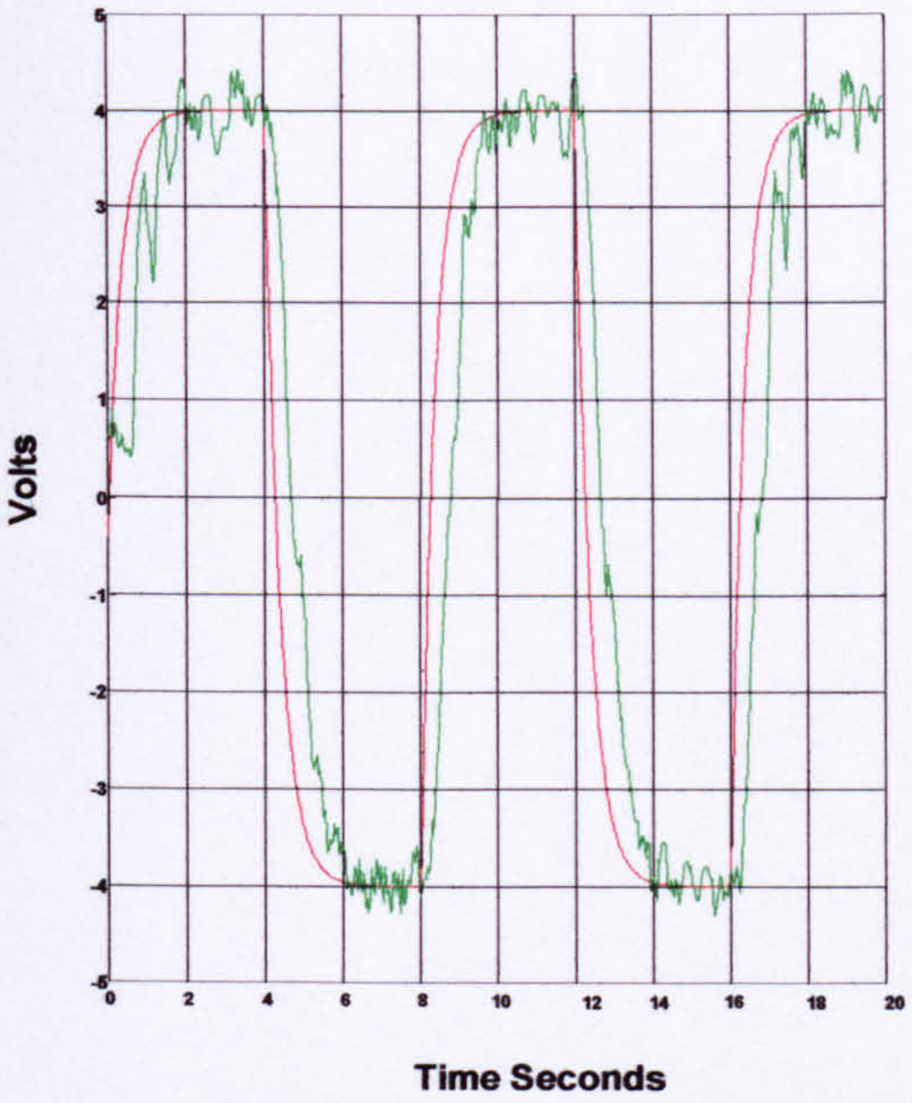

Figure 7.19 Input Output behaviour for Minimum order controller

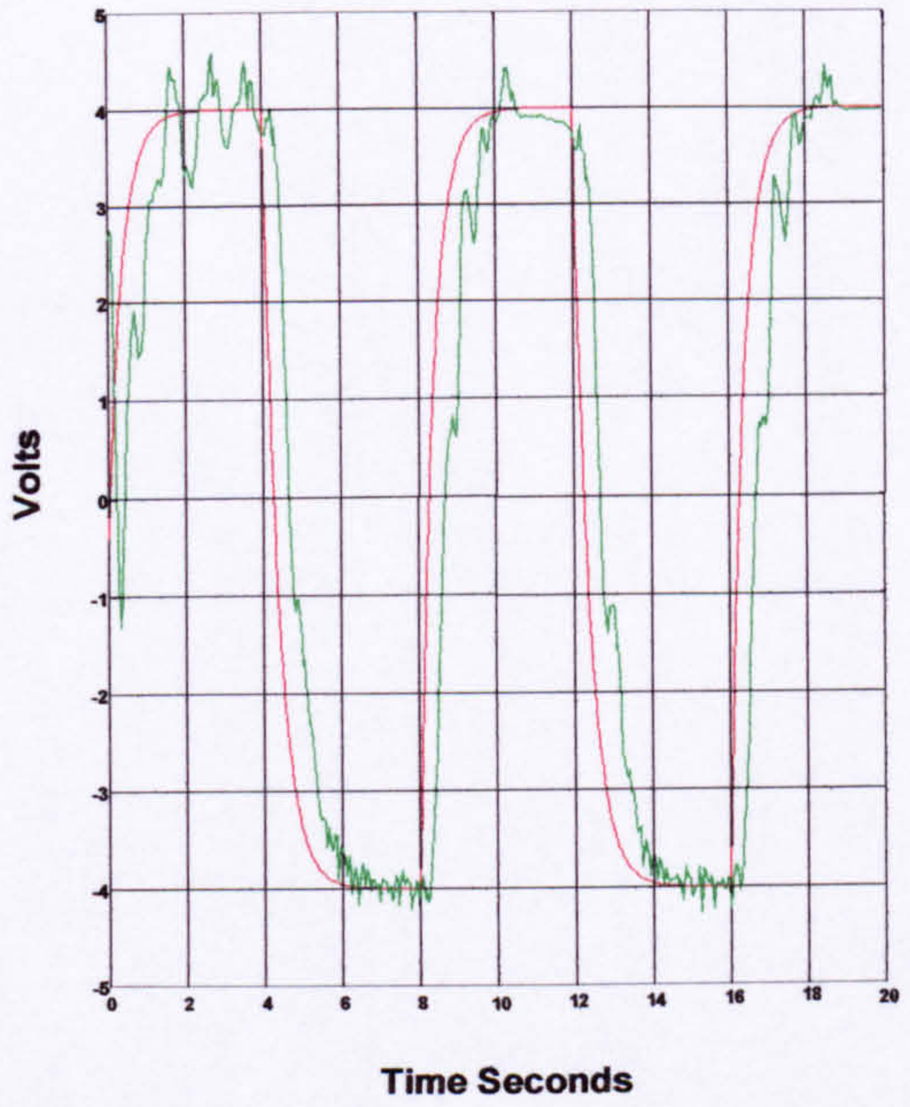

Figure 7.20 Input Output behaviour of 2+minimum order controller

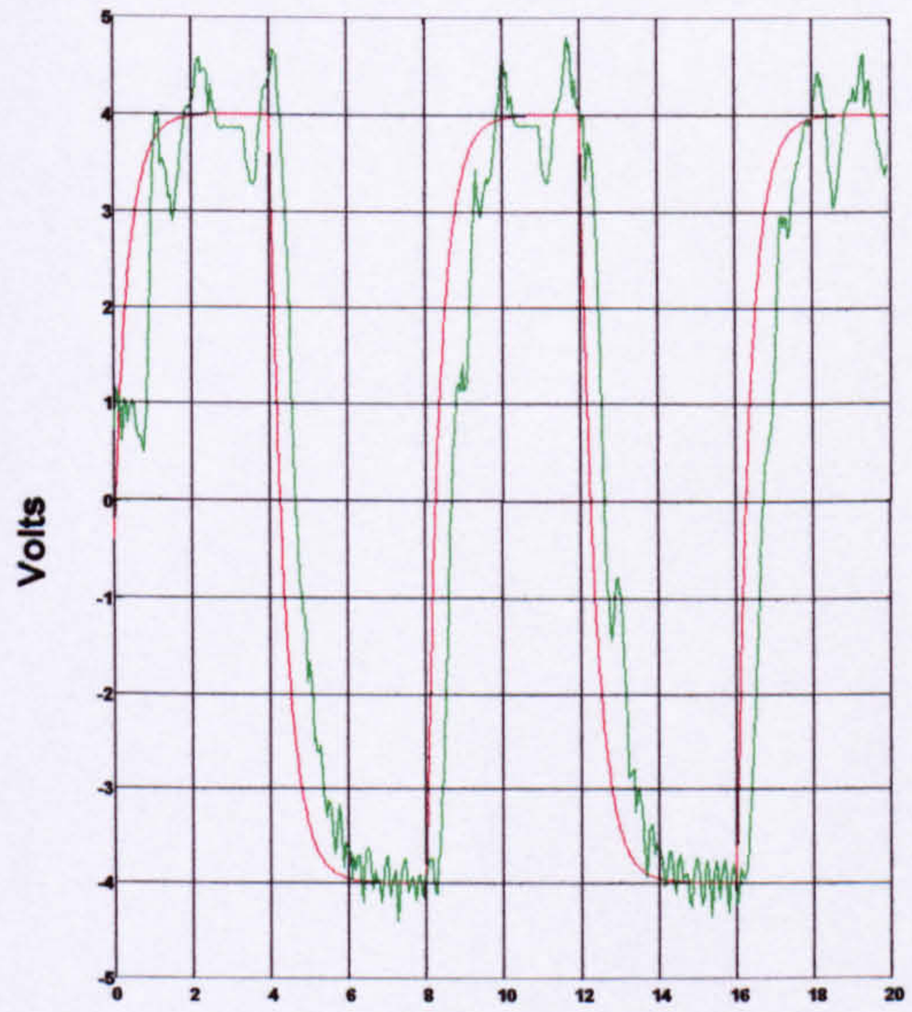

Figure 7.21 Input Output behaviour of of 4+minimum order controller

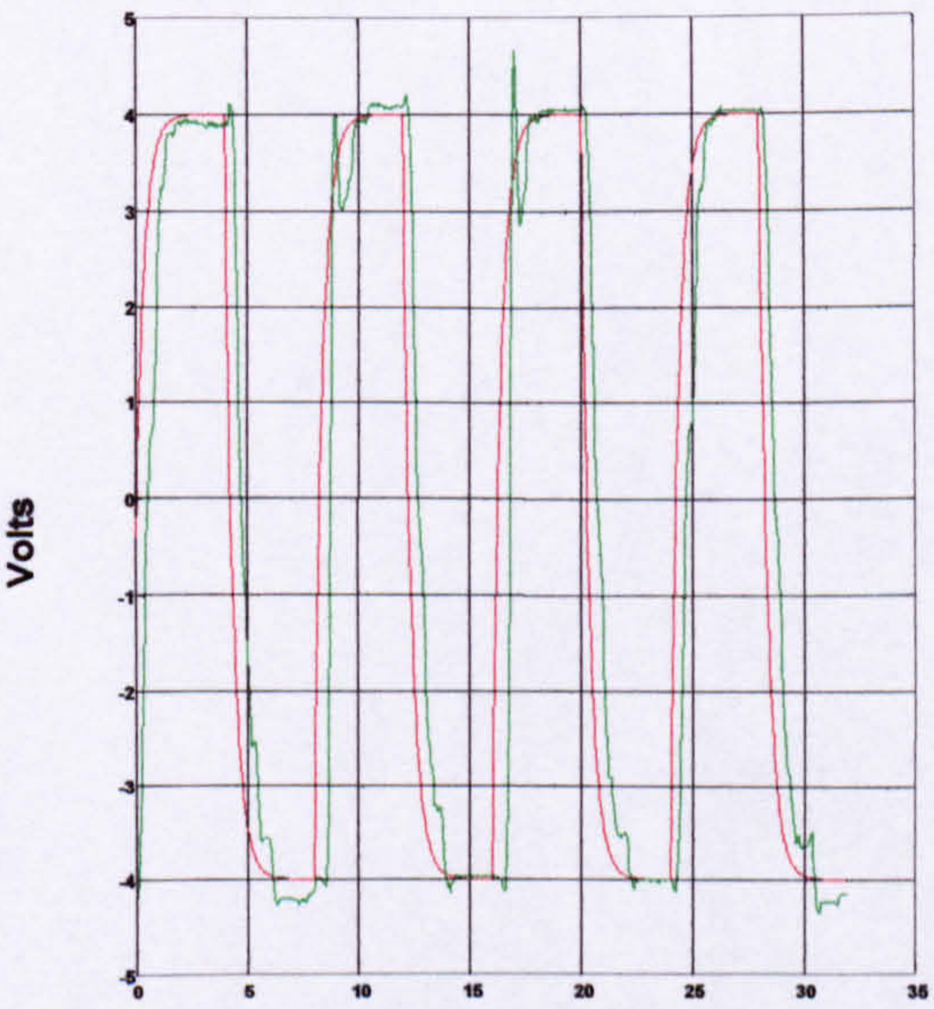

Figure 7.22 Input Output behaviour selected controller

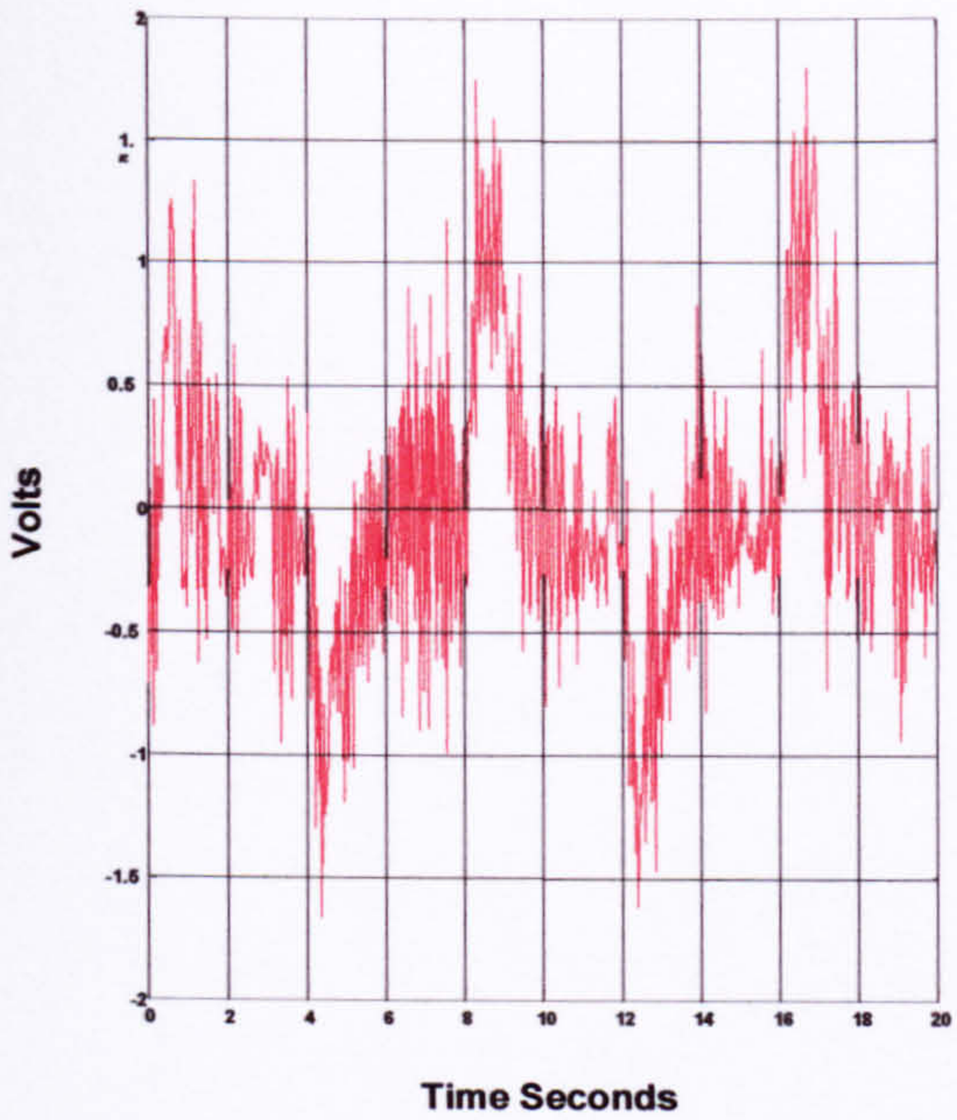

Figure 7.23 Controller effort for input signal in figure 7.19

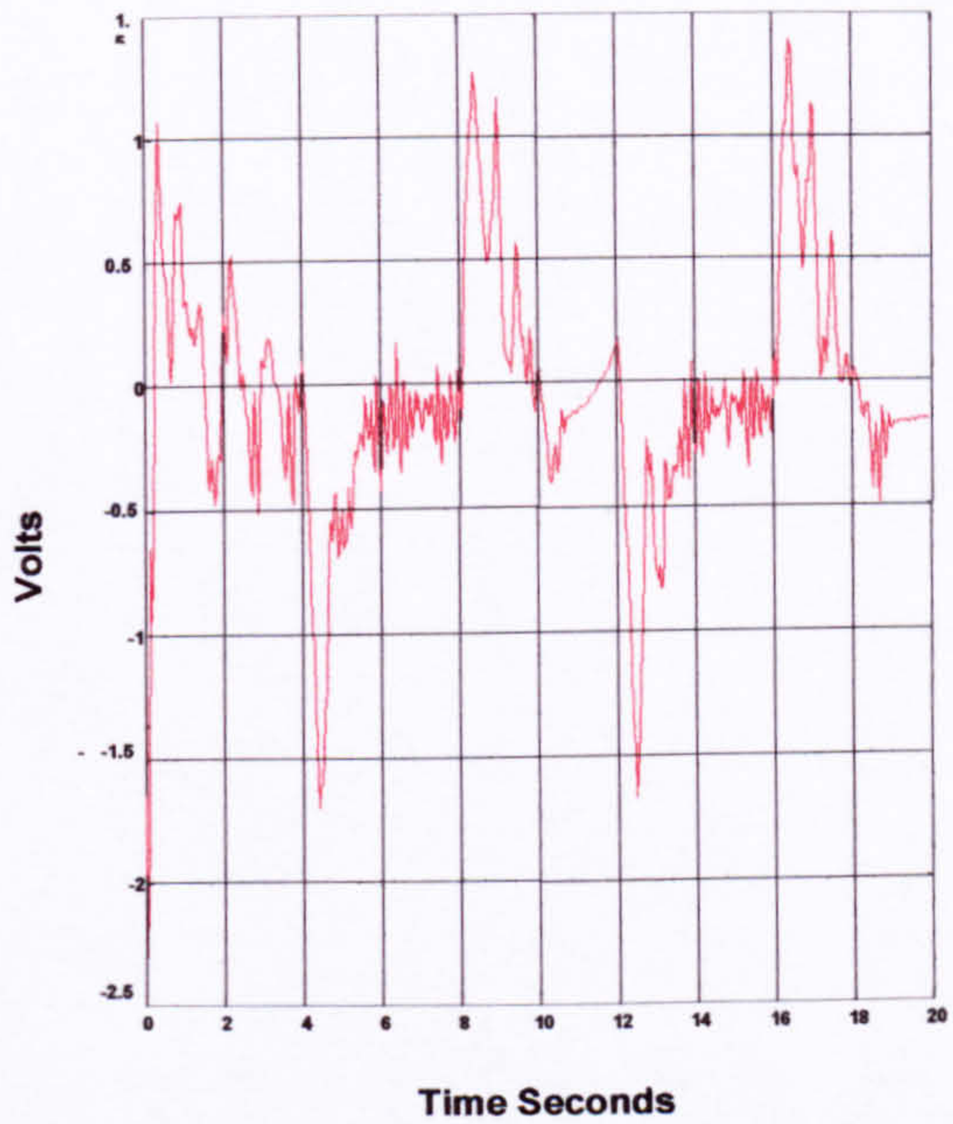

Figure 7.24 Controller effort for input signal in fig 7.20

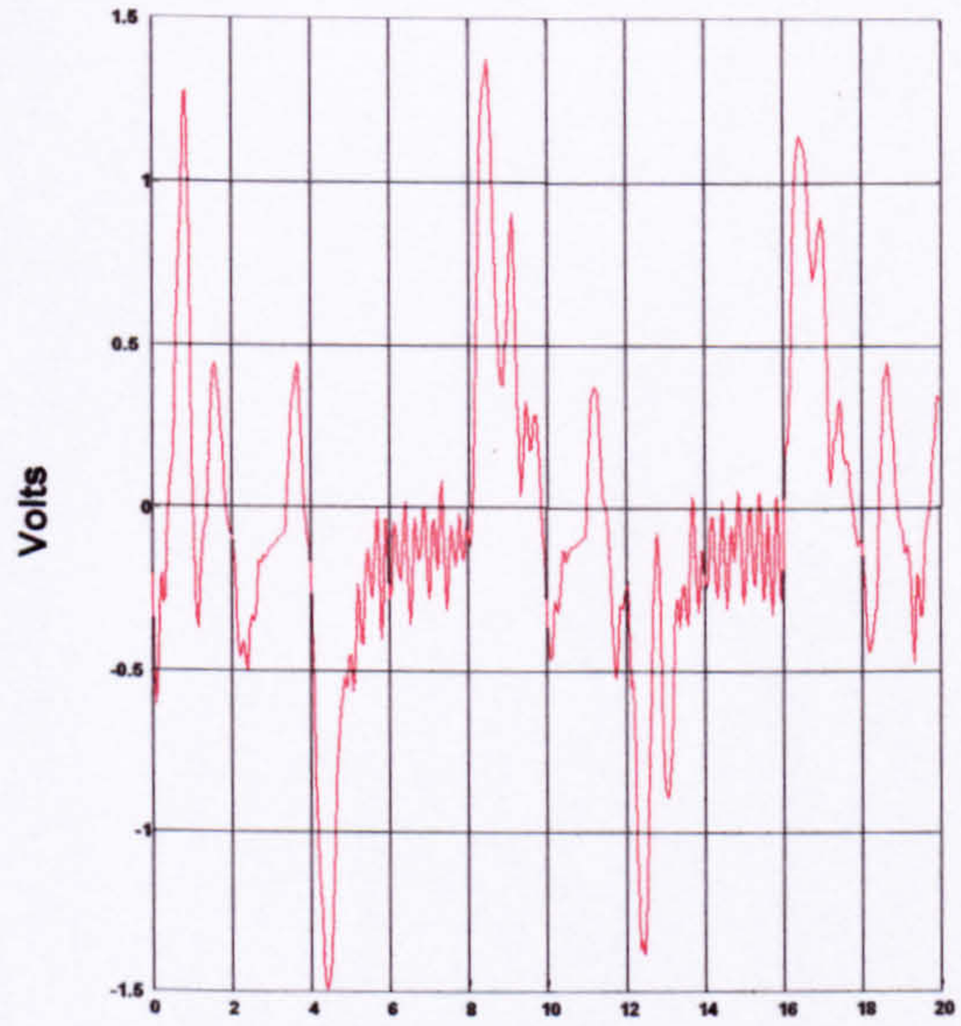

Figure 7.25 Controller effort for input signal in figure 7.21

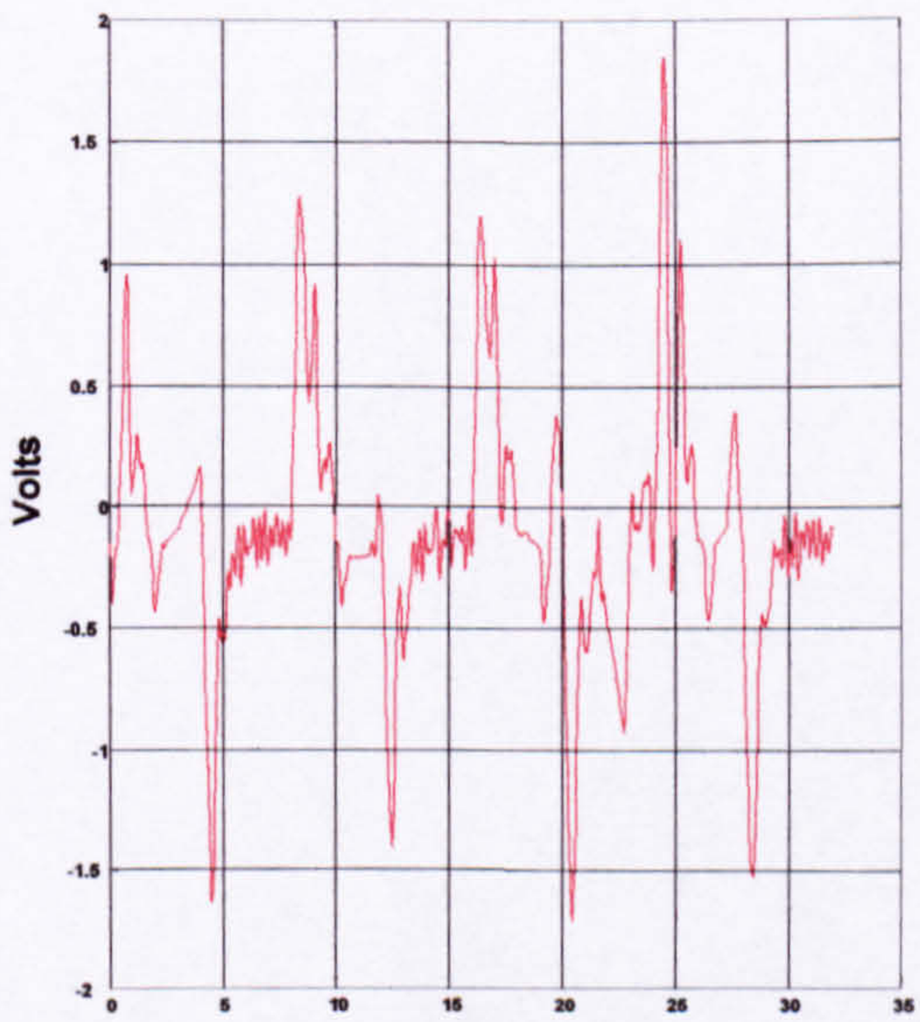

Figure 7.26 Controller effort for input signal in figure 7.22

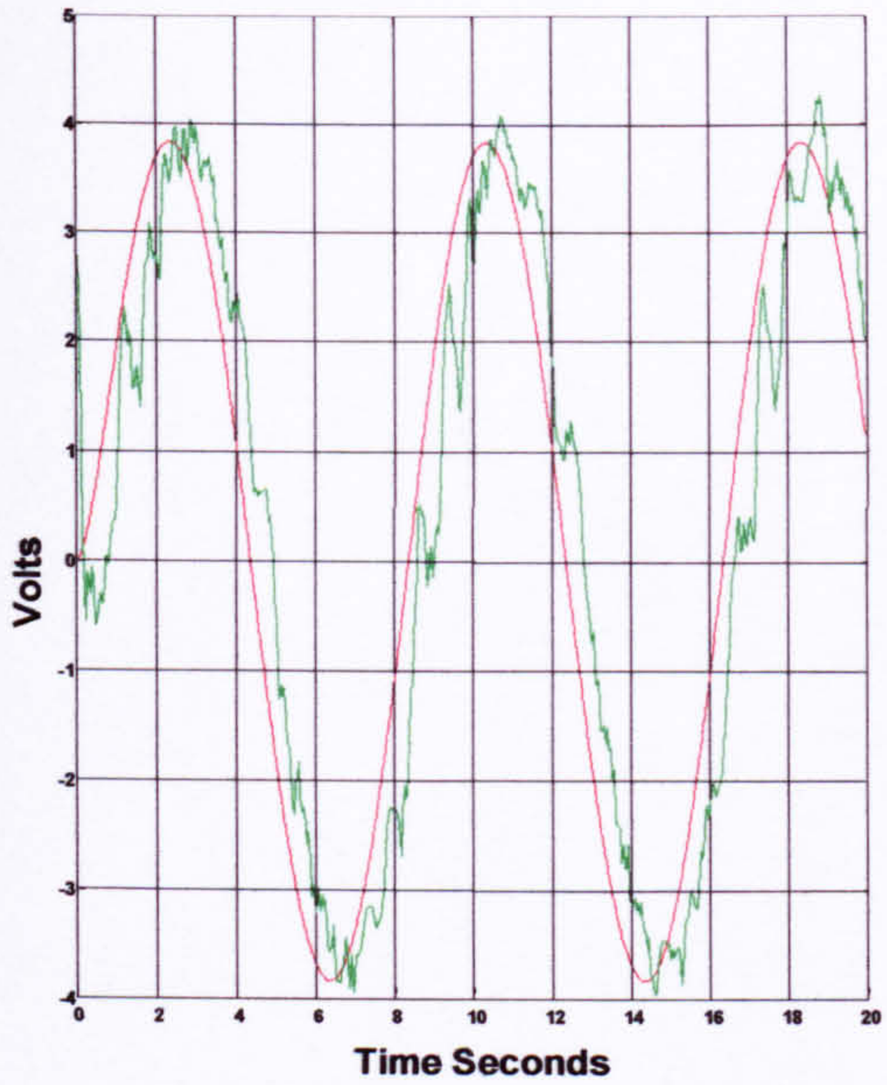

Figure 7.27 Input Output behaviour of minimum order controller

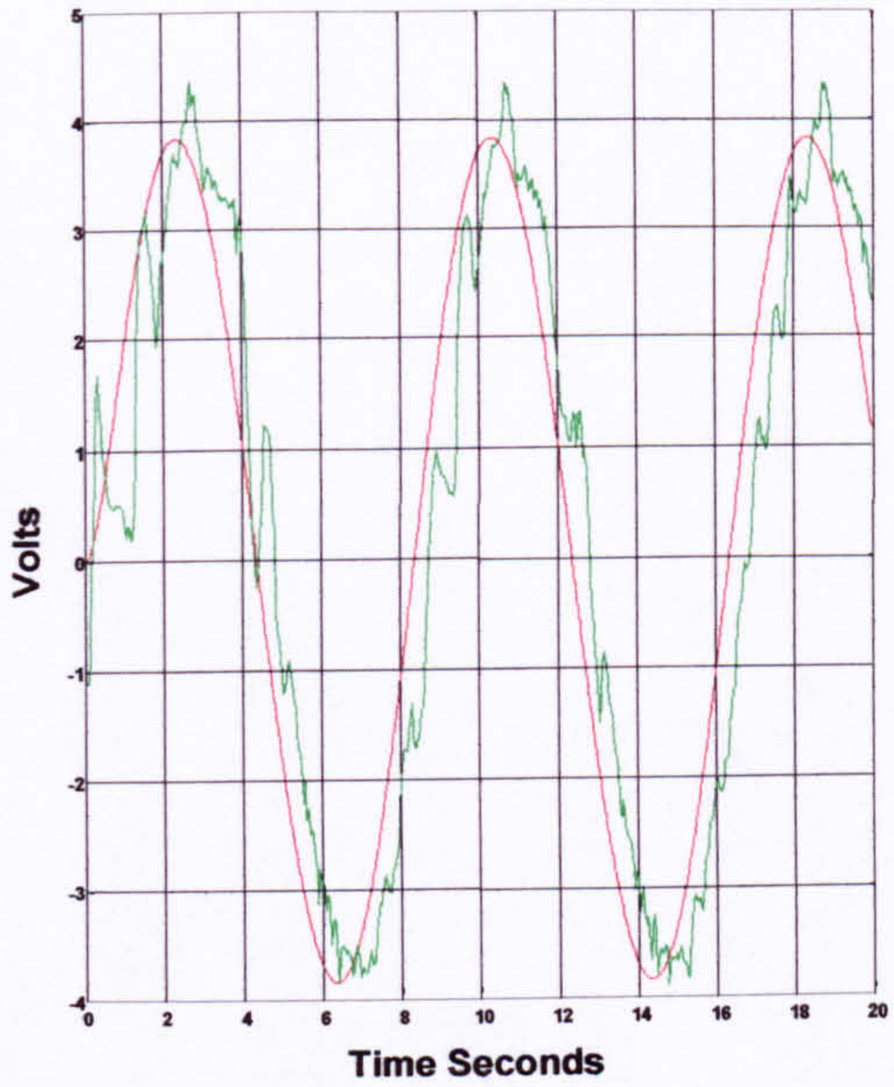

Figure 7.28 Input Output behaviour 0f 2+minimum-order controller

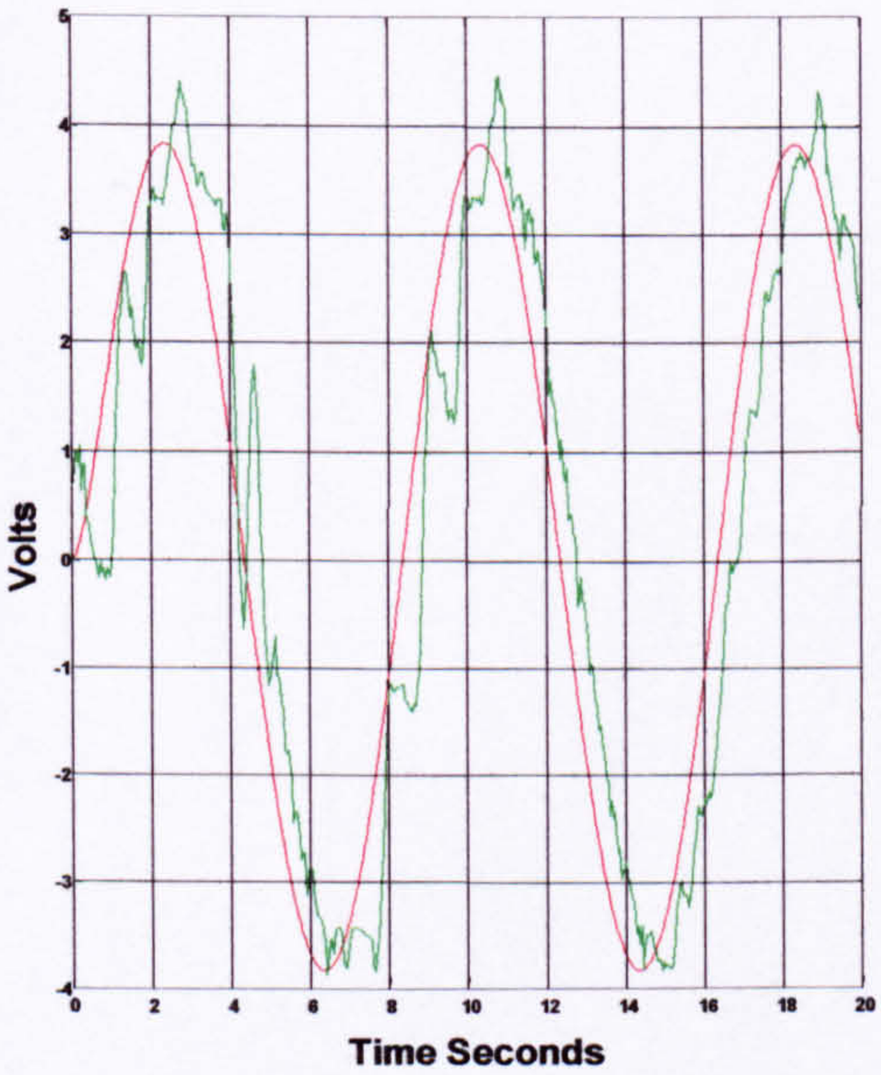

Figure 7.29 Input Output behaviour of 4+minimum order controller

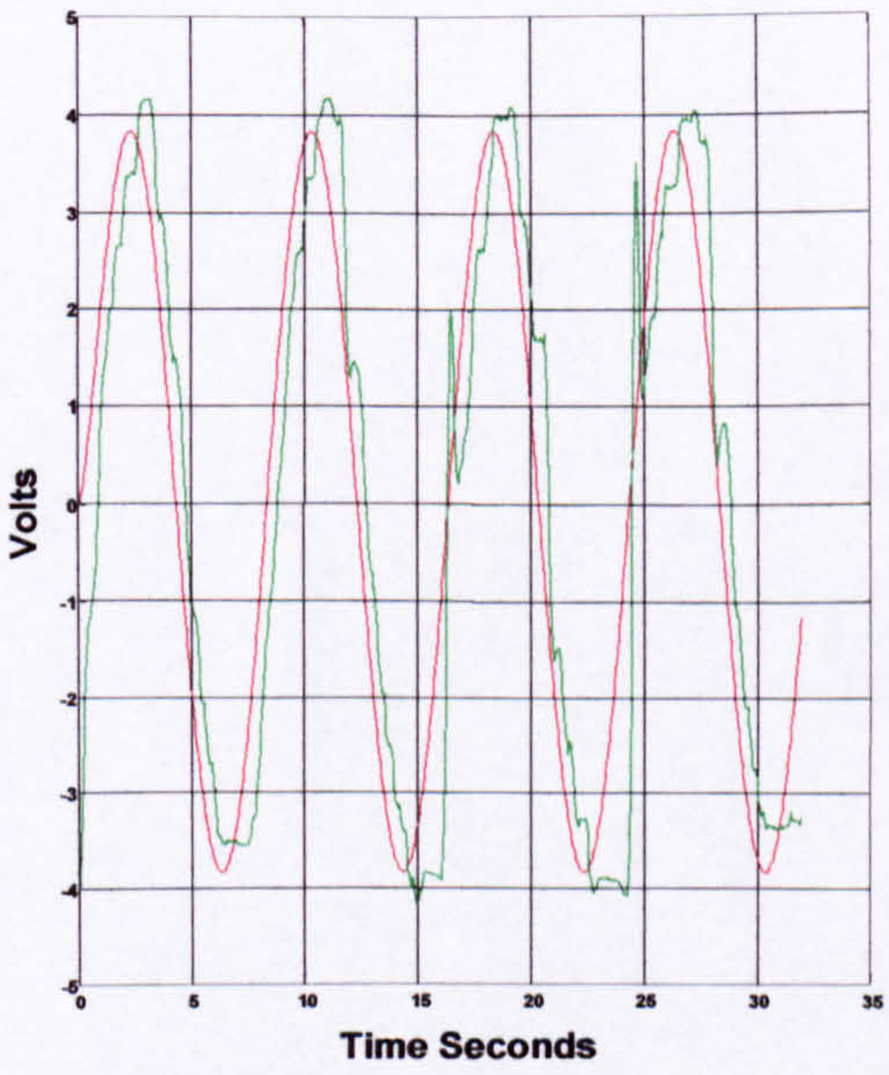

Figure 7.30 Input Output behaviour of selected controller

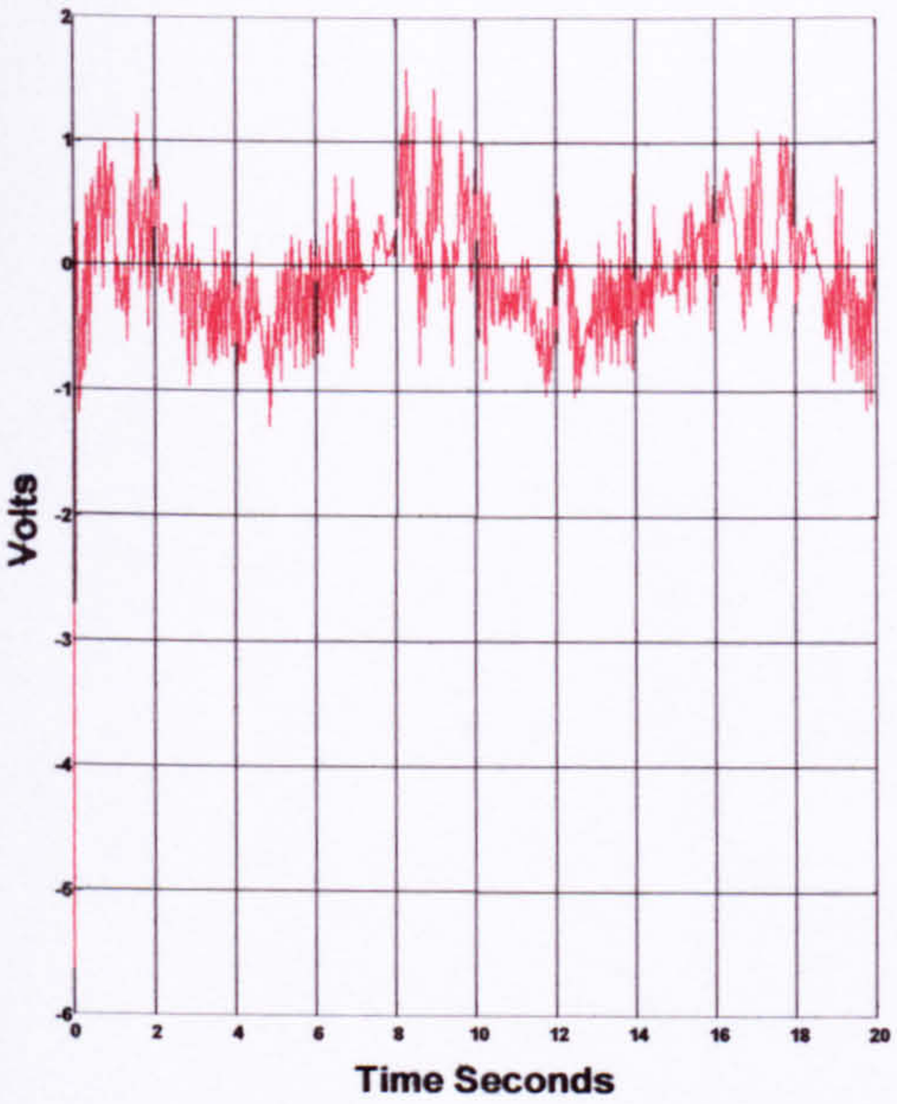

Figure 7.31 Controller effort for

Input signal in figure 7.27

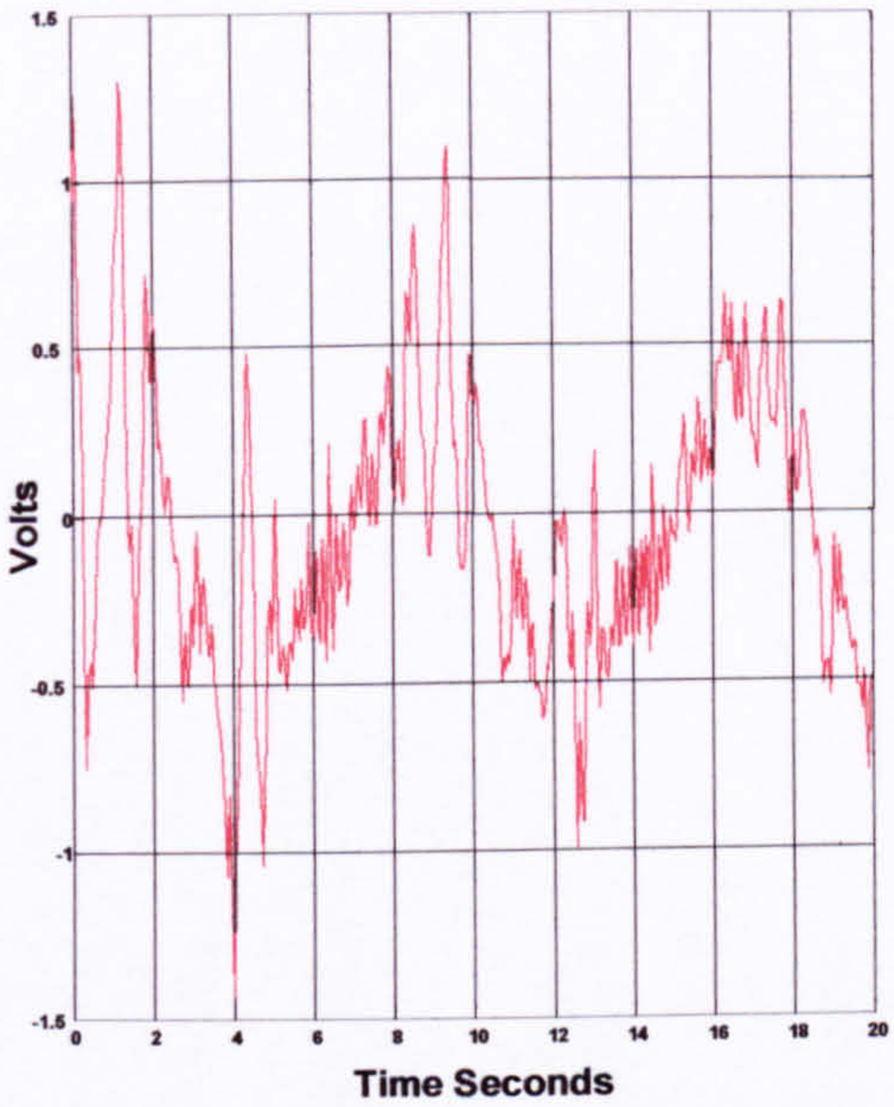

Figure 7.32 Controller effort for

Input signal in figure 7.28

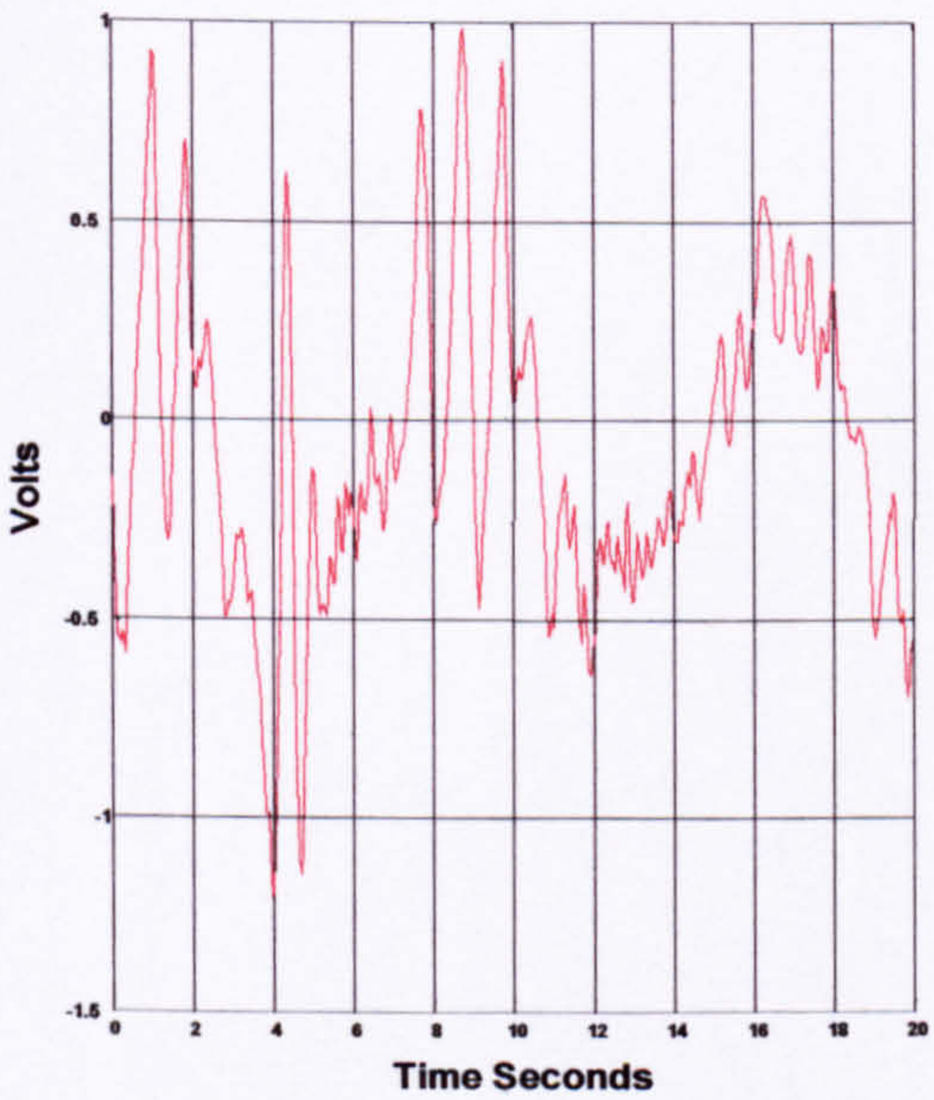

Figure 7.33 Controller effort for

Input signal in figure 7.29

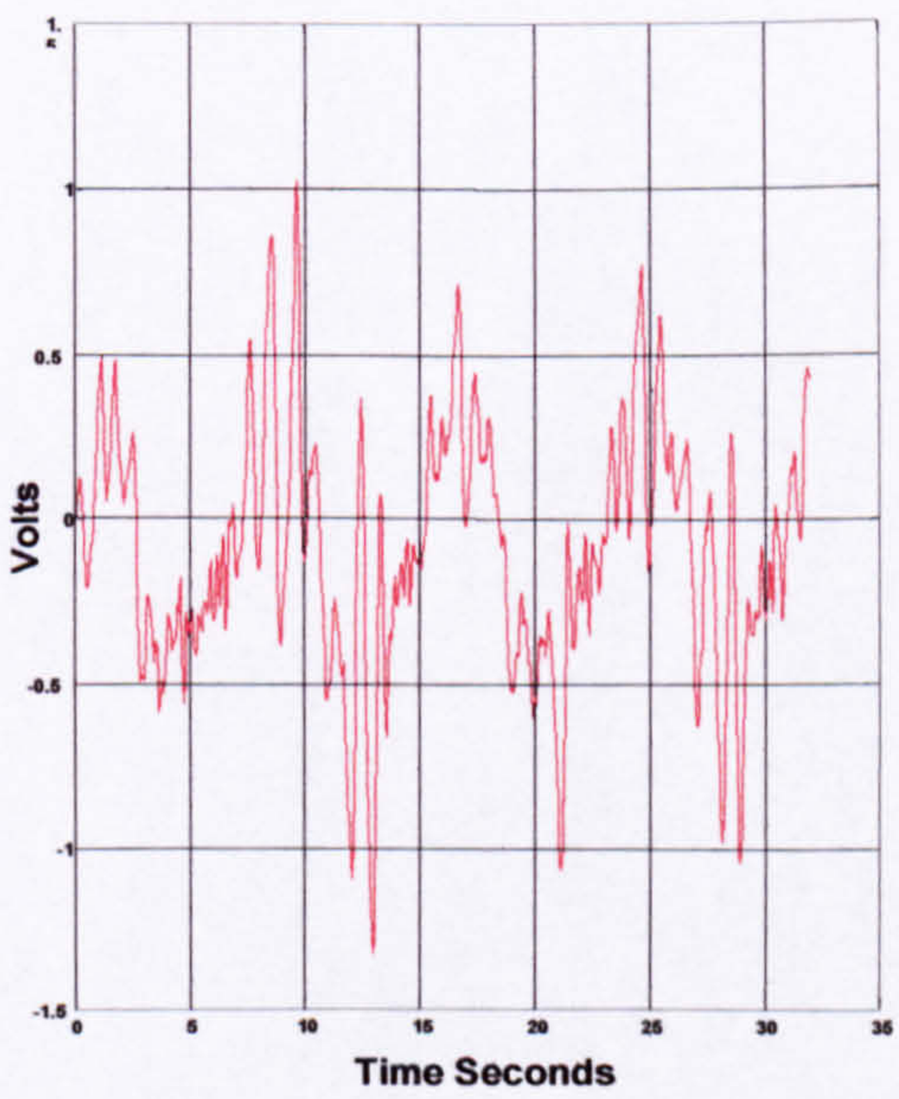

Figure 7.34 Controller effort for

Input signal in figure 7.30

7.7 Comparison of both Legs when the Orthosis is unloaded

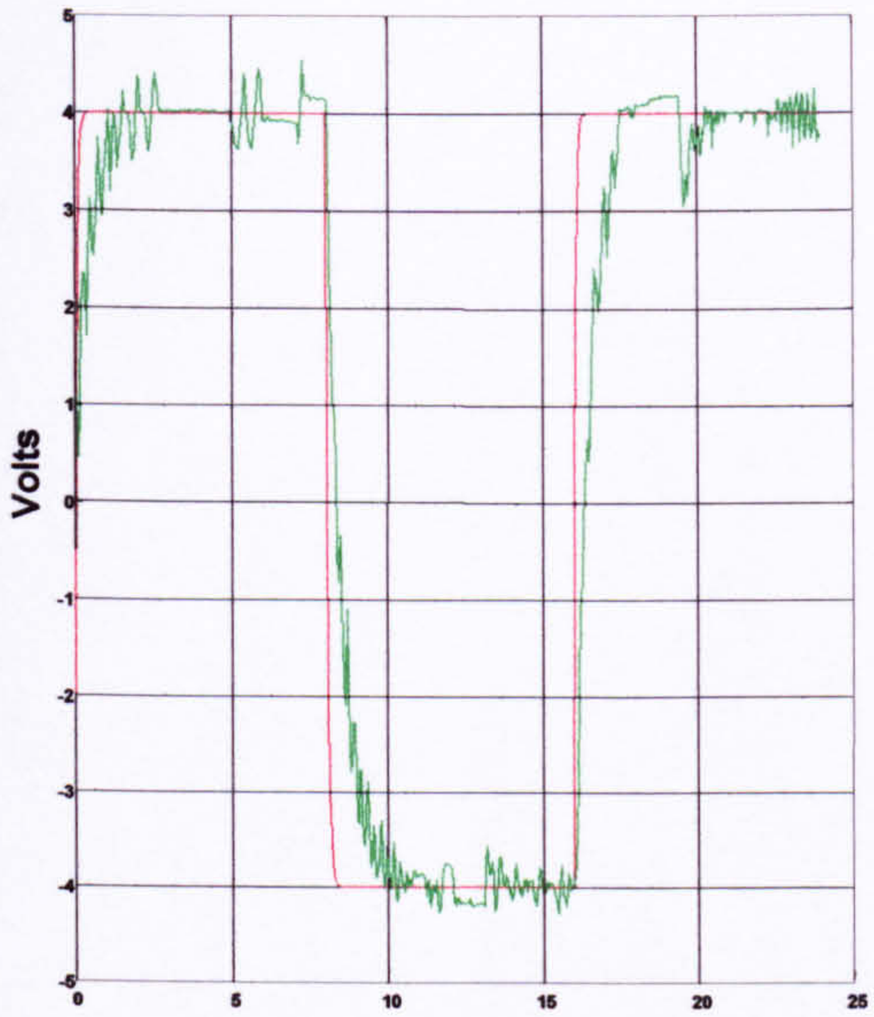

Figure 7.27

Input output behaviour of left leg

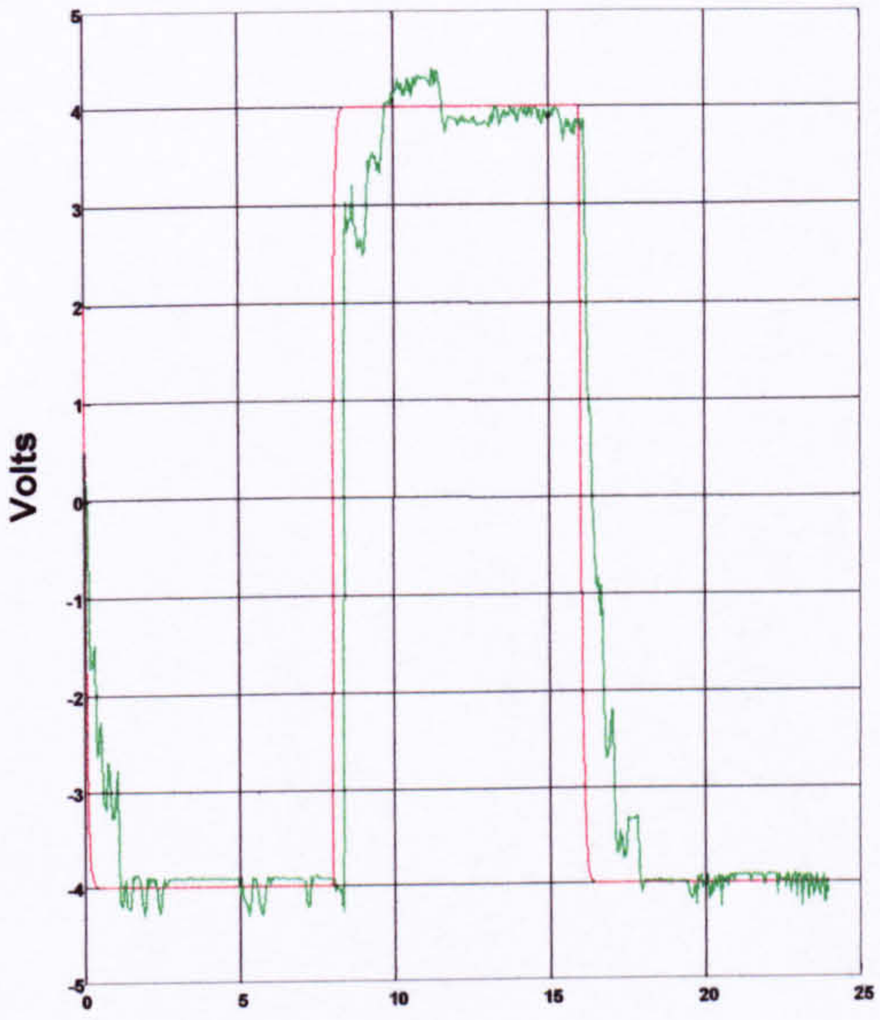

Figure 7.28

Input output behaviour of right leg

The important result with this test is to make sure both legs are in synchrony. That is when one leg is moving forward, the other leg (hip) is moving back. As the Orthosis is suspended during the test, when the leg is driven forward the other leg is driven back. However when the Orthosis is loaded and walking on the ground, one leg is moving forward while the hip of the stance leg is moved back allowing for the first step to be taken. This is then repeated for the other leg. The results in figures (7.47) and (7.48) clearly show both legs to be in synchrony.

7.8 Comparison of both Legs when the Orthosis is loaded

a) Volunteer number 1

Training volunteer number 1 took approximately 45 minutes. The subject was required to take his body weight from the moving leg to the stance leg. Then he was asked to hold that position while the Orthosis is moving one leg forward. Then the subject is required to transfer his body weight to the other leg allowing the stance leg to be moved forward. This procedure had to be repeated continuously. Problems encountered include fighting of the motion by the subject especially with the initial transient. That is when the Orthosis first starts moving the subject seems to stiffen up and try to hold the motion before relaxing again. Another problem was that when the subject was waiting for the Orthosis to move one leg he kept moving the leg, which is about to be moved slightly. In other words non of the two volunteers felt comfortable with standing on one leg and just suspending the other leg freely.

Figures (7.29)-(7.34) show the response of the left and right legs when volunteer no. 1 was walking in the Orthosis. Three different speeds were tested. The results show that the Orthosis followed the pre-set reference signal closely. It can be seen that during the transition cycle of the gait there is a slight hesitancy in the Orthosis movement. Holding position was also slightly difficult for the subject as shown in figures (7.29)-(7.34). This is shown in the figures by the ragged peaks of the response rather than a smooth peak.

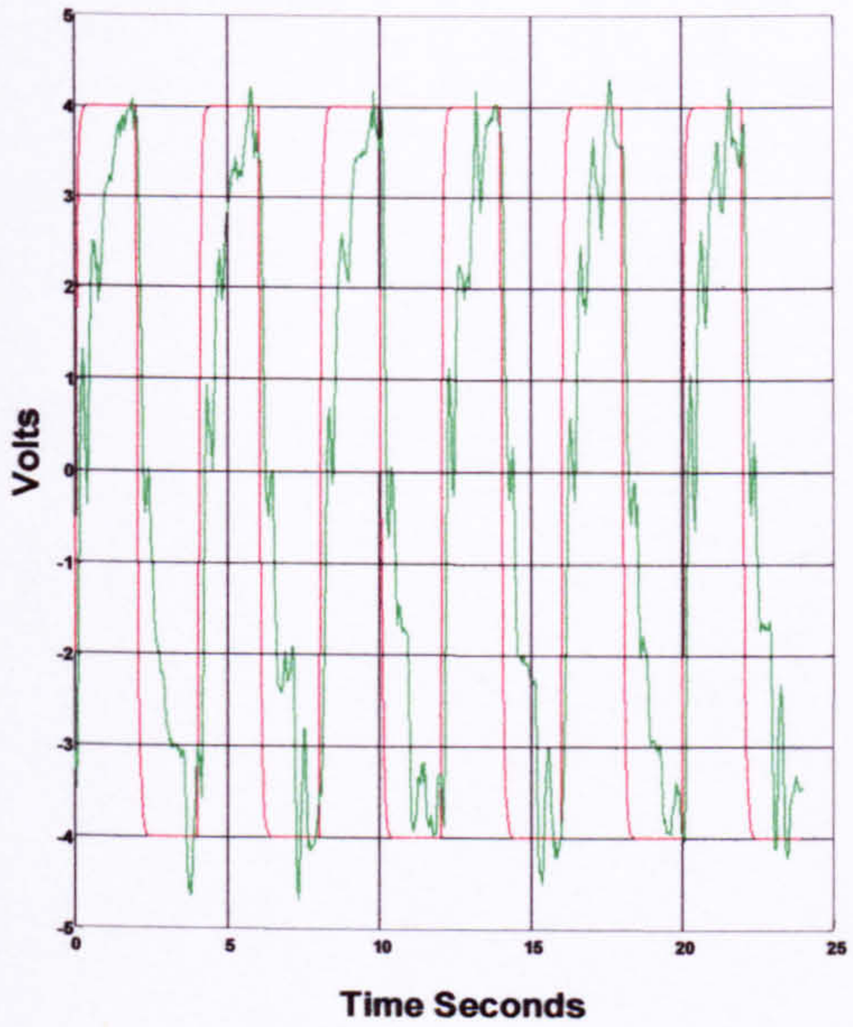

Figure 7.29 Input-Output behaviour of Left leg with volunteer no.1

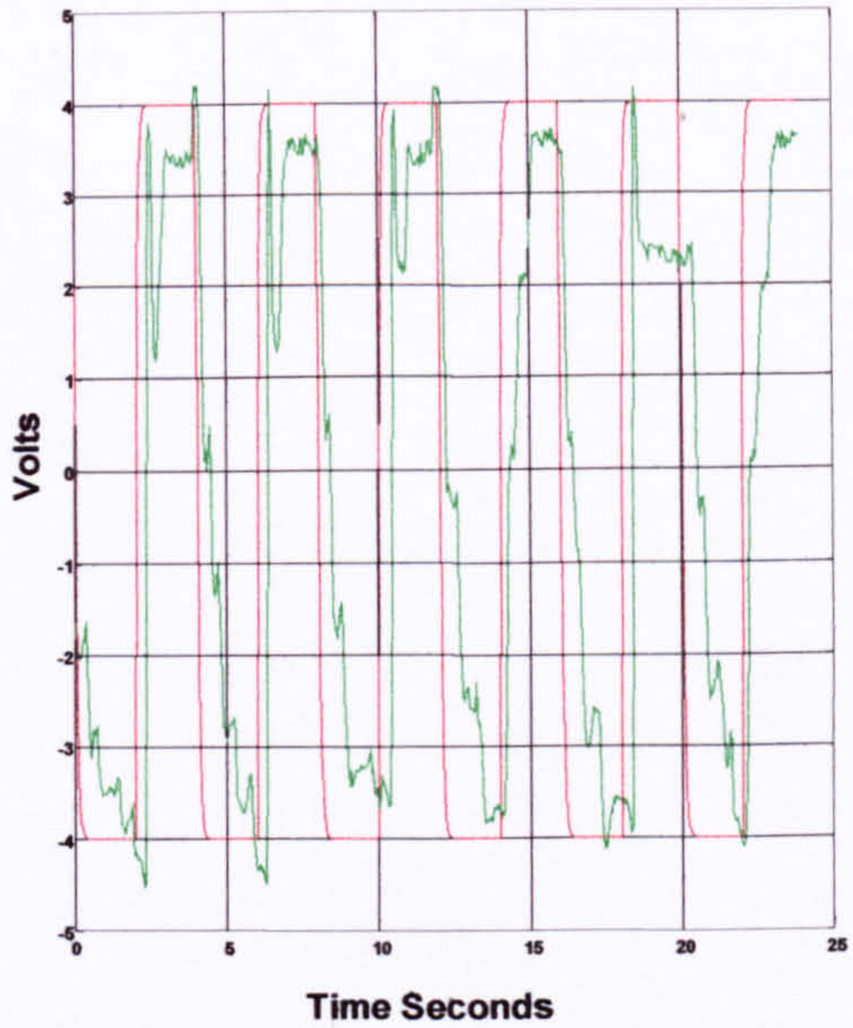

Figure 7.29b Input-Output behaviour of Right leg with volunteer no.1

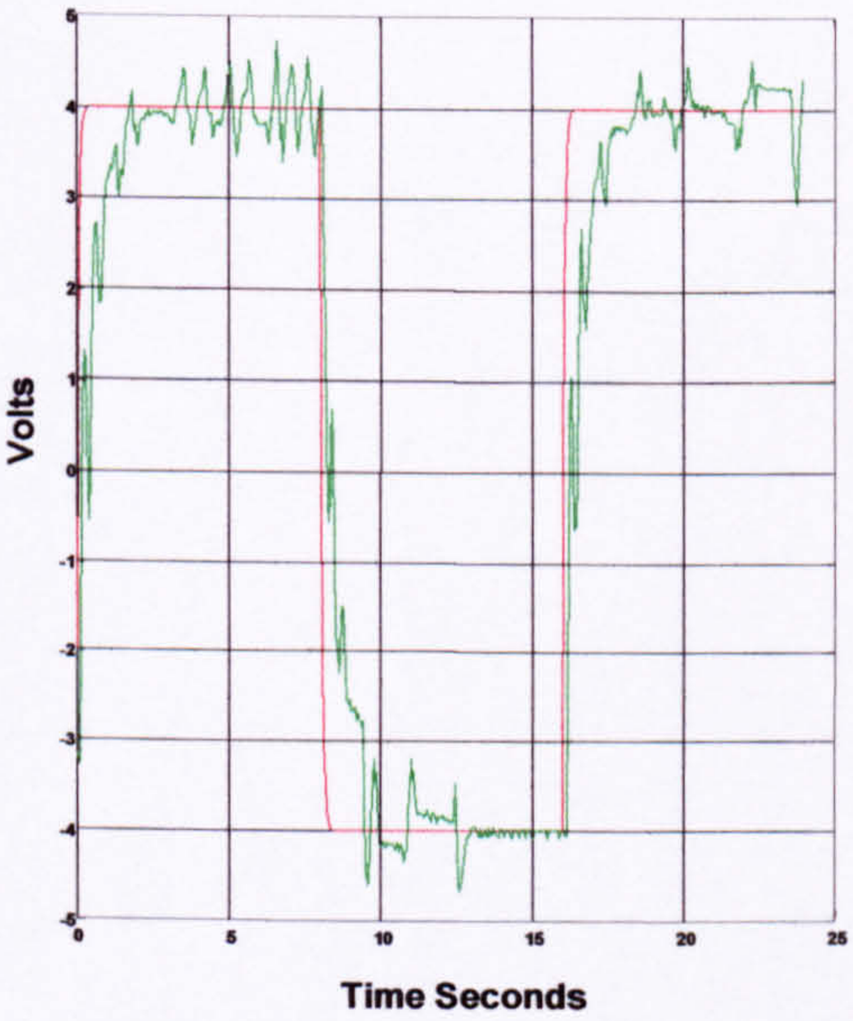

Figure 7.30 Input-Output behaviour of Left leg with volunteer no.1

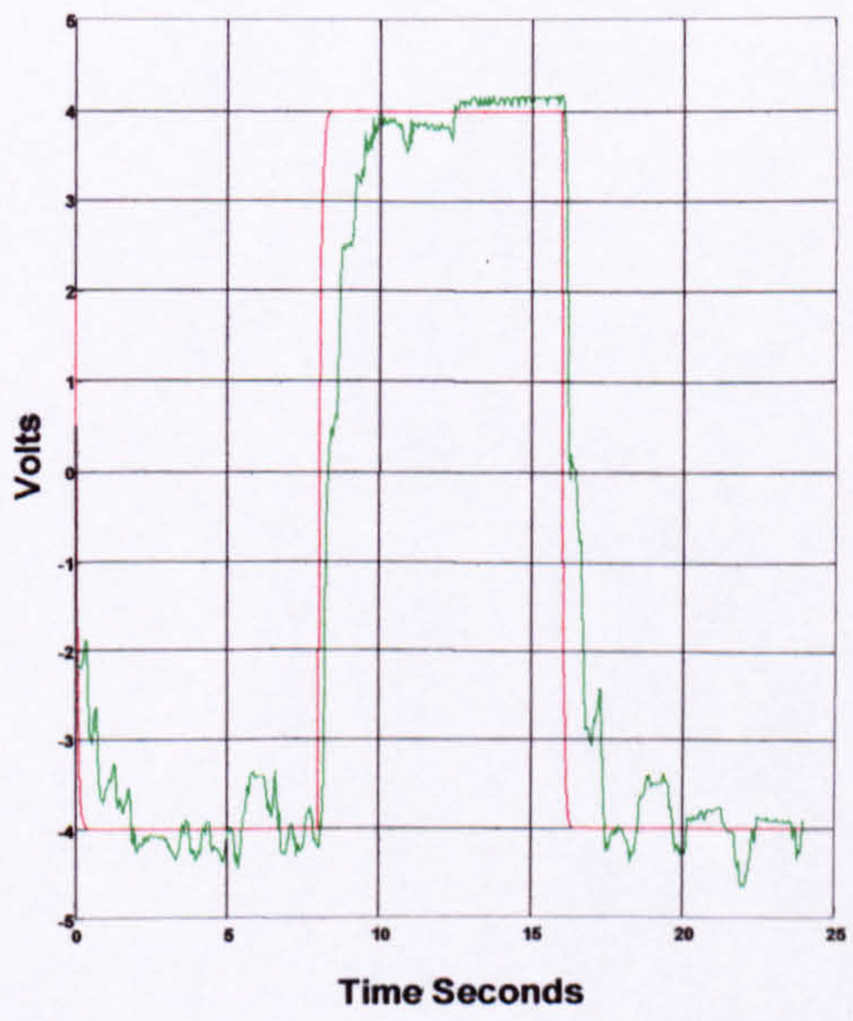

Figure 7.30b Input-Output behaviour of Right leg with volunteer no.1

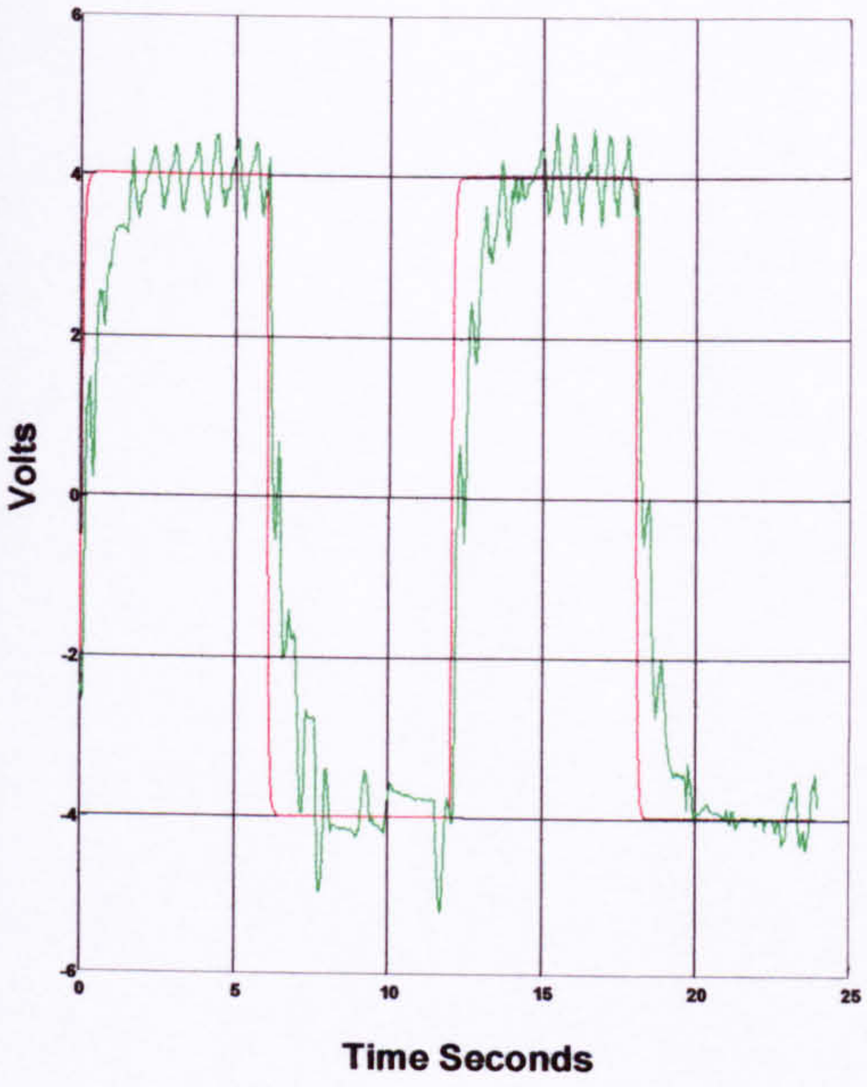

Figure 7.31 Input-Output behaviour of Left leg with volunteer no.1

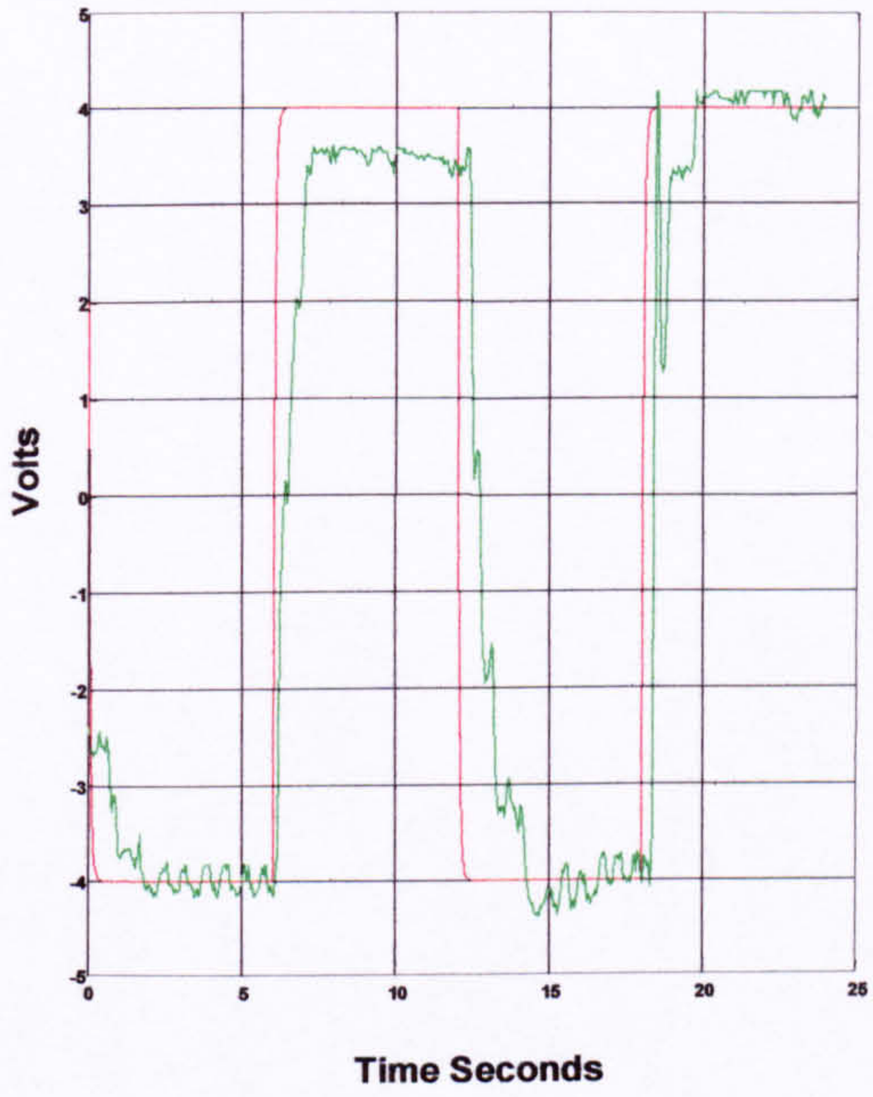

Figure 7.31b Input-Output behaviour of Right leg with volunteer no.1

b) Volunteer number 2

More tests were carried out with subject 2 because his time did not allow for training. In fact only 5 minutes of instruction was given before the tests were carried out. He results clearly show a degradation in performance comparing with subject number 1. One of the major problems encountered by this subject is his ability to hold. Every time he transferred his body weight to the stance leg he also moved his other leg further back resulting in overshoots in the graphs. The Othosis always attempted to correct but the subject was always fighting the motion. He was not very happy in the Orthosis and stated that he felt uncomfortable. All these problems can clearly be ironed out with further training. Another important point to mention is that it is imperative that the person in the Orthosis be the right size to fit in the Orthosis.

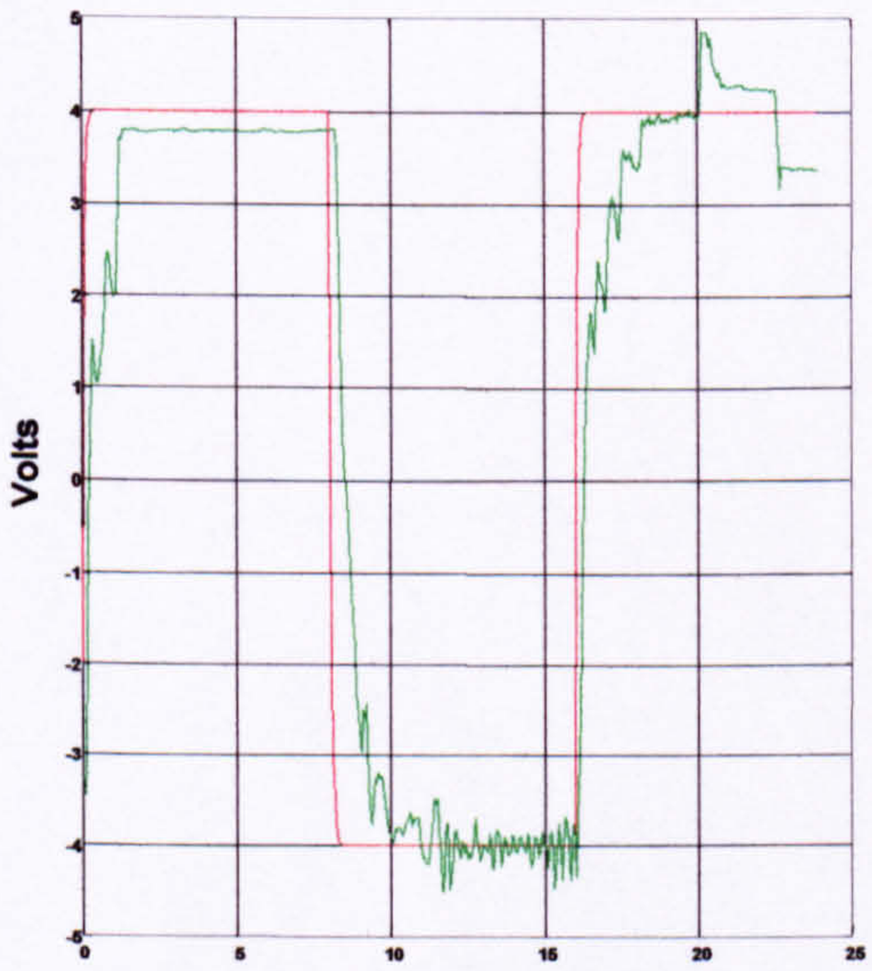

Figure 7.32 Input-Output behaviour of Left leg with volunteer no.2

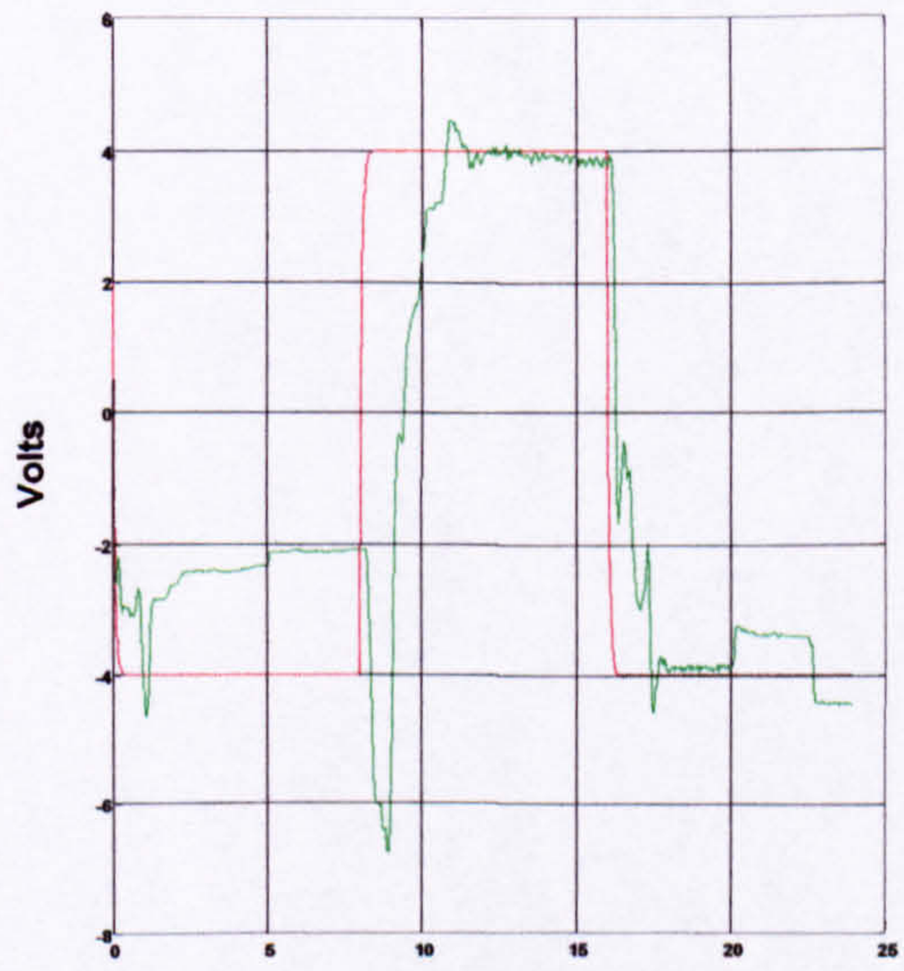

Figure 7.32b Input-Output behaviour of Right leg with volunteer no.2

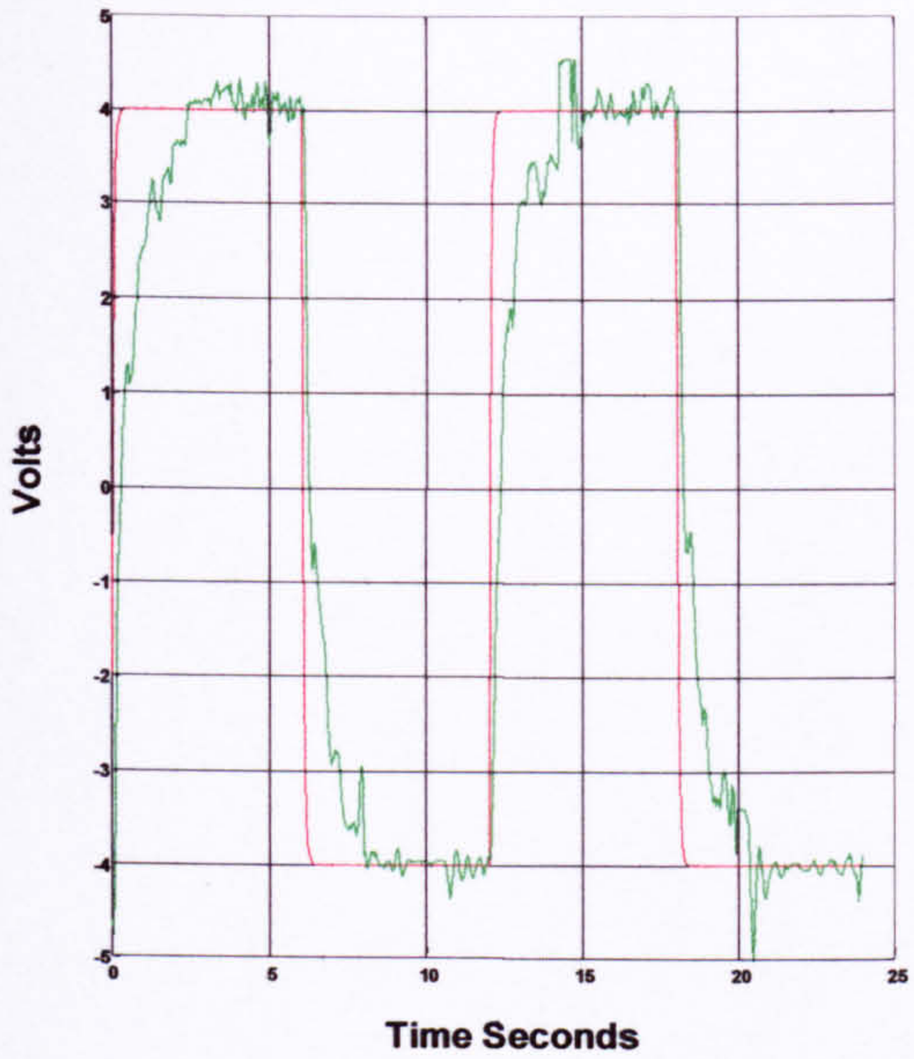

Figure 7.33 Input-Output behaviour of Left leg with volunteer no.2

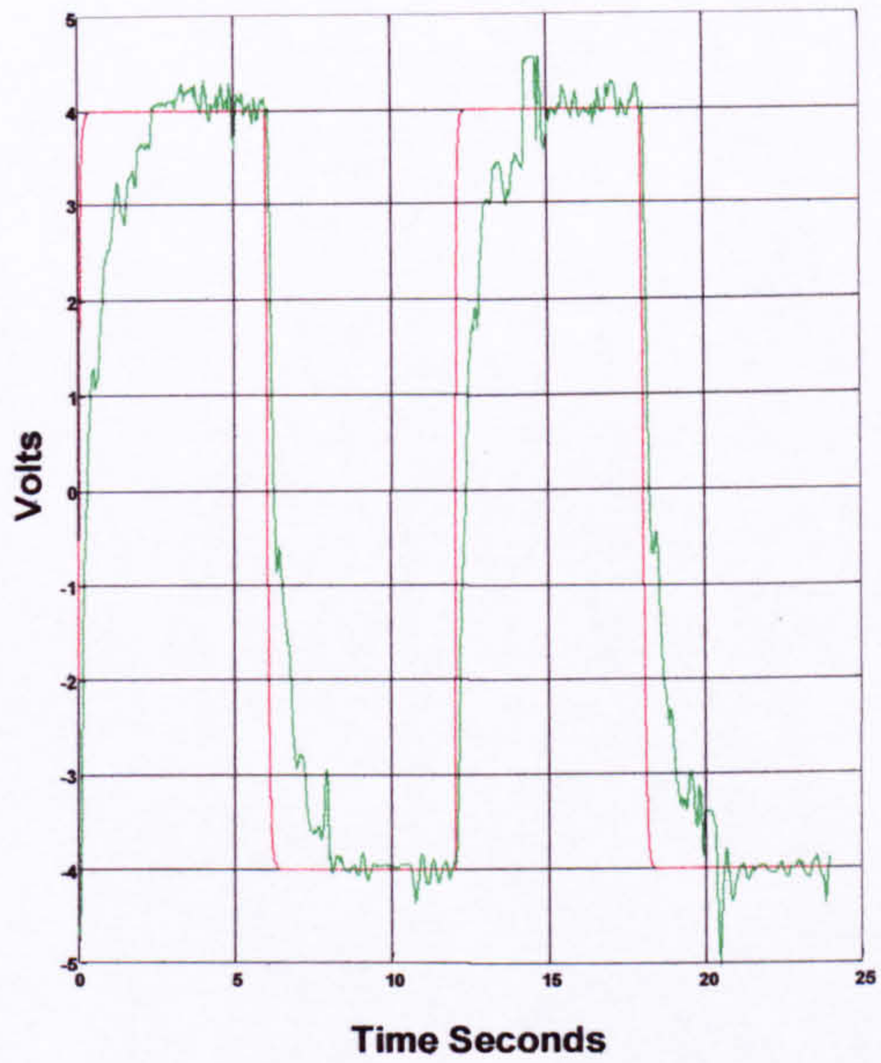

Figure 7.33b Input-Output behaviour of Right leg with volunteer no.2

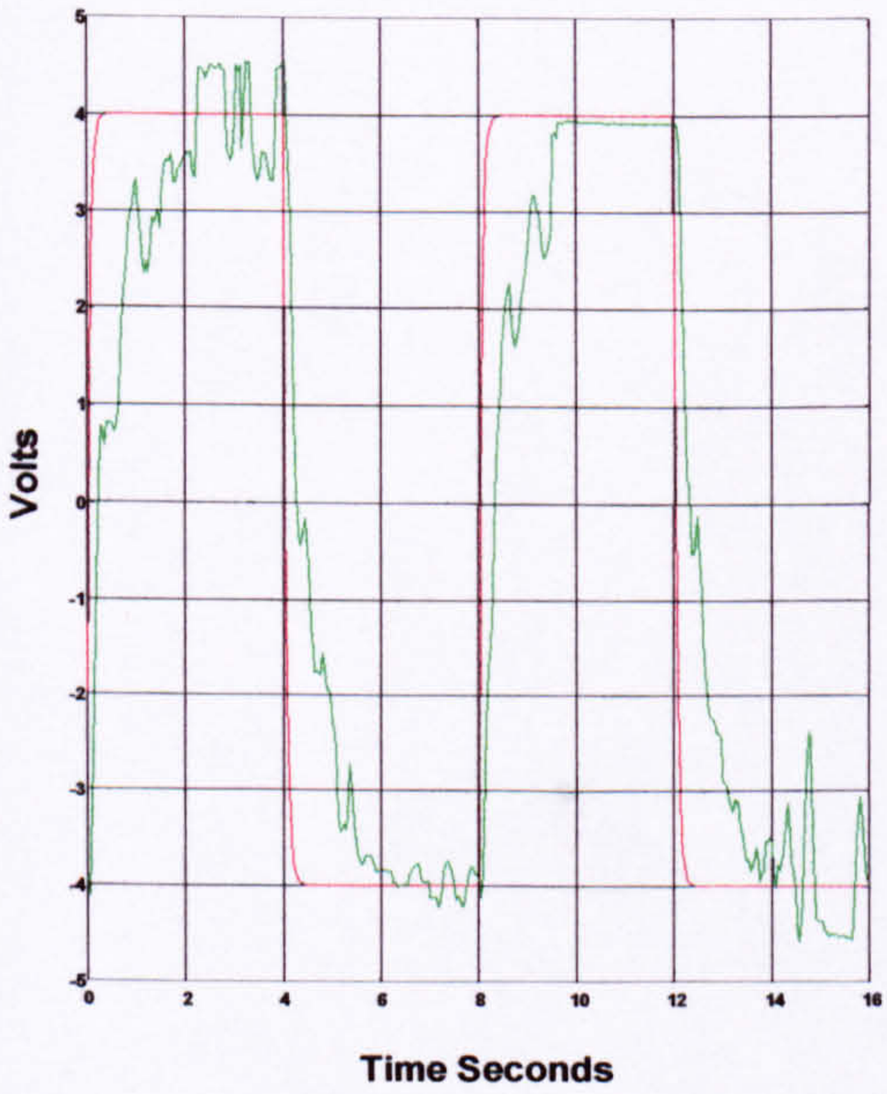

Figure 7.34 Input-Output behaviour of Left leg with volunteer no.2

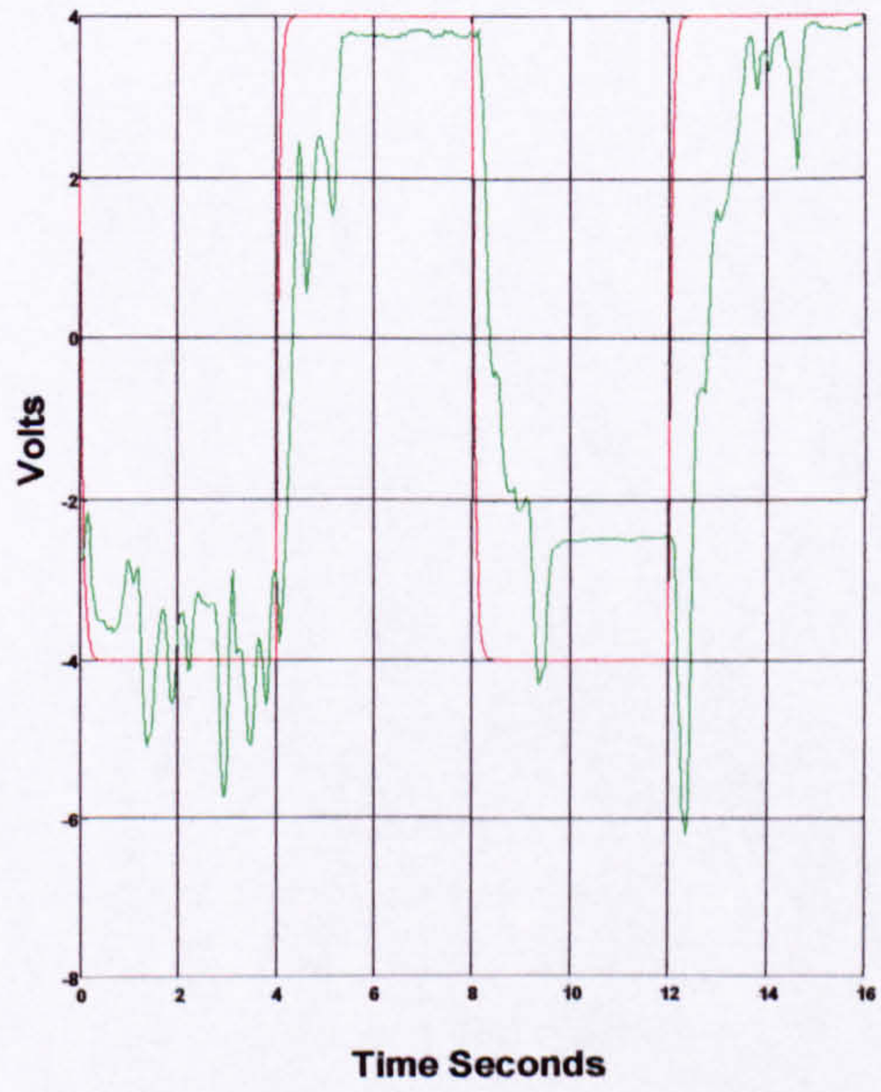

Figure 7.34b Input-Output behaviour of Right leg with volunteer no.2

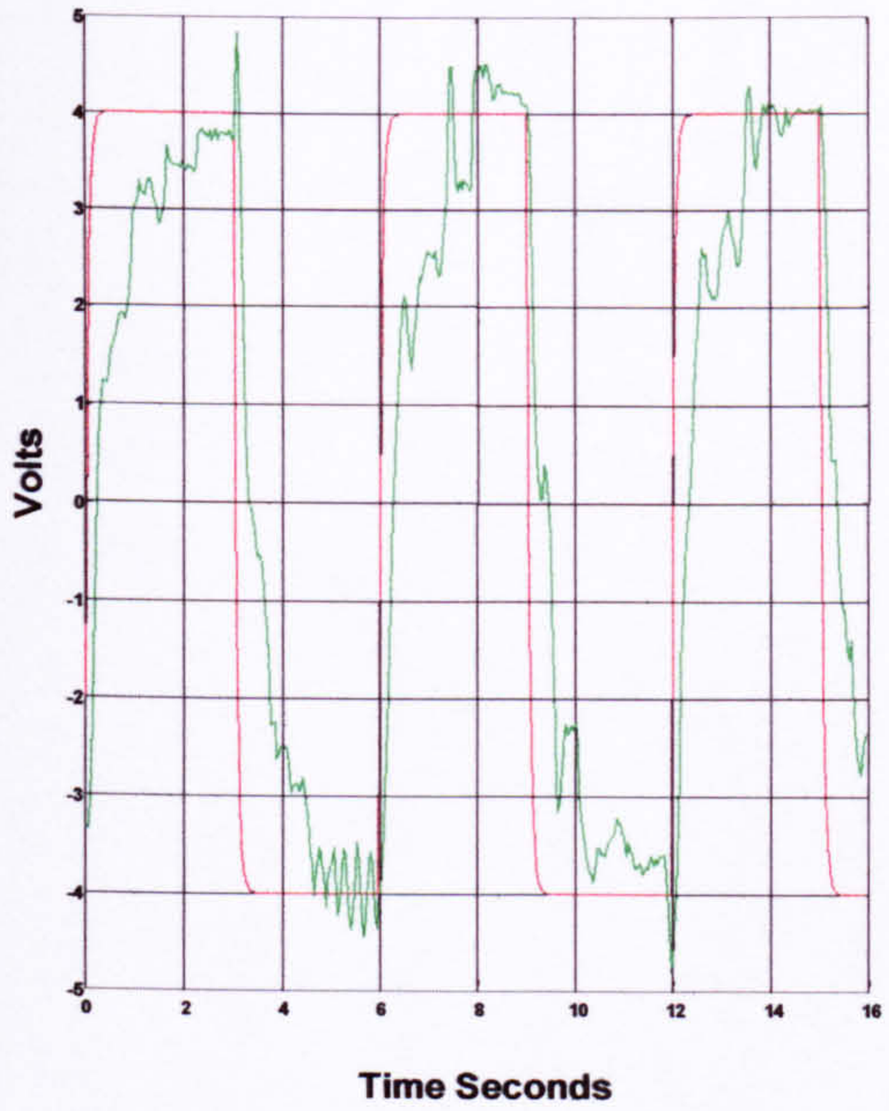

Figure 7.35 Input-Output behaviour of Left leg with volunteer no.2

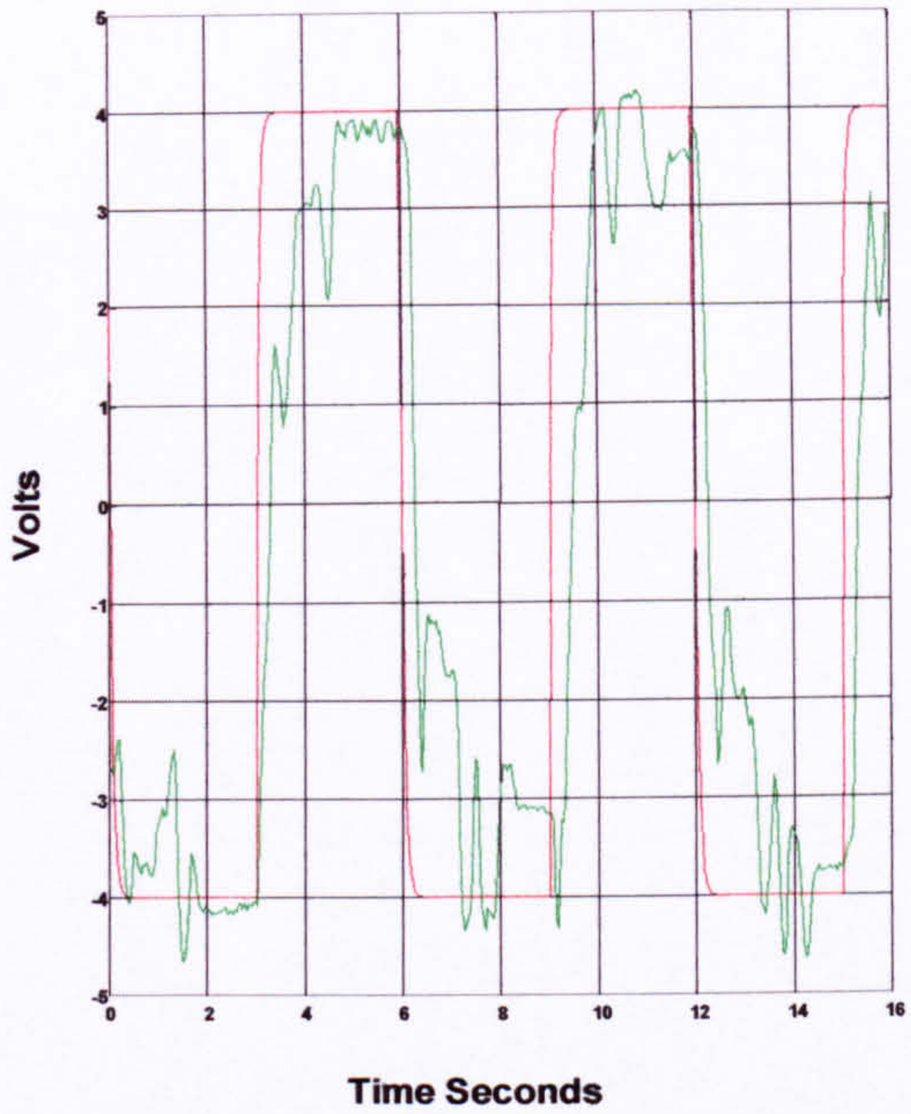

Figure 7.35b Input-Output behaviour of Right leg with volunteer no.2

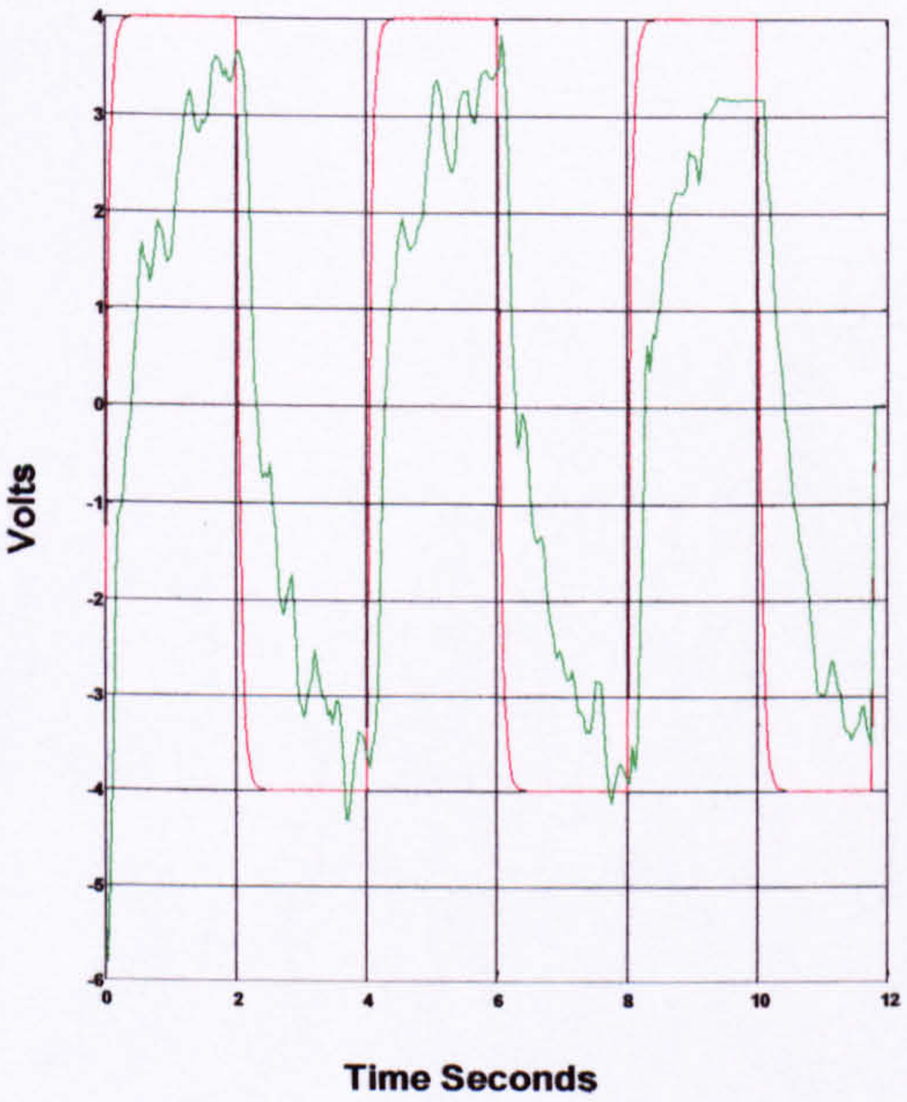

Figure 7.36 Input-Output behaviour of Left leg with volunteer no.2

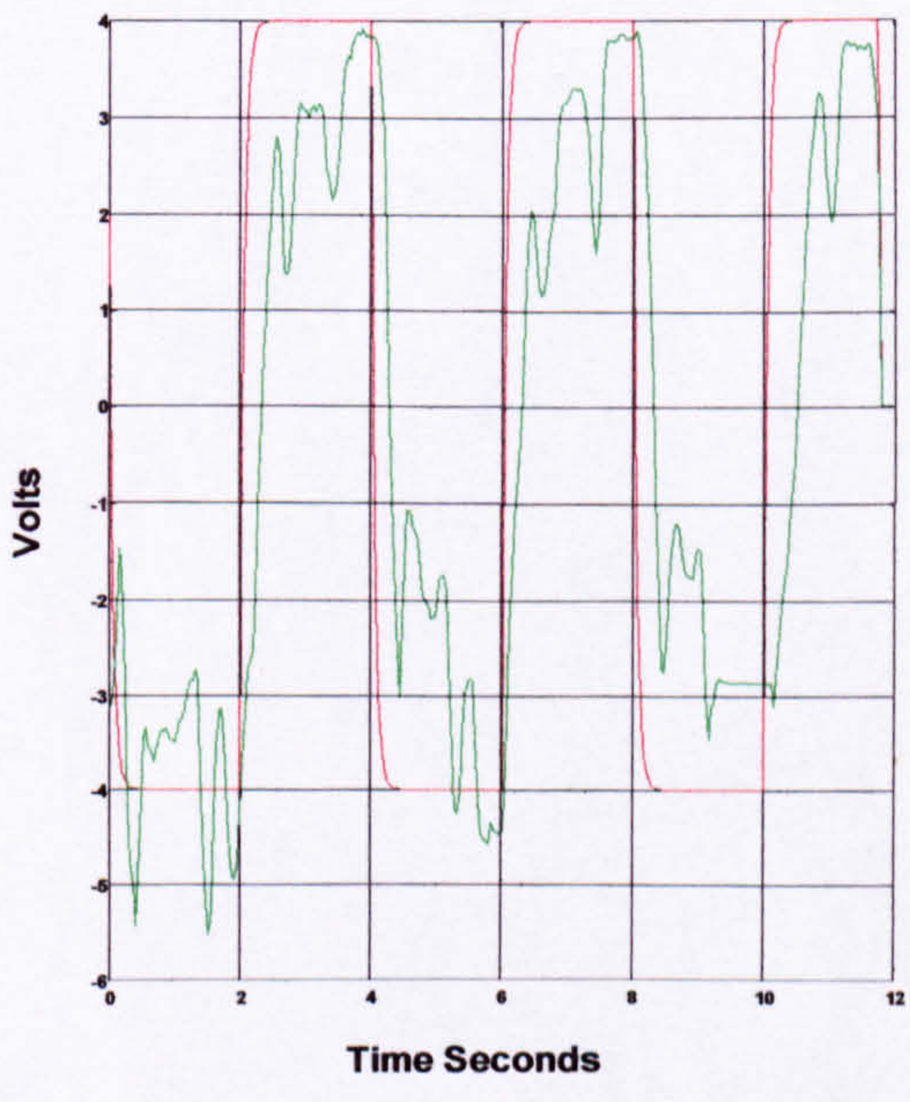

Figure 7.36b Input-Output behaviour of Right leg with volunteer no.2

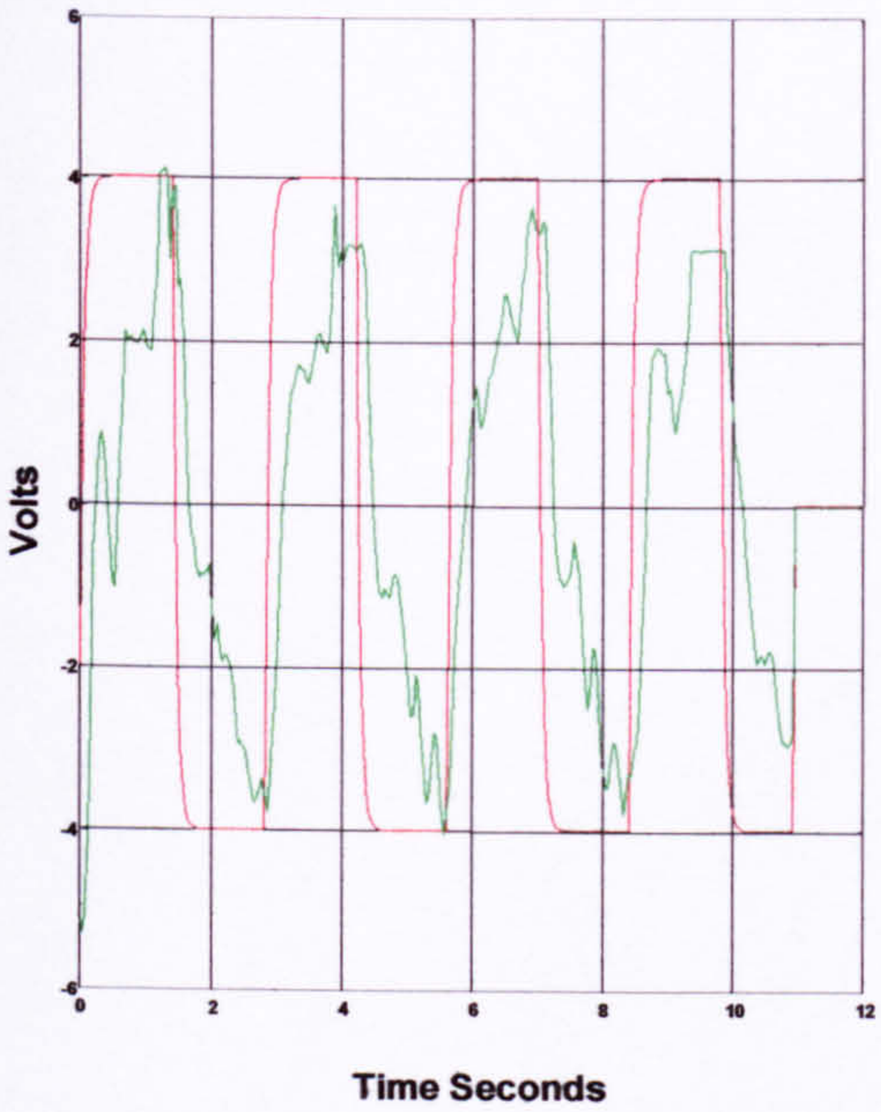

Figure 7.37 Input-Output behaviour of Left leg with volunteer no.2

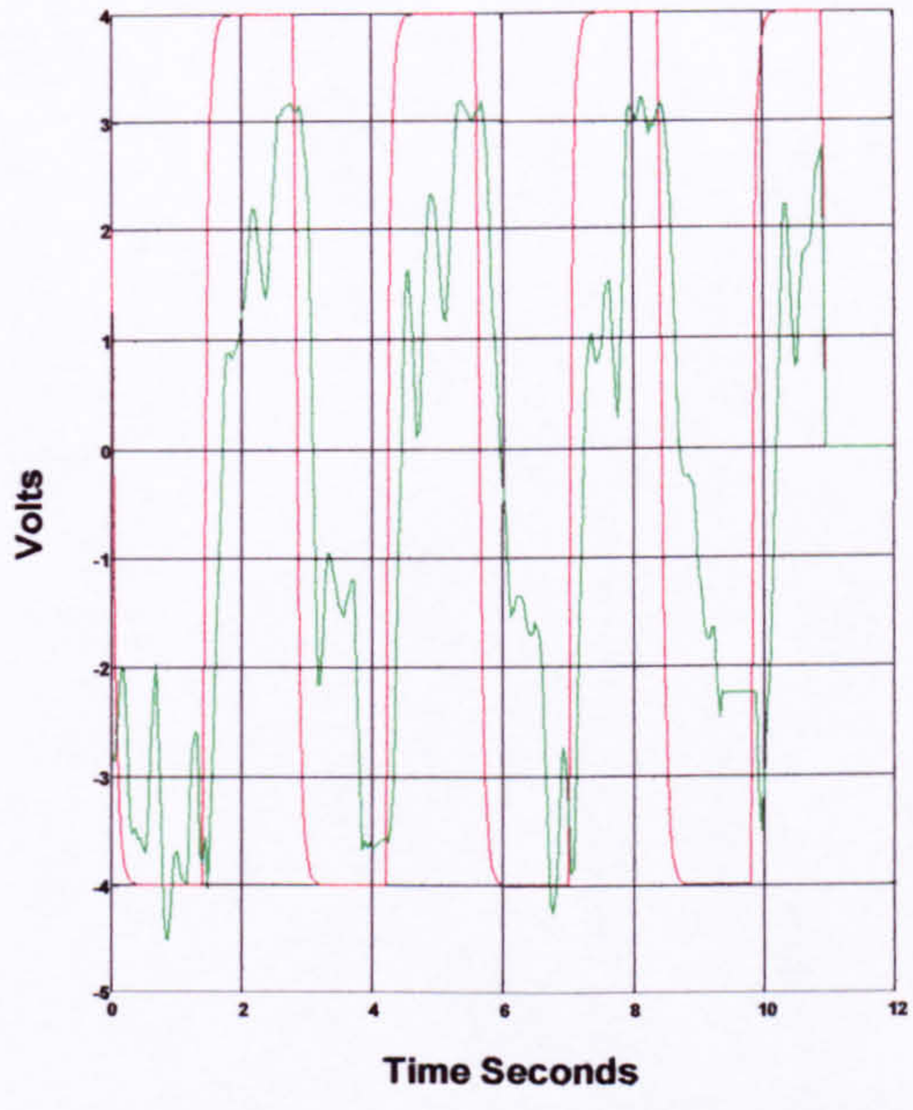

Figure 7.37b Input-Output behaviour of Right leg with volunteer no.2

7.9 Conclusion

It has been mentioned that the problems encountered when testing the Orthosis may be overcome by training. Fighting the motion of the Orthosis comes from the lack of confidence in the Orthosis by the volunteers. It is natural to be apprehensive from something, which you do not have complete control over. However it is worth remembering that some of the problems encountered with the able-bodied volunteers will not actually be the same with paraplegics. Moving the leg when they are required to hold is not an option with paraplegics. What is clear is that a device like the Orthosis would

need a great deal of training before anyone is completely happy with walking with the device.

CHAPTER 8

Conclusion

The reciprocating gait Orthosis and the powered reciprocating gait Orthosis design enables balanced standing and needs much less energy in walking compared with conventional calipers. However these devices are not what you would term as "Plug and Play". These devices are by no means easy to fit and the whole program requires a team effort of specially trained Orthotist, Physiotherapists, specialist's doctors and occupational therapists. The patient may need several weeks of training before they can effectively use these devices [Beckman J., 1987]. The powered Orthosis increases the scope of the R.G.O, The main advantage of the powered Orthosis is that the energy input required to operate the system is much less than that of the conventional R.G.O. It is also considerably faster.

Reciprocal walking for paraplegic patients is now a viable clinical option. At present only mechanical systems are routinely available. As more research is done into powering these systems and as they become more available then the Orthosist will have an extra option when prescribing the systems he thinks is more applicable to different patients.

Research into hybrid and pure F.E.S systems is continuing and as they become available they will inevitably improve and add to the systems available. Whilst such systems may be the ideal solution there are many difficulties to be resolved before all fundamental problems can be overcome. In particular system reliability, energy cost, safe failure mode

for patient, cosmesis of walking and cost are all areas in which pure F.E.S systems can not yet match the mechanical or hybrid approach. Clearly modern technology will have a large role to play in solving these deficiencies. It is unlikely that any one system will provide the ideal solution for every patient and clinicians will need to be able to asses which fundamental approach will suite particular groups of patients. Children, adolescents, young and old patients all present different problems requiring different approaches and subdivisions of needs within these groups will probably occur.

The greatest potential at present seems to be shown by the hybrid approach in which walking is augmented by electrical stimulation. The H.G.O, R.G.O and powered R.G.O. being suitable for this purpose. The F.E.S may be used simply to get the patient onto the standing position with straight knees by stimulating the quadriceps but it could also have an active element in the gait. The use of such hybrid systems improves the walking of those using a walking brace and may extend the use of these braces to those unable to use them at present.

Functional electrical stimulation has not proved beneficial for every paraplegic. It does not work for muscles with damaged secondary motor neurons, or in patients with progressive neuromuscular diseases as an alternative to F.E.S. The purely mechanical systems, require high energy when using them, they are also slow. Therefore the only viable alternative is to add external power to the mechanical system. However introducing external means introducing extra problems. The most important being the issue of control. Pole assignment controllers are used to control the powered Orthosis.

But before a control system is designed and implemented a model for the Orthosis had to be obtained using MATLAB

The ARMAX model structure was used to describe the model initially for power supply, the motor driver unit, EC motor, gearbox and a Tacho as a system. The identification algorithm employing the PC-MATLAB system identification toolbox has successfully identified a model of the system in good agreement with different data. The investigated system was a "nice" simple system to identify, but the success in deriving a model gave us confidence in using the same method with the real system (Orthosis).

When identifying a model of the system many problems were encountered. Initially the sampling time used was 10ms, but because of the mechanical vibrations of the leg when responding to pseudo-random input signals, a model was not successfully derived, not only the parameters were different but even the order and structure of the models was different. The different models derived not only were not good enough to describe the system but inconsistent. Because of the mechanical vibration the non-linear behaviour of the system was captured in the data collected to be used for identification. Matlab was not able to derive a linear model, which could compensate for the non-linear behaviour. When the sampling time was dropped to 40ms we were able to derive a model which accurately described the system and the results were repeatable.

Once a succesful model was derived the next step was to design a controller. The approach taken here is to exploit the non uniqueness of the solutions to the pole

assignment equation. Since the implementation of this method simply requires the knowledge of the model of the system, the approach although presented for the off line design, it could easily be applied to adaptive controllers.

Youlas parameterization is used to parameterize all the high order controllers in terms of minimal order controller and a free polynomial. In this approach the task of finding the optimal controller reduces the optimization with respect to this free polynomial. For computational reasons we have adopted the L_2 norm criterion as a measure for robustness.

The use of high order controllers is a simple but effective method of improving the performance and robustness of pole assignment controllers. The improvement of high order controllers is due to more information about the system being used. While the results show clearly that this type of controller is effective for our system further and future work is still needed. These suggestions include.

1) Self-tuning or adaptive regulators. In this thesis the off line approach was adopted and Youlas parameterization was used to come up with high order controller. It is believed that further improvement may be possible when self-tuning regulators are used. This includes the on line derivation of a model and online implementation of the controller.
2) Energy expenditure. One of the main purposes of adding external power to the Orthosis was to reduce the energy expenditure by the patient and to improve the

speed. A field study would be needed to evaluate the magnitude of these improvements and speeds the Orthosis is capable of.

3) Power Source. This is one of the major problems to be overcome. While in the laboratory the power source is easily available. It is a different case when you are out and about. If batteries are going to be used the then duration of the battery before it needs charging becomes important. If the battery needs charging every 15 minutes say then the whole system will be of no use. The second problem is the size of the power source and where is it going to be placed. It is important for the source to be as light and small as possible.

4) Autonomous, Independent System. The use of a computer to implement the control algorithm may not be a very practical solution. It would be better to use microcontrollers powered from a portable source. That way the system can truly be seen as independent autonomous system.

5) Cosmesis. Research and trials are continuing on new designs to improve the cosmesis, function and greater simplicity of manufacture and fitting of the reciprocating gait Orthosis.

APPENDIX A

C PROGRAM USED FOR DATA STORAGE AND COLLECTION

```
/*
 * load random data from PC-MATLAB
 * and convert these data into analog signal
 * to create random signal in order to drive
 * DC motor and save the data from ADC into
 * PC-MATLAB format
 */


#include "stdlib.h"
#include "stdio.h"
#include "dos.h"
#include "math.h"
#include "conio.h"

/*****************************************************************/
/*****************  D/A conversion Function **********************/
/*****************************************************************/

void digital_to_analog2(output_voltage)

float output_voltage;

{
int temp1;
int base_address;
int da_msb;
int da_lsb;

base_address = 0x700;
temp1 = (output_voltage * 2048.0/-10.0) + 2048.0;
if (temp1>4095) temp1 = 4095;
if (temp1<0) temp1 = 0;

outp(base_address+0x1c,0x20);   /*set DACINV to 1 in ADCCFG*/

da_msb = temp1>>4;
da_lsb = (temp1<<4)&0xf0;

/*set the address for the output so that the output from the
*/
/*computer to the motor is using DAC1 at the 50 ways D connectors.
*/

outp(base_address+0x11,da_msb);
outp(base_address+0x10,da_lsb);

outp(base_address+0x1c,0x00); /*set DACINV to zero in ADCCFG*/
}

/*Digital_to_analog1*/
```

```
void digital_to_analog1(output_voltage)

float output_voltage;

{
int temp1;
int base_address;
int da_msb;
int da_lsb;

base_address = 0x700;
temp1 = (output_voltage * 2048.0/-10.0) + 2048.0;
if (temp1>4095) temp1 = 4095;
if (temp1<0) temp1 = 0;

outp(base_address+0x1c,0x20);   /*set DACINV to 1 in ADCCFG*/

da_msb = temp1>>4;
da_lsb = (temp1<<4)&0xf0;

/*set the address for the output so that the output from the
*/
/*computer to the motor is using DAC0 at the 50 ways D connectors.
*/
outp(base_address+0xd,da_msb);
outp(base_address+0xc,da_lsb);

outp(base_address+0x1c,0x00); /*set DACINV to zero in ADCCFG*/
}

/*************************************************************/
/******************** A/D conversion Function ****************/
/*************************************************************/

float analog_to_digital(channel)
int channel;
{
 int base_address;
 float ad_sample;
 float digital_output;
 int wait;

base_address = 0x700;

// outp(0x700+0x03,0x92);              /*initialize PC-30GA board */
// outp(0x700+0x02,0x02);              /*set ADCCR for software
strobes*/
// wait=inp(0x701);
// wait=inp(0x700);
// for(wait=1;wait<320;wait++);
// wait=inp(0x701);
```

```
// wait=inp(0x700);

outp(base_address+2,(channel<<4)+2);
outp(base_address+2,(channel<<4)+3);
outp(base_address+2,(channel<<4)+2);
/*setting a delay time before starting any conversion          */
for(wait=1;wait<320;wait++);
/*ad_sample is 12 bit data, 8 bit for each address, so we use  */
/*2 address.*/
ad_sample=((inp(base_address+1)&0xf)<<8)+inp(base_address);

digital_output =10.0*((float)ad_sample - 2048.0)/2048.0;

return(digital_output);
}

/*****************************************************************/
/********************* MAIN PROGRAM ******************************/
/*****************************************************************/

#define MAX_DATA 500

main()
{FILE  *fz;
 int i,m,count,count2,dir,tempd,da_msb2,da_lsb2;
 long delay;
 float
y[MAX_DATA],v[MAX_DATA],ref[MAX_DATA],U[MAX_DATA],error,Vref,dVref
,d1,d2;
 char name[20];
 float uo,test,u1=0,u2=0,u0=0,ref1;
 float pi=3.1415,xref=0,dx=pi/30.0;/*generates sine waves,sq waves
at diff fq*/

/* outp(0x700+0x03,0x92);
 outp(0x700+0x07,0x34);
 outp(0x700+0x07,0x74);
 outp(0x700+0x07,0xb6);
 outp(0x700+0x02,0x02);
for(count=1;count<30000;count++);
d1=inp(0x701);
d1=inp(0x700);  */

 outp(0x700+0x03,0x92);              /*initialize PC-30GA board */
 outp(0x700+0x02,0x02);              /*set ADCCR for software
strobes*/
 outp(0x700+0x1c,0x00);              /*clear ADCCFG */
 outp(0x700+0x1d,0xff);              /*set D/A -10V to +10 V */
 outp(0x700+0x18,0x00);              /*set gains of all A/D channels
to 1*/
```

```
 outp(0x700+0x19,0x00);                  /*set gains of all A/D channels
to 1*/
 outp(0x700+0x1a,0x00);                  /*set gains of all A/D channels
to 1*/
 outp(0x700+0x1b,0x00);                  /*set gains of all A/D channels
to 1*/
 outp(0x700+0x0b,0x80);                  /*initialize ppiports a,b,c,as
outputs*/
 outp(0x700+0x08,0x00);                  /*set to zero port a*/
 outp(0x700+0x09,0x00);                  /*set to zero port b*/
 outp(0x700+0x0a,0x00);                  /*set to zero port c*/
/* Read A/D high and low bytes to clear A/D
alternative: use analog_to_digital function before main loop*/
d1=inp(0x701);
d1=inp(0x700);
for(count=1;count<320;count++);
d1=inp(0x701);
d1=inp(0x700);
digital_to_analog1(0.0);
digital_to_analog2(0.0);
for(count=1;count<320;count++){
  d1=analog_to_digital(1);
  d1=analog_to_digital(3);
}
 for (i=0;i<MAX_DATA;i++){
     y[i]=0.0;
     v[i]=0.0;
     U[i]=0.0;
     ref[i]=0.0;
     }
test=5;
uo=0;
count=0;
i=0;
dir=-1;
count2=0;
Vref=-6;
dVref=7.0;
d1=0;
d2=0;

   //  y[i]=analog_to_digital(1);
 do{
   //  y[i]=analog_to_digital(1);
     //d1=y[i];
     v[i]=analog_to_digital(2);



   ref1=2*sin(xref);                     /*3 generates a sin wave*/
//     if(ref1>=0.0) ref1=2.0;
```

```
    //    if(ref1<0.0) ref1=-2.0; /*generates an square wave*/
      xref=xref+dx;
       if(xref>2*pi) xref=xref-2*pi;    /*no overflow*/


                  /*CONTROLLER STARTS HERE*/
       error=(Vref+dVref)-y[i];          /*Vref=reference
voltage,y[i]=reading from kpot*/
//    u1=4*error;   */       /*1.2 is the proportional gain
desined in my controller*/
 //    u1=0.0*u1+1.0*dVref;
//     u1=ref1;
       u1=dVref;
 //    count2=count2+1;
   //       if(count2>0){
      //        count2=0;
         if(rand()>16384) dVref=-dVref;
      // }
//printf("%4f %4f %4f\n",d1,v[i],u1);
/*         if(rand()>16384) u1=5;*/
       u0=u1;
       U[i]=u0;
        //  ref[i]=ref1;
       // test=-test;  /* in order to check the sampling time*/
        uo=u0;
       if(uo>10) uo=10;
       if(uo<-10) uo=-10;
       digital_to_analog1(10.0);

       //  digital_to_analog2(0.0);
/*     if(count2>150)
       {

        dVref=-dVref;
        count2=0;
        }*/
//     if(y[i]<-5.0) dVref=0.0;

//    if(y[i]>5.0)  dVref=0.0;
      for (count=0;count<25000;count++){
      /* three loops of 25000 14500 14500 for 10 ms */
      //three loops of 4200 100 100 for 1 ms;
      //three loops of 950 100 100 for 1/2ms;
      //no count 0.33ms;
      // 8 loops of 30000 for 40ms
}
 for (count=0;count<30000;count++){
 }
 for (count=0;count<30000;count++)
 {
```

```
   }
for(count=0;count<30000;count++)
{
}
      for(count=0;count<30000;count++)
{
}
 for(count=0;count<30000;count++)
{
}
          for(count=0;count<30000;count++)
        {
        }


                  for(count=0;count<30000;count++)
        {
        }
i++;
     }
     while( (i<MAX_DATA) && (kbhit()==0));

   digital_to_analog1(0.0);
   digital_to_analog2(0.0);

   if((fz=fopen("motidnt2.mat","w"))==NULL){
      printf("cannot open file\n");
      exit(1);
      }
   for(i=0;i<MAX_DATA;i++) fprintf(fz," %.4f %.4f \n",U[i],v[i]);
   fclose(fz);

}
```

```
/*
 * load random data from PC-MATLAB
 * and convert these data into analog signal
 * to create random signal in order to drive
 * DC motor and save the data from ADC into
 * PC-MATLAB format
 */


#include "stdlib.h"
#include "stdio.h"
#include "dos.h"
#include "math.h"
#include "conio.h"
#include "loadmat.c"
#define MAX_DATA 1000
#define GLmax 35
#define FLmax 35
#define GRmax 35
#define FRmax 35
#define modelfile "nq4p5.mat"
#define modelfile2 "nq4p5.mat"


/*****************************************************************/
/*****************  D/A conversion Function **********************/
/*****************************************************************/

void digital_to_analog2(output_voltage)

float output_voltage;

{
int temp1;
int base_address;
int da_msb;
int da_lsb;

base_address = 0x700;
temp1 = (output_voltage * 2048.0/-10.0) + 2048.0;
if (temp1>4095) temp1 = 4095;
if (temp1<0) temp1 = 0;

outp(base_address+0x1c,0x20);   /*set DACINV to 1 in ADCCFG*/

da_msb = temp1>>4;
da_lsb = (temp1<<4)&0xf0;

/*set the address for the output so that the output from the
*/
```

```
/*computer to the motor is using DAC1 at the 50 ways D connectors.
*/

outp(base_address+0x11,da_msb);
outp(base_address+0x10,da_lsb);

outp(base_address+0x1c,0x00); /*set DACINV to zero in ADCCFG*/
}

/*Digital_to_analog1*/
void digital_to_analog1(output_voltage)

float output_voltage;

{
int temp1;
int base_address;
int da_msb;
int da_lsb;

base_address = 0x700;
temp1 = (output_voltage * 2048.0/-10.0) + 2048.0;
if (temp1>4095) temp1 = 4095;
if (temp1<0) temp1 = 0;

outp(base_address+0x1c,0x20);   /*set DACINV to 1 in ADCCFG*/

da_msb = temp1>>4;
da_lsb = (temp1<<4)&0xf0;

/*set the address for the output so that the output from the
*/
/*computer to the motor is using DAC0 at the 50 ways D connectors.
*/
outp(base_address+0xd,da_msb);
outp(base_address+0xc,da_lsb);

outp(base_address+0x1c,0x00); /*set DACINV to zero in ADCCFG*/
}

/*****************************************************************/
/******************** A/D conversion Function ********************/
/*****************************************************************/

float analog_to_digital(channel)
int channel;
{
 int base_address;
 float ad_sample;
 float digital_output;
 int wait;
```

```
base_address = 0x700;

// outp(0x700+0x03,0x92);                    /*initialize PC-30GA board */
// outp(0x700+0x02,0x02);                    /*set ADCCR for software
strobes*/
// wait=inp(0x701);
// wait=inp(0x700);
// for(wait=1;wait<320;wait++);
// wait=inp(0x701);
// wait=inp(0x700);
```

```
outp(base_address+2,(channel<<4)+2);
outp(base_address+2,(channel<<4)+3);
outp(base_address+2,(channel<<4)+2);
/*setting a delay time before starting any conversion          */
for(wait=1;wait<320;wait++);
/*ad_sample is 12 bit data, 8 bit for each address, so we use  */
/*2 address.*/

ad_sample=((inp(base_address+1)&0xf)<<8)+inp(base_address);

digital_output =10.0*((float)ad_sample - 2048.0)/2048.0;

return(digital_output);
}
```

```
/*****************************************************************/
/********************* MAIN PROGRAM ******************************/
/*****************************************************************/



void main()
{
FILE  *fz,*fp1;
 int i,count,count2,dir,tempd,da_msb2,da_lsb2;
 float error,Vref,dVref,v1,v2,d1,d2;
 char name[20];
 float
null,uL,uR,test,u1=0.00,refl,refr,ref1=0.0,ur,u2=0.00,u3=0.00;
 float GL[GLmax],FL[FLmax],wL[FLmax],yl[GLmax],eL[GLmax];
 float GR[GRmax],FR[FRmax],wR[FRmax],yr[GRmax],eR[GRmax];
 float fdbckl=0,fdfwdl=0,hl=0;
 float fdbckr=0,fdfwdr=0,hr=0;
 float pL[MAX_DATA],pr[MAX_DATA],vL[MAX_DATA],vR[MAX_DATA];
 float UL[MAX_DATA],UR[MAX_DATA],REFR[MAX_DATA],REFL[MAX_DATA];
 int type,mrows,ncols,imagf,t;
 double *xi,*xr;
```

```
 float pi=3.1415,xref=0,dx=pi/200.0;/*generates sine waves,sq
waves at diff fq*/

 null=0;
 count=0;
 i=0;
 count2=0;
 dVref=4;
 d1=0;
 d2=0;
 test=5;

/* ADC data */

/*initialize arrays*/

for(i=0;i<FLmax;i++)
 {
   FL[i]=0;
   wL[i]=0;
 }
 for(i=0;i<FRmax;i++)
 {
   FR[i]=0;
   wR[i]=0;
   }

for(i=0;i<GLmax;i++)
 {
   GL[i]=0;
   yl[i]=0;
   eL[i]=0;
 }
for(i=0;i<GRmax;i++)
{
  GR[i]=0;
  yr[i]=0;
  eR[i]=0;
  }
    for(i=0;i<MAX DATA;i++){  /*initialitation to zero
(security)*/

          pL[i]=0.0;
          pr[i]=0.0;
          vL[i]=0.0;
          UL[i]=0.0;
          UR[i]=0.0;
          REFR[i]=0.0;
          REFL[i]=0.0;
// printf("%.4f %.4f %.4f %.4f %.4f
%.4f\n",REFL[i],pL[i],UL[i],REFR[i],pr[i],UR[i]);
```

```
    }

clrscr();
printf(" \n\n\n\n");
printf("              * * * * * * * * * * * * * * * * * * * * * * * * * * * *
* *\n");
printf("              *
*\n");
printf("              *                ORTHOSIS DRIVE SYSTEM
*\n");
printf("              *   CHECK THAT COMPUTER IS SET TO TURBO MODE
*\n");
printf("              *  AND OUTPUT OF D/A CONVERTER IS SET TO ZERO
*\n");
printf("              *                PRESS ANY KEY TO STOP
*\n");
printf("              *
*\n");
printf("              *                 ARAFAT A.ZAIDAN
*\n");
printf("              *
*\n");
printf("              *   Supervisor: Dr G. A. Medrano-Cerda
*\n");
printf("              *
*\n");
printf("              *                UNIVERSITY OF SALFORD
*\n");
printf("              *                   JULY/1997
*\n");
printf("              *
*\n");
printf("              * * * * * * * * * * * * * * * * * * * * * * * * * * * *
* *\n");

fp1=fopen(modelfile,"rb");
if (loadmat(fp1, &type, name, &mrows, &ncols, &imagf, &xr, &xi))
            {
                printf("\nREAD ERROR\n");
            }
      free(xr);
      if(imagf)
            {
                free(xi);
            }  /* printf("%d %d %d \n",typel,mrowsl,ncolsl);*/
      for(i=0;i<ncols;i++)
            {
                FL[i]=*(xr+i);
/*              printf("\n%f\n",FL[i]);*/
                }
if (loadmat(fp1, &type, name, &mrows, &ncols, &imagf, &xr, &xi))
```

```
        {
                printf("\nREAD ERROR\n");
        }

free(xr);
if(imagf)
        {
                free(xi);
        }
        /*printf("%d %d %d \n",type,mrows,ncols);*/
        for(i=0;i<ncols;i++)
                {
                        GL[i]=*(xr+i);
/*                      printf("\n%f\n",GL[i]);*/
                }
fclose(fp1);
 fp1=fopen(modelfile2,"rb");
if (loadmat(fp1, &type, name, &mrows, &ncols, &imagf, &xr, &xi))
        {
                printf("\nREAD ERROR\n");
        }
      free(xr);
      if(imagf)
                {
                        free(xi);
                }  /* printf("%d %d %d \n",typel,mrowsl,ncolsl);*/
      for(i=0;i<ncols;i++)
                {
                        FR[i]=*(xr+i);
/*                      printf("\n%f\n",FR[i]);*/
                        }
if (loadmat(fp1, &type, name, &mrows, &ncols, &imagf, &xr, &xi))
                {
                        printf("\nREAD ERROR\n");
                }

      free(xr);
      if(imagf)
                {
                        free(xi);
                }
                /*printf("%d %d %d \n",type,mrows,ncols);*/
        for(i=0;i<ncols;i++)
                {
                        GR[i]=*(xr+i);
/*                      printf("\n%f\n",GR[i]);*/
                }
fclose(fp1);

hl=0;
hr=0;
```

```
for(i=0;i<GLmax;i++) hl=hl+GL[i];
for(i=0;i<GRmax;i++) hr=hr+GR[i];
for(i=0;i<FLmax;i++) printf("\%f\n",FL[i]);
for(i=0;i<FRmax;i++) printf("\%f\n",FR[i]);
for(i=0;i<GLmax;i++) printf("\%f\n",GL[i]);
for(i=0;i<GRmax;i++) printf("\%f\n",GR[i]);
printf("%f\n",hl);
printf("%f\n",hr);

 outp(0x700+0x03,0x92);                /*initialize PC-30GA board */
 outp(0x700+0x02,0x02);                /*set ADCCR for software
strobes*/
 outp(0x700+0x1c,0x00);                /*clear ADCCFG */
 outp(0x700+0x1d,0xff);                /*set D/A -10V to +10 V */
 outp(0x700+0x18,0x00);                /*set gains of all A/D channels
to 1*/
 outp(0x700+0x19,0x00);                /*set gains of all A/D channels
to 1*/
 outp(0x700+0x1a,0x00);                /*set gains of all A/D channels
to 1*/
 outp(0x700+0x1b,0x00);                /*set gains of all A/D channels
to 1*/
 outp(0x700+0x0b,0x80);                /*initialize ppiports a,b,c,as
outputs*/
 outp(0x700+0x08,0x00);                /*set to zero port a*/
 outp(0x700+0x09,0x00);                /*set to zero port b*/
 outp(0x700+0x0a,0x00);                /*set to zero port c*/
/* Read A/D high and low bytes to clear A/D
alternati#ve: use analog_to_digital function before main loop*/
d1=inp(0x701);
d1=inp(0x700);
for(count=1;count<320;count++);
d1=inp(0x701);
d1=inp(0x700);
digital_to_analog1(0.0);
digital_to_analog2(0.0);
for(count=1;count<320;count++){

       digital_to_analog1(null);
       digital_to_analog2(null);
       d1=analog_to_digital(1); /*reading speed from left leg*/
       d2=analog_to_digital(2); /*reading speed from right leg*/
                          }
    for(i=0;i<GLmax;i++) yl[i]=d1; /*to assign the same value at
all
                          the initial conditions, to have the same
value in t=0 and all the previous values*/
    for(i=0;i<GRmax;i++) yr[i]=d2;
    fdbck1=0;
    for(i=1;i<GLmax;i++)
    {
```

```
 fdbckl=fdbckl+GL[i]*yl[i];
}
fdbckr=0;
for(i=1;i<GRmax;i++)
{
fdbckr=fdbckr+GR[i]*yr[i];
}
  count=0;
 // refl=4.0;
      /******************Loop starts here ******************/
       do{
       d1=analog_to_digital(1);/*reading position of left leg*/
       d2=analog_to_digital(2);/*reading position of right leg*/
     //  v1=analog_to_digital(3);/*reading(nothing for now) from
left leg*/
      // v2=analog_to_digital(4);/*reading(nothing for now) from
right leg*/
       yl[0]=d1;
       yr[0]=d2;

       /*PUT REFERENCE SIGNAL FOR LEFT LEG HERE*/

    ref1=2*sin(xref);                  /*generates a sin wave*/
    if(ref1>0) ref1=4;
     if(ref1<=0) ref1=-4;             /*generates an square wave*/
xref=xref+dx;
     if(xref>2*pi) xref=xref-2*pi;     /*no overflow*/

// if(count2<50)  ref1=2;
// if(count2>=50) ref1=-2;
// if(count2>=100) count2=0;
 u2=0.5*u2+0.5*ref1;
 ref1=u2;
//
 count2++;
// printf("%d %.4f\n",count2,u2);

 /*PUT REFERENCE SIGNAL FO RIGHT LEG HERE*/

 //      refr=2+3.0*sin(xref);
/*      if(refr>2) refr=5;
     if(refr>2) refr=3;     */

          refr=-u2;
  //THE REFERENCE FOR RIGHT LEG WILL BE SAME AS LEFT LEG BUT IN
OPPOSIT DIRECTION


     /* PUT CONTROLLER FOR LEFT LEG HERE */
```

```
/* Part on the forward and part on the feedback */
/*************************************************/
 eL[0]=(hl*refl-GL[0]*yl[0]-fdbckl);
   wL[0]=eL[0]-fdfwdl;
   u1=u1+wL[0]; /*effect of the integrator*/
   if(u1>10) u1=10;
   if(u1<-10) u1=-10;
/*************************************************/

     /* PUT CONTROLLER FOR RIGHT LEG HERE*/

/* part on the forward and part on the feedback */
/*************************************************/
eR[0]=(hr*refr-GR[0]*yr[0]-fdbckr);
  wR[0]=eR[0]-fdfwdr;
  u3=u3+wR[0];
  if(u3>10) u3=10;
  if(u3<-10) u3=-10;
/*************************************************/

      uL=u1;
      UL[count]=uL;
      //   if(uL>0) outp(0x700+0x08,0x01); /*sets A0(port a) high
for left leg clockwise rotation */
     // if(uL<0)
     // {
       //   outp(0x700+0x08,0x00);  /*sets A0 low for left leg
anti-clockwise */
       //  uL=-uL;   /*no negative voltage*/
      //   }
      uR=u3;
      UR[count]=uR;
     // if(uR>0) outp(0x700+0x09,0x01);  /*sets B0 high for right
leg clockwise rotation*/
       //  if(uR<0)
      //   {
     //    outp(0x700+0x09,0x00); /*sets B0(port b) low for right
leg anti-clockwise*/
       //  uR=-uR;
     //     }              /*there is no negative voltage used in
this case only 0-10*/

       //    uL=u1/.92;
       if(uL>10) uL=10;
     //  test=-test;

       digital_to_analog1(uL);/*sends control signal ul to left
leg using output DA1*/

       //   uR=u2/.92;
       if(uR>10) uR=10;
```

```
        digital_to_analog2(uR);/*sends control signal uR to right
leg using output DA2*/

          // printf("%d %.4f\n",uL,uR);
       // if(count2>100)
      //   {
        //     dVref=-dVref;
       //      count2=0;
       //      }
        //     count2=count2+1;

/*move arrays*/
 for(i=FLmax-1;i>0;i--)
          {
               wL[i]=wL[i-1];
          }
 for(i=FRmax-1;i>0;i--)
          {
               wR[i]=wR[i-1];
          }
  for(i=GLmax-1;i>0;i--)
          {
               yl[i]=yl[i-1];
               eL[i]=eL[i-1];
          }
        for(i=GRmax-1;i>0;i--)
          {
               yr[i]=yr[i-1];
               eR[i]=eR[i-1];
          }
/* Part on the forward and part on the feedback for left leg */
/*************************************************************/
      fdbckl=0;
      for(i=1;i<GLmax;i++)
          {
               fdbckl=fdbckl+yl[i]*GL[i];
          }
      fdfwdl=0;
      for(i=1;i<FLmax;i++)
          {
               fdfwdl=fdfwdl+FL[i]*wL[i];
          }
/*************************************************************/

/*part on the forward and part on the feedback for right leg*/
      fdbckr=0;
      for(i=1;i<GRmax;i++)
          {
               fdbckr=fdbckr+yr[i]*GR[i];
          }
```

```
      fdfwdr=0;
      for(i=1;i<FRmax;i++)
            {
                  fdfwdr=fdfwdr+FR[i]*wR[i];
            }
/*************************************************************/
       for(i=0;i<31000;i++)
       {
       /* 10 ms sampling three loops 31000 */
       } /*sampling time*/
       for(i=0;i<31000;i++)
       {
       } /*sampling time*/
       for(i=0;i<31000;i++)
       {
       } /*sampling time*/
        for(i=0;i<31000;i++)
       {
       /* 10 ms sampling three loops 31000 */
       } /*sampling time*/
       for(i=0;i<31000;i++)
       {
       } /*sampling time*/
       for(i=0;i<31000;i++)
       {
       } /*sampling time*/
        for(i=0;i<25000;i++)
       {
       } /*sampling time*/
       for(i=0;i<25000;i++)
       {
       } /*sampling time*/
        for(i=0;i<25000;i++)
       {
       } /*sampling time*/



REFL[count]=refl;
REFR[count]=refr;
pL[count]=d1;
pr[count]=d2;
vL[count]=v1;
vR[count]=v2;

/*  printf("%4f %4f %4f\n",wL[0],yl[0],refl);*/

count=count+1;
}
while( (count<MAX_DATA) && (kbhit()==0));
```

```
  /*****************************************************************/
  /*                          END                                  */
  /*****************************************************************/

  digital_to_analog1(null);
  digital_to_analog2(null);
  outp(0x711,0x80);
  outp(0x710,0x00);
  outp(0x700+0x08,0x00);              /*set to zero port a*/
/*   printf("%4f %4f %d\n",d1,uo,count); */

if((fz=fopen("unl2.mat","w"))==NULL){
      printf("cannot open file\n");
      exit(1);
      }
  for(i=0;i<MAX_DATA;i++) fprintf(fz,"%.4f %.4f %.4f %.4f %.4f
%.4f\n",REFL[i],pL[i],UL[i],REFR[i],pr[i],UR[i]);
  fclose(fz);

}
```

APPENDIX B

L_2 NORM FOR POLYNOMIALS

Appendix B: L_2 norm for polynomials

Let $Q(z^{-1}) = q_o + q_1 z^{-1} + \ldots\ldots\ldots\ldots + q_{nq} z^{-nq}$

$$\left\| Q(z^{-1}) \right\|_{L_2}^2 = \frac{1}{2\pi} \int_{-\pi}^{\pi} \left| Q(e^{-jw}) \right|^2 dw$$

$$= \frac{1}{2\pi} \int_{-\pi}^{\pi} \left| q_o + q_1 e^{-jw} + \ldots\ldots\ldots + q_{nq} e^{-jnqw} \right|^2 dw$$

$$= \frac{1}{2\pi} \int \{ | q_0 + q_1 \cos w + \ldots\ldots\ldots + q_{nq} \cos(nqw)$$

$$- j[q_1 \sin w + \ldots\ldots\ldots + q_{nq} \sin(nqw)] |^2 \} dw$$

$$= \frac{1}{2\pi} \int \{ [q_o + q_1 \cos w + \ldots\ldots\ldots + q_{nq} \cos(nqw)]^2$$

$$+ [q_1 \sin w + \ldots\ldots\ldots + q_{nq} \sin(nqw)]^2 \} dw$$

$$= \frac{1}{2\pi} \int_{-\pi}^{\pi} \{ \sum_{i=0}^{nq} (q_i \cos iw)^2 + 2 \sum_{i=0}^{ng-1} \sum_{K=i+1}^{ng} (q_i q_K \cos iw \cos Kw)$$

$$+ \sum_{i=0}^{nq} (q_i \sin iw)^2 + 2 \sum_{i=0}^{ng-1} \sum_{K=i+1}^{ng} (q_i q_K \sin iw \sin Kw) \} dw$$

Now Since $\int_{-\pi}^{\pi} \cos iw \cos Kw = 0 \quad \text{for i} \neq \text{K}$

$$\int_{-\pi}^{\pi} \sin iw \sin Kw = 0 \text{ for i} \neq \text{ K}$$

And $\cos^2 iw + \sin^2 iw = 1$

$$\left\| Q(z^{-1}) \right\|_{L_2}^2 = \frac{1}{2\pi} \int_{-\pi}^{\pi} (q_o{}^2 + q_1{}^2 + \ldots\ldots\ldots + q_{nq}{}^2) dw$$

$$= \sum_{i=0}^{nq} q_i{}^2$$

= euclidean norm of $Q(z^{-1})$

APPENDIX C

MAXON MOTOR DATA SHEET

maxon EC motor

Ø40 mm, brushless, 100 Watt

CE approved

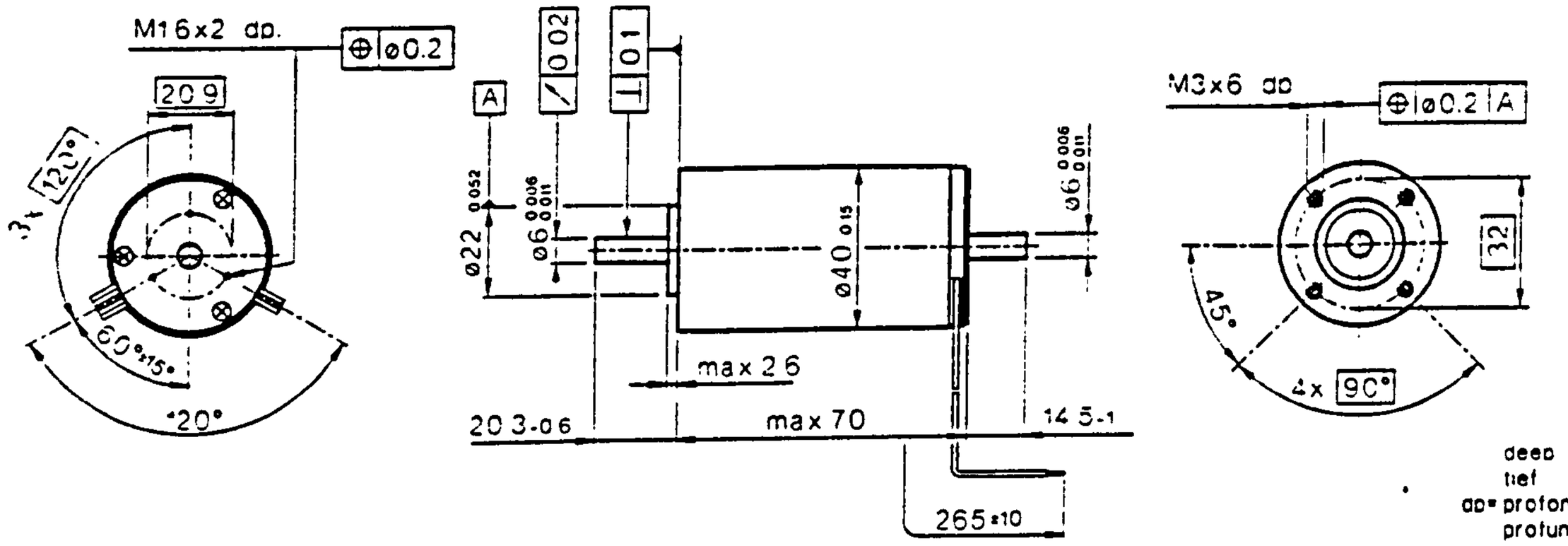

Motor Type:
maxon EC motor Ø40 mm, brushless . . .

Order Number
Motor Data /

. . . "Y-circuit". 100 Watt, ball bearings, 2 shafts		118894	118895	118896	118897	118898	118899	118900	118901
1 Assigned power rating	W	100	100	100	100	100	100	100	100
2 Nominal Voltage	Volt	12.00	12.00	18.00	30.00	36.00	42.00	42.00	42.00
3 No load speed	rpm	6600	4500	4500	4800	4500	2800	2200	1800
4 Stall torque	mNm	543	550	546	589	550	326	260	209
5 Speed/torque gradient	rpm/mNm	12.3	8.3	8.2	8.3	8.3	8.7	8.8	8.8
6 No load current	mA	410	230	150	100	80	30	30	20
7 Terminal resistance phase to phase	Ohm	0.38	0.55	1.26	3.00	4 90	18.3	28.4	43.6
8 Max. permissible speed	rpm	15000	15000	15000	15000	15000	15000	15000	15000
9 Max. continuous current at 5000 rpm	A	4.37	3.63	2.4	1.55	1.22	0.63	0.51	0.41
10 Permiss. continuous power loss	W	13.3	13.3	13.3	13.3	13.3	13.3	13.3	13.3
11 Max. efficiency	%	79.0	80.0	80.8	81 1	80.8	77.5	75.5	73.8
12 Torque constant	mNm/A	17.2	25.2	38.2	58.9	74.9	142	176	217
13 Speed constant	rpm/V	555	379	250	162	127	67 0	54 0	44 0
14 Mechanical time constant	ms	11	7	7	7	7	8	8	8
15 Rotor inertia	gcm²	85	85	85	85	85	85	85	85
16 Terminal inductance (phase to phase)	mH	0.08	0.1	0.3	0.8	1.2	4.4	6.8	10
17 Thermal resistance housing-ambient	K/W	6.3	6.3	6.3	6.3	6.3	6.3	6.3	6.3
18 Thermal resistance winding-housing	K/W	1.2	1.2	1.2	1.2	1.2	1.2	1.2	1.2
19 Thermal time constant winding	s	15	15	15	15	15	15	15	15
20 Thermal time constant stator	s	1050	1050	1050	1050	1050	1050	1050	1050

Operating Range

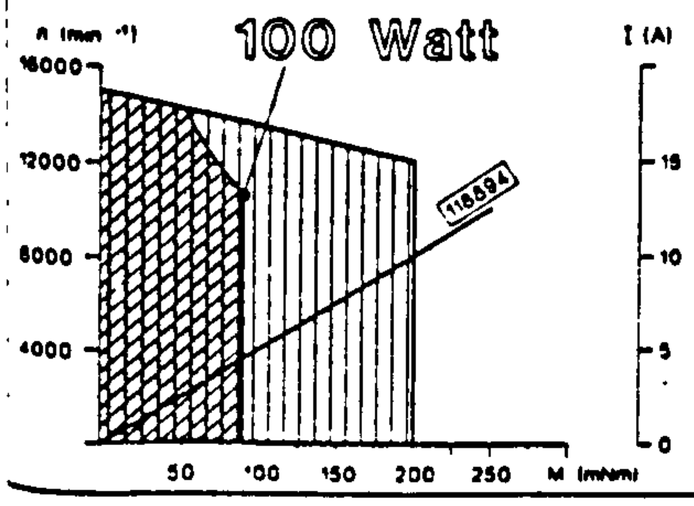

Comments

(Details on page 86)

Continuous operation
In observation of above listed thermal resistances (lines 17 and 18) the maximum permissible winding temperature will be reached during continuous operation at 25°C ambient.
= Thermal limit

Short term operation
The motor may be briefly overloaded (recurring).

- Stock program
- Standard program
- Special program (on request!)

● Axial play	< 8 N	0 mm
	> 8 N max.	0.14 mm
● Preloaded ball bearings min. preloading		8 N
● Max. ball bearing loads		
axial (dynamic)		10 N
radial (5 mm from flange)		70 N
Press-fit force (static)		170 N
same as above, shaft supported		5000 N
● Radial play/ball bearings		0.03 mm
● Ambient temperature range		-20/+125°C
● Max. permissible winding temperature		+125°C
● Weight of motor		390 g

● Values listed in the table are nominal.
For applicable tolerances see page 33.

Cable	Connection
black	motor winding 2
white	motor winding 3
red	motor winding 1
white/gray	Hall sensor 3
green	Vcc Hall
blue	GND
black/gray	Hall sensor 2
red/gray	Hall sensor 1

maxon Modular System

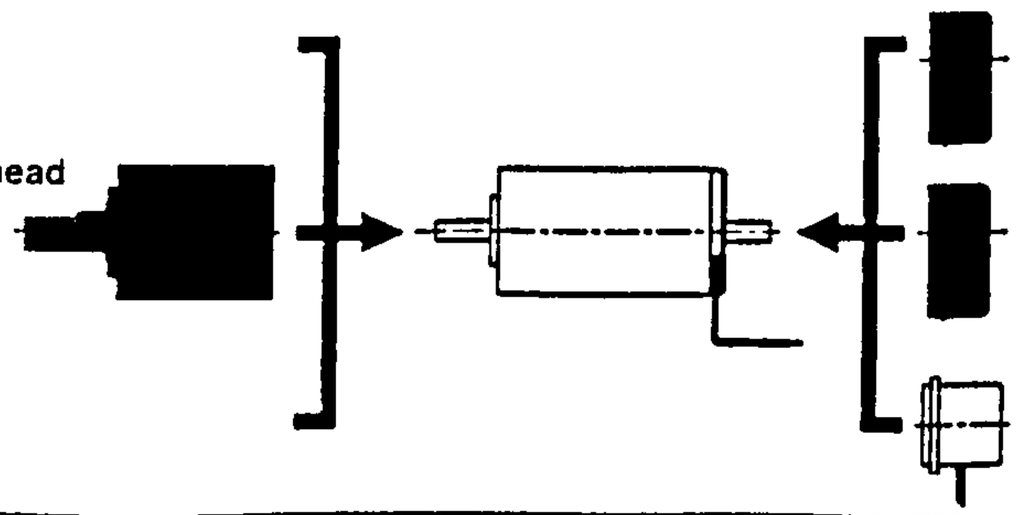

Planetary Gearhead
Ø42 mm
2.94-14 7 Nm
Details page 128

Digital-Encoder
HP HEDS 5540
500 CPT, 3 chan.
Details page 147

Digital-Encoder
HP HEDL 5540
500 CPT, 3 chan
Details page 147

Resolver
Ø26 mm, 10 V
Details page 152

APPENDIX D

MAXON DRIVER DATA SHEET

maxon motor control 4-Q-EC, Type number 132368

Operating instructions April 1997 edition

4-Q -EC Servoamplifier with speed control by encoder signals

The 4-Q-EC is a Servoamplifier for electronic commutated (brushless) DC motors with Hall sensors and mounted encoder.

The speed control of the PWM (pulse wide modulation) servoamplifier is made by the encoder signals.

The servoamplifier controls the three windings in the motor according to the position of the rotor. The position feedback is achieved by Hall sensors. The output power stage is designed in MOS-FET technology for high efficiency.

Pin	4-Q-EC
1	DC Supply voltage
2	Ground
3	Winding 1
4	Winding 2
5	Winding 3
6	Hall Sensor 1
7	Hall Sensor 2
8	Hall Sensor 3
9	Hall Sensor supply voltage +5V/30mA
10	Ground
11	Enable
12	Ground
13	neg. reference voltage -10 VDC
14	pos. reference voltage +10 VDC
15	negative set value speed
16	positive set value speed
17	Ready
18	Encoder supply voltage +5V/100mA
19	Ground
20	Encoder Channel A
21	Encoder Channel B
22	Set value current limit
23	Ground
24	Monitor actual speed tacho

Safety precautions

⚠ Skilled personnel

Installation and starting of the equipment shall only be performed by experienced, skilled personnel.

⚠ Statutory Regulations

The user must ensure that the servo amplifier and the components belonging to it are assembled and connected according to the local statutory regulations.

⚠ Additional Safety Equipment

Electronic apparatus are basically not fail-safe. Machines and apparatus must therefore be fitted with independent monitoring and safety equipment. It must be ensured that, if the equipment breaks down, is operated incorrectly, the control units break down, the cables break etc., the drive or the complete apparatus respectively is kept in a safe operating modus.

⚠ Danger

Do ensure that, during the installation of the Servoamplifier, **no** apparatus is connected to an electric supply! After switching on do not touch any live parts.

⚠ Max. Supply Voltage

Make sure the supply voltage is between 12 - 50 VDC. Attention: higher voltage than 50 VDC or wrong polarity will destroy the unit.

⚠ Load Decoupled

For the primary operation the motor should be free running, i.e. with the load decoupled.

⚠ Repairs

Repairs may only be made by authorised persons or by the manufacturer. It is dangerous for the user to open the unit or make repairs to it.

⚠ Electro Static Discharge (ESD)

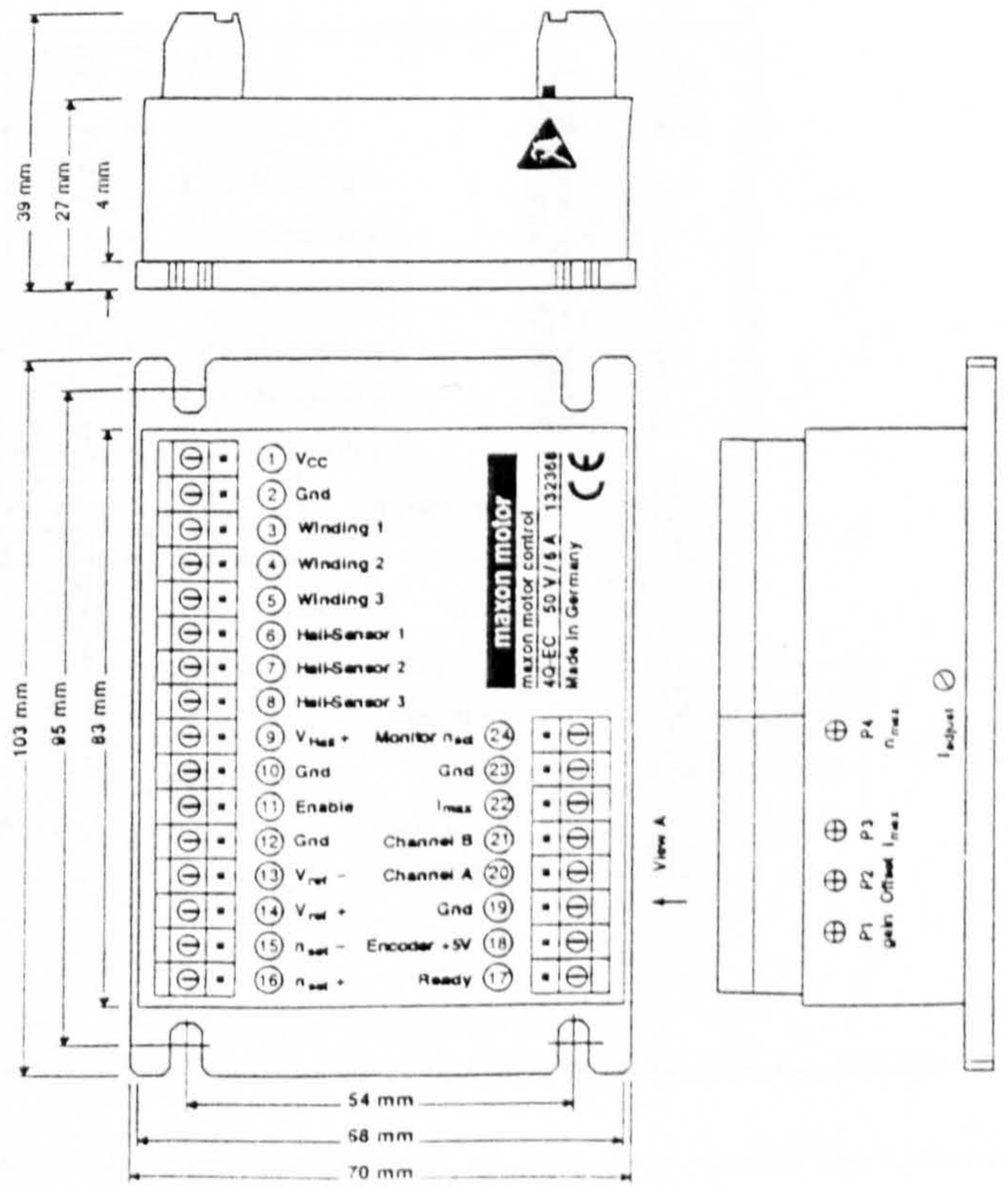

Performance Data

- Supply voltage V_{CC} 12 - 50 VDC
  Ripple < 5%
- max. continuous output current
  with additional heat sink ± 6 A
- absolute current limit
  (cycle by cycle) ± 10 A
- minimum load inductance
  (phase by phase) 400µH
- Switching frequency 20kHz ± 10%

Input

- Set value speed n_{set}
  (differential, Ri > 47kΩ) -10. . . +10 V
- Set value current limit I_{max}
  (Ri > 47kΩ) 0. . . +10 V
- Enable
  Input open = motor disabled
- Encoder signals Channel A, Channel B
  max. 225kHz per channel

Voltage output

- Reference voltage +10 VDC / -10 VDC, max. 5mA
- Hall sensor supply voltage +5 VDC, max. 30mA
- Encoder supply voltage +5 VDC, max. 100mA

Trim potentiometer

- Gain speed controller (gain)
- Offset (Offset)
- Current limit set (I_{max})
- Set value adjustment speed (n_{max})
- Current fine adjustment (I_{adj})

Status reading

- READY max. 30 V
  (Output Open Collector) max. 50mA

Monitor output

- Monitor act. speed tacho n_{act} -5 . . . +5 V, max. 5mA

Ambient temperature range

Operation -10 . . . +45°C
Storage -40 . . . +85°C

Humidity range

- no condensation 20 . . . 80 %

Mechanical Data

Weight 215 g
Size (L x W x H) 103 x 70 x 39 mm
Mounting plate or flange for 4 screws M3
Distance between threads 95 x 54 mm

Connections:

- PCB-clamps 16 and 8 poles
  pitch 5 mm
  suitable for cable profile
  multiple-stranded wire 0,14 - 2,5 mm²
  single wire 0,14 - 4 mm²

Minimum External Wiring

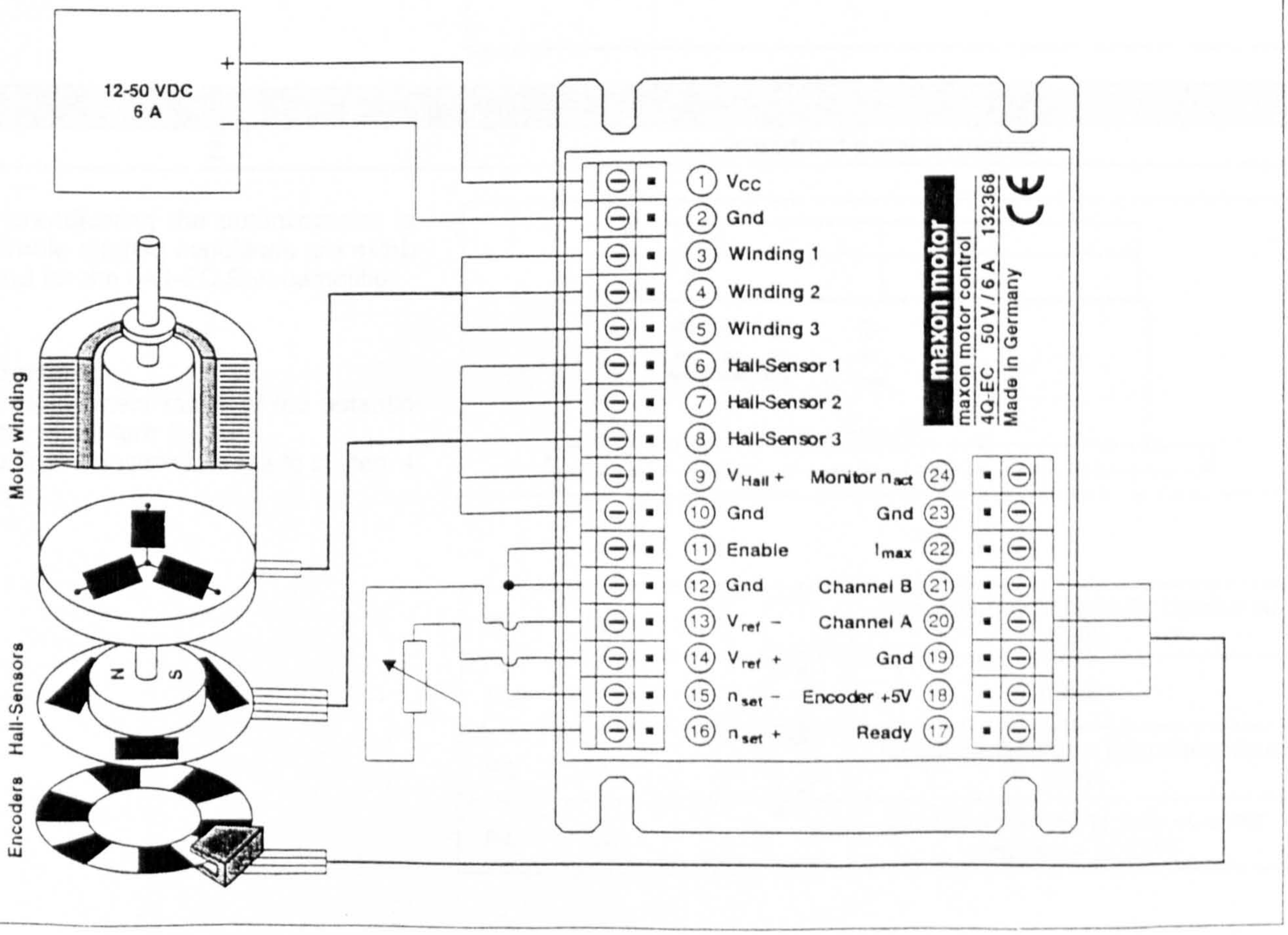

Step	Task
1.	**Determine power supply requirements**

You may make use of any available power supply, as long as it meets the minimal requirements shown on the right.

Please note:
- Regulations for electrical equipment.
- During set up and adjustment phases we recommend to separate the motor mechanically from the machine to prevent damage due to uncontrolled motions!

Important:
The maximum voltage must be in agreement with the desired operating point of the motor.

Power supply requirements	
Output voltage	V_{cc} min.12 VDC V_{cc} max.50 VDC
Ripple	< 5 %
Output current	6 A (constant)

The required voltage can be calculated as follows:

Known values:
- Operating torque M_B [mNm]
- Operating speed n_B [rpm]
- Nominal motor voltage U_N [Volt]
  (according to catalog, Motor Data, Line 2)
- Motor no load speed at U_N, n_0 [rpm]
  (according to catalog, Motor Data, Line 3)
- Speed/torque gradient of the motor
  $\Delta n/\Delta M$ [rpm mNm]
  (according to catalog, Motor Data, Line 5)

Sought values: Supply voltage V_{cc} [Volt]

Solution:
$$V_{cc} = \frac{U_N}{n_0} \bullet (n_B + \frac{\Delta n}{\Delta M} \bullet M_B) + 4\ V$$

Choose a power supply capable of supplying this calculated voltage under load. The formula takes a 4 Volt max. voltage drop at the 4-Q-EC Servoamplifier into account.

Step	Task
2.	**Preadjust potentiometers**

By preadjusting the potentiometer favourable starting conditions are established for the 4-Q-EC Servoamplifier.

Important:
The adjustment range of the potentiometer is 3/4 turn (=270°).
The final adjustment is made in step 4.

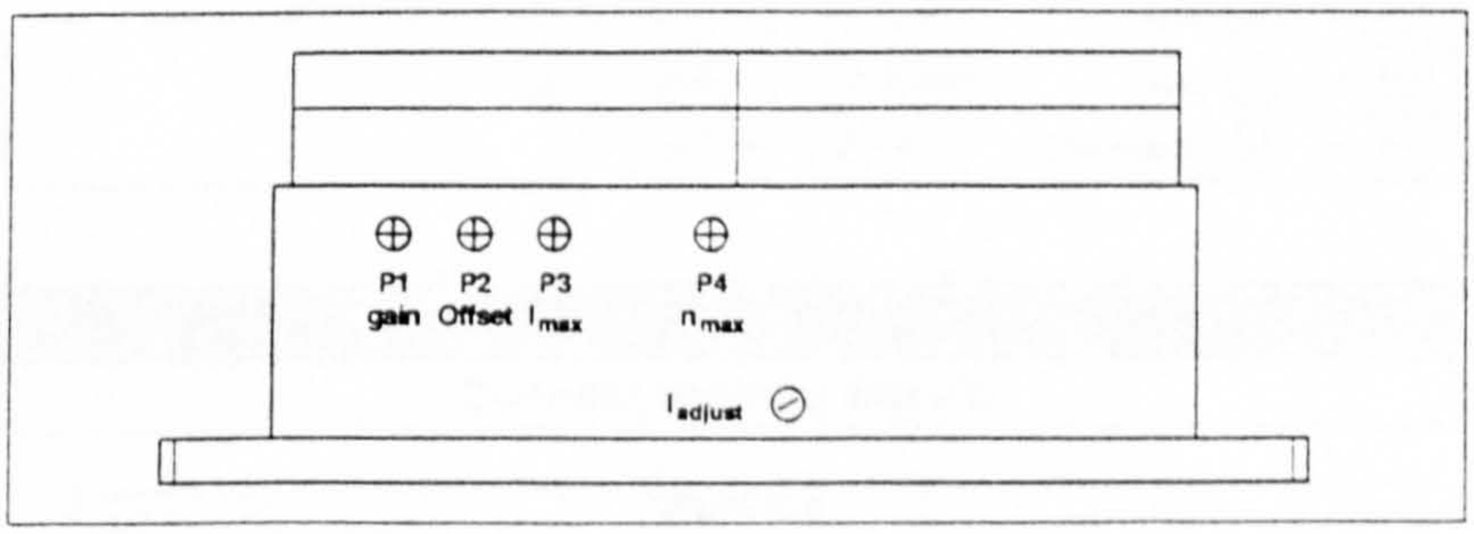

P1	gain	↻	Turn potentiometer fully clockwise (CW)
P2	Offset	↻	Middle
P3	I_{max}	↻	Turn potentiometer fully clockwise (CW)
P4	n_{max}	↻	Turn potentiometer fully counter clockwise (CCW)

Step	Task
3.	Wiring
3.1	Connect motor windings

Connect motor „Winding1" through „Winding3" as shown in diagram.

In case the original motor cable requires extension:

- take into account diameter and length of cable. The motor windings have a low resistance therefore the resistance of the connecting wires can change the motors performance.
- use separately shielded cables for the motor and for the feedback.

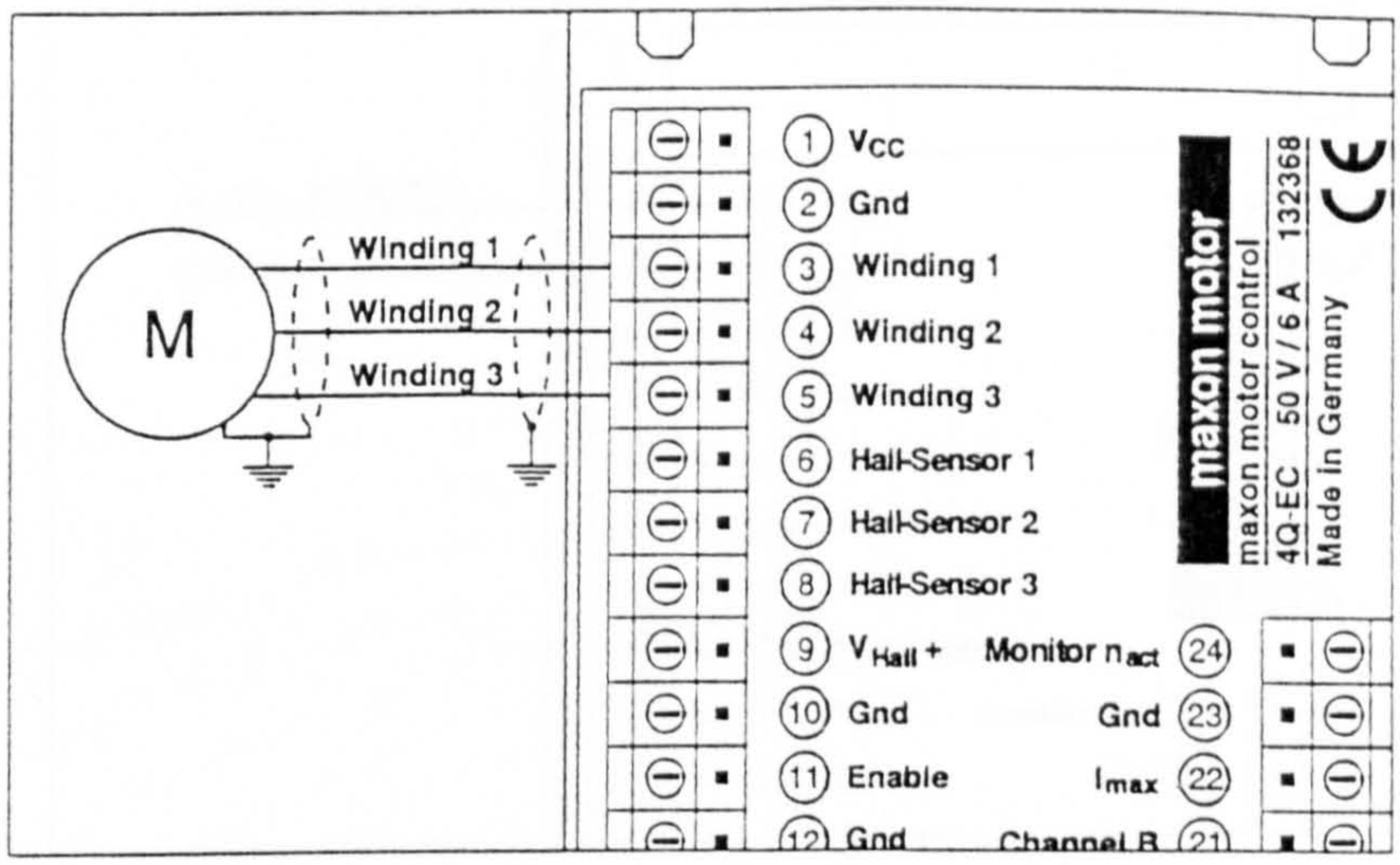

Step	Task
3.2	Connect Hall sensors

Connect Hall sensors as shown in diagram.

In case the original Hall sensor cable requires extension:

- use separately shielded cables for the feedback and for the motor.

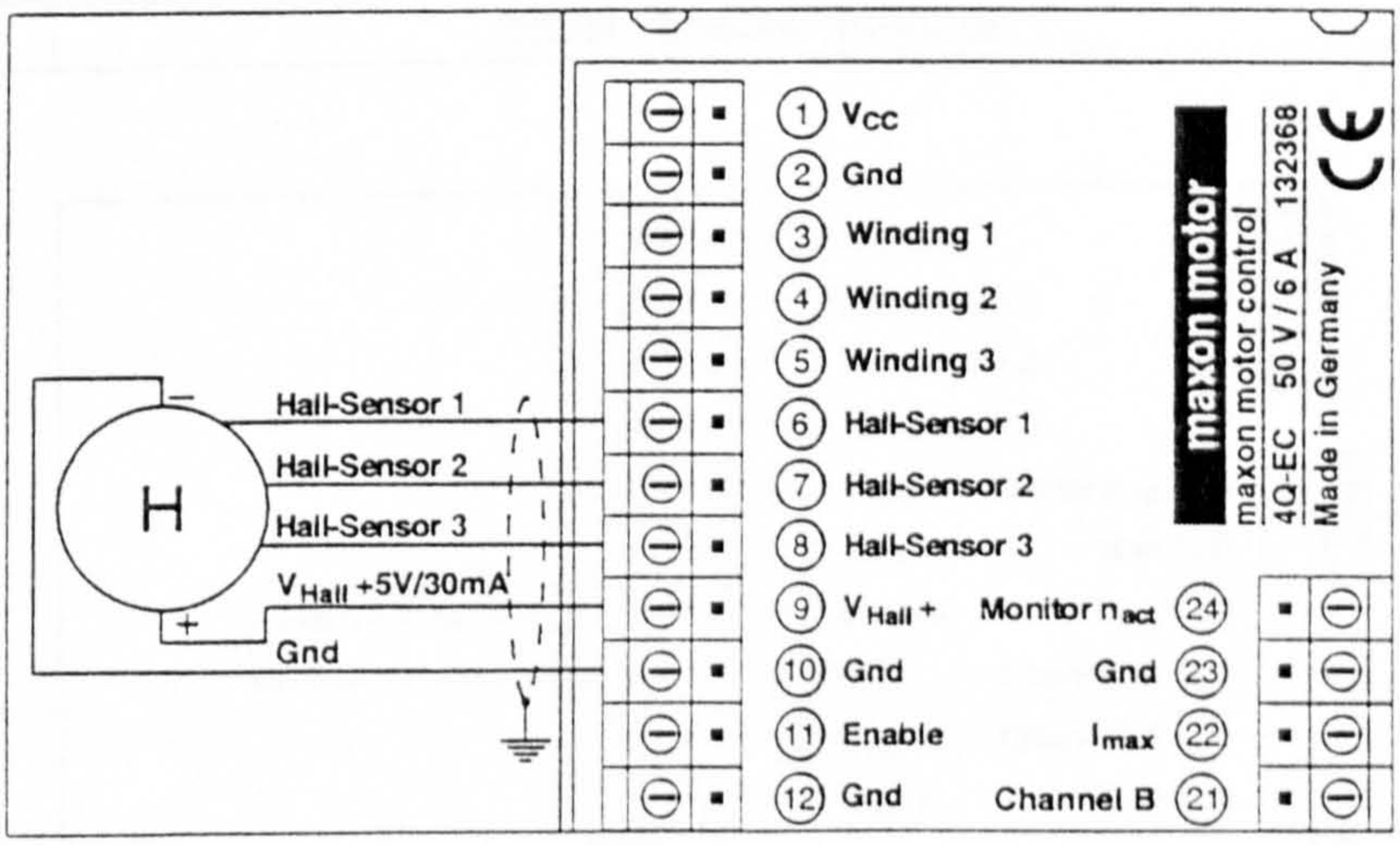

Step	Task
3.3	Connect encoder signals

Connect encoder signals as shown in diagram.

- If cable length l >1,5 m and / or if interference instability exists, use a screened cable and a Line Driver (i.e. AM26LS31 and a Line Reciever i.e. AM26LS32).

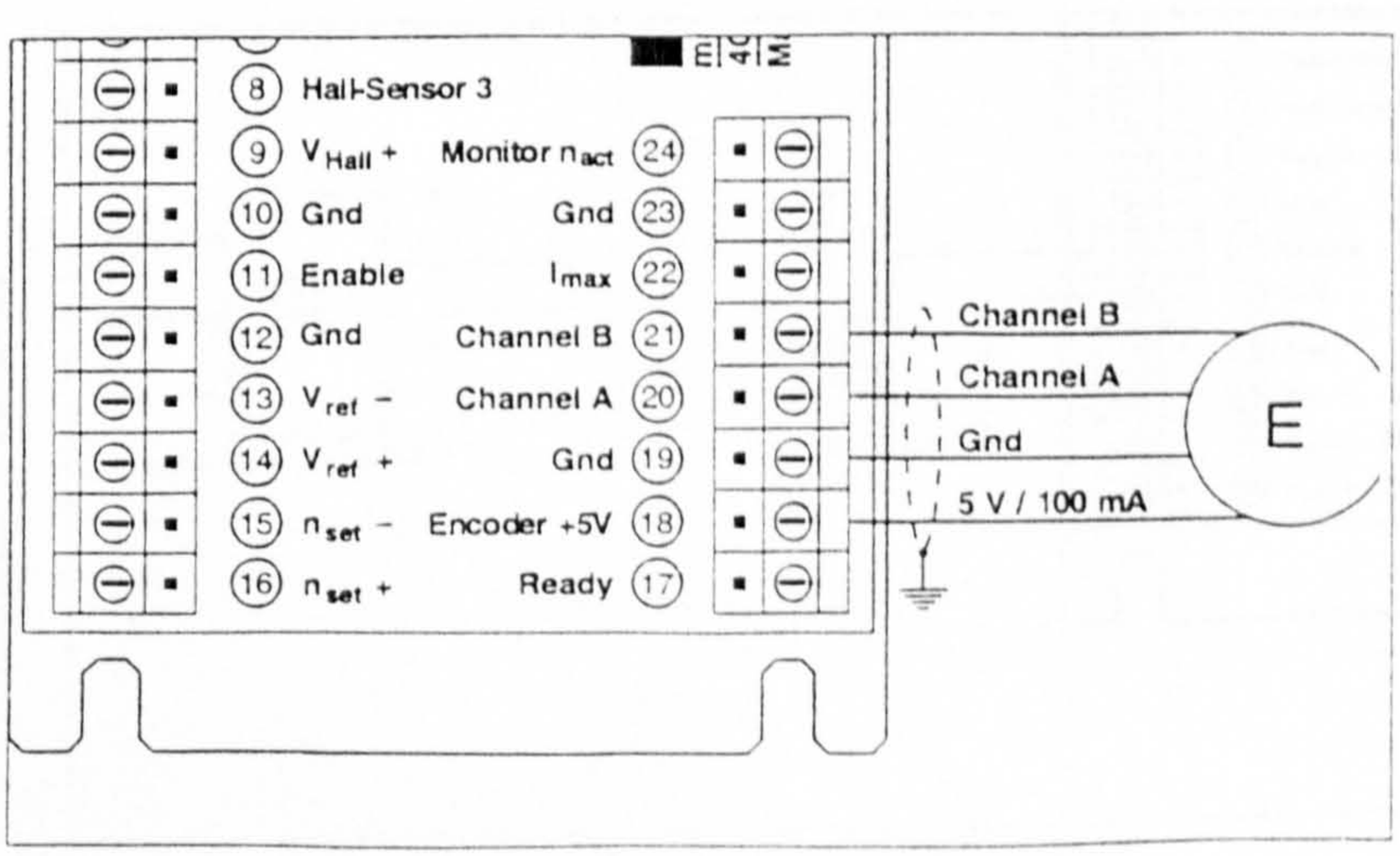

Step	Task
3.4	Connect power supply

- Determine supply voltage (see Step 1).
- Check that the supply voltage V_{cc} is between +12 VDC und +50 VDC
- Switch off supply voltage.
- Connect power supply as shown in diagram.

Caution:
voltages higher than +50 VDC, or wrong polarity, will destroy the unit.

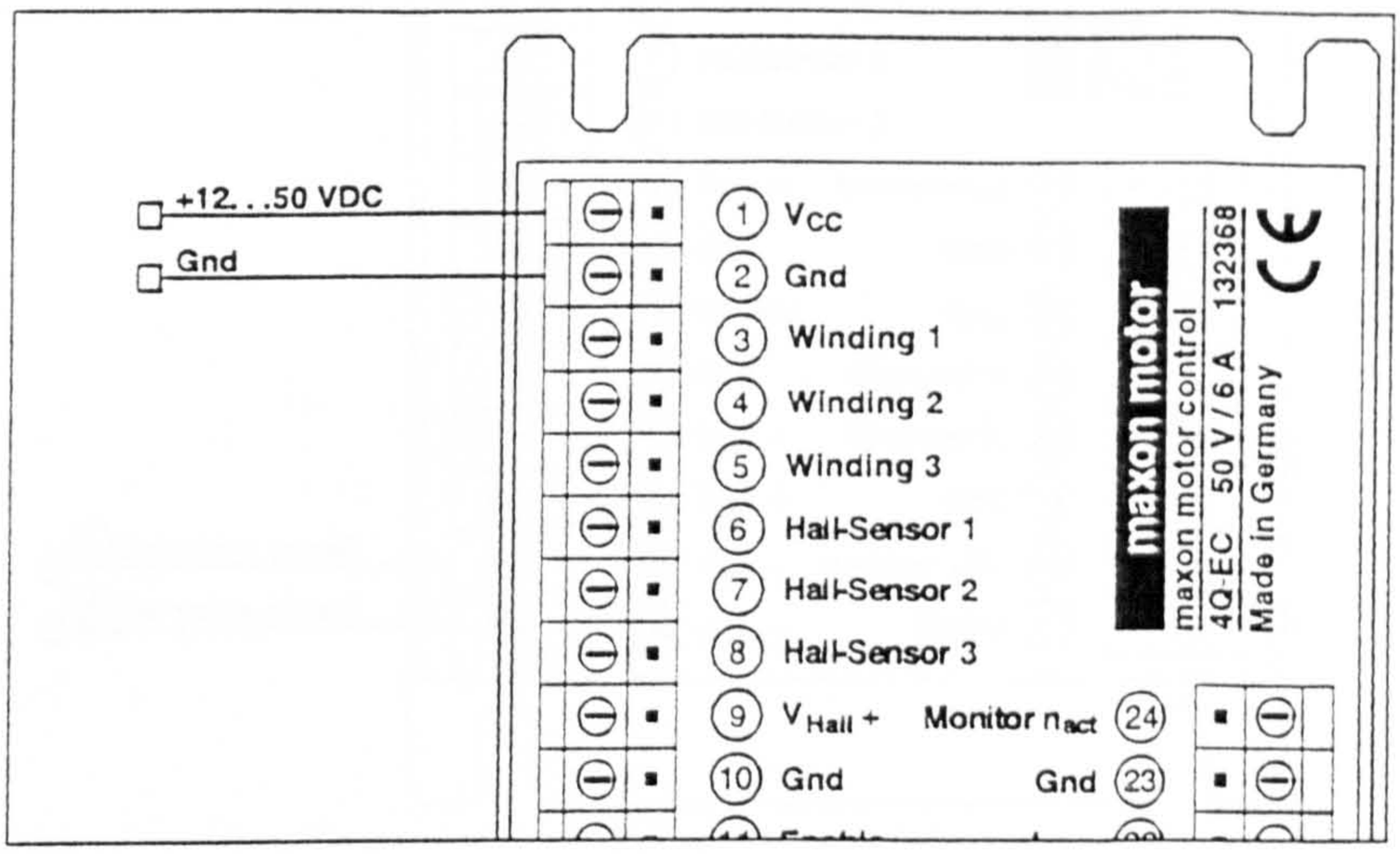

Step	Task
3.5	Effect "Enable" function

To enable the power stage, Pin 11 Enable and Gnd (i.e. Pin 12) must be connected.

Version 1:
Enable with switch

Switch closed	Switch open
Power stage activated	Power stage disabled
Motor connected	Motor not connected

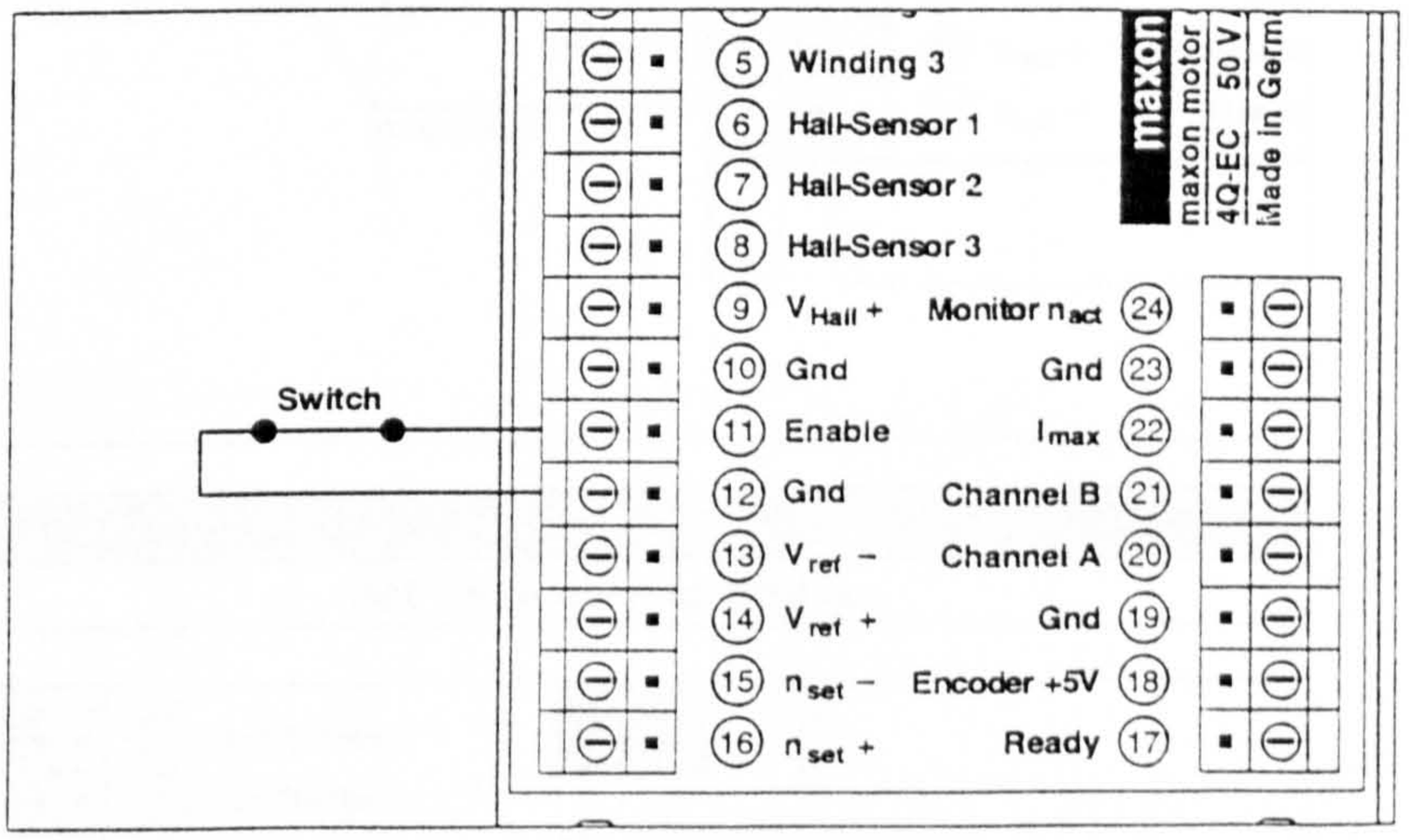

Version 2:
Enable with open collector transistor or TTL / CMOS components

Transistor conducting „Low"	Transistor closed „High"
Power stage activated	Power stage disabled
Motor connected	Motor not connected

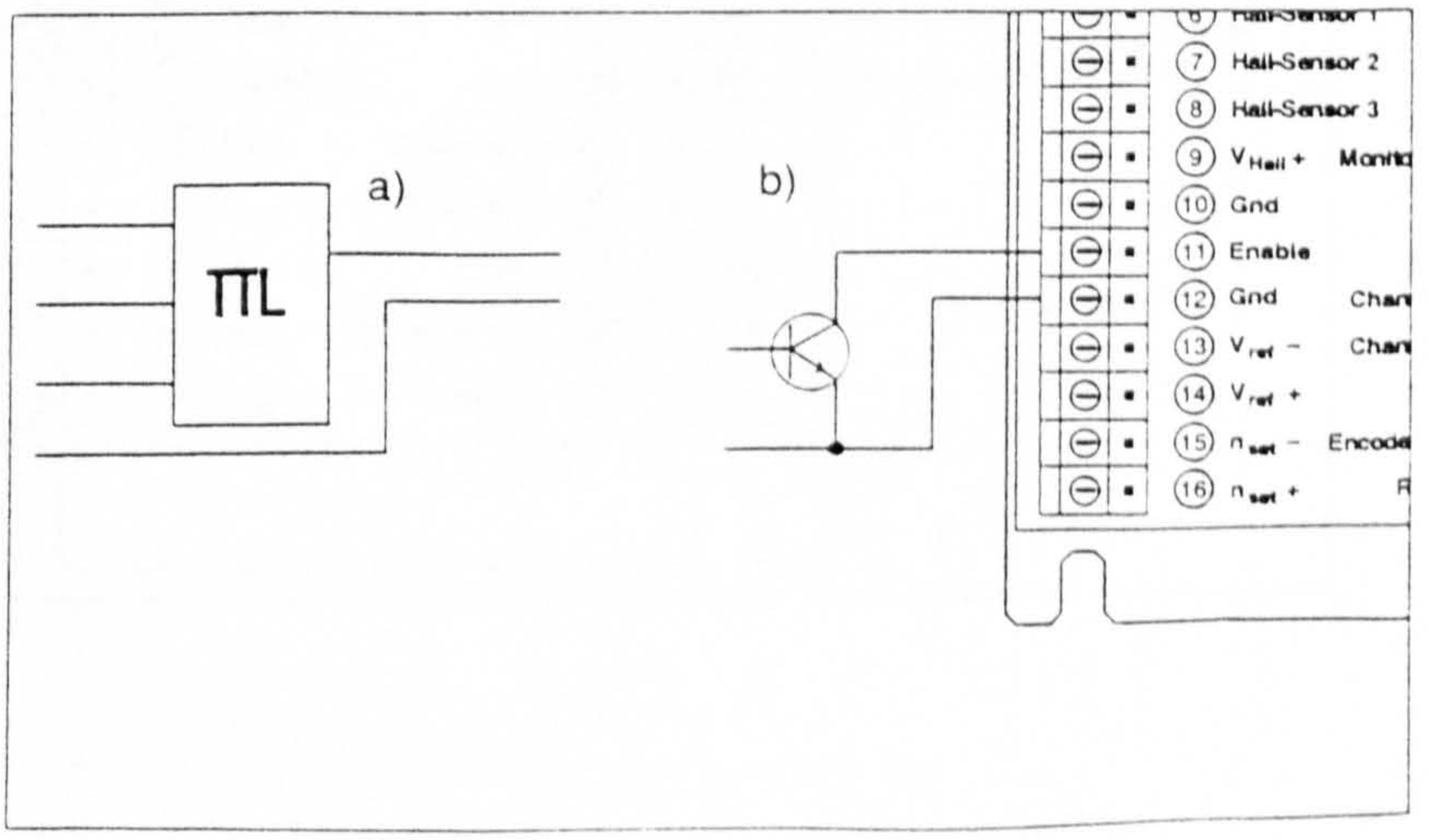

Step	Task
3.6	**Connect Set value speed**

The set value speed can be given through an external voltage or potentiometer.

Version 1:
with external voltage ±10 VDC

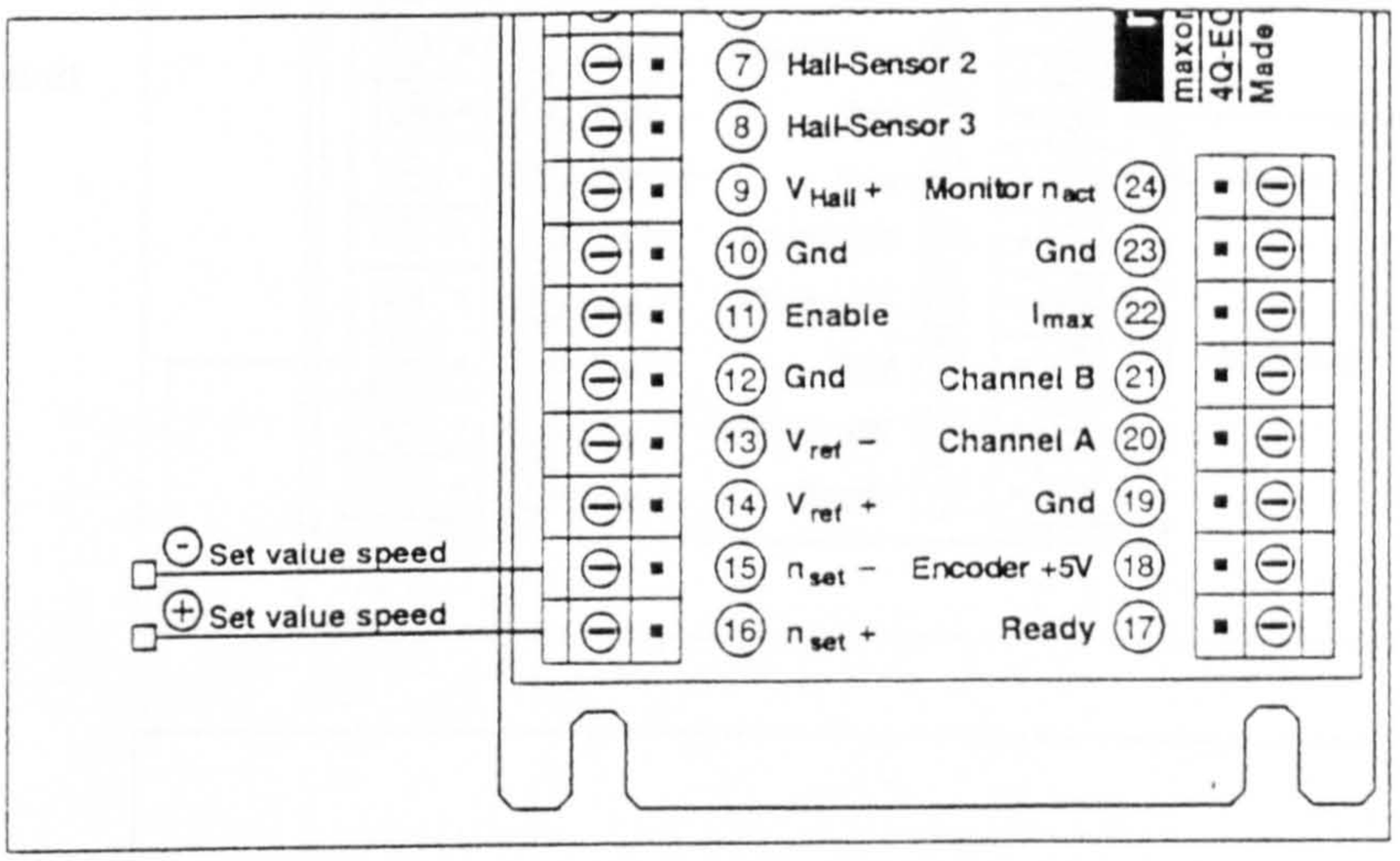

Version 2:
with external potentiometer.
Recommended potentiometer 10 KΩ

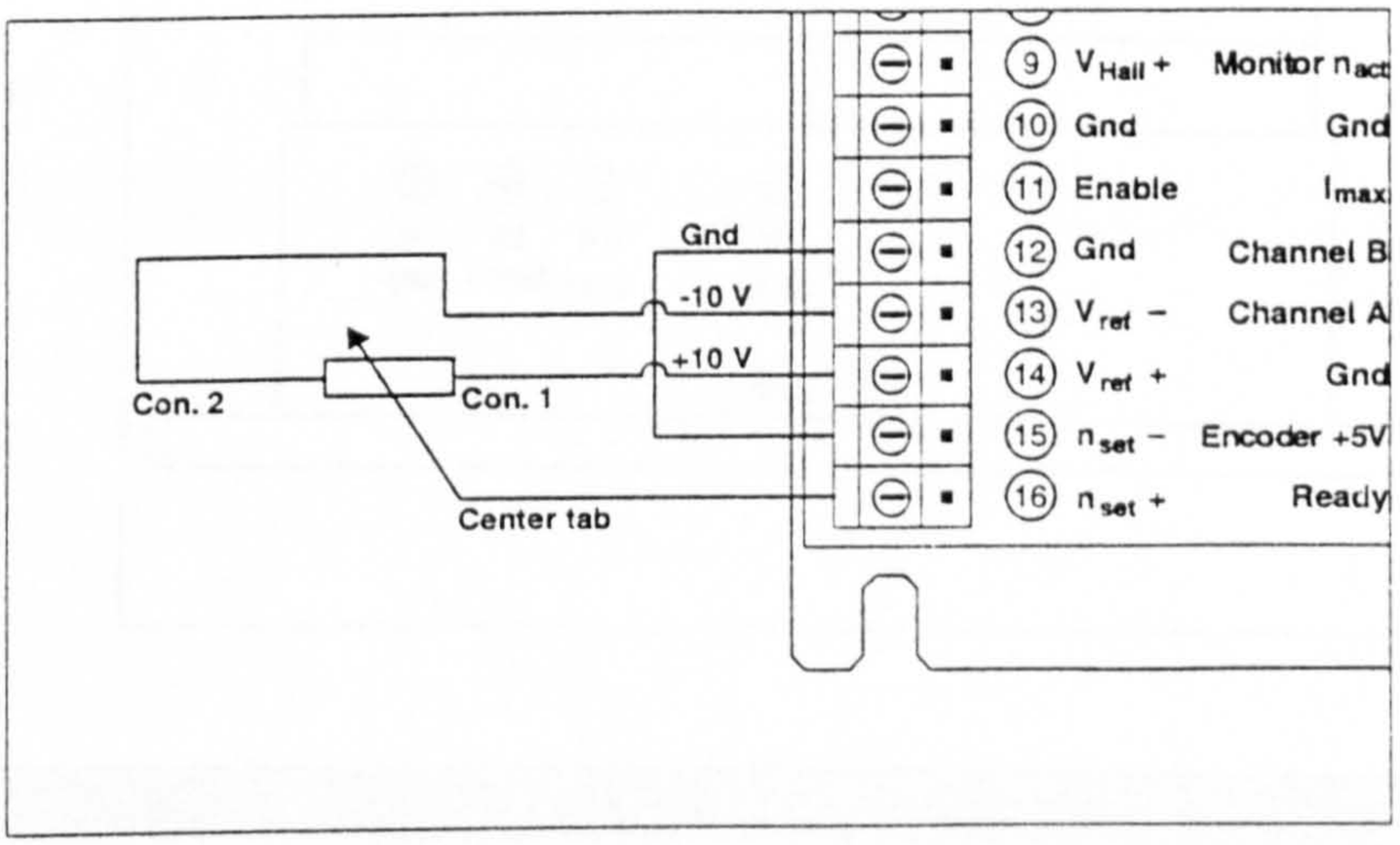

Step	Task
3.7	**Set value current limit I_{max}**

The set value current limit I_{max} can be given through an external voltage or internal potentiometer P3 I_{max} .

Version 1:
with external voltage 0. . .10 VDC

Basic requirements:
internal potentiometer (I_{max}) must be at the left limit stop.

Caution:
If set value current limit is 0 V the motor does not run.

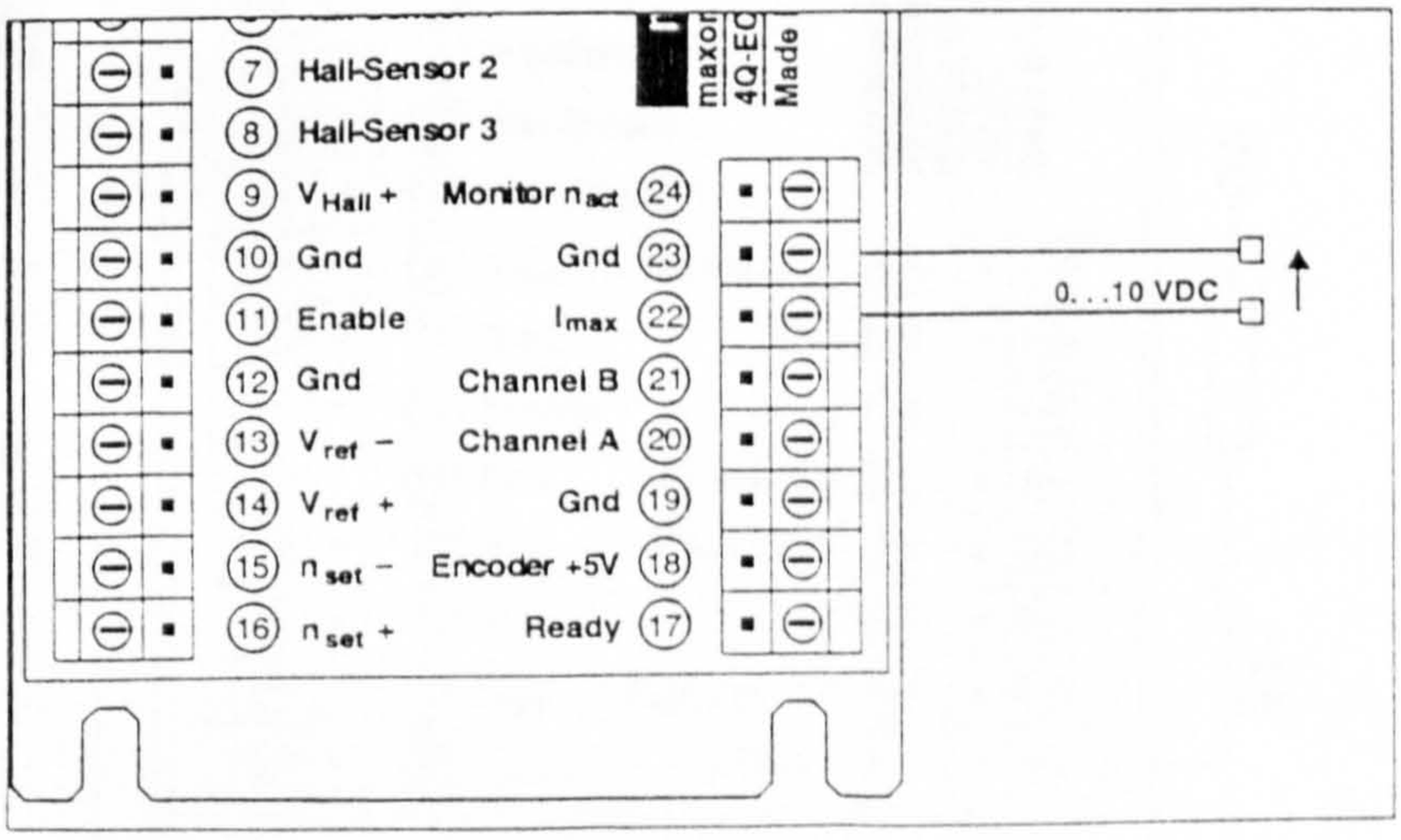

Note versions 2 and 3 on page 7.

Version 2:
with external potentiometer.
Recommended potentiometer 10 KΩ

Basic requirements:
internal potentiometer (I_{max}) must be at the left limit stop.

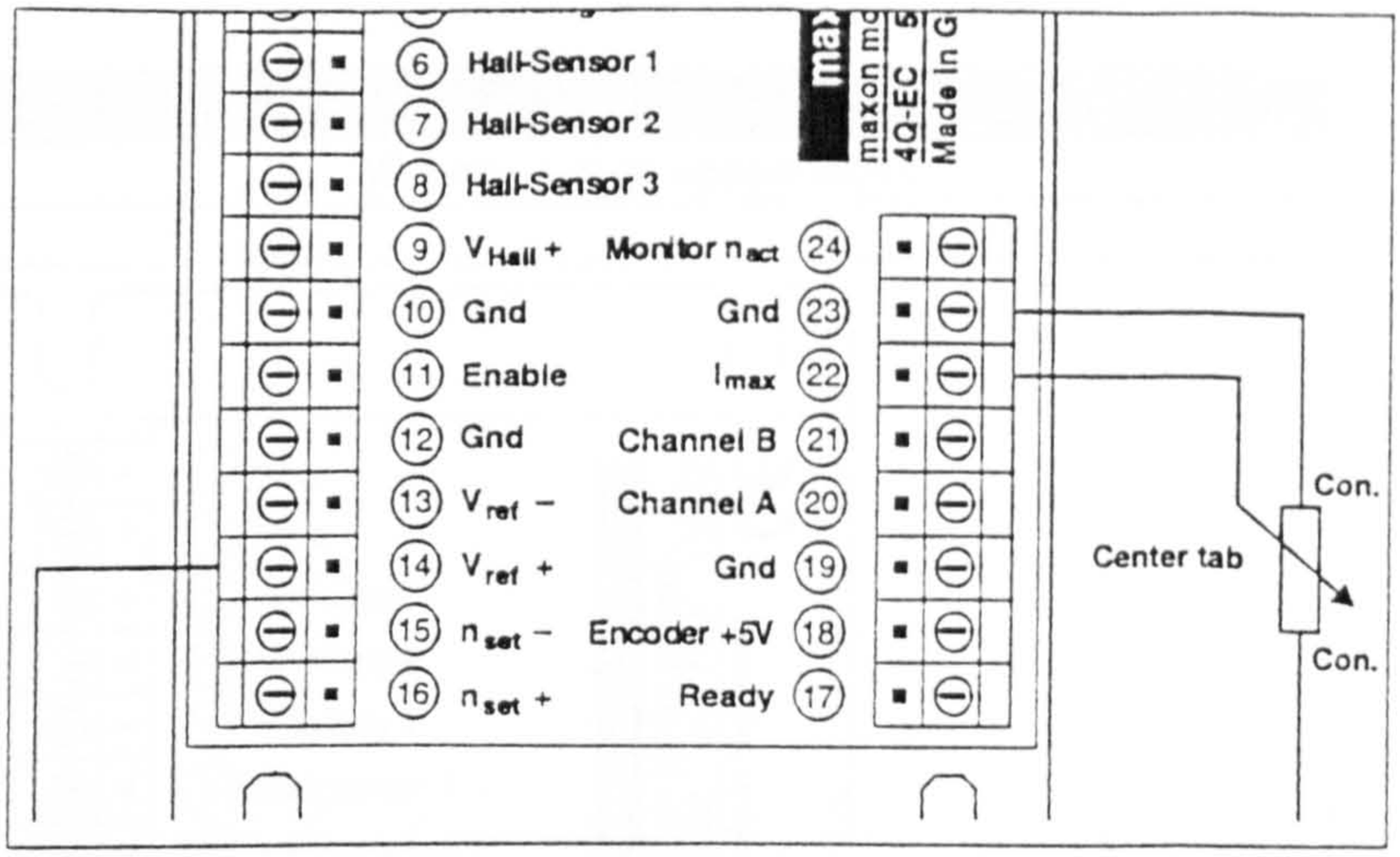

Version 3:
internal potentiometer P3 I_{max}

Caution:
If the set value current limit (Pin 22) I_{max} is not connected, this Pin should be connected to Gnd.

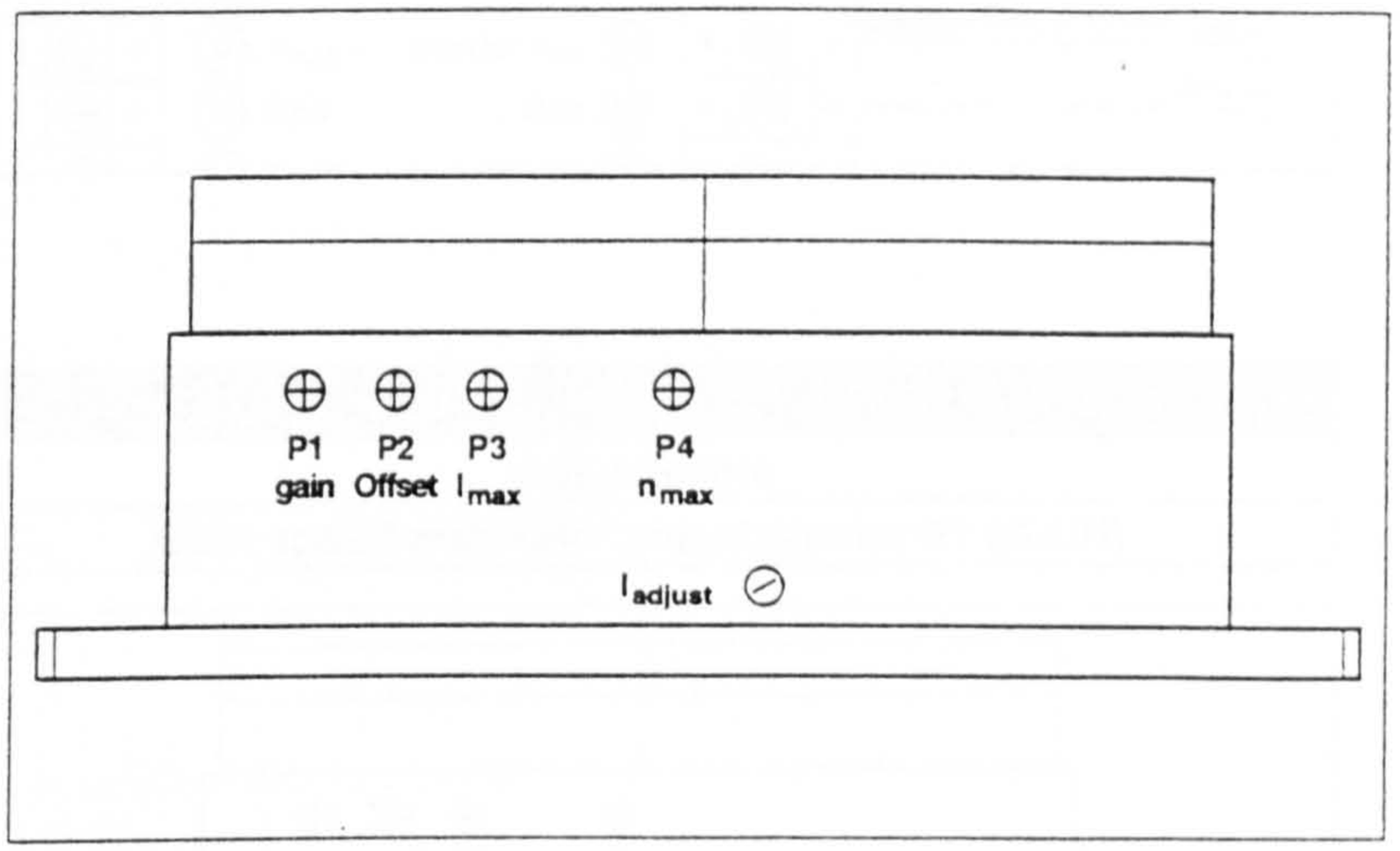

Step	Task
3.8	Ready

Enable and temperature o.k.	Disabled and / or over temperature
Pin 17 Ready "Low"	Pin 17 Ready "High"

The signal READY is an „Open Collector" output, it is active low (Gnd connected).

An external additional voltage is required:
max. 30 VDC
I_{LOAD} max. 50 mA

This solution is therefore load break resistant, i.e. even a broken connection between the Ready output signal and the controller lead to an error message.

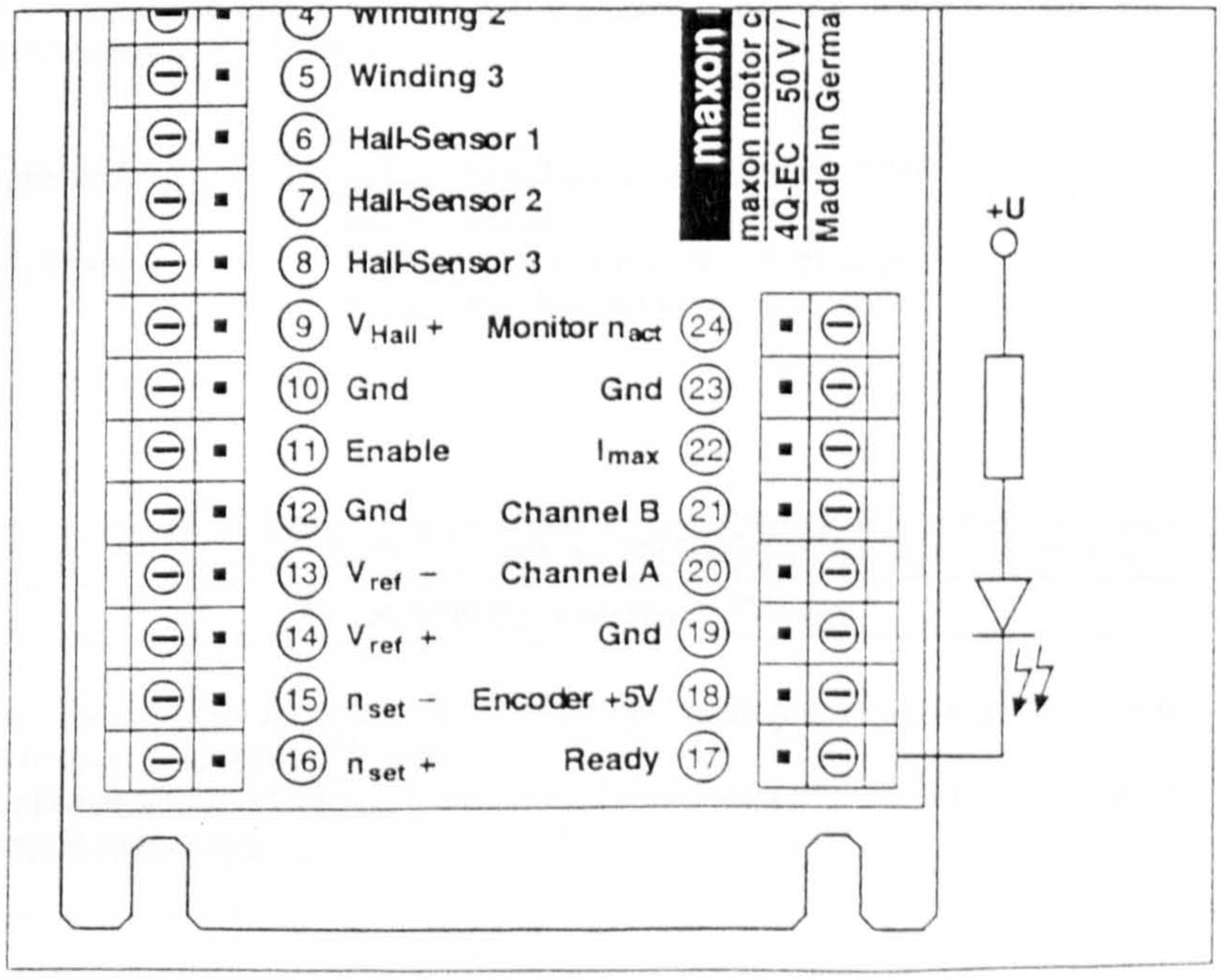

Step	Task
3.9	**Monitor actual speed tacho**

Monitor actual speed tacho n_{act} -5V... +5V
max. 5mA

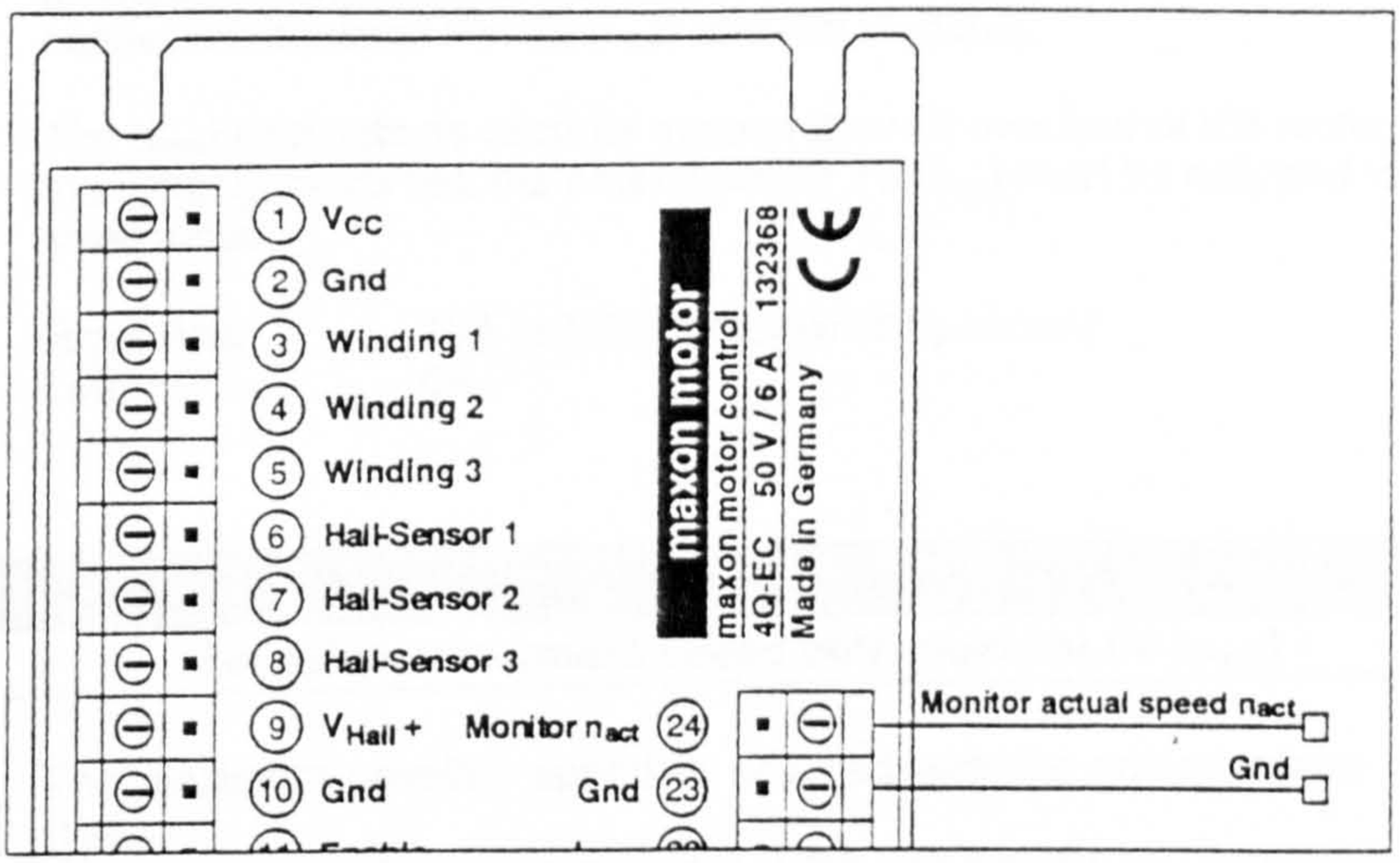

Caution:
Primarily the monitor signals are for assessing the dynamic of the speed controller and not for quantified measurements.
An exact adjustment of the maximum speed should be made, for example, with the help of an incremental pulse.

- Another voltage may not be connected to the monitor outputs.
- The monitor output signal ±5V corresponds to the adjusted max. speed n_{max}. at ±10V set value input.

Step	Task
4.	**Adjustments**
4.1	**Gain speed controller potentiometer P1 (GAIN)**

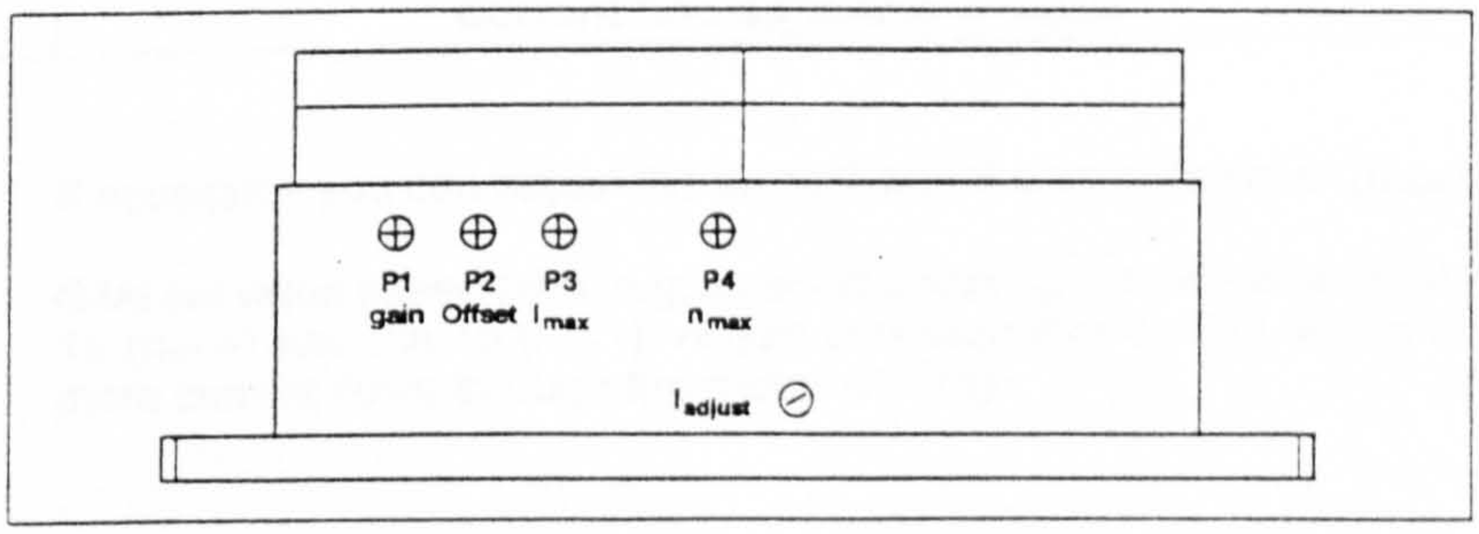

Attention:
If the motor vibrates or becomes loud the amplification is adjusted too high and the potentiometer P1 (GAIN) must be readjusted until the instability of the closed loop of the drive under all loads disappears.

The amplification of the speed controller can be adjusted with the potentiometer P1 (GAIN).

Right limit: small amplification of the controller
slow reaction

Left limit: high amplification of the controller
faster reaction but high overshoot

Step	Task
4.2	**Offset potentiometer P2 (Offset)**

Note:
The adjustment of the offset can be influenced by temperature changes.

Give speed set value zero, e.g. by short circuiting the set value input Pin 16 (n_{set} +) and Pin 15 (n_{set} -).
Set the motor speed to zero with the potentiometer P2 (Offset) until motor shaft is stationary.

Step	Task
4.3	**Current limit potentiometer P3 (I_{max})**

Caution:
The current limit is depends on the motor type used and on the supply voltage (current ripple). If the current limit has to be adjusted precisely, the motor current must be measured with a clamp-on probe.

The current limit can be adjusted by the potentiometer P3 (I_{max}).
In case of using the internal current limit P3 (I_{max}), there should be a connection between Pin 22 (I_{max}) and Pin 23 (Gnd).

The (I_{max}) limit acts as security against thermal overload of the motor. If the motor gets too hot, the potentiometer P3 (I_{max}) must be adjusted to a lower value.

Right limit: 10A (±20%) motor winding current
Left limit: 0A

Step	Task
4.4	**Set value adjustment speed potentiometer P4 (n_{max})**

Caution:
The max. speed depends on the motor type used and on the supply voltage (current ripple).

The maximum possible speed is adjusted with the potentiometer P4 (n_{max}).
Give the max. set value speed (e.g. 10V) and turn P4 (n_{max}) so far that the required speed is achieved.

Right limit: maximal possible speed
Left limit: minimal possible speed

Step	Task
4.5	**Current fine adjustment (I_{adjust})**

Caution:
Normally it is **not** necessary to adjust the potentiometer (I_{adjust}).

If necessary you can adjust the current with the potentiometer (I_{adjust}).

Give set value speed zero, e.g. by short circuiting the set value input Pin 16 (n_{set} +) and Pin 15 (n_{set} -). Adjust potentiometer current fine until no more current flows through the motor winding.

Step	Task
5.	**Error Handling**

Defect	Possible source of defect	Measures
Shaft doesn't rotate	Supply voltage <12 VDC	check Pin 1
	Enable not activated	check Pin 11
	set value speed is 0	check Pin 15, 16
	current limit too low	Check adjustment Poti P3 (or external set value to low)
	bad contacts	check wiring
	wrong wiring	check wiring
Speed is not controlled	encoder signals	check Pin 18 - Pin 21

Interelectric AG specializes in the development, manufacturing and sales of **high quality drive components and systems** under the trade mark **maxon motor**.
The **maxon DC motor** range quite likely represents the world's most extensive variety of moving coil motors.

Interelectric's newly established manufacturing facility in the heart of Switzerland features the most modern equipment. Interelectric presently employs approximately 400 people. All key components are manufactured inhouse with custom design machinery. This is your assurance for efficient production of large to very large quantities, as well as maximum flexibility where special requirements are to be met. Our «modular system» provides for great flexibility and rapid and cost-effective deliveries. Interelectric's extensive R & D department is able to meet the requirements of the rapidly developing market of high technology drive systems. Our sales engineers are at your disposal to discuss tailored solutions for your specialized requirements.

Our expertise:
To convert electronic signals into highly dynamic mechanical motion. Our up to date quality assurance procedures provide for the highest possible quality.
We fulfil quality standard ISO 9001, EN 29001 and BS 5750.

Sales engineers at the factory, in our subsidiaries, as well as carefully and continuously educated distribution partners offer you expert support and consulting – call for the **maxon** advantage!

maxon DC motor

maxon DC motors are high quality drive components and are equipped with high performance permanent magnets.

The patented moving coil rotor represents the heart of our motor. For you, this means the latest technology in compact, high performance, low inertia drives. The program is complemented with precision gearheads for a wide range of speeds and torques. High resolution analog and digital encoders, coupled with state of the art electronics are your assurance of dynamic motion control.

The maxon A-max program

The new **maxon A-max** breakthrough DC motor-program that gives you luxury performance at economy costs. New motor housing, precision-made from rolled steel. New, reduced diameter commutator, employing more segments, provides longer life. Newly designed precious-metal brushes ensure longer life and help minimize power consumption. The added benefit of „snap on" technology allows for greater flexibility in mounting gearheads, encoders and tachometers.

The **maxon A-max** comprises 7 different motors in Ø from 12 to 40 mm; versions with precious-metal or graphite brushes, sleeve or ball bearings and with double ended shafts.

InnovationAward 96
CHAMBER OF COMMERCE OF CENTRAL SWITZERLAND

maxon EC motor

The electronically commutated **maxon EC motors** are particularly noteworthy for their excellent torque handling characteristics, high performance, extremely wide speed range and, of course, their unsurpassed service life.

maxon motor control

This electronic control system is optimized for use with maxon motors. Various 4-quadrant servo-amplifiers meet your needs regarding performance and speed accuracy with **maxon DC motors.** The most sophisticated electronic commutation is available with **maxon EC motors.**
We offer comprehensive solutions for applications requiring precise positioning and controlled rotational motion.

maxon gear

Precision spur and planetary gearheads matched to **maxon motors.**

maxon tacho

maxon tachos and encoders: Only mounted to motors with through shafts for reasons of precision and resonance.

Order the new **maxon**-catalogue with CD-ROM and maxon selection program.
180 pages of helpful information on motors, gears, tachos and positioning control units.

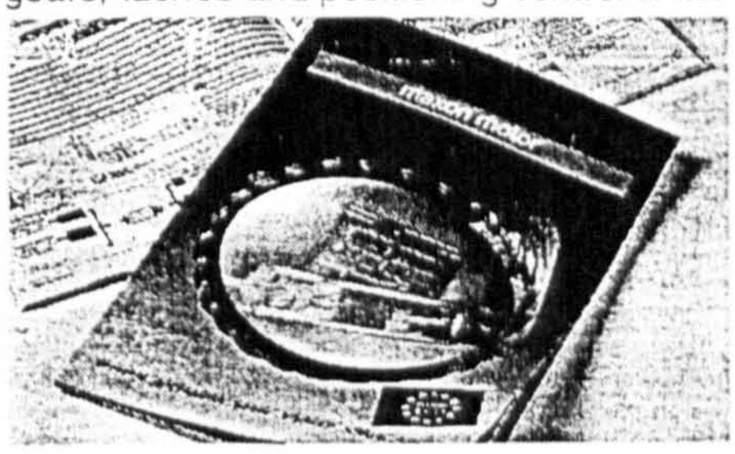

Interelectric AG CH-6072 Sachseln/OW Switzerland Tel.: +41/41-666 15 00 Fax: +41/41-666 16 50

Interelectric SA
Office West Switzerland
Case postale 11
CH-1110 Morges
Tel.: +41/21 - 803 45 48
Fax: +41/21 - 803 45 50

Subsidiaries:
Germany
maxon motor gmbh
Wardeinstrasse 3
D-81825 München
Tel.: +49/89 - 42 04 93-0
Fax: +49/89 - 42 10 89

Germany (North)
maxon motor gmbh
Beithanstrasse 16
D-34637 Schrecksbach
Tel.: +49/6698 96 11-0
Fax: +49/6698 17 16

BENELUX
Sanders-Birnie B.V.
De Giem 22
NL-7547 SV Enschede
Tel.: +31/53 - 432 05 66
Fax: +31/53 - 430 36 65

Spain (Head Office)
maxon motor ibérica s.a.
P. Empres. San Fernando
Edificio Italia
E-28831 Madrid
Tel.: +34/1 - 656 49 73
Fax: +34/1 - 656 48 72

Spain
maxon motor ibérica s.a.
Avenida de Roma, 2 y 4
Oficina 1508
E-08014 Barcelona
Tel.: +34/3 - 425 09 36
Fax: +34/3 - 423 13 52

USA (West)
maxon precision motors, inc.
838 Mitten Road
Burlingame CA 94010 USA
Tel.: +1/415 - 697 96 14
Fax: +1/415 - 697 28 87

USA (East)
maxon precision motors, inc.
231 Weaver Street
Fall River, MA 02720 USA
Tel.: +1/508 - 677 05 20
Fax: +1/508 - 677 05 30

Japan
maxon japan corporation
Shinjuku-Ku
Tokyo 160 Japan
Tel.: +81/3 - 3350 42 61
Fax: +81/3 - 3350 42 30

Representatives:
Australia/New Zealand
M. Rutty & Co. Pty. Ltd.
Mount Kuring-Gai
NSW 2080 Australia
Tel.: +61/2 - 9457 22 22
Fax: +61/2 - 9457 22 99

Austria
Kwapil & Co. GmbH
A-1210 Wien
Tel.: +43/1 - 278 85 85
Fax: +43/1 - 278 85 86

Brazil
AGMS Automação Ind. Ltda.
CEP-01544-010 São Paulo-SP
Tel.: +55/11 - 591 16 32
Fax: +55/11 - 272 01 69

China
Suzhou Servo Dynamics Co. Ltd.
Suzhou, Jiangsu
Tel.: +86/512 - 53 06 167
Fax: +86/512 - 53 03 199

Denmark
Famell Compower A/S
DK-2730 Herlev
Tel.: +45/44 - 92 66 20
Fax: +45/44 - 92 66 02

Finland
Oy Stork AB
SF-01300 Vantaa
Tel.: +35/89 - 873 40 11
Fax: +35/89 - 873 41 33

France
mdp
21, Porte du grand Lyon, Neyron
F-01707 Miribel Cedex
Tel.: +33/472 - 01 83 00
Fax: +33/472 - 01 83 09

Great Britain
Trident Engineering Ltd.
Winnersh, Wokingham
Berks, RG41 5AS,
Tel.: +44/1189 - 78 64 44
Fax: +44/1189 - 77 63 45

Hong Kong
Servo Dynamics (H.K.) Ltd.
Tsuen Wan, N.T. Hong Kong
Tel.: +852/240 999 86
Fax: +852/240 978 72

Hungary
Uzimex AG Budapest
H-1325 Budapest
Tel.: +36/1 - 120 82 58
Fax: +36/1 - 129 62 14

Israel
Servotronix Ltd.
12 Hachoma St. P.O.B. 5096
Rishon le Zion, 75105
Tel.: +972/3 - 961 65 95 /6
Fax: +972/3 - 961 65 79

Italy
Abaco S.r.L.
I-20020 Arese MI
Tel.: +39/2 - 9358 01 88
Fax: +39/2 - 9358 22 03

Korea
E.G. Incorporated
104-10, Kuro Dong
Kuro-Ku, Seoul, Korea
Tel.: +82/2 - 839 42 52
Fax: +82/2 - 839 42 55

Norway
Stork AS
N-1300 Sandvika
Tel.: +47/67 - 56 76 20
Fax: +47/67 - 56 90 20

Singapore
Servo Dynamics Pte Ltd
SIN-349247 Singapore
Tel.: +65/2 - 98 60 11
Fax: +65/2 - 96 92 76

South Africa
A.S.D.
2128 Rivonia/South Africa
Tel.: +27/11-444 23 33
Fax: +27/11-444 17 06

Sweden
AB D.J. Stork
S-172 21 Sundbyberg
Tel.: +46/8 - 635 60 00
Fax: +46/8 - 635 60 01

Taiwan
USE Electronics Co., Ltd.
Chung Hsiao E. Road
Taipei, Taiwan, R.O.C.
Tel.: +88/62 - 393 48 25
Fax: +88/62 - 341 49 00

Czech Rep./Slovakja
Uzimex Praha spol.s.r.o. GmbH
Na Celne 5/524
CS-150 00 Prag 5
Tel.: +42/2 - 54 45 01
Fax: +42/2 - 53 46 05

BG/PL/R/SLO/YU
Uzimex AG
CH-8834 Schindellegi
Tel.: +41/1 - 787 31 61
Fax: +41/1 - 784 82 65

APPENDIX E

TACHOGENERATOR DATA SHEET

Tlx 844 605 mimo
Fax 091 59 51 08

DC-Tachogenerators

Type 2225, 2233

Tacho type		2225 U 4,3 G9	2233 U 007 G9	2233 U 011 G9	
EMF constant	e_s	4,3	7,0	11,0	mV/rpm
		4,11	6,69	10,51	mV/rad/s
Tolerance of EMF constant		± 1	± 1	± 1	%
Load resistance	RL ≥	25	35	81	KΩ
Operating speed, max. recommended	$n_{e\,max.}$	5 000	5 000	3 000	rpm
Current, max. recommended		limited by the load resistance			
Terminal resistance	R	260	350	810	Ω
Ripple voltage, average (peak-peak)	≤	7	5	5	%
Ripple frequency, cycles		10	14	14	per rev.
Linearity error, unloaded					
between 500 and 5 000 rpm	+/–	0,2	0,2	0,2	%
Reversion error	+/–	0,2	0,2	0,2	%
Temperature coefficient of EMF		0,02	0,02	0,02	%/°C
Temperature coefficient of resistance		0,4	0,4	0,4	%/°C
Inductance	L	7	15	30	mH
Armature inertia	J	1,65	2,5	2,5	gcm²
Number of poles		2	2	2	
Commutator segments		5	7	7	gold alloy
Brush leaves		5	5	5	gold alloy
Magnet		permanent Alnico magnet, calibrated			
Direction of rotation		reversible			
Polarity		+ on plus pole if shaft is driven in clockwise direction			
Operating temperature range					
– standard		– 30 ... + 85			°C
– optional		– 55 ... + 125			°C
Shaft load max.					
– radial at 3 000 rpm (3 mm from bearing)		1,2	1,2	1,2	N
– axial at 3 000 rpm		0,2	0,2	0,2	N
– axial at standstill		20	20	20	N
Shaft bearings					
– standard		sintered sleeve bearings (optional ball bearings)			
Weight		45	61	61	g

Features

Design
These tachogenerators feature the patented skew wound ironless rotors (System Faulhaber®).

Commutation system
Commutator and brushes are made of high quality gold alloy and provide a minimized but constant contact resistance as well as insensibility to changes in environment.

Advantages
This unique design results in following advantages:
- linear speed/back-EMF characteristics
- extreme low starting friction – even after long standstill
- low armature inertia
- high efficiency
- smooth running

MINIMOTOR SA
CH-6982 Agno
Switzerland
Tel 091 59 18 21
Tlx 844 605 mimo
Fax 091 59 51 08

DC-Tachogenerators

Type 2225, 2233

Dimensional drawings

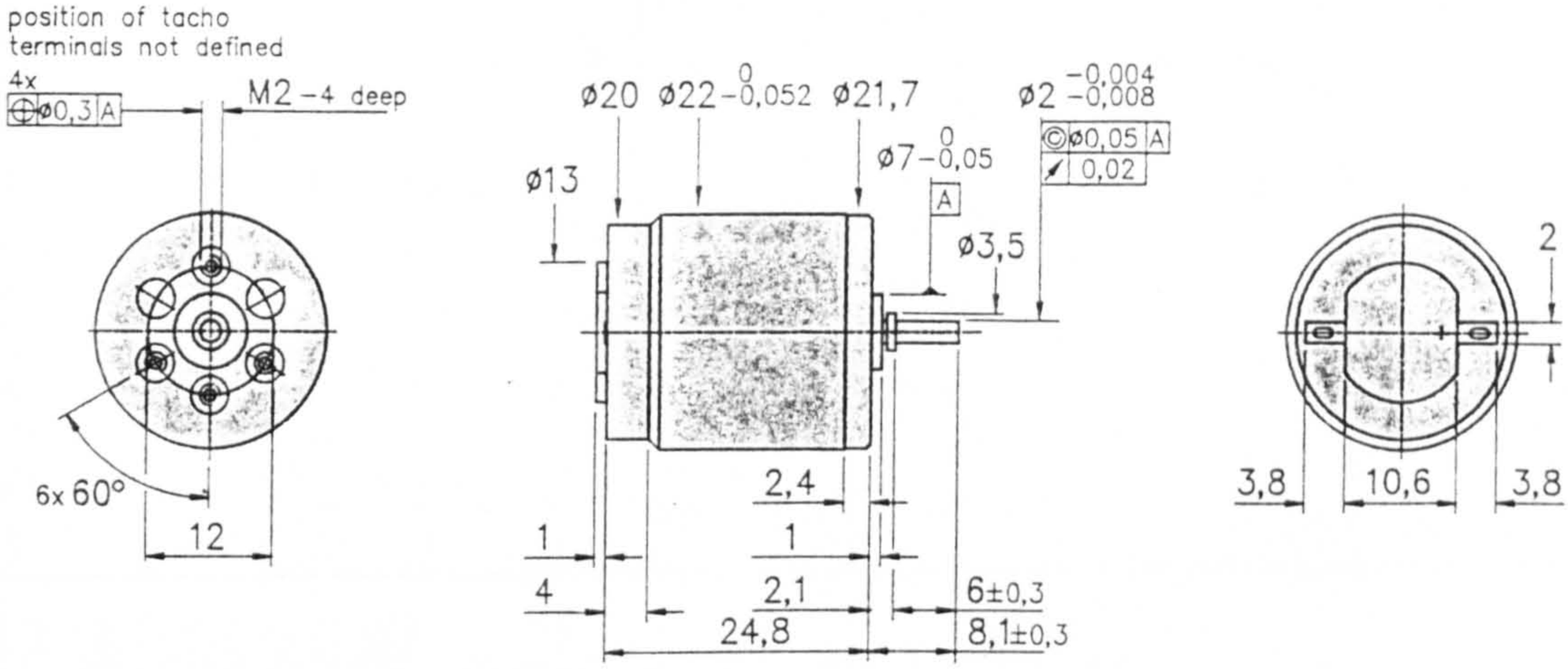

2225 U 4,3 G9

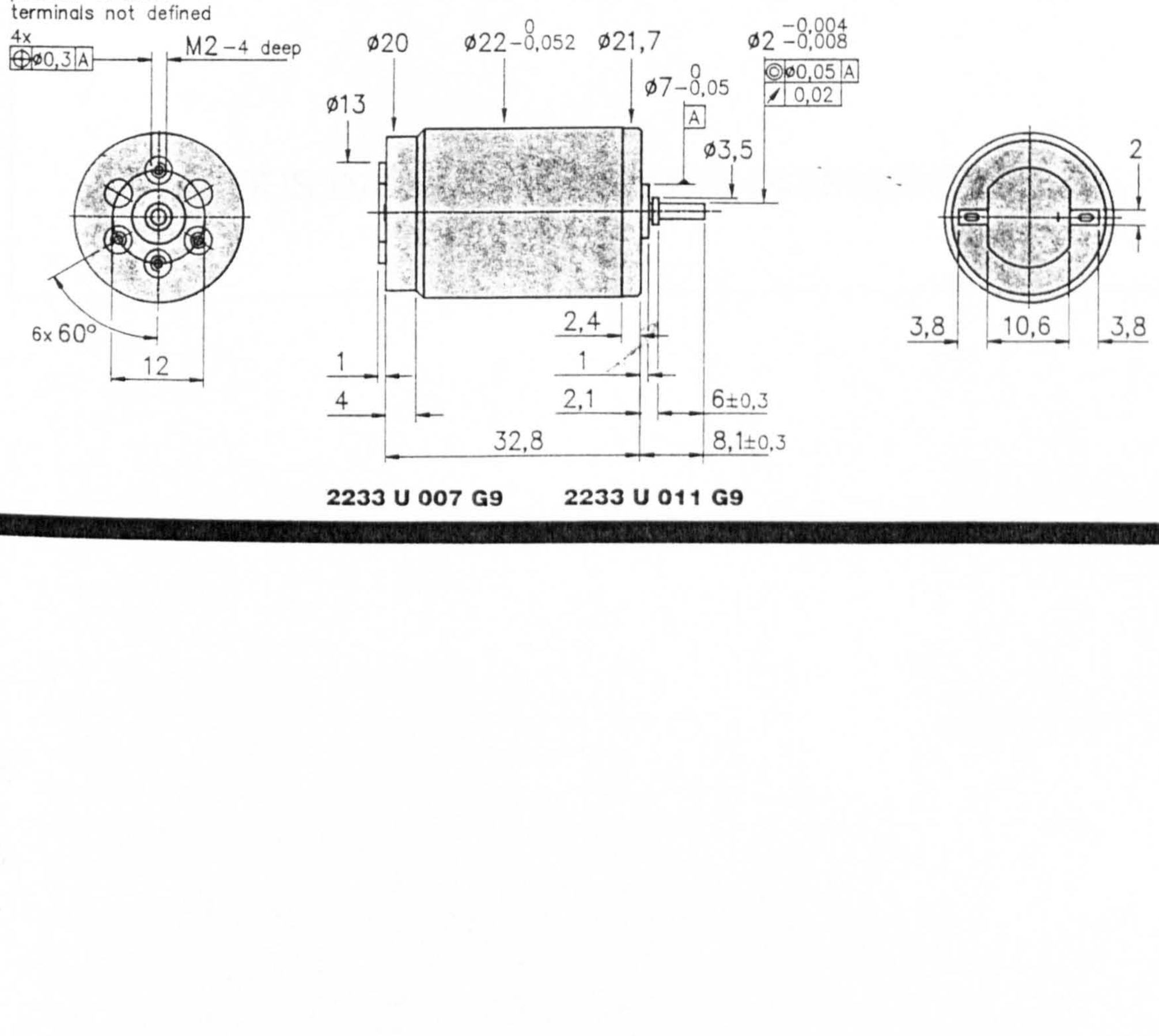

2233 U 007 G9 **2233 U 011 G9**

APPENDIX F

VARIOUS DATA SHEETS FOR EQUIPMENT USED

Separate drivers for each type of device means enhanced device performance

EDRE Control Panel Applet supplies information on installed boards

Software driver libraries included support all popular 32-bit programming languages. These include Delphi, C/C++ Builder, Visual C/C++, Visual Basic, Visual J++, Win 95/98, Windows NT, etc. Drivers will also be available for TestPoint, DasyLab, LabView and HP VEE.

The EDRE SDK allows the user to control the board via Win32 API calls.

Demo examples using polled I/O and interrupts under Windows as well as VBX, OCX and ActiveX Control software is included in the EDRE.

SPECIFICATION

ANALOG INPUTS

Input channels	16/32 single-ended or 8/16 differential
Overvoltage protection	±35V (powered on); ±25V powered off
Resolution	12 bit (1 in 4096)
Input ranges	±5V, ±10V, 0 to 10V
Input coupling	DC
System accuracy	±1 LSB depending on environment
A/D linearity	Differential ±¾ LSB max
SNR	84dB typ
Total harm dist.	-98dB
System accuracy	±2 LSB depending on environment
Acquisition rate	F series 330KS/s max G series 100KS/s
A/D FIFO buffer	2k samples
Acquisition modes	Polled I/O, interrupts, REP INSW

AMPLIFIER CHARACTERISTICS

Input Impedance	10GΩ/20pF (On chan) 10GΩ/100pF (Off chan)
Offset voltage	Adjustable to zero
Input Gains	1, 10, 100, 1000 (or 1, 2, 4, 8) Error: Adjustable to 0 Nonlinearity: 0.002% (typ), 0.015% (max) [G<1000] 0.02% (typ), 0.06% (max) [G=1000]
	Accuracy: 0.25% max, 0.05% typ CMRR: 100dB typ, 80dB max for G=1 Monotonicity: 0 to 70°C
Temperature drift	6ppm/°C (Full scale) 1ppm/°C (Bipolar zero) ±30ppm/°C (Gain typ)

DYNAMIC CHARACTERISTICS

Bandwidth (small signal)	1.0MHz (G<1000) 250kHz (G=1000)
Full power bandwidth	1MHz for G<1000, 100kHz for G=1000
Crosstalk	-85dB, DC to 100kHz
System Noise	±1LSB (G=1)

ANALOG OUTPUTS

No of Channels	4 x 12 bit
Accuracy	±1 LSB
DNL	½ LSB max
Output Ranges	±5V, ±10V, 0 to 10V, 0 to 13V
Update Rate	100kHz (depending on computer)
Offset Error:	Unipolar: ¼ LSB typ, 1 LSB (max) Bipolar: ½ LSB typ, 2 LSB (max)
Resolution	16 bits

DIGITAL I/O

No of TTL I/O lines	24 in 3 ports (8255 PPI)
Digital Logic Levels	High: 2.0V (min), 5.0V max Low: 0.0V (min), 0.8V (max)
Current Output	±3mA (source/sink)
Interrupt support	Yes (Mode 0, Mode 1, Mode 2)

EXTERNAL INTERFACE

Connector Types	SCSI 50-way Right Angle Female IDC40 Header (for digital I/O)

COUNTER TIMERS

Resolution	16-bit
Clock Frequency	2 or 8 Mhz (for A/D)
No of counters	3 (2 used for A/D conv.)

PCI INTERFACE

Base Address	Auto selected
No of registers	Sixteen 32 bit
Interrupts	Auto selected

ENVIRONMENTAL

Rel. humidty	0% to 90% (non-condensing)
Operating temp	0°C to 70°C
Board dimensions	193mm x 111mm
Power requirements	+5V @ 1.2A typ

(G = gain)

Separate drivers for each type of device means enhanced device performance

EDRE Control Panel Applet supplies information on installed boards

Software driver libraries included support all popular 32-bit programming languages. These include Delphi, C/C++ Builder, Visual C/C++, Visual Basic, Visual J++, Win 95/98, Windows NT, etc. Drivers will also be available for TestPoint, DasyLab, LabView and HP VEE.

The EDRE SDK allows the user to control the board via Win32 API calls.

Demo examples using polled I/O and interrupts under Windows as well as VBX, OCX and ActiveX Control software is included in the EDRE.

SPECIFICATION

ANALOG INPUTS

Input channels	16/32 single-ended or 8/16 differential
Overvoltage protection	±35V (powered on); ±25V powered off
Resolution	12 bit (1 in 4096)
Input ranges	±5V, ±10V, 0 to 10V
Input coupling	DC
System accuracy	±1 LSB depending on environment
A/D linearity	Differential ±¾ LSB max
SNR	84dB typ
Total harm dist.	-98dB
System accuracy	±2 LSB depending on environment
Acquisition rate	F series 330KS/s max G series 100KS/s
A/D FIFO buffer	2k samples
Acquisition modes	Polled I/O, interrupts, REP INSW

AMPLIFIER CHARACTERISTICS

Input Impedance	10GΩ/20pF (On chan) 10GΩ/100pF (Off chan)
Offset voltage	Adjustable to zero
Input Gains	1, 10, 100, 1000 (or 1, 2, 4, 8) Error: Adjustable to 0 Nonlinearity: 0.002% (typ), 0.015% (max) [G<1000] 0.02% (typ), 0.06% (max) [G=1000]
	Accuracy: 0.25% max, 0.05% typ CMRR: 100dB typ, 80dB max for G=1 Monotonicity: 0 to 70°C
Temperature drift	6ppm/°C (Full scale) 1ppm/°C (Bipolar zero) ±30ppm/°C (Gain typ)

DYNAMIC CHARACTERISTICS

Bandwidth (small signal)	1.0MHz (G<1000) 250kHz (G=1000)
Full power bandwidth	1MHz for G<1000, 100kHz for G=1000
Crosstalk	-85dB, DC to 100kHz
System Noise	±1LSB (G=1)

ANALOG OUTPUTS

No of Channels	4 x 12 bit
Accuracy	±1 LSB
DNL	½ LSB max
Output Ranges	±5V, ±10V, 0 to 10V, 0 to 13V
Update Rate	100kHz (depending on computer)
Offset Error:	Unipolar: ¼ LSB typ, 1 LSB (max) Bipolar: ½ LSB typ, 2 LSB (max)
Resolution	16 bits

DIGITAL I/O

No of TTL I/O lines	24 in 3 ports (8255 PPI)
Digital Logic Levels	High: 2.0V (min), 5.0V max Low: 0.0V (min), 0.8V (max)
Current Output	±3mA (source/sink)
Interrupt support	Yes (Mode 0, Mode 1, Mode 2)

EXTERNAL INTERFACE

Connector Types	SCSI 50-way Right Angle Female IDC40 Header (for digital I/O)

COUNTER TIMERS

Resolution	16-bit
Clock Frequency	2 or 8 Mhz (for A/D)
No of counters	3 (2 used for A/D conv.)

PCI INTERFACE

Base Address	Auto selected
No of registers	Sixteen 32 bit
Interrupts	Auto selected

ENVIRONMENTAL

Rel. humidty	0% to 90% (non-condensing)
Operating temp	0°C to 70°C
Board dimensions	193mm x 111mm
Power requirements	+5V @ 1.2A typ

(G = gain)

Separate drivers for each type of device means enhanced device performance

EDRE Control Panel Applet supplies information on installed boards

Software driver libraries included support all popular 32-bit programming languages. These include Delphi, C/C++ Builder, Visual C/C++, Visual Basic, Visual J++, Win 95/98, Windows NT, etc. Drivers will also be available for TestPoint, DasyLab, LabView and HP VEE.

The EDRE SDK allows the user to control the board via Win32 API calls.

Demo examples using polled I/O and interrupts under Windows as well as VBX, OCX and ActiveX Control software is included in the EDRE.

SPECIFICATION

ANALOG INPUTS

Input channels	16/32 single-ended or 8/16 differential
Overvoltage protection	±35V (powered on); ±25V powered off
Resolution	12 bit (1 in 4096)
Input ranges	±5V, ±10V, 0 to 10V
Input coupling	DC
System accuracy	±1 LSB depending on environment
A/D linearity	Differential ±¼ LSB max
SNR	84dB typ
Total harm dist.	-98dB
System accuracy	±2 LSB depending on environment
Acquisition rate	F series 330KS/s max G series 100KS/s
A/D FIFO buffer	2k samples
Acquisition modes	Polled I/O, interrupts, REP INSW

AMPLIFIER CHARACTERISTICS

Input Impedance	10GΩ/20pF (On chan) 10GΩ/100pF (Off chan)
Offset voltage	Adjustable to zero
Input Gains	1, 10, 100, 1000 (or 1, 2, 4, 8) Error: Adjustable to 0 Nonlinearity: 0.002% (typ), 0.015% (max) [G<1000] 0.02% (typ), 0.06% (max) [G=1000]
	Accuracy: 0.25% max, 0.05% typ CMRR: 100dB typ, 80dB max for G=1 Monotonicity: 0 to 70°C
Temperature drift	6ppm/°C (Full scale) 1ppm/°C (Bipolar zero) ±30ppm/°C (Gain typ)

DYNAMIC CHARACTERISTICS

Bandwidth (small signal)	1.0MHz (G<1000) 250kHz (G=1000)
Full power bandwidth	1MHz for G<1000, 100kHz for G=1000
Crosstalk	-85dB, DC to 100kHz
System Noise	±1LSB (G=1)

ANALOG OUTPUTS

No of Channels	4 x 12 bit
Accuracy	±1 LSB
DNL	½ LSB max
Output Ranges	±5V, ±10V, 0 to 10V, 0 to 13V
Update Rate	100kHz (depending on computer)
Offset Error:	Unipolar: ¼ LSB typ, 1 LSB (max) Bipolar: ½ LSB typ, 2 LSB (max)
Resolution	16 bits

DIGITAL I/O

No of TTL I/O lines	24 in 3 ports (8255 PPI)
Digital Logic Levels	High: 2.0V (min), 5.0V max Low: 0.0V (min), 0.8V (max)
Current Output	±3mA (source/sink)
Interrupt support	Yes (Mode 0, Mode 1, Mode 2)

EXTERNAL INTERFACE

Connector Types	SCSI 50-way Right Angle Female IDC40 Header (for digital I/O)

COUNTER TIMERS

Resolution	16-bit
Clock Frequency	2 or 8 Mhz (for A/D)
No of counters	3 (2 used for A/D conv.)

PCI INTERFACE

Base Address	Auto selected
No of registers	Sixteen 32 bit
Interrupts	Auto selected

ENVIRONMENTAL

Rel. humidty	0% to 90% (non-condensing)
Operating temp	0°C to 70°C
Board dimensions	193mm x 111mm
Power requirements	+5V @ 1.2A typ

(G = gain)

Filter and Amplifier used from figure 5.11

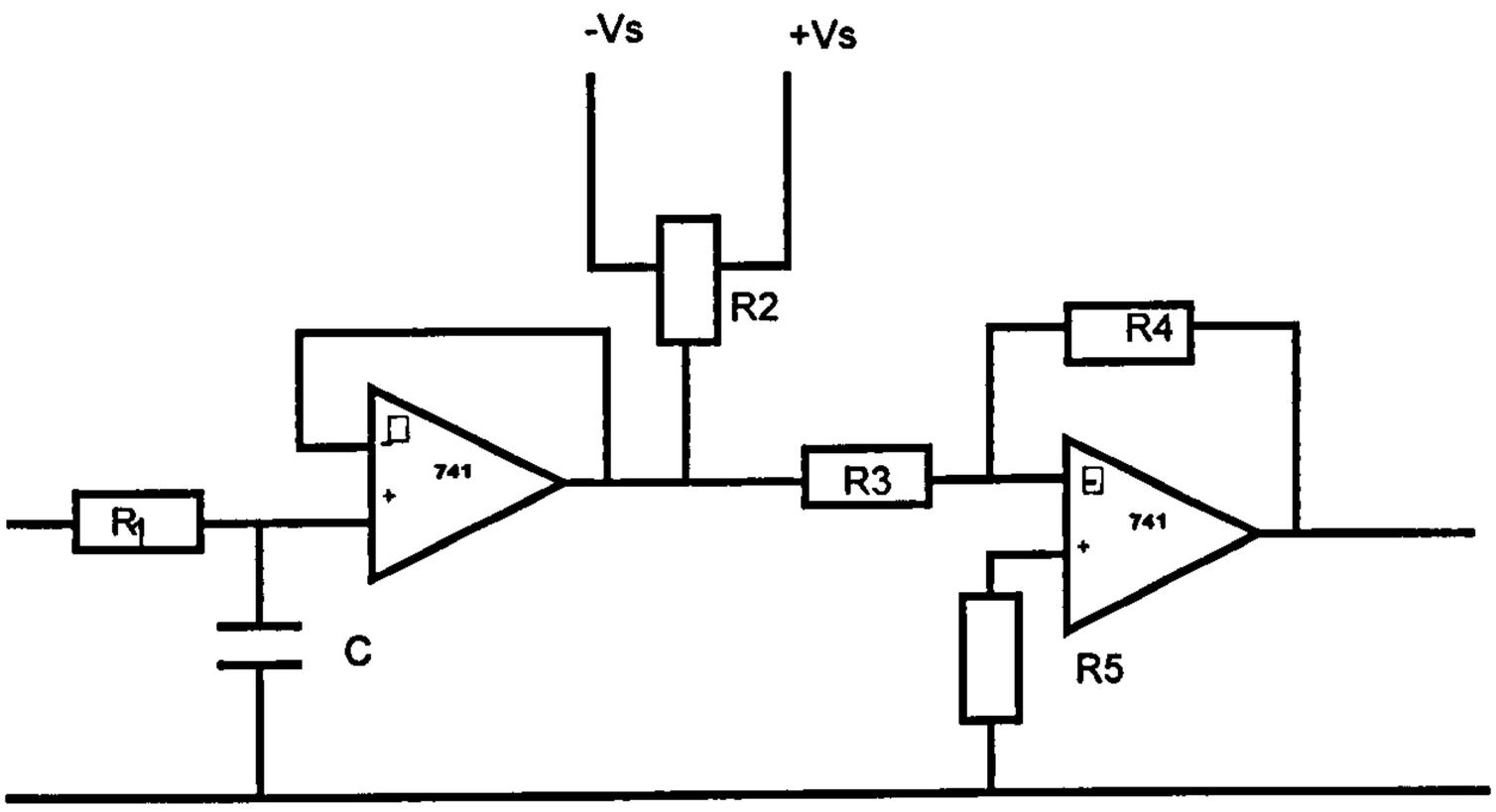

The maximum voltage change when the Orthosis foot moved the full step was 2.4 volts. However to use the maximum possible resolution of the D/A converter, an amplifier was used. R3 and R4 were chosen so as to give an amplification factor of 3.5.

The filter used was the same one shown in figure 4.12.

Dynamometer Specification

Manufactureres	JJ. Lloyd Instruments Limited
Type No.	FH1
Ser. No.	3128301
Resolution	0-2 Nm

Potentiometer Used

Manufacturers	RS
Resistance	$20K\Omega \pm 20\%$
Lin	0.5%
Part No.	173-1596 01

PAGE NUMBERING AS ORIGINAL

References

Allidina, A.Y. and H. Yin, Explicit pole assignment self-tuning algorithm "International Journal of Control, Vol 42, PP 113-1130, (1985).

Astrand P.O., Rodhal K., (1970), "Textbook of Work Physiology", New York. Mcgraw Hill.

Astrom k.J., and Wittenmark B., (1990) "Computer controlled Systems: Theory and design, 2nd edition, Prentice-Hall, Inc. PP 19, PP 511.

Astrom, K.J., (1980), "Robustness of a design method based on assignment of poles zeros" IEEE Transactions on Automatic control, Vol. AC-25 No 3, June 1980.

Astrom, K.J., Jury E.I., and Angiel, R>G, (1970), "A numerical method for the evaluation of complex integrals. "IEE Transaction on Automatic control" August, PP 468-471.

Beckmann J. (1987) "The Louisiana State University Reciprocating Gait Orthosis". Physiotherappy 73(8): 386-392.

Bessey E.J., Bendall M.J., Pearson M., (1988). "Muscle strength in the triceps surae and objectively measured customary walking activity in men and women over 65 years of age. Clin Sci 74, 85-89.

Blessey R. (1978), Energy cost of normal Walking, "Orthopedic Clinics of North America PP 356-358.

Butler P. Engelbrecht M., Major R., Tah J., Stallard J., Patric J. (1989). "Physiological cost index of walking for normal children and its use as an indicator of physical handicap" Developmental Medicine and Child Neurology 26:607-612.

Butler P.B., Major R.E. (1987), The Parawalker a rational approach to the provision of reciprocal ambulation for paraplegic patients. "Physiotherapy 73(8): 393-397.

Butler P.B., Major R.E. and Patrick J.H., (1984). "The technique of reciprocal walking using the hip guidance Orthosis (H.G.O) with crutches" Prosthetics and Orthotics International, 8, 33-38.

Butler P.B., Farmer I.R., Poiner R., Patrick J.H., "Use of the Orlau Swivel Walker for the Severely Handicapped Patient" October (1982), Physiotherapy , Vol. 68, No. 10.

Caldwell D.G., Medrana-Cerda G.A. & Goodwin M.J. "Braided Pneumatic Actuator control of a multi jointed manipulator", IEE Int. Conf. on Systems, Man and Cybemetic Vol. 1, 423-428, 1993

Cerny K., Waters R., Hislop H., Perry J., (1980). "Walking and wheelchair energetics in persons with paraplegia. Physical Therapy 60: 1133-1139.

Chantraine A., Crielaard J.M., Onkelinx A., Pirnay F., (1984), "Energy expenditure of ambulation in paraplegics; effects of long term use of bracing". Paraplegia 22: 173-181.

David A. Yngve. Roy Douglas and John M. Roberts. "The reciprocating Gait Orthosis in Myelomeningocele Journal of Padiatric Orthopedics 4: 304-310, (1984) Raven Press, New York.

Davies J.B., (1977) "Use of heart rate in assessment of Orthoses" Physiotherapy, April 1977, Vol. 63.

Dounis E., Rose G.K., Wilson R.S.E., Steventon R.D (1980). "A comparison of efficiency of three Types of Crutches using Oxygen Consumption" Rheumatology and Rehabilitation, 19, 252-255.

Downes C.G., Hill S.L., Gray J.O., "Distributed Control of an Electrically Powered Hip Orthosis". Proc. of Control 1994, Int. Conf. on Control, Vol. 1, 24-30, march (1994).

Downes C.G., Hill S.L., Gray J.O., "Control Aspects of a Powered Hip Orthosis", Proc. of 13th IASTED. Int. Conf, on Modelling, Identification and Control, 31-34, February (1994).

Djaferis, T.E. (1983), "Robust Pole-assignment for system with parameters". Proceedings of the 22nd IEEE Conf. on Decision and Control, San Antonio PP 636-639.

Djaferis, T.E. (1983) " Achieving Robust Stability by sensing additional System outputs". Proceedings of the 25th IEEE Conf. on Decision and Control, Athens PP 1451-1456.

Dyson, R.J. "The physiological cost of amputee locomotion" PhD thesis, University of Strathclyde, Glasgow, (1977).

Edwards J.,Gray J.O., "Powered Hip Orthosis" UK Patent application N0. 9314825, (1993).

Edwards J. University of Salford U.K, Powel E. and Sykes L.(1993), North Western Orthotic Unit. Salford U.K, "RGO restoration of upright mobility in paraplegics" The English experience.

Eldaw E.E. (1991). Adaptive Position Control of a D.C Motor Based on Robust Controller Design.

Electro-Craft Corporation, Fifth Edition, (1980) "DC Motors, Speed Controls, Servo Systems" An Engineering Handbook.

Ferrate G.A., (1986), About low Cost Automation Proceedings of IFAC Low cost Automation, Spain PP 1-3.

Florence J. (1986). Roy Douglas Brace. Letter in Link, May/June.

Francesco Donati and Maurizio Vallauri, (1984) "Guaranteed Control of Almost Linear Plants", IEE Transactions on Automatic Control Vol. AC-29, NO. 1, January 1984.

Garcia C.E. and Morari M. (1982). Internal model control 1: A unifying review and some new results. Industrial engineering chemical process, Design and Development, 21, PP 308-323.

Goodwin G.C. and Payne, R.L. (1977), Dynamic system identification Experimental design and data analysis, Academic press INC.

Grundman J. and Sierg A., Computer Control of Multi-task exoskeleton for paraplegics. In: on theory and practice of robots and manipulators II CISM-IFTOMM symposium, Warszawa, PNN, (1976).

Guttmann L. (1976). Spinal Cord Injuries, Blackwell Scientific Publivations, 2nd edn, ch 35, 605-607.

Hassan K.Khalil (1981). "On the Robustness of Output Feedback Control Methods to modelling Errors", IEEE Transaction on Automatic Control Vol. AC-26 No.2 April.

Hector Roistein, Alfredo Desages and Jose A. Romagnoli (1989), "Robustness Consideration in Reduced-Order Controller", IEE Transactions on Automatic Control, Vol. 34, No. 4, April 1989.

Henshaw J.T., and Griffiths J.C. (1981), "Walking appliances for paraplegics and tetraplegics In: " Orthopedic Mechanics Vol. III (Ed). Ghista D.N. and Road R. Academic press, London 115-135.

Hill J.W. Hydraulically Powered Lower Limb Orthosis, Stanford Research Institute Mento Park California 94025, U.S.A

Hirokawa S., Grimm M., Thanah L., Solomonow M., Baratta R.V., (1990). "Energy consumption in paraplegic ambulation using the reciprocating gait orthosis and electric stimulation of the thigh muscles. Arch Phys Med Rehabil 71:687-694.

Hoffer M.M., Feiwell E. Perry R. Perry J. and Bonnett C. (1973). "Functional Ambulation in Patients with Myelomeningocele". Journal of Bone and Joint Surgery, 55A, 1, 137-148.

Huang C.T., Kuhlemeier K.V., Moore M.B., Fine P.R., (1979). "Energy cost of ambulation in paraplegic patients using Craig Scott braces. Archives of Physical Medicine and Rehabilitation 60:595-600.

Hyde S.A., Scott O. M. Goddard C.M. and Dubowitz V. (1982). "Prolongation of Ambulation in Duchenne muscular dystrophy by appropriate Orthoses". Physiotherapy, 68,4, 105-108.

Isakov E., Douglas R., Berns P., (1992). "Ambulation using the reciprocating gait orthosis and functional electrical stimulation" Paraplegia 30, 239-245.

Iserman R. (1980), "Practical Aspects of Process identification, Automatic Vol. 16, PP 575-578.

Lehman J.F., and Redford J.B. (Ed), In "Orthotics Etcetra", Baltimore U.S.A, Williams & Wilkins, (1986). Lower Limb Orthotics, 278-351.

Leigh J.R. (1985). "Applied Digital Control. Prentice Hall International.

Levy R., (1980). "The objective measurement of disability in the physical handicapped", Ph.D thesis, University of Strathclyde, Glasgow.

Limo and M.M. Bayoumi (1989), "A Novel Approach to the Explicit Pole Assignment Self-Tuning Controller design" IEEE Transactions on Automatic Control. Vol. 34, No.3, March 1989.

Ljung L. 1991. Issues in System Identification IEEE Control System Magazine, Vol. 11, No.1 PP 25.

Ljung L. (198), System Identification: Theory for the user. Englewood cliffs N.J, Prentice Hall Inc.

MacGregor J., (1981) " The evaluation of patient performance using long-term ambulatory monitoring technique in the domiciliary environment" February, Physiotherapy, Vol. 67, No. 2.

MacGregor J., (1979a)"The objective measurement of physical performance wit long term ambulatory physiological surveillance equipment". Proceedings of the *third* International Symposium on Ambulatory Monitoring, Stott, Raftery and Goulding (eds), 29-39.

McCall, R.E., and Schmidt, W.T., (1986), "Clinical Experience with the Reciprocal Gait Orthosis in Myelodysplasia", Journal of Paediatric Orthopaedics, 6, 2, 157-161.

Merkel K.D., Miller N.E., Merritt J.L., (1985). "Energy expenditure in patients with low, mid or high thoracic paraplegia using Scott Craig knee ankle foot Orthoses. Mayo Clinical Proceedings 60:165-168.

Merkel K.D., Miller N.E., Westbrooke P.R., Merritt J.L., (1984). "Energy expenditure of paraplegic patients standing and walking with two knee ankle foot orthoses". Archives of Physical Medicine and Rehabilitation 65:121-124.

Micallef J.P. & Rabischong E. " Active Electrical Orthosis as a simulation tool for F.E.S Program, Abs. of the commission of European Communities, 1st European Conf. on Biomedical Engineering, R.B.M. 1,13,129-130, (1991).

Michael W. Whittle, Paraplegic Locomotion "Clinical Rehabilitation (1988), 2: 45-49.

Miller N.E., Merritt J.L., Merkel K.D., Westbrook P.R., (1984). "Paraplegic energy expenditure during negotiation of architectural barriers. Arch Phys Med Rehabil 65:778-779.

Miyamoto H., Israel I., Miyamoto H., Mori S., Sono A. & Sakurai Y. (1985), "Approach to a Powered Orthosis for Paralysed Lower Limbs", Proc. of Int Conf. of Advanced Robotics, ICAR 85, 451-458.

Miyamoto H., Sano A. Mari S., Sand Sakuri Y., (1983), " Use of a Powered Orthosis for Paralysed Lower Limbs Progress in Artificial Organs (3rd ISAO Symposium) Kyoto, Japan, November, PP 957-961.

Mossberg K.A., Linion K.A., Friskf K., (1990), "Ankle-foot Orthoses: effect on energy expenditure of gait in spastic diplegic children. Arch Phys Med Rehabil 71, 490-494.

Motloch W., (1992). Principles of Orthotic management for child and adult paraplegia and clinical experience with the Isocentric R.G.O. In: Proceedings of the 7th world congress of the International Society for Prosthetics and Orthotics, Chicago, II, June 28- July 3, 1992-Copenhagen: ISPO. P28.

Mulder A.J., Veltink P.H. & Boom H.B.K., (1992) "On/Off Control in F.E.S induced standing up: a model study and experiments", Medical & Biological Engineering & Computing, 30, 205-212.

Mustafa, M.M. (1989), "Pole-assignment higher Order Controllers and applications to adaptive Control with on-line Supervision, PhD Salford University.

Mustaffa, M.M., and Medrano-Cerda G.A., (1989b), "On the use of High Order Controllers to Improve the Robustness and Performance of Pole-Assignment Controllers". 28th IEEE Conf. On Decision and Control, Tampa, PP. 1234-1235.

Nakagiri K.I., (1976), "Energy Cost of Floor Walking in Static Encephalopthy Children with and without their Plastic ankle-Foot-Orthosis. Stanford University, California, division of Physical Therapy, Thesis.

Nene A.V., M.B., B.S., Dorth, MS(ORTH), Mch Orth, Patrick J.H., Paraplegia, Vol 27, Part 1, (1989), NEME AV ET AL, "Energy Cost of Paraplegic Motion With the ORLAN Para walker.

Patrick J.H., (1986), "Developmental research in Paraplegic Walking, "British Medical Journal 262,2788.

Paul J. (1975) in book by Grive D.W., " Techniques for analysis of human movement Lepus books, London fig 12, PP 169.

Petrofsky J.S., Smith J.B., (1991). Physiologic costs of computer-controlled walking in persons with paraplegia using a reciprocating gait Orthosis. Arch Phys Med Rehabil 72, 890-896.

Petrofsky J.S., Phillips C.A., Larson P., and Douglas R. (1985). "Computer Synthesized Walking: An application of Orthosis and functional electrical Stimulation (F.E.S), Journal of Neurological and Orthopaedic Medicine and Surgery, 6,3, 219-230.

Phillips C.A., Hendershot D.M., "Functional electrical stimulation and reciprocating gait Orthosis for ambulation exercise in a tetraplegic patient" a case study. Paraplegia 29, 268-276.

Postlethwait I., Gu D.W., O'Young S.D. and Tombs M.S. (1986). Industrial Control Systems design using H_∞ optimisation, "Proceedings of the 25th IEEE Conference on Decision and Control, Athens PP. 12-13.

Rabischong P., Bel J.P., Hill J., Peruchon E. Simon M., Screve J., Pelegrin M., Benzaken A., Tomovic R., Lazarevic S., Javkovic S. & clot A. (1975), "The Amol Project", Proc. of 5th International Symp. On Advances in External Control of Human Extremities, 33-42.

Ralston H.J., (1965). "Effect of immobilisation of various body segments on energy costs of human locomotion". Proc. 2nd I.E.A. Conf. Dartmund (Supplement to Ergonomics, p 53).

Rose G.K., (1986), "Principles & Practice of Orthotics" William Heinemann, Medical books London PP 47-48.

Riadi I.C.J. (1990), "Robust Controller design and Identification of Position Controller design and Identification of Position Control System for a DC motor, Msc dissertation Salford University.

Rose G.K., Stallard J. and Sankarankutty M. (1983). "A clinical review of the Orthotic treatment of Myelomeningocele patients". Journal of Bone and Joint Surgery, 65B, 3, 242-246.

Rose G.K., Stallard J. and Sankarankutty M. (1981). "Clinical evaluation of Spina bifida patients using Hip Guidance Orthosis". Developmental Medicine and Child Neurology, 23, 30-40.

Rose G.K. (1980) "Orthosis for Severely Handicapped –rational or empirical choice. Physiotherapy 66: 76-81.

Rose G.K. (1979), "Principles and Practice of Hips Guidance Articulation " Prosthetics and Orthotics International 3:37-43.

Scrutton D. (1971). " A Reciprocating Brace with Polyplanar Hip Hinges used on Spina Bifida Children". Physiotherapy, 57,2, 61-66.

Solomonow M. Baratta R., Hirokaw S., Rightor N., Walker W., Beaudette P., Shoj H., Ambrosia D. (1989), "The R.G.O. Generation II, Muscle Stimulation Powered Orthosis as a Practical Walking System for Thoracic Paraplegics; Orthopedics, 12(10): 1309-1315.

Stallard J. Major R.E. Poiner R. Farmer I.R. Jones N. (1986), "Engineering design Consideration of the ORLAU Para Walker and F.E.S Hybrid System". Engineering in Medicine 15: 123-129.

Stallard J. and Rose G.K. (1981). "Independence for adult paraplegics in Swivel Walkers". Journal of Medical Engineering and Technology, 5, 3, 136-7.

Stallard J. Rose G.K. (1980), "Clinical Decision making with the Aid of ambulatory of heart rate". Prosthetics and Orthotics International 4, 91-96.

Stallard J. Tait J.H., Davies J.R., (1978), " Assessment of Orthotics by means of Speed and Heart Rate" Journal of Medical Engineering and Technology 2, 22-24.

Stanic U. & Tmkoczy A., (1974), "Closed loop Positioning of Hemiplegics Patients Joint by Means of Functional Electrical Stimulation:, IEE Trans, BME-21, 365-370.

Stauffer E.S. Hoffer M. and Nickel V.L., (1987). "Para Walker Paraplegic Walking", Physiotherapy, 73, 2, 99-100.

Summers B.N., McClelland M.R. Patrick J.H., EI, Masrib W.S., (1986). "A Clinical Review of the Adult Hip Guidance Orthosis". Paper read at the Scientific Meeting of the IMSP, Oslo, Norway, August .

Sykes L., Ross E.R.S., Powell E.S. and Edwards J., (1996) "Objective measurement of use of the reciprocating gait Orthosis (R.G.O.) and the electrically augmented R.G.O. in adult patients with spinal cord lesion" Prosthetics and Orthotics International, 20, 182-190.

Tomovic R., Popovic D., & Tepavac D., (1990), "Rule Based Control of Sequential Hybrid Assistive Systems (SHAS)". Proc. of 10th Int. Symp. On Advances in External Control of Human Extremities ECHEX 11-19.

Vukobratovich M., Shagayushchiye Roboty. (1976),"Anthropomorphous Mechanisms". Moscow Mir Press,

Waters R.L., Yakura J.S., Adkins R., Barnes G. (1989). Determinants of gait performance following spinal cord injury. Arch Phys Med Rehabil 70:811-818.

Waters R.L., and Lunsford B.R. (1985). "Energy cost of paraplegia locomotion. Journal of Bone and Joint Surgery 76A: 1245-1250.

Watkins E.M., Edwards D.E., and Patrick J.H., (1987) "Para Walker paraplegic walking". Physiotherapy 73,2, 99-100.

Winchester P.K., Carollo J.J., Parekh R.N., Lutz L.M., Aston Jr J.W. (1993) " A comparison of paraplegic gait performance using two types of reciprocating gait Orthosis" Prosthetics and Orthotics International. 17, 101-106.

Xu J.H and Mansour M. (1986), "Design of H_∞ optimal Robust Controller. Stability, Asymptotic regulation and disturbances rejection". Proceedings of the 25th IEE conference on Decision and Control, Athens, PP 1-6.

Youla D.C., Bongiorno J.J. and Jabr H.A., (1985), " A Feedback Theory of Two-Degree of Freedom Optimal Wiener-Hopf Design" IEEE Trans. Automatic Control, Vol. AC-30, No.7, PP. 652-665.

Youla D.C., Bongiorno J.J. and Jabr H.A., (1976a), " Modern Wiener-Hopf Design of Optimal Controllers, Part I: The single-Input Single-Output Case", IEEE Trans. Automatic Control, Vol. AC-21, No.1, PP. 3-13.

Youla D.C., Bongiorno J.J. and Jabr H.A., (1976b), "Modern Wiener-Hopf Design of Optimal Controllers, Part II: Multivariable Case", IEEE Trans. Automatic Control, Vol. AC-21, No.3, PP. 319-338.

Youla D.C., Bongiorno J.J. and Jabr H.A., (1974), " Single Loop Feedback Stabilization of Linear Multivariable Dynamical Plants", Automatica, Vol. 10, PP. 159-173.

Young P. (1981), Parameter Estimation for Continuous time models a Survey". Automatica, Vol. 17, PP 23-29.

Zarrop B. and Fisher M. (1985),"Reduced Variance Pole-Assignment Self-Tuning Regulation". International Journal of Control, Vol. 42, No.5, PP 1013-1033.

References

References